OPTIMAL CONTROL OF FULLY ROUTED AIR TRAFFIC IN THE PRESENCE OF UNCERTAINTY AND KINODYNAMIC CONSTRAINTS

DISSERTATION

Christopher D. Arendt, Major, USAF

AFIT-ENS-DS-14-S-15

DEPARTMENT OF THE AIR FORCE
AIR UNIVERSITY

AIR FORCE INSTITUTE OF TECHNOLOGY

Wright-Patterson Air Force Base, Ohio

The views expressed in this dissertation are those of the author and do not reflect the official policy or position of the United States Air Force, the Department of Defense, or the United States Government.

AFIT-ENS-DS-14-S-15

OPTIMAL CONTROL OF FULLY ROUTED AIR TRAFFIC IN THE PRESENCE OF UNCERTAINTY AND KINODYNAMIC CONSTRAINTS

DISSERTATION

Presented to the Faculty

Graduate School of Engineering and Management

Air Force Institute of Technology

Air University

Air Education and Training Command

in Partial Fulfillment of the Requirements for the

Degree of Doctor of Philosophy in Operations Research

Christopher D. Arendt, B.A., M.S.

Major, USAF

September 2014

AFIT-ENS-DS-14-S-15

OPTIMAL CONTROL OF FULLY ROUTED AIR TRAFFIC IN THE PRESENCE OF UNCERTAINTY AND KINODYNAMIC CONSTRAINTS

Christopher D. Arendt, B.A., M.S.
Major, USAF

Approved:

/signed/	14 Aug 2014
James W. Chrissis, PhD (Chairman)	Date
/signed/	14 Aug 2014
Darryl K. Ahner, PhD (Member)	Date
/signed/	14 Aug 2014
Richard F. Deckro, DBA (Member)	Date
/signed/	14 Aug 2014
Mark E. Oxley, PhD (Member)	Date

Accepted:

ADEDEJI B. BADIRU, PhD Dean, Graduate School of Engineering and Management	Date

AFIT-ENS-DS-14-S-15

Abstract

A method is presented to extend current graph-based Air Traffic Management optimization frameworks. In general, Air Traffic Management is the process of guiding a finite set of aircraft, each along its pre-determined path within some local airspace, subject to various physical, policy, procedural and operational restrictions. This research addresses several limitations of current graph-based Air Traffic Management optimization methods by incorporating techniques to account for stochastic effects, physical inertia and variable arrival sequencing. In addition, this research provides insight into the performance of multiple methods for approximating non-differentiable air traffic constraints, and incorporates these methods into a generalized weighted-sum representation of the multi-objective Air Traffic Management optimization problem that minimizes the total time of flight, deviation from scheduled arrival time and fuel consumption of all aircraft. The methods developed and tested throughout this dissertation demonstrate the ability of graph-based optimization techniques to model realistic air traffic restrictions and generate viable control strategies.

To my wife, for her patience and inspiration

Table of Contents

Page

Page

Page

List of Figures

Figure Page

List of Tables

List of Acronyms

Acronym	Definition
APF	Artificial Potential Field
ATC	Air Traffic Control
ATM	Air Traffic Management
ESP	Euclidean Shortest Path
FAA	Federal Aviation Administration
FCFS	First-Come-First-Served
HCS	Hybrid Control System
KKT	Karush-Kuhn-Tucker
LGR	Legendre-Gauss-Radau
MLD	Minimum Lateral Distance
NAS	National Airspace System
NASA	National Aeronautics and Space Administration
NextGen	Next-Generation Air Transportation System
SCP	Sequential Convex Programming
SQP	Sequential Quadratic Programming
STOP	Shadow Time Overshoot Phase

OPTIMAL CONTROL OF FULLY ROUTED AIR TRAFFIC IN THE PRESENCE OF UNCERTAINTY AND KINODYNAMIC CONSTRAINTS

I. Introduction

1.1 Background

Air Traffic Management (ATM) is the process of guiding a finite set of aircraft within some local airspace from their initial positions (or *originations*) to their respective destinations, subject to various physical, policy, procedural and operational restrictions [41]. If each aircraft has a pre-defined route through the airspace and a scheduled (or *nominal*) time of arrival, the process is known as the *Fully Routed Nominal Arrival Problem* in ATM [75]. Solving this problem involves generating feasible speed advisories (also known as *control strategies*) for all aircraft within the finite set. Clearly, for airspace on the order of the National level, there can be many aircraft comprising this set. Thus, problems of this nature tend to be large and difficult to solve.

Ghrist and Koditschek [32] developed a framework that defines the finite set of allowable or pre-determined vehicle routes as a directed graph with vertices corresponding to points in two- or three-dimensional physical space, and with edges corresponding to oriented curves in the space. The physical position of each vehicle is thus represented by its arc-length along one of the graph edges. Sadovsky, Davis, and Isaacson [72, 73, 76] at the National Aeronautics and Space Administration (NASA) Ames Research Center have applied this framework to compute for each aircraft within a local airspace *speed* advisories that are feasible with respect to various restrictions, focusing on separation assurance requirements. However, this framework does not model aircraft acceleration and assumes zero winds and zero deviation from pre-defined aircraft routes or arrival sequence. Thus, there exists no graph-based ATM framework that generates optimal control strategies based on kinodynamic constraints, stochastic flight control properties and variable arrival sequencing.

This research extends current graph-based methods used to address the Fully Routed Nominal Arrival Problem in ATM by generalizing the ATM framework of Sadovsky, *et al.*, to account for stochastic effects, physical inertia and variable arrival sequences. In addition, this research provides insight into the performance of multiple methods for approximating non-differentiable air traffic constraints, and incorporates these methods into a scalarized representation of the multi-objective Air Traffic Management optimization problem that evaluates trade-offs between the total time of flight, deviation from scheduled arrival time and fuel consumption of all aircraft based on notional priorities.

1.2 Overview

This research focuses on modeling local Air Traffic that falls under the responsibility of terminal Air Traffic Control (ATC) (*i.e.*, aircraft in flight near an airport), as opposed to optimizing Air Traffic across multiple ATC sectors or optimizing ground traffic operations (*e.g.*, sequencing take-off order, aircraft taxiing between runways and terminal gates, *etc.*). One of the fundamental objectives of this research is to demonstrate that the roadmap coordination space framework developed by Sadovsky, *et al.*, is suitable for mapping general airspace graphs. While the current framework, detailed in Section 2.5.1, is able to represent special airspace graphs that include only lateral separation requirements [72, 73], Federal Aviation Administration (FAA) policies define safe separation in terms of each aircraft maintaining some minimum lateral distance from any other aircraft in the terminal airspace or maintaining a distinct minimum vertical distance from any other aircraft in the terminal airspace [27]. This *anisotropic* property of the safe separation requirement results in non-differentiable constraint functions when formulating the ATM optimization problem. Therefore, this research develops and analyzes three differentiable methods of approximating the anisotropic safe separation constraint. These approximations are defined such that the modeled feasible region of the ATM optimization problem is a subset of the true feasible region; that is, solutions that satisfy the differentiable constraint approximations never violate the actual anisotropic constraints. Furthermore, error bounds are derived for each approximation method indicating the anisotropic constraints can be approximated with arbitrary precision. Additionally, FAA procedures to account for the "effects of wake turbulence" in the terminal airspace introduce asymmetry to the

safe separation requirements [27]. For example, if a designated "small" aircraft is flying behind a designated "heavy" aircraft, ATC is directed to ensure at least 5 miles of lateral separation between the aircraft [27]. However, if a designated "heavy" aircraft is flying behind a designated "small" aircraft, ATC is directed to ensure at least 3 miles of lateral separation between the aircraft [27]. This research develops a hybrid approximation scheme that incorporates two differentiable methods to approximate the asymmetric lateral separation constraint.

Modeling the management of commercial air traffic in the terminal airspace as an optimization problem requires the definition of an objective function. However, real-world conditions and FAA policies may imply a preference or ordering among certain competing objectives. For example, commercial airlines may seek to minimize fuel consumption and deviation from scheduled arrival times, while the priority of Air Traffic Controllers may be to guide aircraft out of the terminal airspace as quickly and safely as possible. Taking these factors into consideration, this research defines and evaluates a notional weighted-sum objective function that represents the relative priorities assigned to a fuel consumption measure, a deviation from scheduled arrival time measure and a total time in flight (or *makespan*) measure as either a linear or exponential weight. This research evaluates variants of this weighted-sum approach to provide insight into how to incorporate the relative priorities of these competing objectives when defining the ATM optimization problem.

Furthermore, the current graph-based ATM optimization framework of Sadovsky, *et al.*, detailed in [75], does not model aircraft acceleration and assumes each aircraft achieves zero deviation from its assigned path or speed. That is, the model does not incorporate random lateral deviations from path due to wind, nor vertical deviations from path due to turbulence. Additionally, the current model does not account for random perturbations in aircraft speed due to mechanical or control lag or human error. The research presented here defines aircraft acceleration as the control variable and incorporates a *positional probability ellipsoid model* to account for stochastic effects when estimating the lateral and vertical separation between each aircraft.

The incorporation of flight time measures, such as schedule deviation or makespan, as objectives in an ATM optimization problem introduces the issue of allowing the aircraft arrival sequence to vary. While variable arrival sequences could be accounted for by enumerating and

evaluating all feasible arrival sequences, such a method would introduce combinatoric complexity to the ATM optimization problem. Therefore, this research leverages the assumption of positive aircraft speed to define an on-time arrival constraint that allows the ATM optimization problem with variable arrival sequences to be evaluated without explicitly defining the aircraft arrival sequence.

This research combines these extensions and generalizations into a novel ATM optimization framework that accounts for aircraft acceleration, anisotropic and asymmetric separation requirements, variable arrival sequences and stochastic effects. The suitability of these extensions and generalizations of the current graph-based ATM optimization framework is demonstrated through the use of notional test cases with increasing complexity. The simplest test case is evaluated to characterize how the performance of the new framework varies based on changes in model parameters and on variations of the weighted-sum objective formulation. The model parameters and weighted-sum objective formulation that generate the best overall results are then used to demonstrate how the new framework could be applied in more complicated cases.

1.3 Organization

This document is organized as follows. Chapter 2 reviews the relevant literature concerning current ATM problems and research, as well as pertinent mathematical and optimization techniques that have been applied to similar problems. Chapter 3 describes methods to synthesize previous research and novel approaches into a robust ATM optimization framework. Chapter 4 provides the results of implementing those methods, while Chapter 5 provides a summary and conclusion of the research and results presented.

II. Literature Review

This chapter presents background information and research concerning Air Traffic Management (ATM) in general, as well as techniques that are currently applied to ATM optimization problems and topics that are relevant to this research.

2.1 Air Traffic Management

Air Traffic Management is defined by the Federal Aviation Administration (FAA) as the process of guiding a finite set of aircraft through some local airspace, subject to various physical, policy, procedural and operational restrictions [27]. In practice, this process consists of Air Traffic Control (ATC) operators (or *controllers*) giving navigational instructions (consisting of directional heading, speed and target altitude) to aircraft within the controller's designated airspace; providing these instructions is known as *vectoring*. The principal restriction in this research is *minimum separation assurance*. While exact separation requirements are location-specific, Isaacson and Robinson [40] state that aircraft typically must be separated *vertically* by at least $1,000$ feet (ft) or *laterally* by at least 3 nautical miles (nmi). This restriction defines a set of cylinders centered on each aircraft (Figure 2.1), and admissible air traffic advisories (also known as *vectors* or *control strategies*) must result in trajectories in which no aircraft intersects another's cylinder at any time. That is, for every instant of time, t, all pairs of aircraft i and j must satisfy *at least one* of the constraints:

$$\left\|\mathbf{x}_i(t) - \mathbf{x}_j(t)\right\|_L \geq r_{i,j}(t) \tag{2.1a}$$

or

$$\left\|\mathbf{x}_i(t) - \mathbf{x}_j(t)\right\|_V \geq h_{i,j}(t), \tag{2.1b}$$

where $\mathbf{x}_i(t)$ is the three-dimensional position of aircraft i at time t, $\mathbf{x}_j(t)$ is the three-dimensional position of aircraft j at time t, $\|\cdot\|_L$ is the lateral (two-dimensional Euclidean) distance function, $r_{i,j}(t)$ is the minimum allowable lateral separation between aircrafts i and j at time t, $\|\cdot\|_V$ is the vertical (one-dimensional absolute) distance function, and $h_{i,j}(t)$ is the minimum allowable vertical separation between aircrafts i and j at time t. Since only one of the constraints from (2.1) must be satisfied at any time, inadmissible air traffic advisories violate *both* constraints at some instant, t.

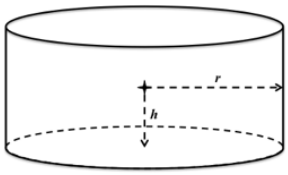

Figure 2.1: Notional Aircraft Separation Cylinder

2.1.1 Current Operations and Developing Issues.

The primary concern of air traffic controllers is ensuring the safe separation of aircraft in the terminal airspace. While en-route traffic follows routes that ensure safe separation, Sadovsky [72] states that in the terminal airspace, controllers are required to detect potential safety conflicts and provide timely trajectory advisories, including speed, altitude and heading, in order to ensure safe separation through the terminal airspace. Furthermore, the FAA has projected air traffic demand to increase significantly in the upcoming years [26]. According to Davis, Erzberger, Green and Nedell [20], and Sadovsky [72], this increased demand and workload for air traffic controllers is expected to result in increasing delays and airspace congestion, as well as increased costs due to fuel consumption.

2.1.2 Next-Generation Air Transportation System (NextGen).

To address these developing issues, the Next-Generation Air Transportation System (NextGen) is being developed by the FAA as a comprehensive overhaul of the National Airspace System (NAS) [26]. NextGen includes ATC navigational and communications technology modernization, as well as policy and procedural changes that reflect the capabilities of the new infrastructure. One of the intended goals of NextGen is to mitigate the safety, schedule and congestion issues associated with increasing air traffic demand through the use of increasingly precise navigation methods and the development of automated ATM support tools. Thus, a critical component of NextGen is the efficient generation of admissible trajectories for aircraft in the terminal airspace; that is, the "specification of a path from origin to destination for each flight" that does not violate applicable physical, policy, procedural or operational requirements [72]. The success of the NextGen system depends heavily on the performance and validity of its automated ATM support tools, including

trajectory planning for the terminal airspace. Therefore, the algorithms and frameworks that NextGen implements for trajectory generation must be robust and thoroughly analyzed.

2.2 Optimization Problems

This section lists various types of optimization problems and describes how they may apply to this ATM optimization research. Many of these problems are related to vehicle routing problems, where the goal is to find the optimal route from a given initial position (or *origination*) to the final position (or *destination*), or to optimal control problems, where the goal is to find the control strategy (*e.g.*, heading, speed or acceleration) that minimizes the *measure of performance*. Indeed, the key distinction between these types of problems is generally the measure of performance that defines optimality: total distance travelled, time of completion, fuel consumed, and so on.

2.2.1 Shortest Path Problem.

Given a graph $\mathcal{G} = (\mathcal{N}, \mathcal{A})$, where $\mathcal{N}$ is a set of nodes (or *vertices*) and $\mathcal{A}$ is a set of edges (or *arcs*), and a set of *arc lengths*, C, for each element in $\mathcal{A}$, a set of arcs that connects a given origination vertex to a given destination vertex is a *path* [7]. The *path length* is the sum of all arc lengths corresponding to the arcs in the path. The path with the minimum length is the *shortest path* [7]. This problem of finding the shortest path is represented as:

$$\text{minimize} \quad \sum_{i=1}^{n} \sum_{j=1}^{n} c_{ij} x_{ij} \tag{2.2a}$$

$$\text{subject to} \quad \sum_{j=1}^{n} x_{ij} - \sum_{k=1}^{n} x_{ki} = \begin{cases} 1, & i = 1 \\ 0, & i \notin \{1, n\} \\ -1, & i = n \end{cases} \tag{2.2b}$$

$$x \in \{0, 1\} \quad i, j = 1, 2, \ldots, n, \tag{2.2c}$$

where n is the total number of vertices in the graph $\mathcal{G}$, $c_{ij} \in C$ is the length of the arc connecting vertices $i \in \mathcal{N}$ and $j \in \mathcal{N}$, x_{ij} is equal to 1 if the arc connecting vertices i and j is in the path, and x_{ij} is equal to 0 otherwise [7]. Several methods exist to solve this shortest path problem, including Dijkstra's Algorithm [21], the "A-star" heuristic [34] and dynamic programming.

The shortest path problem does not need to minimizes literal distances, since the set C of arc lengths could represent some other cost or weighting associated with traversing the arcs. For example, Sadovsky, *et al.*, represent aircraft route segments in [72] as arcs in the graph, but the arc lengths are not defined as distances. Instead, they are defined by a weighting function that represents the likelihood of admitting separation compliant routings along those arcs. Thus, the shortest path problem in [72] does not necessarily generate paths of minimal distances, but is intended to generate paths that are more likely to keep pairs of aircraft safely separated.

The shortest path problem is called a *Euclidean Shortest Path (ESP)* problem if the arc lengths are defined as Euclidean distances, and the goal of the ESP is to find the minimum distance route (or set of routes for multiple vehicles) [7]. This representation of the shortest path problem is valid for vehicle routings when the set of paths from the vehicle initial position to the final position constitutes a *roadmap* of a countable number of arcs [52, 66]. Transforming an ATM problem into an ESP network optimization problem can be accomplished a variety of ways. For example, if aircraft are only permitted to fly through predefined routes in the airspace near an airport, and aircraft altitude is allowed only a finite number of values, then the path of an aircraft through the terminal airspace consists of a discrete and countable set of physical route segments connected at physical waypoints that can be modeled as a *roadmap* network of arcs connected at vertices [72]. On the other hand, if there are no predefined routes in the airspace, it is possible to construct a graph, known as a *Voronoi diagram*, whose arcs represent the safest routes that avoid obstacles in the environment, and to find the shorts path along these safety arcs [9]. This method is discussed in more detail in Section 2.3.3.

If aircraft altitude is not constrained to a finite number of values, then the number of paths from the initial position to the final position may become uncountable, and no graph representation may be practical. However, the shortest path problem can be generalized to account for when the number of paths from the initial position to the final position is uncountable. The objective function of the continuous shortest path problem can be given as

$$\underset{\mathbf{f}}{\text{minimize}} \quad \int_{t_0}^{t_f} \left\| \dot{\mathbf{f}}(t) \right\| dt, \tag{2.3}$$

where t_0 is the initial time (when the initial position is departed), t_f is the final time (when the final position is reached), and $\dot{\mathbf{f}}(t)$ is the vehicle velocity at time t [39]. Depending on the dynamics or constraints involved in the problem, continuous shortest path problems are typically approximated by selecting discrete values from the time interval, $[t_0, t_f]$, and applying a numerical solver to optimize the problem at the selected time values [39].

Shortest path problems have been used extensively in collision avoidance and vehicle navigation problems with direct application to ATM. Suh and Shin proposed a shortest path method for path planning of robots with distance safety criterion that could be applied to aircraft that must navigate within predefined airspace corridors [82]. Asano, Kirkpatrick and Yap presented a pseudo approximation algorithm for the three-dimensional ESP that "generalizes the shortest path for ... moving amidst polyhedral obstacles" [4], which could apply to inclement weather avoidance in ATM. Mitchell and Sharir provide a polynomial-time algorithm for the shortest path problem that avoids "terrain-like" stacked polygonal obstacles [62] that could also apply to aircraft weather or terrain avoidance. Furthermore, the ESP in two-dimensions is shown by Hershberger and Suri [35] to be computable in polynomial time, while Canny and Reif [17] show that, in general, three-dimensional ESP problems are not computable in polynomial time. Thus, it may be impractical to formulate a terminal airspace ATM optimization problem as a three-dimensional ESP.

2.2.2 Minimum Time.

Given a general shortest path problem as defined by equation (2.2) or (2.3), if the arc lengths are defined as task times or durations, then the shortest path problem represents a minimum time or minimum final time problem (also known as *makespan* [67]). In many cases, the ESP solution also defines the minimum time solution, since the total distance travelled can be parameterized by the instantaneous vehicle velocity and time, as given in the continuous shortest path objective function (2.3).

However, path-dependent restrictions on vehicle speeds may generate a difference between the minimum distance path and the minimum time path. For example, if a path of distance d permits a maximum speed of u, the minimum time required to traverse the path is d/u. However, if a path

of distance $2d$ permits a maximum speed of $3u$, the minimum time required to traverse the path is $2d/3u$. Thus, between the two paths, the minimum distance path is not the minimum time path.

Indeed, for ATM problems, the minimum time route may not correspond to the minimum distance route; thus, if the goal is to minimize the travel time from the initial position to the final position, then time should occur explicitly in the objective function formulation, such as

$$\text{minimize} \quad t_f. \tag{2.4}$$

Makespan problems are used extensively in obstacle avoidance vehicle routing problems [1, 66, 78]. Thus, while the objective function evaluation may be very simple in obstacle avoidance problems, it may be very difficult and time consuming to generate feasible solutions and guarantee that an optimal solution has been found. Methods for generating feasible obstacle avoidance solutions are described in Section 2.3. Furthermore, when multiple vehicles with separation requirements are involved, minimum time problems may include the additional difficulty of determining the optimal vehicle arrival sequence, as described in Section 2.2.4.

2.2.3 Minimum Control.

For many vehicle routing problems, the objective is to minimize a function that measures the *control variable* (or set of variables) used to control changes in the vehicle's state (*e.g.*, position, weight, speed, *etc.*). These *optimal control* problems are often defined by the objective function

$$\underset{\mathbf{u}(t)}{\text{minimize}} \quad \int_{t_0}^{t_f} \Big[\sum_{i=1}^{m} \beta_i \big| u_i(t) \big| \Big] dt, \tag{2.5a}$$

$$\text{subject to} \qquad \dot{\mathbf{x}}(t) = \mathbf{f}\left(\mathbf{x}(t), \mathbf{u}(t)\right), \tag{2.5b}$$

where t_0 is a fixed or variable initial time, t_f is a fixed or variable final time, $\mathbf{x}(t)$ is the state of a vehicle (or the state of the system under control) at time t, $\dot{\mathbf{x}}(t)$ is the instantaneous change in state at time t, $\mathbf{u}(t) = [u_1(t), u_2(t), \ldots, u_m(t)]$ is the vector of control variables that vary as a function of time, $\beta_i > 0$ is a weighting that represents the relative importance of control variable i, and $\mathbf{f}\left(\mathbf{x}(t), \mathbf{u}(t)\right)$ is the function that relates changes in the control variables to changes in the state at time t (thus, equations similar to equation (2.5b) define the *dynamics* of the problem [46]).

A similar measure, presented in [73], to require vehicles "to move as slowly as possible" is given as

$$\underset{\mathbf{u}(t)}{\text{minimize}} \quad \sum_{i=1}^{m} \Big[\int_{t_0}^{t_{[f,i]}} \Big(u_i(t) \Big)^2 dt \Big], \tag{2.6a}$$

$$\text{subject to} \qquad \dot{\mathbf{x}}(t) = \mathbf{u}(t), \tag{2.6b}$$

where $t_{[f,i]}$ is the final time for vehicle i.

Optimal control vehicle routing problems that seek to minimize the amount of fuel consumed, or *fuel burn* [16], are studied extensively in ATM since fuel costs are of great interest to commercial airlines and other operators. Bowe and Lauderdale studied the effects of generating individual collision avoidance maneuvers based on optimal fuel consumption instead of minimal schedule delay [16]. Erzberger illustrated the cost savings associated with on-board trajectories generated to minimize fuel consumption [24]. Neuman and Erzberger compared fuel minimizing ATM techniques to standard First-Come-First-Served (FCFS) arrival sequencing [63]. However, [16] and [24] consider only individual conflict maneuvers or the trajectory of a single aircraft, while [63] is primarily concerned with efficiently scheduling and sequencing airport landings from the perspective of runway operations, as opposed to congested airspace operations.

2.2.4 Minimum Delay.

Minimum delay vehicle routing problems can be seen as a generalized makespan problem in which each vehicle is given a target start time or a target time of completion. With respect to air traffic operations, the start time may be the aircraft's scheduled departure time from its origination, while the time of completion is typically the aircraft's scheduled arrival time at its destination. Deviations from scheduled departure and arrival times can result in significant costs for airlines. Although the exact cost of delay as determined by the airlines may be unknown, ATM solutions that minimize schedule delay certainly contribute to minimizing the cost of delay [15, 19, 44].

Time targets could be generalized for any point along an aircraft's route; for example, each aircraft could have a scheduled arrival time at each waypoint along its path. If the number of target times is countable for each aircraft, the minimum delay problem for a single aircraft can be given

by

$$\text{minimize} \quad \sum_{i=1}^{m} w_i T_i, \tag{2.7a}$$

$$\text{subject to} \quad T_i \triangleq \max\{t_i - \tau_i, 0\}, \tag{2.7b}$$

where m is the number of waypoints with scheduled arrival times, w_i is a weighting that represents the relative importance of meeting the scheduled time of arrival at waypoint i, τ_i is the scheduled or target time of arrival at waypoint i, t_i is the actual time of arrival at waypoint i, and T_i, known as the *tardiness* at waypoint i, is 0 if the actual time of arrival is equal to or less than the scheduled time of arrival, and the difference between the two otherwise [68]. It is important to note that no cost is incurred for the minimum delay problem if the aircraft arrives *before* its scheduled arrival time.

As in the makespan problem, generating feasible solutions in the presence of obstacles or multiple aircraft that share resources (*e.g.*, the same route segments or runways) can be difficult. For example, when multiple vehicles with separation requirements are involved, the makespan and minimum delay problems could involve the additional difficulty of determining the optimal arrival sequence. If the arrival sequence is not fixed, then for A aircraft, there could be $A!$ possible arrival sequences. Thus, determining which arrival sequence provides the minimum feasible makespan or delay could require evaluating $A!$ makespan or delay sub-problems. In [63], Neuman and Heinz analyze how optimal arrival sequencing and "FCFS" sequencing rules can affect aircraft arrival delays. In [71], Robinsin, Davis and Isaacson, compare FCFS sequencing methods to a "fuzzy reasoning-based sequencing" of aircraft arrivals. In [80], Soler, Olivares, Staffetti and Bonami propose a "branch-and-bound"-based heuristic for selecting and optimizing an arrival sequence. Section 3.1.3.1 presents a method for evaluating feasible arrival sequences implicitly, without having to define all $A!$ sub-problems and evaluate all feasible arrival sequences.

2.2.5 Minimum Deviation.

The minimum deviation problem can be seen as a generalization of the minimum delay problems. The minimum delay problem seeks to minimize tardiness, and ignores cases in which the aircraft arrives before the scheduled arrival time. Although it is important for an aircraft to arrive at each waypoint (including its destination) with minimal delay, it may also be important to prevent

aircraft from arriving too soon before their scheduled arrival time, since this could interfere with other aircrafts' scheduled arrivals and departures, and may result in greater fuel consumption if the aircraft is forced to loiter until it can safely land [3]. Therefore, an ATM problem may seek to minimize the *absolute deviation*, positive and negative, from schedule.

However, it may also be important to minimize an aircraft's absolute deviation from a planned trajectory, or any target that can be parameterized as a function of time. Thus, if the measure of comparison can be given as a function of time, the minimum absolute deviation objective function for a single aircraft is given as

$$\int_{t_0}^{t_f} \Big[\sum_{i=1}^{m} |\tau_i(t) - x_i(t)| \Big] dt, \tag{2.8}$$

where $|\cdot|$ represents the absolute value, m is the number of target measures of comparison (schedule, trajectory, *etc*.), $\tau_i(t)$ is the target value of measure of comparison i at time t, and $x_i(t)$ is the actual value of measure i at time t. For computational simplicity, the minimum deviation objective function may also appear as

$$\int_{t_0}^{t_f} \Big[\sum_{i=1}^{m} \big(\tau_i(t) - x_i(t)\big)^2 \Big] dt. \tag{2.9}$$

2.2.6 Min-max.

Min-max (or *minimax*, or *max ordering*) problems typically involve multiple objectives, or multiple vehicles, each with its own measure of performance. The goal of the min-max problem is to find the feasible solution that minimizes the maximal element of the set of all objectives or vehicles. The min-max problem takes the form

$$\underset{\mathbf{x}\in\mathbf{\Omega}}{\text{minimize}} \quad \max\{f_1(\mathbf{x}), \ldots, f_i(\mathbf{x}), \ldots, f_m(\mathbf{x})\}, \tag{2.10}$$

where m is the number of objective functions or vehicles of interest, $\mathbf{x} \in \mathbf{\Omega}$ is the vector of decision variables in the feasible space $\mathbf{\Omega}$, and $f_i(\mathbf{x})$ is the value of objective i evaluated at $\mathbf{x}$.

An important feature of the min-max formulation is that it gives a weakly efficient solution [23]; that is, no feasible solution can improve upon any of the m objective function values given by the min-max solution without generating an inferior value in another objective function. However,

the min-max objective function may be non-differentiable even if the individual objective functions are differentiable, which can make optimization difficult [11].

2.2.7 Weighted-Sum.

Another method of evaluating problems that involve multiple objectives, or multiple vehicles, each with its own measure of performance, is to define the objective function as a weighted-sum of the multiple objectives or measure of performance for each vehicle. This weighted-sum transforms the vector of values of each objective function into a single value, or scalar. The weighted-sum objective function takes the form

$$\underset{\mathbf{x}\in\mathbf{\Omega}}{\text{minimize}} \quad \sum_{i=1}^{m} \lambda_i f_i(\mathbf{x}), \tag{2.11}$$

where m is the number of objective functions or vehicles of interest, $\mathbf{x} \in \mathbf{\Omega}$ is the vector of solution values in the feasible space $\mathbf{\Omega}$, $f_i(\mathbf{x})$ is the value of objective i evaluated at $\mathbf{x}$, and λ_i is the relative weighting associated with objective function i, often defined such that $\sum_{i=1}^{m} \lambda_i = 1$ (*i.e.*, normalized weights).

An important feature of the weighted-sum formulation is that it gives a weakly efficient solution [23]; that is, no feasible solution can improve upon any of the m objective function values given by the weighted-sum solution without generating an inferior value in another objective function. While the weighted-sum objective function is differentiable if the individual objective functions are differentiable, for certain problems, the weighted-sum objective function method may be unable to generate large regions of efficient solutions. For example, if some of the multiple objectives are non-convex, the weighted-sum method "may work poorly" and generate solutions corresponding to individual objective minima rather than solutions that represent trade-offs between the multiple objectives [23].

2.3 Obstacle Avoidance

In addition to a measure of performance and dynamics equations, an ATM or vehicle routing problem may involve a set of obstacles that must be avoided. Obstacle avoidance problems seek to generate vehicle trajectories that guide the vehicle from its origination to its destination such that the vehicle trajectory does not intersect the boundary of any obstacle in the set. The separation

assurance criteria of ATM can be seen as part of an obstacle avoidance problem, with each aircraft being considered a moving obstacle in relation to all other aircraft. Furthermore, ATM strategies that seek to avoid inclement weather or restrict aircraft trajectories to predefined routes in the airspace can also be formulated as obstacle avoidance problems [4, 82]. This section describes typical obstacle avoidance techniques and details how they have been applied to ATM related problems.

2.3.1 Path Constraints.

One approach for dealing with obstacles is to define vehicle path constraints based on each obstacle. Path constraints define the minimum allowable distance from the vehicle to an obstacle, or the distance from a time-dependent state of the system to the boundary of a set of inadmissible states (as described in Section 2.5.1). For example, the time-dependent path constraint for a single obstacle may be given by

$$\min_{\mathbf{b}(t)} \left\{ \mathcal{D}\Big(\mathbf{x}(t), \mathbf{b}(t)\Big) \;\mid\; \mathbf{x}(t) \right\} \geq \mathbf{r}(t), \tag{2.12}$$

where $\mathcal{D}(\cdot)$ represents the distance function chosen for the problem, the vector $\mathbf{x}(t)$ represents the given system state or the position of the vehicle at time t, $\mathbf{b}(t)$ represents the boundary of the obstacle or inadmissible state set at time t, and $\mathbf{r}(t)$ is the minimum separation allowed between the vehicle or state and the boundary of the obstacle. In this case, the path constraint indicates that the vehicle path must be at least a distance of $\mathbf{r}(t)$ from the nearest point on the boundary of the obstacle at time t. For circular or spherical obstacles with known radii, the path constraint can be simplified as the minimum allowable distance from the center of the obstacle, since the point on the obstacle boundary nearest to the vehicle path will always be a single radius from the obstacle center. Therefore, some obstacle avoidance techniques seek to approximate obstacles with a circle or sphere that encompasses the actual shape of the obstacle [28]. Suppose, however, that an obstacle, O, is defined as the intersection of K constraint-defined sets, formulated as

$$O \triangleq \bigcap_{k=1}^{K} \mathbf{G}_k, \tag{2.13a}$$

where for each $k \in \{1, 2, \ldots, K\}$

$$\mathbf{G}_k \triangleq \{\mathbf{x}(t) \;\mid\; g_k(\mathbf{x}(t)) > 0\}, \tag{2.13b}$$

and $\mathbf{x}(t)$ is the position of a vehicle or the system state at time t. That is,

$$\mathcal{O} \triangleq \left\{ \mathbf{x}(t) \;\middle|\; \min\left\{g_1(\mathbf{x}(t)), g_2(\mathbf{x}(t)), \ldots, g_K(\mathbf{x}(t))\right\} > 0 \right\}. \tag{2.14}$$

For example, the ATM constraints in equation (2.1) define each aircraft as a cylindrical obstacle that is the intersection of the lateral separation constraint and the vertical separation constraint. In this case, the intersection of sets is not circular or spherical, so approximating such an obstacle with a single radius will reduce the apparent feasible region for the problem and could result in paths that are not optimal. Thus, the path constraints should model the obstacle boundary with as much accuracy as is practical. Sections 2.3.1.1 - 2.3.1.6 describe methods of modeling obstacles and obstacle boundaries that seek to reduce the over-estimation error of the path constraints.

2.3.1.1 Elliptical Methods.

Elliptical methods approximate each path obstacle with an ellipsoid or the *union* of multiple ellipsoids. The equation of the boundary of an ellipsoid centered at the origin and oriented in the direction of each coordinate axis is given by [86]

$$\sum_{k=1}^{K} \left(\frac{x_k}{r_k}\right)^2 = 1, \tag{2.15}$$

where K is the dimensionality of the ellipsoid, x_k is the coordinate in the kth dimension of a point on the boundary, and r_k is the distance from the center of the ellipsoid to the boundary in the kth coordinate direction. Therefore, the time-dependent path constraint for a single *stationary* elliptical obstacle may be given by

$$1 - \sum_{k=1}^{K} \left(\frac{\hat{c}_k(t)}{r_k}\right)^2 \leq 0, \tag{2.16}$$

where $\hat{c}_k(t)$ is the kth state coordinate at time t transformed to account for the location of the center and orientation of the elliptical obstacle. If an obstacle is approximated by the combination (or *union*) of multiple ellipsoids, then the path constraint for the single obstacle would consist of a set of ellipsoid constraints of the form given by equation (2.16). For example, in [43], Kamgarpour, Dadok and Tomlin use a set of "minimum volume bounding ellipses" to model inclement weather obstacles for aircraft to avoid.

While elliptical methods can more closely approximate obstacles than a single radius (circular) approximation, they are inappropriate for path obstacles defined as the *intersection* of shapes or

sets, rather than the union. For example, the ATM cylindrical constraint from equation (2.1) could be approximated with the equation of the minimum volume ellipsoid that contains the minimum separation cylinder. However, the approximation could greatly overestimate the volume of the cylindrical ATM obstacle.

2.3.1.2 Indicator Methods.

One method of formulating path obstacles as the intersection of sets involves the use of *indicator functions*. In reference to equation (2.13), for each set $\mathbf{G}_k$ in the obstacle-defining intersection of K such sets, an indicator function, y_k, is defined such that

$$y_k(t) = \begin{cases} 1 & \text{if } \mathbf{x}(t) \in \mathbf{G}_k, \\ 0 & \text{otherwise,} \end{cases} \tag{2.17}$$

where $\mathbf{x}(t)$ is the state of the system at time t. If an obstacle is defined as the intersection of K such sets, then the obstacle is avoided when there exists some $\mathbf{G}_k$ such that $\mathbf{x}(t) \notin \mathbf{G}_k$; that is whenever at least one indicator function is equal to zero, the obstacle is avoided. Thus, the path constraint can be formulated as

$$1 - K + \sum_{k=1}^{K} y_k(t) \leq 0 \tag{2.18a}$$

or

$$\prod_{k=1}^{K} y_k(t) \leq 0. \tag{2.18b}$$

However, neither formulation of the indicator function path constraint given in (2.18) is guaranteed to be differentiable at all values of t, since each indicator function y_i defined by equation (2.17) becomes discontinuous at the boundary of the set $\mathbf{G}_k$. The non-differentiability of the constraint formulation makes the obstacle avoidance problem difficult to solve using the standard methods described in Section 2.4. Therefore, many differentiable approximations or alternative formulations have been developed to address this issue [10].

2.3.1.3 Piece-wise Methods.

Piece-wise methods of formulating obstacle path constraints are similar to indicator methods in that they are based on conditionally (or *piece-wise*) defined constraint functions of the form

$$G(t) = \begin{cases} y_1(t) & \text{if } \mathbf{x}(t) \in \mathbf{D}_1, \\ \vdots & \\ y_K(t) & \text{if } \mathbf{x}(t) \in \mathbf{D}_K, \\ 0 & \text{otherwise,} \end{cases} \tag{2.19}$$

where the *subdomains* $\mathbf{D}_1, \ldots, \mathbf{D}_k$ are mutually exclusive: $\bigcap_{k=1}^{K} \mathbf{D}_k = \varnothing$ [2]. That is, for $k = 1, \ldots, K$, if the state variable $\mathbf{x}$ is in the subdomain $\mathbf{D}_k$ at time t, the value $G(t)$ of the piece-wise defined constraint function is given by $y_k(t)$; otherwise, $G(t) = 0$. However, for use with standard optimization methods, the piece-wise defined constraint functions should be defined such that they are continuous and differentiable. For example [29], the piece-wise defined constraint function, G_{pw}, given by

$$G_{pw}(t) = \begin{cases} -1 + e^{-(d_1(t)-1)^2} & \text{if } d_1(t) \geq 1 \text{ and } d_2(t) < 1, \\ -1 + e^{-(d_2(t)-1)^2} & \text{if } d_1(t) < 1 \text{ and } d_2(t) \geq 1, \\ -1 + e^{-(d_1(t)-1)^2-(d_2(t)-1)^2} & \text{if } d_1(t) \geq 1 \text{ and } d_2(t) \geq 1, \\ 0 & \text{otherwise,} \end{cases} \tag{2.20}$$

is continuous for $d_1(t), d_2(t) \geq 0$ since each subdomain's function is continuous over its subdomain, and at the shared boundary of any two subdomains, their functions evaluate to the same value. Note that the piece-wise defined function (2.20) may be used to represent the ATM cylindrical path obstacle as

$$G_{pw}(t) < 0, \tag{2.21a}$$

with

$$d_1(t) = \frac{\left\|\mathbf{x}_i(t) - \mathbf{x}_j(t)\right\|_L}{r_{i,j}(t)} \tag{2.21b}$$

and

$$d_2(t) = \frac{\left\|\mathbf{x}_i(t) - \mathbf{x}_j(t)\right\|_V}{h_{i,j}(t)}. \tag{2.21c}$$

This piece-wise defined constraint function is once-differentiable for $d_1(t), d_2(t) \geq 0$ since each subdomain's function is differentiable over its subdomain, and at the shared boundary of any two subdomains, their function's derivatives evaluate to the same value. However, the strict inequality of this formulation treats the boundary of the path obstacle as infeasible, and the constraint function is not *twice*-differentiable [29], since at the shared boundary of any two subdomains, their function's second derivatives do not evaluate to the same value.

2.3.1.4 Multiplier Methods.

In [69], Raghunathan, Gopal, Subramanian and Biegler address the non-differentiability of the ATM cylindrical path constraint (2.1) by introducing two artificial control variables, λ_1 and λ_2, that are included as multipliers in the path constraint formulation, and as terms in an addition to the objective function. Thus, the minimum separation path constraint is given by

$$\lambda_1(t)\Big(\big\|\mathbf{x}_i(t) - \mathbf{x}_j(t)\big\|_L - r_{i,j}(t)\Big) + \lambda_2(t)\Big(\big\|\mathbf{x}_i(t) - \mathbf{x}_j(t)\big\|_V - h_{i,j}(t)\Big) \geq 0, \tag{2.22a}$$

$$\lambda_1(t) + \lambda_2(t) = 1, \tag{2.22b}$$

$$\lambda_1(t), \lambda_2(t) \geq 0, \tag{2.22c}$$

for every $t \in \Big[t_0, t_f\Big]$, and the addition to the objective function is given by

$$\int_{t_0}^{t_f} \Big[\lambda_1(t)^2 + \lambda_2(t)^2\Big] dt. \tag{2.23}$$

While this method appears to work well with obstacles that can be defined as the intersection of only two constraints, it requires the introduction and optimization of a new control variable for each constraint in the intersection of constraints that defines the obstacle. Therefore, the Multiplier Method in [69] may be inappropriate for formulations that involve the intersection of more than two constraints.

In [10], Bertsekas discusses Multiplier Methods that approximate multiple non-differentiable functions with piece-wise defined functions whose subdomains are determined by a sequence of multipliers and a sequence of accuracy parameters. These methods are designed for problems with

"simple kinks" [10] of the form

$$G(t) = \max\{0, g(t)\} \tag{2.24a}$$

or

$$G(t) = \max\{g_1(t), \ldots, g_k(t), \ldots, g_K(t)\}, \tag{2.24b}$$

where the function G is the *only* source of non-differentiability in an objective function or constraint function, and g and each g_k are assumed to be continuously differentiable functions. For example, (2.24a) would be approximated as

$$\tilde{G}(g(t), \lambda, \gamma) = \begin{cases} g(t) - (1-\lambda)^2/2\gamma & \text{if } (1-\lambda)/\gamma \leq g(t), \\ \lambda g(t) + \frac{1}{2}\gamma[g(t)]^2 & \text{if } -\lambda/\gamma \leq g(t) \leq (1-\lambda)/\gamma, \\ -\lambda^2/\gamma & \text{if } g(t) \leq -\lambda/\gamma, \end{cases} \tag{2.25}$$

where $0 \leq \lambda \leq 1$ is a multiplier that "determines whether the approximation is more accurate for positive or negative values", and $\gamma > 0$ is a parameter that "controls the accuracy of the approximation" [10]. Using (2.25), functions of the form (2.24b) would be approximated by a series of embedded approximations, such that

$$\begin{aligned} \tilde{G}(g_1(t), \ldots, g_K(t), \boldsymbol{\Lambda}, \boldsymbol{\Gamma}) = & g_1(t) + \\ & \tilde{G}(g_2(t) - g_1(t) + \\ & \tilde{G}(\ldots \tilde{G}(g_{K-1}(t) - g_{K-2}(t) + \\ & \tilde{G}(g_K(t) - g_{K-1}(t), \lambda_{K-1}, \gamma_{K-1}))\ldots), \lambda_1, \gamma_1), \end{aligned} \tag{2.26}$$

where $\boldsymbol{\Lambda} = [\lambda_1, \ldots, \lambda_{K-1}]$ is a vector of multipliers and $\boldsymbol{\Gamma} = [\gamma_1, \ldots, \gamma_{K-1}]$ is a vector of accuracy parameters. Note that this formulation can be simplified by setting $\lambda_k = \lambda$ for all $k = 1, \ldots, K-1$ and $\gamma_k = \gamma$ for all $k = 1, \ldots, K-1$.

From (2.14), the path obstacle, $\mathcal{O}$, may be defined as

$$\mathcal{O} \triangleq \left\{ \mathbf{x}(t) \;\middle|\; \min\left\{g_1(\mathbf{x}(t)), g_2(\mathbf{x}(t)), \ldots, g_K(\mathbf{x}(t))\right\} > 0 \right\}. \tag{2.27}$$

However, since

$$\min_{k\in\{1,\ldots,K\}} \left\{g_k(\mathbf{x}(t))\right\} > 0 \iff -\left(\max_{k\in\{1,\ldots,K\}} \left\{-g_k(\mathbf{x}(t))\right\}\right) > 0, \tag{2.28}$$

the ATM cylindrical obstacle for the interaction between aircraft i and aircraft j would appear as

$$O_{i,j} \triangleq \Big\{ \mathbf{x}(t) \;\Big|\; -\Big(\max\Big\{ -g_1(\mathbf{x}(t)), -g_2(\mathbf{x}(t)) \Big\} \Big) > 0 \Big\}, \tag{2.29}$$

where $O_{i,j}$ is the cylindrical obstacle, $\mathbf{x}(t)$ is the system state at time t,

$$g_1(\mathbf{x}(t)) = r_{i,j}(t) - \Big\| \mathbf{x}_i(t) - \mathbf{x}_j(t) \Big\|_L, \tag{2.30a}$$

$$g_2(\mathbf{x}(t)) = h_{i,j}(t) - \Big\| \mathbf{x}_i(t) - \mathbf{x}_j(t) \Big\|_V, \tag{2.30b}$$

and the remaining terms are as defined in equation (2.1). Thus, the piece-wise defined multiplier approximation of the path constraint for the required separation between aircraft i and aircraft j would be formulated as

$$-\Big(-g_1(\mathbf{x}(t)) + \tilde{G}\big(-g_2(\mathbf{x}(t)) - (-g_1(\mathbf{x}(t))), \lambda, \gamma \big) \Big) \leq 0, \tag{2.31a}$$

or, equivalently, as

$$g_1(\mathbf{x}(t)) - \tilde{G}(g_1(\mathbf{x}(t)) - g_2(\mathbf{x}(t)), \lambda, \gamma) \leq 0. \tag{2.31b}$$

While the piece-wise defined Multiplier Methods can account for multiple non-differentiable functions, and may produce approximations that are twice-differentiable, they introduce two new sets of parameters, both of which are iteratively updated throughout the optimization process, either through the "repetitive solution of the approximate problem for ever increasing values" of the parameter, or using a fixed step size change in the multiplier [10]. The approximation error associated with this method is discussed in Section 3.1.2.1.

2.3.1.5 Max-Norm Methods.

A *max-norm* (or *mixed-norm* [74]) method uses a maximum-norm as a way to intersect multiple constraints (that is, more than two) so as to define an obstacle or region to avoid. For a finite-dimensional vector space $\mathbb{R}^K$, the maximum-norm is formulated in [58] as

$$\Big\| (g_1, g_2, \ldots, g_K) \Big\|_{\max} \triangleq \max\Big\{ |g_1|, |g_2|, \ldots, |g_K| \Big\}. \tag{2.32}$$

Thus, the max-norm simply maps a vector $\mathbf{g} \in \mathbb{R}^K$ to the absolute value of the element of the vector $\mathbf{g}$ that is largest in absolute value. In reference to (2.13), the max-norm method formulates the

obstacle, O, as

$$O \triangleq \left\{ \mathbf{x}(t) \;\middle|\; \max\left\{ |\hat{g}_1(\mathbf{x}(t))|, |\hat{g}_2(\mathbf{x}(t))|, \ldots, |\hat{g}_K(\mathbf{x}(t))| \right\} < 1 \right\}, \tag{2.33}$$

where $|\hat{g}_k(\mathbf{x}(t))| > 1$ if and only if $g_k(\mathbf{x}(t)) > 0$ and $|\hat{g}_k(\mathbf{x}(t))| \leq 1$ if and only if $g_k(\mathbf{x}(t)) \leq 0$. That is, each constraint involved in the obstacle definition is replaced with an equivalent *normalized* constraint. For example, the ATM cylindrical obstacle for the interaction between aircraft i and aircraft j would be formulated as

$$O_{i,j} \triangleq \left\{ \mathbf{x}(t) \;\middle|\; \max\left\{ \frac{\left\|\mathbf{x}_i(t) - \mathbf{x}_j(t)\right\|_L}{r_{i,j}(t)}, \frac{\left\|\mathbf{x}_i(t) - \mathbf{x}_j(t)\right\|_V}{h_{i,j}(t)} \right\} < 1 \right\}, \tag{2.34}$$

where $O_{i,j}$ is the cylindrical obstacle, $\mathbf{x}(t)$ is the system state at time t, and the remaining terms are as defined in equation (2.1). The path constraint for the required separation between aircraft i and aircraft j would be given by

$$\max\left\{ \frac{\left\|\mathbf{x}_i(t) - \mathbf{x}_j(t)\right\|_L}{r_{i,j}(t)}, \frac{\left\|\mathbf{x}_i(t) - \mathbf{x}_j(t)\right\|_V}{h_{i,j}(t)} \right\} \geq 1, \tag{2.35a}$$

or equivalently by

$$\left\| \left(\frac{\|\mathbf{x}_i(t) - \mathbf{x}_j(t)\|_L}{r_{i,j}(t)}, \frac{\|\mathbf{x}_i(t) - \mathbf{x}_j(t)\|_V}{h_{i,j}(t)} \right) \right\|_{\max} \geq 1. \tag{2.35b}$$

From equation (2.32), the derivative with respect to time of the max-norm is

$$\frac{d}{dt}\left\|(g_1(t), g_2(t), \ldots, g_K(t))big\right\|_{\max} = \frac{d}{dt} \max\left\{ |g_1(t)|, |g_2(t)|, \ldots, |g_K(t)| \right\}. \tag{2.36}$$

However, if for some value of t, there exist $k_1, k_2 \in \{1, 2, \ldots, K\}$ such that $k_1 \neq k_2$, $|g_{k_1}(t)| = |g_{k_2}(t)| = \max\left\{ |g_1(t)|, |g_2(t)|, \ldots, |g_K(t)| \right\}$, but $\frac{d}{dt}|g_{k_1}(t)| \neq \frac{d}{dt}|g_{k_2}(t)|$, then there is no unique value for equation (2.36), and the derivative of the max-norm is not defined for that value of t. That is, unless the derivative is identical for each maximal term of the set for all t, the max-norm is not differentiable for some values of t. Thus, the max-norm method may be impractical for use with the gradient-based optimization methods that are typically applied to ATM optimal control problems. Therefore, Section 2.3.1.6 outlines an approximation of a max-norm method that is differentiable and thus suitable for use with typical optimization methods.

2.3.1.6 p-Norm Approximation Methods.

In [56], Lewis, Ross and Gong define two-dimensional obstacles for ground vehicle routing problems using a p-norm formulated as

$$\| (g_1, g_2) \|_p \triangleq (|g_1|^p + |g_2|^p)^{1/p}, \quad p \in [0, \infty) . \tag{2.37}$$

However, a p-norm may also be used as a differentiable approximation of a max-norm intersection method described in Section 2.3.1.5. In addition to equation (2.32), the max-norm can also be defined as [85]

$$\left\|(g_1, g_2, \ldots, g_K)\right\|_{\max} \triangleq \lim_{p\to\infty} \left(\sum_{k=1}^{K} |g_k|^p \right)^{1/p}. \tag{2.38}$$

Therefore, a p-norm approximation of the max-norm simply evaluates $\left(\sum_{k=1}^{K} |g_k|^p \right)^{1/p}$ for some large value of p. Since the p-norm approximation is a polynomial, it resolves the non-differentiability issue inherent in the max-norm formulation. However, defining an obstacle with the p-norm approximation is not trivial. For example, if the p-norm approximation were used to substitute the max-norm in equation (2.35), the following *erroneous* constraint would result

$$\left(\frac{\left\|\mathbf{x}_i(t) - \mathbf{x}_j(t)\right\|_L^p}{r_{i,j}(t)^p} + \frac{\left\|\mathbf{x}_i(t) - \mathbf{x}_j(t)\right\|_V^p}{h_{i,j}(t)^p} \right)^{1/p} \geq 1, \tag{2.39a}$$

or equivalently,

$$\frac{\left\|\mathbf{x}_i(t) - \mathbf{x}_j(t)\right\|_L^p}{r_{i,j}(t)^p} + \frac{\left\|\mathbf{x}_i(t) - \mathbf{x}_j(t)\right\|_V^p}{h_{i,j}(t)^p} \geq 1. \tag{2.39b}$$

The formulation given in equation (2.39) is satisfied if

$$\left\|\mathbf{x}_i(t) - \mathbf{x}_j(t)\right\|_L = r_{i,j}(t) \left(\frac{1}{2}\right)^{1/p} \tag{2.40a}$$

and

$$\left\|\mathbf{x}_i(t) - \mathbf{x}_j(t)\right\|_V = h_{i,j}(t) \left(\frac{1}{2}\right)^{1/p}. \tag{2.40b}$$

However, if $1 < p < \infty$, then $(1/2)^{1/p} < 1$, so the values given in (2.40) fail to satisfy each of the exact constraints given in (2.1). Thus, the formulation given in equation (2.39) is not a suitable approximation. In [79], Smith and Arendt provide a formulation that accounts for this error. Their formulation is given as

$$\frac{\left\|\mathbf{x}_i(t) - \mathbf{x}_j(t)\right\|_L^p}{r_{i,j}(t)^p} + \frac{\left\|\mathbf{x}_i(t) - \mathbf{x}_j(t)\right\|_V^p}{h_{i,j}(t)^p} \geq 2. \tag{2.41}$$

Additionally, since the p-norm approximation involves normalized constraints, care must be taken to ensure the obstacle constraints are properly normalized. In [55], Lewis and Ross address the issue of non-normalized constraints for a p-norm approximation method by defining the obstacle path constraint as the natural logarithm of the p-norm of the exponential function of each constraint. In standard form, the approximate constraint function would be defined as

$$G_p(g_1, g_2, \ldots, g_K) \triangleq -\ln\left[\left(\sum_{k=1}^{K} (e^{-g_k})^p\right)^{1/p}\right], \tag{2.42}$$

where $g_1, g_2, \ldots, g_K$ are the constraints from (2.13) whose intersection defines the obstacle. Thus, the obstacle path constraint is simply

$$G_p(g_1(\mathbf{x}(t)), g_2(\mathbf{x}(t)), \ldots, g_K(\mathbf{x}(t))) \leq 0. \tag{2.43}$$

However, if $g_k(\mathbf{x}(t)) = \frac{1}{p}\ln(K)$, for $k = 1, \ldots, K$, then each $g_k(\mathbf{x}(t)) > 0$ so the state $\mathbf{x}$ is actually infeasible at t, but the approximate constraint evaluates as

$$\begin{aligned} G_p\left(\tfrac{1}{p}\ln(K), \ldots, \tfrac{1}{p}\ln(K)\right) &= -\ln\left[\left(\sum_{k=1}^{K}\left(e^{-\frac{1}{p}\ln(K)}\right)^p\right)^{1/p}\right] \\ &= -\ln\left[\left(\sum_{k=1}^{K}\left(e^{-\ln(K)}\right)\right)^{1/p}\right] \\ &= -\ln\left[\left(\sum_{k=1}^{K}\left(\frac{1}{K}\right)\right)^{1/p}\right] \\ &= -\ln[1] \\ &= 0 \end{aligned}$$

so the path *appears* feasible. Therefore, care must be taken so that exponential p-norm approximation does not underestimate the obstacle and lead to paths that would fail to avoid the exact obstacle. Section 3.1.2.4 outlines a method of accomplishing this task.

2.3.1.7 Sigmoid Approximation Methods.

In [70], Ren, McIsaac and Huang use sigmoid approximation functions to define physical terrain obstacles for vehicles to avoid in an optimal control problem. A sigmoid approximation method is a differentiable approximation of an indicator function intersection method described in Section 2.3.1.2. An exponential sigmoid approximation of the indicator functions given in equation

(2.17) is formulated as

$$\tilde{g}_k(t) = \frac{1}{1 + e^{-\mathsf{s} g_k(t)}}, \tag{2.44}$$

where s is some large positive number and the constraint function $g_k(t)$ is defined in reference to (2.13) such that

$$g_k(t) > 0 \iff \mathbf{x}(t) \in \mathbf{G}_k \tag{2.45a}$$

and

$$g_k(t) \leq 0 \iff \mathbf{x}(t) \notin \mathbf{G}_k. \tag{2.45b}$$

Thus, the sigmoid approximation $\tilde{g}_k$ is continuously differentiable if the constraint function g_k is continuously differentiable. Additionally, for $\mathsf{s} > 0$,

$$\mathbf{x}(t) \in \mathbf{G}_k \Rightarrow \tilde{g}_k(t) \to 1 \text{ as } \mathsf{s} \to \infty \tag{2.46a}$$

and

$$\mathbf{x}(t) \notin \mathbf{G}_k \Rightarrow \tilde{g}_k(t) \to 0 \text{ as } \mathsf{s} \to \infty. \tag{2.46b}$$

However,

$$\mathbf{x}(t) \notin \mathbf{G}_k, \;\; g_k(t) = 0 \Rightarrow \tilde{g}_k(t) = \frac{1}{2}, \forall \mathsf{s}. \tag{2.47}$$

That is, on the boundary of the path obstacle, the sigmoid function will evaluate to $\frac{1}{2}$. Therefore, for an individual sigmoid approximation function $\tilde{g}_k$, its path constraint would be given by

$$\tilde{g}_k(t) \leq \frac{1}{2}. \tag{2.48}$$

Thus, if the sigmoid approximation is used to define the path obstacle as the intersection of K constraints, as in (2.18b), it should be formulated as

$$\prod_{k=1}^{K} \tilde{g}_k(t) \leq \left(\frac{1}{2}\right)^K, \tag{2.49a}$$

or

$$-\left(2^{-K}\right) + \prod_{k=1}^{K} \tilde{g}_k(t) \leq 0. \tag{2.49b}$$

Substituting (2.44) for $\tilde{g}_k(t)$ gives

$$-\left(2^{-K}\right) + \prod_{k=1}^{K} \frac{1}{1 + e^{-\mathsf{s} g_k(t)}} \leq 0. \tag{2.50}$$

For example, a sigmoid formulation of the ATM path constraint for the required separation between aircraft i and aircraft j would be given by

$$-\left(2^{-2}\right)+\left(\frac{1}{1+e^{-\mathsf{s}g_1(t)}}\right)\left(\frac{1}{1+e^{-\mathsf{s}g_2(t)}}\right)\leq 0, \tag{2.51}$$

where

$$g_1(t) = r_{i,j}(t) - \left\|\mathbf{x}_i(t) - \mathbf{x}_j(t)\right\|_L \tag{2.52a}$$

and

$$g_2(t) = h_{i,j}(t) - \left\|\mathbf{x}_i(t) - \mathbf{x}_j(t)\right\|_V. \tag{2.52b}$$

Since $\tilde{g}_k(t)$ only approximates an indicator function, the sigmoid formulation of the path constraint overestimates the true region of the obstacle in every set $\mathbf{G}_k$. For example, in (2.49b) with $K = 2$, if $\tilde{g}_1(t) = 0.9999$ and $\tilde{g}_2(t) = \frac{1}{2}$, then the state is *actually* feasible, but the sigmoid constraint function would evaluate to

$$\begin{aligned}
&-\left(2^{-2}\right) + (0.9999)\,(0.50)\\
&= 0.24995\\
&> 0,
\end{aligned}$$

so the state would *appear* to be infeasible. For $K = 2$, if $\tilde{g}_1(t) = 0.9999$, then $\tilde{g}_2(t)$ would have to satisfy $\tilde{g}_2(t) \leq \frac{2^{-2}}{0.9999}$ in order for the state to appear feasible. Since $\tilde{g}_1(t)$ is bounded above by 1, the worst case feasibility bound for $\tilde{g}_2(t)$ at the boundary of the path obstacle is $\tilde{g}_2(t) \leq 2^{-2}$. Similarly, for any $K \geq 2$, the worst case feasibility bound for a sigmoid indicator approximation $\tilde{g}_k$ at the boundary of the path obstacle is given by

$$\tilde{g}_k(t) \leq 2^{-K}. \tag{2.53}$$

From (2.44),

$$\tilde{g}_k(t) \leq 2^{-K} \iff 1 + e^{-\mathsf{s}g_k(t)} \geq 2^K, \tag{2.54a}$$

or, equivalently,

$$\tilde{g}_k(t) \leq 2^{-K} \iff g_k(t) \leq \frac{1}{\mathsf{s}} \ln\left(2^K - 1\right). \tag{2.54b}$$

Therefore, the sigmoid approximation of the ATM cylindrical obstacle constraint with $K = 2$ is equivalent to the conditional constraint:

$$\left\|\mathbf{x}_i(t) - \mathbf{x}_j(t)\right\|_L \geq r_{i,j}(t) + \frac{1}{\mathsf{s}} \ln(3) \tag{2.55a}$$

or

$$\left\|\mathbf{x}_i(t) - \mathbf{x}_j(t)\right\|_V \geq h_{i,j}(t) + \frac{1}{\mathsf{s}} \ln(3). \tag{2.55b}$$

The parameter s controls the accuracy of the approximation, similar to the effect of γ in Section 2.3.1.4, without the need for additional multiplier variables or iterative updates to the parameter.

2.3.2 Penalty Functions.

The penalty function approach to obstacle avoidance problems is to define an additional cost function based on the system state's proximity to an obstacle. Thus, the minimum cost path should avoid states that approach too close to the path obstacles. However, since the penalty function associated with an obstacle replaces path constraints for the obstacle [54], it may be possible to generate a path that intersects an obstacle, but is still considered feasible by the penalty function formulation of the optimization problem. Therefore, it is important to formulate the obstacle-based penalty function so that the minimum cost path is very likely to avoid intersecting an obstacle. Some common penalty function methods that can be applied to obstacle avoidance problems follow.

2.3.2.1 Barrier Functions.

One method of decreasing the likelihood of generating an obstacle-intersecting path is to use a *barrier function* to define the obstacle's penalty. For example, a logarithmic barrier function is defined such that the cost of intersecting an obstacle approaches infinity:

$$f_b(t) \triangleq -\mu \ln\left(g(\mathbf{x}(t))\right), \tag{2.56}$$

where f_b is the barrier function, $\mu > 0$ is a scaling parameter (or "barrier parameter" [84]) that controls the relative importance of avoiding the obstacle, and $g(\cdot) \geq 0$ is defined such that $g(\mathbf{x}(t)) = 0$ if and only if the state at time t, $\mathbf{x}(t)$, intersects the obstacle. However, if $\ln\left(g(\mathbf{x}(t))\right) > 0$, the $f_b(t) < 0$, so the barrier and similar penalty function methods may generate paths that stay as far away from obstacles as possible, to maximize $\ln\left(g(\mathbf{x}(t))\right)$. While such paths are likely to be feasible for the original obstacle avoidance problem, they may result in increases in the original measure of

performance. That is, if the minimum cost path in the original obstacle avoidance problem (*without* penalty functions) requires the state to approach very close to an obstacle, penalty function methods may not generate that solution, since the penalty function could reduce the apparent cost of a path by requiring the state to remain very far from an obstacle. This deviation from the optimal path of the non-penalty problem can be mitigated by choosing the barrier parameter μ to be very small.

2.3.2.2 Artificial Potential Fields.

An alternative to using barrier penalty functions is to define an Artificial Potential Field (APF) for each obstacle. An APF is defined to act analogously to a repulsive force emanating outward from an obstacle so the trajectory of the state is unlikely to approach the obstacle [54]. As with barrier functions, the APF may cause the trajectory to avoid obstacles by more than is actually necessary, resulting in sub-optimal paths. In [70], Ren, McIsaac and Huang employ sigmoid-type functions so that the simulated repulsive force only significantly affects trajectories that are relatively close to an obstacle, and has negligible effect elsewhere. In [6], Barnes, Fields and Valvanis also use a sigmoid "limiting function" to control where an artificial potential field can significantly affect the cost of a candidate trajectory. Additionally, since each obstacle requires its own APF, problems with multiple obstacles may cause the multiple APFs to interact problematically. In [45], Kim and Khosla introduce *harmonic* APFs that are designed to minimize or eliminate problematic interactions.

2.3.3 Voronoi Diagrams.

Another approach to obstacle avoidance is to generate a Voronoi diagram to partition the entire traversable space (*i.e.*, the feasible space if there were no obstacles) into regions defined by each obstacle [64]. Each region of the diagram is defined as the points in the space that are closer to the obstacle contained in the region than to any other obstacle. The boundary of each region is either the boundary of the traversable space or the set of points equidistant from two or more obstacles. Typically, Voronoi diagrams are generated by first transforming the traversable space so that all obstacles can be represented as single points in the transformed space [64]. The region boundaries can then be produced from the perpendicular bisectors of every combination of pairs of point obstacles. If no obstacle-to-point transformation is used, then the obstacle boundaries determine the Voronoi diagram. Figure 2.2 shows an example Voronoi diagram for a rectangular

traversable space with three circular obstacles. The solid boundary lines define the regions based on the obstacle center points. Note that a Voronoi diagram based on obstacles boundaries may not be identical to the diagram based on point obstacles, since points that are equidistant from obstacle centers are not necessarily equidistant from obstacle boundaries.

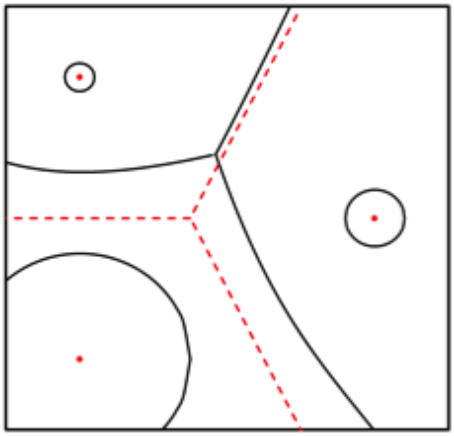

Figure 2.2: Obstacle center-based and Obstacle boundary-based Voronoi Diagrams

For cases where the originations and destinations of a vehicle are located on the boundary of a two-dimensional traversable space, the Voronoi diagram can be used to define the graph for a shortest path problem; the origination and destination, as well as points where the boundaries of the traversable space intersect, can be considered graph vertices, and segments connecting these points can be considered graph arcs if they do not intersect any obstacles. Thus, any path from the origination vertex to the destination vertex in a graph generated in this manner will avoid all obstacles.

In [13] and [12], Bhattacharya and Gavrilova present an efficient optimal path planning algorithm based on the Voronoi diagram generated from "simple disjoint polygonal obstacles" with applications to aircraft terrain following or avoidance. The resulting Voronoi diagram is then considered a roadmap for the vehicle, and any shortest path algorithm can then be applied to find the shortest obstacle avoiding path. If the sharp corners of the Voronoi diagram path are impractical for the vehicle, an approximation of the Voronoi diagram path may be generated [42, 57]. If the

Voronoi diagram method is extended to a three-dimensional traversable airspace or the obstacles are time-dependent (in effect, moving), the region boundaries could become surfaces oriented in three dimensions. Since these boundary surfaces admit a continuum of paths, each boundary would need to be discretized into a countable number of paths in order to generate a shortest path graph from the boundaries.

2.4 Optimization Methods

The preceding sections outlined various objective function and constraint formulations associated with ATM. This section details the optimization approaches that may be used to obtain an optimal solution given some combination of the objective function and constraint formulations describe in Section 2.2 and Section 2.3.1.

2.4.1 Optimal Control Problem Discretization.

Continuous-time optimal control problems as described in Section 2.2.3 fall under the study of *functional optimization*, and can be analyzed using indirect methods based on optimality conditions derived from variational calculus [31, 46]. However, since these indirect methods may have no analytical solution, and the problems involve differential equations that may require numerical approximation methods to evaluate, many continuous-time optimization problems are instead evaluated using direct numerical methods based on discretization and large-scale *static* optimization [46]. That is, the continuous-time optimal control problem is typically given by

$$\text{minimize} \quad \phi(\mathbf{x}(t_f)) + \int_{t_0}^{t_f} L(\mathbf{x}(t), \mathbf{u}(t), t)dt, \tag{2.57a}$$

$$\text{subject to} \qquad \dot{\mathbf{x}}(t) = \mathbf{f}\left(\mathbf{x}(t), \mathbf{u}(t), t\right), \tag{2.57b}$$

where $\mathbf{x}(t)$ is the vector of the values of n state variables at time t, $\mathbf{u}(t)$ is the vector of the values of m control variables at time t, t_0 is a fixed or variable initial time, ϕ is the function that represents a cost incurred at the fixed or variable final time, t_f, L is a function that represents the *running cost* incurred at each instant, t, and $\mathbf{f}$ is the function that represents the dynamics that relate changes in

the control $\mathbf{u}$ to changes in the state $\mathbf{x}$ [46]. Then, the discretized approximation would be given by

$$\text{minimize} \quad \hat{\phi}(\hat{\mathbf{x}}_N, t_f) + \sum_{i=0}^{N-1} \hat{L}_i(\hat{\mathbf{x}}_i, \hat{\mathbf{u}}_i, i), \tag{2.58a}$$

$$\text{subject to} \quad \hat{\mathbf{x}}_{i+1} = \hat{\mathbf{f}}_i\left(\hat{\mathbf{x}}_i, \hat{\mathbf{u}}_i, i\right), , \quad i = 1, \ldots, N-1 \tag{2.58b}$$

which is a static optimization problem with decision variable $[\hat{\mathbf{x}}_0, \ldots, \hat{\mathbf{x}}_N, \hat{\mathbf{u}}_0, \ldots, \hat{\mathbf{u}}_N]$, for fixed or chosen t_0 and t_f, where $\hat{\mathbf{x}}_i \in \mathbb{R}^n$ and $\hat{\mathbf{u}}_i \in \mathbb{R}^m$ [46].

A simple method for discretizing the optimal control problem is to divide the interval $[t_0, t_f]$ into N sub-intervals of equal length $\Delta t = \frac{t_f - t_0}{N}$, and to define the state and control within each interval as a vector that is constant over the sub-interval. That is, for the simple discrete approximation [46],

$$\mathbf{x}(t) \approx \hat{\mathbf{x}}_i, \quad t_i < t \leq t_{i+1} \tag{2.59a}$$

$$\mathbf{u}(t) \approx \hat{\mathbf{u}}_i, \quad t_i < t \leq t_{i+1}, \tag{2.59b}$$

$$\hat{\mathbf{f}}_i\left(\hat{\mathbf{x}}_i, \hat{\mathbf{u}}_i, i\right) \triangleq \hat{\mathbf{x}}_i + \mathbf{f}\left(\hat{\mathbf{x}}_i, \hat{\mathbf{u}}_i\right) \Delta t, \tag{2.59c}$$

$$\hat{L}_i(\hat{\mathbf{x}}_i, \hat{\mathbf{u}}_i, i) \triangleq L(\hat{\mathbf{x}}_i, \hat{\mathbf{u}}_i)\Delta t, \tag{2.59d}$$

$$\hat{\phi}(\hat{\mathbf{x}}_N) \triangleq \phi(\hat{\mathbf{x}}, t_f). \tag{2.59e}$$

In [65], Patterson and Rao describe a "Radau collocation method" for discretizing the optimal control problem. This method introduces a new variable $\tau \in [-1, 1]$ and defines the time parameter, t, as a function of τ, such that

$$t = \frac{t_f - t_0}{2}\tau + \frac{t_f - t_0}{2}. \tag{2.60}$$

The interval $[-1, 1]$ for τ is then partitioned into a "mesh" of K sub-intervals $[T_{k-1}, T_k]$, $k = 1, \ldots, K$, such that [30]

$$-1 = T_0 < T_1 < T_2 < \cdots < T_k = 1. \tag{2.61}$$

While the simple discretization method approximates the state as a constant over an interval, the Radau collocation method approximates the state in each mesh sub-interval $[T_{k-1}, T_k]$ with a

polynomial of degree N_k, such that

$$\mathbf{x}_k(\tau) \approx \sum_{j=1}^{N_k+1} \hat{\mathbf{x}}_{k,j} \mathcal{L}_{k,j}(\tau), \tag{2.62}$$

where $\mathbf{x}_k(\tau)$ is the state at time τ in mesh k, $\hat{\mathbf{x}}_{k,j}$ is the approximation of the state in mesh k at time $\tau_{k,j}$, where $\{\tau_{k,1}, \ldots, \tau_{k,j}, \ldots, \tau_{k,N_k}\}$ are the *Legendre-Gauss-Radau (LGR)* [30] collocation points in mesh k while $\tau_{k,N_k+1} = T_k$, and $\mathcal{L}_{k,j}(\tau)$ is a basis of *Lagrange polynomials* such that

$$\mathcal{L}_{k,j}(\tau) = \prod_{\substack{l=1 \\ l \neq j}}^{N_k+1} \frac{\tau - \tau_{k,l}}{\tau_{k,j} - \tau_{k,l}}. \tag{2.63}$$

An approximation of the control, $\hat{\mathbf{u}}_{k,j}$, is then generated for each of the $\hat{\mathbf{x}}_{k,j}$ state approximations. Given these state and control approximations, the dynamics and objective functions are then approximated using LGR differentiation and integration matrices and LGR quadrature weights for each mesh interval [30].

2.4.2 Optimal Control Problem Phases.

Regarding optimal control formulations for the ATM problem, once an aircraft reaches its destination (or leaves the airspace under control), it should no longer affect the objective function or the trajectories of the remaining aircraft [76]. Such time-dependent changes in the dynamics or constraints imposed on an optimal control problem are typically addressed by defining a *phase* for each interval of the problem that has dynamics or constraints that are different from another interval of the problem [65]. The P phases of the problem are linked through a set of constraints that define how the final conditions of one phase are related to the initial conditions of another. For example, in an ATM optimal control problem, the first phase may end the instant the first aircraft reaches its destination, and the second phase begins at that same instant, with constraints dictating that the speed and position of each remaining aircraft at the initiation of the second phase must equal the speed and position of the aircraft at the final instant of the first phase. Then, the final objective function value is optimized as the sum of the objective function values from each phase. The "branch-and-bound"-based ATM heuristic proposed by Soler, *et al*, in [80] and the Radau collocation-based GPOPS-II Matlab package detailed in [65] both implement the phase sub-problem method for optimal control problems.

In [22], Dmitruk and Kaganovich propose an alternative method of modeling time-dependent changes in the optimal control problem dynamics or constraints without *explicit* phase definitions. Instead, new time, state and control variables are defined for each possible change in dynamics or constraints. The problem is then defined as a function of a "joint" time variable, with dynamic equations defined to relate the change in the joint time to the change in each phase-implied time dependent variable. Thus, instead of optimizing P phase-defined sub-problems, with n_p state and m_p control variables defined for each sub-problem $p \in \{1, \ldots, P\}$, the Dmitruk and Kaganovich method optimizes a single optimal control problem with $\sum_{p=1}^{P} n_p$ state and $\sum_{p=1}^{P} m_p$ control variables. In [74], Sadovsky, *et al*., formulate the ATM nominal arrival problem using the method proposed by Dmitruk and Kaganovich.

2.4.3 Sequential Quadratic Programming.

Sequential Quadratic Programming (SQP) algorithms, as described in [8] by Bazarra, Sherali and Shetty, apply Newton's method or the Newton-Raphson method to directly solve the Karush-Kuhn-Tucker (KKT) conditions derived from the Lagrangian form of the objective function and constraints. Since Newton's method requires second-order derivatives for the functions involved, the second-order term is often replaced with a quasi-Newton positive definite approximation (for minimization). Additionally, since SQP algorithm convergence to optimality depends on the proximity of the initial solution to the optimal solution, a merit or penalty function may be introduced so that the SQP algorithm iterations approach a KKT solution in the limit.

In [74], Sadovsky, *et al*., use an SQP algorithm to generate optimal speed advisories for the sample roadmap coordination space problems presented therein. Patterson and Rao [65] also employ an SQP algorithm to generate solutions to optimal control problems that have been discretized using the Radau collocation method in the GPOPS-II optimal control software. This research used the GPOPS-II software to generate SQP-approximated optimal solutions.

2.4.4 Sequential Convex Programming.

In [81], Sriver describes several Sequential Convex Programming (SCP) algorithms that approximate the objective function at a point with a convex function of the original variables, their reciprocals and an approximation of the gradient of the objective function evaluated at the point.

The resulting approximation is separable; that is, it is a linear combination of functions that each depend on only one of the original variables.

At each iteration of an SCP algorithm, the gradient of the Lagrangian function of the convex approximation is itself approximated with respect to the primal variables and set to zero. This system of equations is used to define each primal variable in terms of the dual (or *Lagrange*) variables, and the dual of the convex approximation is constructed and optimized with respect to the dual variables only. The primal-dual variable equations are then used to equate the optimal dual solution to an optimal primal solution for the current iteration. As with SQP, a penalty function may be added to the algorithm to improve its iterative convergence to optimality.

In [81], Sriver employs SCP methods to solve large-scale structural optimization problems that involve thousands of design variables. These methods could prove to be useful in discretized optimal control problems, since the discretization process can result in thousands of time-increment control variables.

2.4.5 Interior Point Methods.

Interior point method (or *barrier method* [84]) algorithms introduce a *barrier term* to the objective function being minimized. A logarithmic form for the barrier term is often used. For example, given an optimization problem with objective function $f(\mathbf{x})$, inequality constraints $g_i(\mathbf{x}) \leq 0$, for $i = 1, \ldots, K$, and set of equality constraints $\mathbf{h}(\mathbf{x}) = \mathbf{0}$, the interior-point optimization problem would appear as [84]

$$\text{minimize} \quad f(\mathbf{x}) - \mu \sum_{i=1}^{K} \ln\Big(-g_i(\mathbf{x})\Big), \tag{2.64a}$$

$$\text{subject to} \quad \mathbf{h}(\mathbf{x}) = \mathbf{0}, \tag{2.64b}$$

where $\mu > 0$ is the "barrier parameter" [84]. Since $\ln\Big(-g_i(\mathbf{x})\Big) \to -\infty$ as $-g_i(\mathbf{x}) \to 0$, the optimal solution to (2.64) will satisfy $g_i(\mathbf{x}) > 0$, for $i = 1, \ldots, K$, and the solution to (2.64) is a point in the interior the feasible region.

Given a formulation of the form (2.64), interior-point optimization algorithms iteratively decrease the value of the barrier term, μ, and apply Newton-type methods to directly solve a sequence of KKT conditions derived from the barrier form of the objective function and constraints.

Primal-dual interior-point algorithms introduce a set of dual variables that involve the iteratively decreasing barrier parameter, μ, and the reciprocal of the primal variables, and apply Newton-type methods to solve a sequence of "perturbed" KKT conditions derived from the barrier form of the objective function and the dual variables [84].

Patterson and Rao [65] employ an interior-point algorithm called *IPOPT* to generate solutions to optimal control problems that have been discretized using the Radau collocation method in GPOPS-II. As detailed in Section 3.1.4.2, this research uses the GPOPS-II software to generate interior-point approximated optimal solutions.

2.5 Path Coordination and Resolution

Path coordination refers to generating trajectories for all vehicles in the problem setting such that each vehicle's path does not conflict with the path of another vehicle, where conflict definition may vary based on the problem setting. *Path resolution* refers to problem settings in which the trajectories of some vehicles may be controlled but others may not be, and trajectories for the vehicles under control must be generated such that their paths do not conflict with each other's paths or with the paths of vehicles that are not under control. This section describes various approaches to these types of problems.

2.5.1 Roadmap Coordination.

In [14], Bien and Lee provide examples of the conflict-free state space (or *coordination space*) for the motion of two robotic manipulators under direct control and show how changes in the motion of each manipulator affect the state space representation of when they are in conflict. These examples were based on the path-position parameterization technique developed in [77]. In [33], Ghrist, O'Kane and LaValle propose a similar coordination space approach to the path coordination problem for multiple vehicles. This *roadmap* coordination method requires that each vehicle have a predefined set of allowable paths, called a roadmap, from its origination to its destination. The roadmap coordination space is then defined as the product space of all roadmaps, excluding positions that satisfy the problem's pair-wise conflict definition.

In [74] and [75], Sadovsky, *et al.*, apply this roadmap coordination method to the Fully Routed Nominal Arrival Problem, in which each aircraft in the problem setting has a predefined

origination, destination, scheduled (or *nominal*) time of arrival, and path from its origination to its destination. To apply the roadmap coordination method, the airspace is represented as a graph, with arcs corresponding to aircraft route segments, assumed to be linear, and vertices corresponding to airspace waypoints or the intersection of route segments. This graph could be based on actual policy mandated flight corridors, or generated using the Voronoi diagram method discussed in Section 2.3.3, or some other technique. Pair-wise conflict regions for two aircraft are then defined for route segments that share a common vertex in the graph using the following steps from [74] and [75] for each pair-wise interaction of two aircraft, $aircraft_1$ and $aircraft_2$:

1. Define unit vectors in the direction of the route segments of each aircraft by

$$\mathbf{a}_1 \triangleq \frac{\mathbf{v}_1 - \mathbf{v}_c}{\|\mathbf{v}_1 - \mathbf{v}_c\|} \tag{2.65a}$$

and

$$\mathbf{a}_2 \triangleq \frac{\mathbf{v}_2 - \mathbf{v}_c}{\|\mathbf{v}_2 - \mathbf{v}_c\|}, \tag{2.65b}$$

where $\mathbf{a}_1$ is the unit vector given as the direction from the common vertex, $\mathbf{v}_c$, to the other segment endpoint $\mathbf{v}_1$ for $aircraft_1$ of the the pair and $\mathbf{a}_2$ is the unit vector given as the direction from the common vertex, $\mathbf{v}_c$, to the other segment endpoint $\mathbf{v}_2$ for $aircraft_2$ of the pair.

2. Translate the space so that the common vertex, $\mathbf{v}_c$, becomes the coordinate origin, and the position of each aircraft along its route segment becomes a scalar multiple of its unit direction vector.

3. Parameterize the position of each aircraft with the state scalars c_1 for $aircraft_1$ and c_2 for $aircraft_2$ such that the state space $\mathcal{X}^{1,2}$ for the pair can be defined as

$$\mathcal{X}^{1,2} \triangleq \left\{ (c_1, c_2) \;\middle|\; \begin{array}{ll} 0 \le c_1 \le l_1, & \text{(2.66a)} \\ 0 \le c_2 \le l_2 & \text{(2.66b)} \end{array} \right\}$$

where $l_1 \triangleq \|\mathbf{v}_1 - \mathbf{v}_c\|$ is the route segment length for $aircraft_1$ and $l_2 \triangleq \|\mathbf{v}_2 - \mathbf{v}_c\|$ is the route segment length for $aircraft_2$.

4. Define the state space conflict region $C^{1,2}$ for an airspace with minimum allowable separation requirement r as

$$C^{1,2} \triangleq \{ (c_1, c_2) \in \mathcal{X}^{1,2} \;\middle|\; \|c_1\mathbf{a}_1 - c_2\mathbf{a}_2\|^2 < r^2 \}, \tag{2.67a}$$

or equivalently as

$$C^{1,2} \triangleq \{ (c_1, c_2) \in \mathcal{X}^{1,2} \;\middle|\; (c_1)^2 + (c_2)^2 - 2c_1c_2\langle \mathbf{a}_1, \mathbf{a}_2 \rangle < r^2 \}, \tag{2.67b}$$

where r is the minimum allowable separation requirement and $\langle \mathbf{a}_1, \mathbf{a}_2 \rangle$ is the inner-product of the direction vectors $\mathbf{a}_1$ and $\mathbf{a}_2$.

From [75], this process can be extended to define the conflict region, C^A, and the set of feasible states (or *coordination space*), $\Omega^A_{\mathcal{X}}$, for the set of A aircraft, denoted $\{\alpha_1, \alpha_2, \ldots, \alpha_A\}$ with the corresponding set of unit direction vectors $\{\mathbf{a}_1, \mathbf{a}_2, \ldots, \mathbf{a}_A\}$, that share a common vertex:

1. Define the state space $\mathcal{X}^A$ as

$$\mathcal{X}^A \triangleq \left\{ (c_1, c_2, \ldots, c_A) \;\middle|\; \begin{array}{ll} 0 < c_1 \leq l_1, & (2.68a) \\ 0 < c_2 \leq l_2, & (2.68b) \\ \quad \vdots & \\ 0 < c_A \leq l_A & (2.68c) \end{array} \right\}$$

where $l_i \triangleq \|\mathbf{v}_i - \mathbf{v}_c\|$ is the route segment length for aircraft α_i for $i = 1, 2, \ldots, A$.

2. Define the conflict region C^A for the route segments with a common vertex in an airspace with minimum allowable separation requirement r as the union of all pair-wise conflict regions:

$$C^A \triangleq \bigcup_{(i,j) \in A \times A, i \neq j} \{ (c_1, c_2, \ldots, c_A) \in \mathcal{X}^A \;\middle|\; (c_i)^2 + (c_j)^2 - 2c_ic_j\langle \mathbf{a}_i, \mathbf{a}_j \rangle < r^2 \}, \tag{2.69}$$

3. Define the coordination space $\Omega^A_{\mathcal{X}}$ as the complement of C^A in $\mathcal{X}^A$:

$$\Omega^A_{\mathcal{X}} \triangleq \mathcal{X}^A \setminus C^A = \{ (c_1, c_2, \ldots, c_A) \in \mathcal{X}^A \;\middle|\; (c_1, c_2, \ldots, c_A) \notin C^A \}, \tag{2.70}$$

where the back-slash symbol, \ , represents the set-theoretic difference or relative-complement operator [36]. Thus, the coordination space $\Omega^A_{\mathcal{X}}$ is defined equivalently as the intersection of all regions that do not contain a pair-wise conflict:

$$\Omega^A_{\mathcal{X}} \triangleq \bigcap_{(i,j)\in A\times A, i\neq j} \{(c_1, c_2, \ldots, c_A) \in \mathcal{X}^A \;\Big|\; (c_i)^2 + (c_j)^2 - 2c_i c_j \langle \mathbf{a}_i, \mathbf{a}_j \rangle \geq r^2\}, \tag{2.71}$$

This state space feasible region definition can then be used to find the optimal trajectory of each aircraft along its route segment, subject to its own physical, policy, procedural or operational restrictions. Sadovsky, *et al*., use this framework to derive optimal aircraft trajectories based on SQP, described in Section 2.4.3, under the simplifying assumptions [75]:

- Vehicles change direction instantaneously at each waypoint
- Vehicle state is controlled directly by vehicle velocity only; acceleration is not modeled
- All vehicle pairs have the same, symmetric minimum separation requirement, r

Nonetheless, this roadmap coordination method was then generalized in [73] and [76] to nominal arrival time problems without pre-defined paths. To accomplish this, a Hybrid Control System (HCS) is defined by enumerating all possible paths in a given graph from each aircraft's initial position to its final position along the route segment network. Each enumerated combination consisting of A paths defines a discrete *mode*, and each mode thus defines a Fully Routed Nominal Arrival problem that can be analyzed using the roadmap coordination space approach. Thus, choosing the best solution from all modes gives the overall optimal solution.

2.5.2 Non-cooperative Path Resolution.

Non-cooperative path resolution problems model cases in which some of the vehicles in the setting are not under control and must be considered independent obstacles. In [5], Bach, Chu and Erzberger present methods for generating temporary path deviations for the aircraft under control in order to avoid the paths of uncontrolled aircraft. Similarly in [16], Bowe and Lauderdale demonstrate path resolution techniques based on minimizing fuel consumption. Tomlin, Pappas and Sastry develop a game-theoretic approach to non-cooperative conflict resolution in [83]. This approach defines the game theoretic optimal reaction to the worst possible action of the other

aircraft as each aircraft's resolution maneuver. However, these methods are designed for one-on-one conflicts, as opposed to the multiple independent conflicts that could arise in terminal airspace ATM problems. Kosecka, Tomlin, Pappas and Sastry present a method to resolve path conflicts for multiple moving agents in [48], but the method is only applicable to a few specific conflict scenarios (*e.g.*, head-on conflicts of aircraft at constant altitude).

2.6 Stochastic Components

This section outlines research related to incorporating stochastic weather, aircraft maneuver and control (*i.e.*, mechanical) lag and random human effects (such as control implementation error) into ATM frameworks.

2.6.1 Wind and Weather.

The stochastic effects of wind and weather on aircraft trajectory may invalidate some of the roadmap-type approaches to ATM, since weather avoidance may force an aircraft to deviate from a predefined route, and wind may affect the aircraft's ability to execute optimal speed advisories precisely [53]. Additionally, in [25], Erzberger, Paielli, Isaacson and Eshow state that "the effects of wind modeling and prediction errors accumulate with time", leading to greater uncertainty in the true position of an aircraft. In [51] and [49], Lauderdale further simulates how such wind prediction uncertainty can affect trajectory planning algorithms, and suggests in [50] that a normal probability distibution-based ellipse can be used to model the likely position of an aircraft in the presence of wind and speed uncertainty.

In [43] Karmgarpour suggests a "receding horizon trajectory" generation method to iteratively optimize weather avoidance paths based on incremental weather forecast updates. In this procedure, weather features are approximated as ellipsoid obstacles for the current planning and execution horizons, and the shortest obstacle avoidance path for each aircraft is determined. Then, the most recent weather forecast is used to update the weather approximating obstacles, and the process is repeated. While this method treats weather forecasts as deterministic obstacles, in [53] Lee, Weygandt, Schwartz and Murphy study how wind and weather uncertainty can cause uncertainty in aircraft trajectories. Since trajectory uncertainty is positively correlated with wind and weather forecast uncertainty, the study indicates the common procedure of adding a standard buffer to the

minimal separation requirement to account for trajectory uncertainty should be replaced with a method of adding a dynamic buffer based on the uncertainty of the wind and weather forecast.

2.6.2 Execution Delay.

According to Cone [18], *execution delay* refers to the "delay between when a conflict resolution maneuver is sent to an aircraft ... and when the aircraft actually begins flying this maneuver". Thus, execution delay is a random process that comprises both human and mechanical effects. Unfortunately, many automated conflict detection and resolution algorithms are designed and tested without taking execution delay into consideration, and McNally and Gong [59] and McNally and Thipphavong [60] showed that the performance of these algorithms is highly dependent on the level of uncertainty present.

In [18], Cone indicates that adding a buffer to minimal separation requirements to account for execution delay leads to path inefficiencies that cause aircraft to fly longer routes than necessary and generates schedule inefficiencies that cause unnecessary arrival or departure delays. Instead, the study [18] simulates a process of generating conflict resolution maneuvers and evaluates the effects of starting the maneuvers with varying time errors. It shows that starting maneuvers late is more detrimental than starting maneuvers early, but that starting maneuvers early still results in failures to resolve minimal separation conflicts and the generation of new conflicts. Nonetheless, [18] suggests, but does not present, generating resolution maneuvers that are robust to a range of both positive and negative execution time errors.

In [47], Knorr and Walter state that "(u)ncertainty can be captured with 3-dimensional ellipsoids, covering all aircraft positions at a specific instant of time ahead," and they suggest that separation conflicts are less likely to occur as the volume of an uncertainty ellipsoid decreases as a result of more accurate estimates of aircraft positions, and in [61], Meckiff estimates this aircraft position uncertainty ellipsoid using the normal distribution to model the uncertainty in each of the three dimensions. Thus, the position uncertainty ellipsoid radii in each of the three directions (latitudinal, longitudinal and vertical) is equated to the distance of three standard deviations of the normal distribution associated with that direction's uncertainty. In [37] and [38], Hu, Prandini and

Sastry apply *Brownian Motion* theory to justify modeling the aircraft position uncertainty with such an ellipsoid.

2.7 Summary

The background information and optimization techniques outlined in this chapter represent the variety of methods that have been applied to ATM optimization problems. While many of these techniques have been developed to address individual ATM components, no robust model has been constructed to address simultaneously many of the limitations of current roadmap-based ATM optimization methods. Chapter 3 presents the methods developed in this research that extend and modify current roadmap-based ATM models to account for aircraft inertia, position uncertainty and realistic safe separation requirements.

III. Research Methodology

The Hybrid Control System (HCS) for Air Traffic Management (ATM) proposed by Sadovsky, *et al*., lists the following suggested extensions [76]:

1. Optimize feasible control strategies using alternative measures of performance (*e.g.* fuel consumption, safety, or deviation from schedule).
2. Include inertia into the HCS by using aircraft accelerations as control variables with corresponding minimum and maximum values
3. Investigate the effects of asymmetric and anisotropic pair-wise separation requirements.
4. Incorporate stochastic components to account for the effects of wind, transportation performance, or human factors.

This chapter describes the approaches used to address these extensions and modifications to the current HCS framework. Section 3.1 provides the multi-objective formulation of the HCS ATM problem. Section 3.1.2 details methods for estimating the anisotropic pair-wise conflict regions for all aircraft in the problem. Section 3.3 provides a formulation of the multi-objective HCS ATM problem that incorporates acceleration controls, and Section 3.4 outlines a method for incorporating uncertainty into the HCS framework. Section 3.5 incorporates asymmetric lateral separation features into the stochastic multi-objective HCS ATM problem with kinodynamic constraints.

3.1 Objective Function Extension

Real-world conditions and Federal Aviation Administration (FAA) policies may imply a preference or ordering among competing objectives associated with ATM. For example, commercial airlines may wish to minimize their measures of fuel consumption and deviation from scheduled arrival times, while the priority of Air Traffic Control (ATC) may be to guide aircraft out of the terminal airspace as quickly and safely as possible. The focus of this research is not to determine the specific priorities that should be assigned to each measure, rather, the focus is to demonstrate the ability of the roadmap-based optimization framework to incorporate these priorities

to generate feasible control strategies. Therefore, this section details a *notional* weighted-sum objective function that is formulated to incorporate the relative priorities that *could* be assigned to a measure of fuel consumption, a measure of schedule deviation and a measure of total time (*i.e.*, the *makespan*.

3.1.1 Mutli-Objective Formulation.

The multi-objective HCS problem is formulated as the weighted-sum of the notional fuel consumption measure, the deviation from scheduled arrival time measure and the makespan measure. Thus, the weighted-sum objective may be given as

$$\hat{F} \triangleq \lambda_1 F_1 + \lambda_2 F_2 + \lambda_3 F_3 \tag{3.1}$$

where $\lambda_1 \geq 0$ is the scalar that represents the relative importance of the notional fuel consumption measure, F_1, $\lambda_2 \geq 0$ is the scalar that represents the relative importance of the schedule deviation measure, F_2, and $\lambda_3 \geq 0$ is the scalar that represents the relative importance of the total time measure, F_3. For the weighted-sum objective, it is common to require that $\lambda_1 + \lambda_2 + \lambda_3 = 1$, and to *normalize* the competing objectives so that $0 \leq F_k \leq 1$ for each $k \in \{1, 2, 3\}$ [23]. However, parameter screening test results, provided in Appendix A, indicated that the linear combination of normalized objectives were not suitable for representing the priorities assigned to the schedule deviation or makespan measures. For example, when λ_1 and λ_3 were set to zero while λ_2 was set to 1, indicating that only the schedule deviation should be minimized, the solution did not result in zero schedule deviation. However, several non-linear weighting schemes resulted in much smaller measures of schedule deviation than the standard linear weighting scheme. Therefore, in order to model non-linear priority weightings, this research generalized the weighted-sum objective formulation. The generalized weighted-sum objective is

$$F \triangleq \left(\lambda_1{}^{\beta_1}\right) F_1{}^{\left(\lambda_1{}^{1-\beta_1}\right)} + \left(\lambda_2{}^{\beta_2}\right) F_2{}^{\left(\lambda_2{}^{1-\beta_2}\right)} + \left(\lambda_3{}^{\beta_3}\right) F_3{}^{\left(\lambda_3{}^{1-\beta_3}\right)} \tag{3.2}$$

where each $\beta_k \in \{0, 1\}$ is a binary term for $k \in \{1, 2, 3\}$ that determines how each measure is weighted. That is, if $\beta_k = 1$, then F_k is weighted on a linear scale, but if $\beta_k = 0$, then F_k is weighted exponentially. Note that the weights are not required to sum to unity for the generalized weighted-

sum objective (3.2); as such, exponent values of λ_k much greater than 1 would cause values of F_k less than 1 to become insignificant in the optimization problem.

Additionally, since this research is intended to extend and generalize the framework from [73], the "move as slowly as possible" objective from [73] was selected as the notional measure representing fuel consumption. Thus, the fuel consumption objective, F_1, is

$$F_1(\mu, \mathbf{u}, \mathbf{t}_0, \mathbf{t}_f, t) = \sum_{\alpha=1}^{A} \left[\int_{t_{[0,\alpha]}}^{t_{[f,\alpha]}} \left[u_{[\mu,\alpha]}(t) \right]^2 dt \right], \tag{3.3}$$

where μ is the selected control mode which designates the pre-defined set of paths for each aircraft $\alpha \in \{1, 2, \ldots, A\}$, $\mathbf{u} = [u_{[\mu,1]}, u_{[\mu,2]}, \ldots, u_{[\mu,A]}]$ is a feasible vector of control strategies, $\mathbf{t}_0 = [t_{[0,1]}, t_{[0,2]}, \ldots, t_{[0,A]}]$ is the vector of initial times for each aircraft, and $\mathbf{t}_f = [t_{[f,1]}, t_{[f,2]}, \ldots, t_{[f,A]}]$ is the vector set of final (or actual arrival) times for each aircraft. However, if the control strategies are required to satisfy $u_{[\mu,\alpha]_{\min}} \leq u_{[\mu,\alpha]}(t) \leq u_{[\mu,\alpha]_{\max}}$ for each $\alpha \in \{1, 2, \ldots, A\}$, then the normalized fuel consumption objective, $\hat{F}_1$, could be given as

$$\hat{F}_1(\mu, \mathbf{u}, \mathbf{t}_0, \mathbf{t}_f, t) = \left(\sum_{\alpha=1}^{A} \left[t_{[f,\alpha]_{\max}} - t_{[0,\alpha]} \right] \right)^{-1} \sum_{\alpha=1}^{A} \left[\int_{t_{[0,\alpha]}}^{t_{[f,\alpha]}} \frac{\left[u_{[\mu,\alpha]}(t) - u_{[\mu,\alpha]_{\min}} \right]^2}{u_{[\mu,\alpha]_{\max}} - u_{[\mu,\alpha]_{\min}}} dt \right], \tag{3.4}$$

where $t_{[f,\alpha]_{\max}}$ is the latest allowable arrival time for aircraft α, such that $[t_{[f,\alpha]} \leq t_{[f,\alpha]_{\max}}$ for each $\alpha \in \{1, 2, \ldots, A\}$. Therefore, the normalized $\hat{F}_1$ given in equation (3.4) was used in the initial parameter screening tests, while the original F_1 given in equation (3.3) was used in subsequent demonstration tests.

F_2 is the measure of deviation from scheduled arrival time given by

$$F_2(\mu, \kappa_2, \mathbf{t}_f, \mathbf{t}_S) = \kappa_2 + \sum_{\alpha=1}^{A} \left[t_{[f,\alpha]} - t_{[S,\alpha]} \right]^2, \tag{3.5}$$

where $\mathbf{t}_S = [t_{[S,1]}, t_{[S,2]}, \ldots, t_{[S,A]}]$ is the vector of scheduled arrival times for each aircraft and $\kappa_2 \geq 1$ is a scalar term added to ensure ${F_2}^{\lambda_2} \geq 1$. The normalized measure of deviation from scheduled arrival time, $\hat{F}_2$, is given by

$$\hat{F}_2(\mu, \mathbf{t}_f, \mathbf{t}_S) = \left(\sum_{\alpha=1}^{A} \left[\max \left\{ \left[t_{[S,\alpha]} - t_{[f,\alpha]_{\min}} \right]^2, \left[t_{[S,\alpha]} - t_{[f,\alpha]_{\max}} \right]^2 \right\} \right] \right)^{-1} \sum_{\alpha=1}^{A} \left[t_{[f,\alpha]} - t_{[S,\alpha]} \right]^2, \tag{3.6}$$

where $t_{[f,\alpha]_{\min}}$ is the earliest allowable arrival time for aircraft α, such that $t_{[f,\alpha]} \geq t_{[f,\alpha]_{\min}}$ for each $\alpha \in \{1, 2, \ldots, A\}$. The normalized $\hat{F}_2$ given in equation (3.6) was used in the initial parameter screening tests, while the original F_2 given in equation (3.5) was used in subsequent demonstration tests.

F_3 is the measure of total time (or makespan) given by

$$F_3(\mu, \kappa_3, \mathbf{t}_f, \mathbf{t}_{f_{\min}}) = \kappa_3 + \sum_{\alpha=1}^{A} \left[t_{[f,\alpha]} - t_{[f,\alpha]_{\min}} \right]^2, \tag{3.7}$$

where $\mathbf{t}_{f_{\min}} = [t_{[f,1]_{\min}}, t_{[f,2]_{\min}}, \ldots, t_{[f,A]_{\min}}]$ is the vector of earliest allowable arrival times for each aircraft, and $\kappa_3 \geq 1$ is a scalar term added to ensure ${F_3}^{\lambda_3} \geq 1$. The normalized measure of total time, $\hat{F}_3$, is given by

$$\hat{F}_3(\mu, \mathbf{t}_f, \mathbf{t}_{f_{\min}}) = \left(\sum_{\alpha=1}^{A} \left[t_{[f,\alpha]_{\max}} - t_{[f,\alpha]_{\min}} \right]^2 \right)^{-1} \sum_{\alpha=1}^{A} \left[t_{[f,\alpha]} - t_{[f,\alpha]_{\min}} \right]^2. \tag{3.8}$$

The normalized $\hat{F}_3$ given in equation (3.8) was used in the initial parameter screening tests, while the original F_3 given in equation (3.7) was used in subsequent demonstration tests.

For each objective, a control strategy $u_{[\mu,\alpha]}$ is feasible if and only if it satisfies the problem's dynamic equations, boundary conditions, and its intermediate state, control and ATM separation constraints. Using roadmap coordination space notation, the dynamic equations of the HCS problem without inertia are

$$\frac{d}{dt} c_{[\mu,\alpha]}(t) = u_{[\mu,\alpha]}(t), \quad \forall \alpha \in \{1, 2, \ldots, A\}, \tag{3.9}$$

where $c_{[\mu,\alpha]}(t)$ is the path-length parameterized position at time t of aircraft α along its route defined by control mode μ. Thus, $u_{[\mu,\alpha]}(t)$ directly controls the instantaneous change in position of aircraft α along its route.

In order to define the boundary conditions and intermediate constraints for the HCS ATM problem, it is necessary to define more precisely how the control mode μ relates to the three-dimensional airspace position $(x_\alpha(t), y_\alpha(t), z_\alpha(t))$ of aircraft α to its roadmap state $c_{[\mu,\alpha]}(t)$. In control mode μ, each aircraft $\alpha \in \{1, 2, \ldots, A\}$ is assigned a set of n_α way-points in the three-dimensional airspace that must be visited in order. The set of way-points is given as

$$WP_{[\mu,\alpha]} = \{(x_{[1,\alpha]}, y_{[1,\alpha]}, z_{[1,\alpha]}), (x_{[2,\alpha]}, y_{[2,\alpha]}, z_{[2,\alpha]}), \ldots, (x_{[n_\alpha,\alpha]}, y_{[n_\alpha,\alpha]}, z_{[n_\alpha,\alpha]})\}, \tag{3.10}$$

so the route of aircraft α is partitioned into a set of $(n_\alpha - 1)$ route segments (or *arcs*) defined by the airspace way-points. Thus, the total path-length for the route of aircraft α in control mode μ, denoted $l_{[\mu,\alpha]}$, is given by

$$l_{[\mu,\alpha]} = \sum_{i=0}^{n_\alpha - 1} \left\| \mathbf{a}_{[i,\alpha]} \right\|, \tag{3.11a}$$

where

$$\mathbf{a}_{[i,\alpha]} \triangleq \begin{cases} [0,0,0] & \text{if } i = 0, \\ [x_{[i+1,\alpha]}, y_{[i+1,\alpha]}, z_{[i+1,\alpha]}] - [x_{[i,\alpha]}, y_{[i,\alpha]}, z_{[i,\alpha]}] & \text{if } i \geq 1, \end{cases} \tag{3.11b}$$

is a vector representation of the route segment that connects way-point i to way-point $(i + 1)$. Thus, the roadmap state $c_{[\mu,\alpha]}(t) \in [0, l_{[\mu,\alpha]}]$ in control mode μ is related to the three-dimensional airspace position of aircraft α by the relationship

$$\begin{bmatrix} x_\alpha(t) \\ y_\alpha(t) \\ z_\alpha(t) \end{bmatrix} = \begin{bmatrix} x_{[1,\alpha]} \\ y_{[1,\alpha]} \\ z_{[1,\alpha]} \end{bmatrix} + \hat{c}_{[\mu,\alpha]}(t) \mathbf{a}_{[\hat{n}_\alpha,\alpha]} + \sum_{i=0}^{\hat{n}_\alpha - 1} \mathbf{a}_{[i,\alpha]}, \tag{3.12a}$$

where

$$\sum_{i=0}^{\hat{n}_\alpha - 1} \left\| \mathbf{a}_{[i,\alpha]} \right\| \leq c_{[\mu,\alpha]}(t) \leq \sum_{i=0}^{\hat{n}_\alpha} \left\| \mathbf{a}_{[i,\alpha]} \right\| \tag{3.12b}$$

and

$$\hat{c}_{[\mu,\alpha]}(t) = \frac{c_{[\mu,\alpha]}(t) - \sum_{i=0}^{\hat{n}_\alpha - 1} \| \mathbf{a}_{[i,\alpha]} \|}{\| \mathbf{a}_{[\hat{n}_\alpha,\alpha]} \|}. \tag{3.12c}$$

Alternatively, the three-dimensional airspace position of aircraft α at time t in control mode μ can be determined using Algorithm 3.1.

Algorithm 3.1 Calculate airspace position given roadmap state $c_{[\mu,\alpha]}(t)$

$\mathbf{a}_\alpha = [0, 0, 0]$

$l_\alpha = 0$

$\hat{n}_\alpha = 1$

while $l_\alpha + \|\mathbf{a}_{[\hat{n}_\alpha,\alpha]}\| \leq c_{[\mu,\alpha]}(t)$ **do**

$\mathbf{a}_\alpha = \mathbf{a}_\alpha + \mathbf{a}_{[\hat{n}_\alpha,\alpha]}$

$l_\alpha = l_\alpha + \|\mathbf{a}_{[\hat{n}_\alpha,\alpha]}\|$

$\hat{n}_\alpha = \hat{n}_\alpha + 1$

end while

$\hat{c}_{[\mu,\alpha]}(t) = \dfrac{c_{[\mu,\alpha]}(t) - l_\alpha}{\|\mathbf{a}_{[\hat{n}_\alpha,\alpha]}\|}$

$\mathbf{a}_\alpha = \mathbf{a}_\alpha + \hat{c}_{[\mu,\alpha]}(t)(\mathbf{a}_{[\hat{n}_\alpha,\alpha]})$

$[x_\alpha(t), y_\alpha(t), z_\alpha(t)] = [x_{[1,\alpha]}, y_{[1,\alpha]}, z_{[1,\alpha]}] + \mathbf{a}_\alpha$

Given equations (3.10) - (3.12), the boundary conditions of the HCS ATM problem are given by

$$t_{[0,\alpha]} = 0, \quad \forall \alpha \in \{1, 2, \ldots, A\}, \tag{3.13a}$$

$$c_{[\mu,\alpha]}\left(t_{[0,\alpha]}\right) = c_{[\min,\alpha]}, \quad \forall \alpha \in \{1, 2, \ldots, A\}, \tag{3.13b}$$

$$c_{[\mu,\alpha]}\left(t_{[f,\alpha]}\right) = l_{[\mu,\alpha]}, \quad \forall \alpha \in \{1, 2, \ldots, A\}, \tag{3.13c}$$

where $l_{[\mu,\alpha]}$ is the path length of the route defined by control mode μ for aircraft α. That is, all aircraft are assumed to enter the problem at the same initial time, $t = 0$, at some distance $c_{[\min,\alpha]}$ along their path, and they are required to travel the remaining distance, $l_{[\mu,\alpha]} - c_{[\min,\alpha]}$, of their path defined by the control mode μ.

Given equations (3.10) - (3.12), the intermediate state and control constraints for all aircraft $\alpha \in \{1, 2, \ldots, A\}$ are given by

$$c_{[\min,\alpha]} \leq c_{[\mu,\alpha]}(t) \leq l_{[\mu,\alpha]}, \tag{3.14a}$$

$$u_{[\min,\alpha]} \leq u_{[\mu,\alpha]}(t) \leq u_{[\max,\alpha]}, \tag{3.14b}$$

for all intermediate time $0 \leq t \leq t_{[f,\alpha]}$, where $u_{[\min,\alpha]} > 0$ is the minimum allowable speed control value for aircraft α and $u_{[\max,\alpha]}$ is the maximum allowable speed control value for aircraft α.

Given equations (3.10) - (3.12) and Algorithm 3.1, for each pair of aircraft (α_1, α_2) such that $\alpha_1 \in \{1, 2, \ldots, A\}$, $\alpha_1 \in \{1, 2, \ldots, A\}$ and $\alpha_1 \neq \alpha_2$, the intermediate ATM separation constraint function is given by

$$G^{\text{ATM}}_{[\alpha_1,\alpha_2]}(t) \triangleq 1 - \max\left\{\frac{\left(x_{\alpha_1}(t) - x_{\alpha_2}(t)\right)^2 + \left(y_{\alpha_1}(t) - y_{\alpha_2}(t)\right)^2}{r(t)^2}, \frac{\left(z_{\alpha_1}(t) - z_{\alpha_2}(t)\right)^2}{h^2}\right\}, \quad (3.15a)$$

or equivalently,

$$G^{\text{ATM}}_{[\alpha_1,\alpha_2]}(t) \triangleq \min\left\{r(t)^2 - \left(x_{\alpha_1}(t) - x_{\alpha_2}(t)\right)^2 - \left(y_{\alpha_1}(t) - y_{\alpha_2}(t)\right)^2, h^2 - \left(z_{\alpha_1}(t) - z_{\alpha_2}(t)\right)^2\right\}, \quad (3.15b)$$

where $r(t)$ is the minimum allowable lateral separation at time t, as described in Section 3.5, h is the minimum allowable vertical separation, and all other values are as defined in equations (3.10) - (3.12) and Algorithm 3.1. The ATM separation constraint is thus,

$$G^{\text{ATM}}_{[\alpha_1,\alpha_2]}(t) \leq 0 \quad (3.16)$$

for all intermediate time $0 \leq t \leq \min\left\{t_{[f,\alpha_1]}, t_{[f,\alpha_2]}\right\}$. Therefore, the pair-wise ATM separation constraint is only defined until aircraft α_1 or aircraft α_2 reaches its destination.

3.1.2 Differentiable ATM Separation Constraint Approximation.

As described in Section 2.3.1, the ATM separation constraints given by equation (3.15) are not differentiable, so they must be approximated in order to evaluate the ATM optimization problem using gradient-based numerical methods. This section details four methods for approximating the multi-objective HCS optimization problem's ATM separation constraints.

3.1.2.1 Multiplier Method ATM Separation Constraint Approximation.

From Section 2.3.1.4, the differentiable Multiplier Method approximation of the ATM separation constraints given in equation (3.15a) should appear as

$$g_1(t) - \tilde{G}(g_1(t) - g_2(t), \lambda, \gamma) \leq 0, \quad (3.17a)$$

where

$$g_1(t) = r(t)^2 - \Big(\big(x_{\alpha_1}(t) - x_{\alpha_2}(t)\big)^2 + \big(y_{\alpha_1}(t) - y_{\alpha_2}(t)\big)^2\Big), \tag{3.17b}$$

$$g_2(t) = h^2 - \big(z_{\alpha_1}(t) - z_{\alpha_2}(t)\big)^2, \tag{3.17c}$$

and

$$\tilde{G}(g_1(t) - g_2(t), \lambda, \gamma) = \begin{cases} g_1(t) - g_2(t) - \frac{(1-\lambda)^2}{2\gamma} & \text{if } \frac{1-\lambda}{\gamma} \le g_1(t) - g_2(t), \\ \begin{pmatrix} \lambda\big(g_1(t) - g_2(t)\big) \\ +\frac{1}{2}\gamma\big(g_1(t) - g_2(t)\big)^2 \end{pmatrix} & \text{if } -\frac{\lambda}{\gamma} \le g_1(t) - g_2(t) \le \frac{1-\lambda}{\gamma}, \\ -\frac{\lambda^2}{\gamma} & \text{if } g_1(t) - g_2(t) \le -\frac{\lambda}{\gamma}, \end{cases} \tag{3.17d}$$

with $0 \le \lambda \le 1$ and $\gamma > 0$.

Note that if $x_{\alpha_1}(t) = x_{\alpha_2}(t)$ and $y_{\alpha_1}(t) = y_{\alpha_2}(t)$, then $g_1(t) = r^2 > 0$. Thus, in order to satisfy the ATM separation constraint, it must be that $g_2(t) \le 0$. Therefore, $g_1(t) - g_2(t) \ge r^2$. From equation (3.17a), if $\gamma > \frac{1}{r^2}$, then $\frac{1-\lambda}{\gamma} \le g_1(t) - g_2(t)$, so the Multiplier Method constraint approximation becomes

$$r(t)^2 - \tilde{G}(r(t)^2 - g_2(t), \lambda, \gamma) \le 0 \tag{3.18a}$$

$$\implies \quad r(t)^2 - \Big(r(t)^2 - g_2(t) - \frac{(1-\lambda)^2}{2\gamma}\Big) \le 0 \tag{3.18b}$$

$$\implies \quad g_2(t) + \frac{(1-\lambda)^2}{2\gamma} \le 0 \tag{3.18c}$$

$$\implies \quad g_2(t) \le -\frac{(1-\lambda)^2}{2\gamma}. \tag{3.18d}$$

That is, if the lateral separation is zero, then the Multiplier Method ATM separation approximation requires the square of the vertical separation to be at least $\frac{(1-\lambda)^2}{2\gamma}$ greater than the square of the minimum allowable vertical separation. Since the actual ATM separation requirement is that if the lateral separation is zero, then the square of the vertical separation must be at least equal to the square of the minimum allowable vertical separation, the maximum error of the Multiplier Method ATM separation approximation in the vertical direction, denoted $\varepsilon_V(\lambda, \gamma)$ is bounded by the relationship

$$0 \le \varepsilon_V(\lambda, \gamma) \le \frac{(1-\lambda)^2}{2\gamma}. \tag{3.19}$$

Similarly, if $z_{\alpha_1}(t) = z_{\alpha_2}(t)$, then $g_2(t) = h^2 > 0$. Thus, in order to satisfy the ATM separation constraint, it must be that $g_1(t) \leq 0$. Therefore, $g_1(t) - g_2(t) \leq -\left(h^2\right)$. From equation (3.17a), if $\gamma > \frac{1}{h^2}$, then $g_1(t) - g_2(t) \leq -\frac{\lambda}{\gamma}$, so the Multiplier Method constraint approximation becomes

$$g_1(t) - \tilde{G}(g_1(t) - h^2, \lambda, \gamma) \leq 0 \tag{3.20a}$$

$$\implies \quad g_1(t) - \left(-\frac{\lambda^2}{\gamma}\right) \leq 0 \tag{3.20b}$$

$$\implies \quad g_1(t) + \frac{\lambda^2}{\gamma} \leq 0 \tag{3.20c}$$

$$\implies \quad g_1(t) \leq -\frac{\lambda^2}{\gamma}. \tag{3.20d}$$

That is, if the vertical separation is zero, then the Multiplier Method ATM separation approximation requires the square of the lateral separation to be at least $\frac{\lambda^2}{\gamma}$ greater than the square of the minimum allowable lateral separation. Since the actual ATM separation requirement is that if the vertical separation is zero, then the square of the lateral separation must be at least equal to the square of the minimum allowable lateral separation, the maximum error of the Multiplier Method ATM separation approximation in the lateral plane, denoted $\varepsilon_L(\lambda, \gamma)$ is bounded by the relationship

$$0 \leq \varepsilon_V(\lambda, \gamma) \leq \frac{\lambda^2}{\gamma}. \tag{3.21}$$

It is interesting to note that the maximum error of a constraint in the Multiplier Method is dependent on its order of appearance in the approximation. For example, if the Multiplier Method ATM separation approximation had been constructed as

$$g_2(t) - \tilde{G}(g_2(t) - g_1(t), \lambda, \gamma) \leq 0, \tag{3.22}$$

then the maximum error in the vertical direction would have been $\frac{\lambda^2}{\gamma}$, instead of $\frac{(1-\lambda)^2}{2\gamma}$, and the maximum error in the lateral plane would have been $\frac{(1-\lambda)^2}{2\gamma}$, instead of $\frac{\lambda^2}{\gamma}$. However, the two maximum error values are equal if $\frac{(1-\lambda)^2}{2\gamma} = \frac{\lambda^2}{\gamma}$, which is satisfied when $\lambda = \left(\sqrt{2} - 1\right)$. Nonetheless, increasing the parameter $\gamma > 0$ should result in more accurate approximations of the ATM separation constraint. However, as $\gamma \to \infty$, the Multiplier Method approximation becomes computationally unstable when evaluated with numerical differentiation methods. Section 3.1.2.5 describes the tests constructed to determine appropriate values of γ and λ for use with the multi-objective HCS optimization problem.

3.1.2.2 Sigmoid ATM Separation Constraint Approximation.

From Section 2.3.1.7, the differentiable sigmoid approximation of the ATM separation constraints given in equation (3.15b) appear as

$$-\left(2^{-2}\right)+\left(\frac{1}{1+e^{-\mathsf{s}g_1(t)}}\right)\left(\frac{1}{1+e^{-\mathsf{s}g_2(t)}}\right)\leq 0, \tag{3.23}$$

where

$$g_1(t)=r(t)^2-\left(\left(x_{\alpha_1}(t)-x_{\alpha_2}(t)\right)^2+\left(y_{\alpha_1}(t)-y_{\alpha_2}(t)\right)^2\right) \tag{3.24a}$$

and

$$g_2(t)=h^2-\left(z_{\alpha_1}(t)-z_{\alpha_2}(t)\right)^2. \tag{3.24b}$$

Note that if $x_{\alpha_1}(t)=x_{\alpha_2}(t)$ and $y_{\alpha_1}(t)=y_{\alpha_2}(t)$, then $g_1(t)=r(t)^2$ and the sigmoid constraint approximation becomes

$$-\left(2^{-2}\right)+\left(\frac{1}{1+e^{-\mathsf{s}r(t)^2}}\right)\left(\frac{1}{1+e^{-\mathsf{s}g_2(t)}}\right)\leq 0, \tag{3.25a}$$

or equivalently,

$$\left(\frac{1}{1+e^{-\mathsf{s}r(t)^2}}\right)\leq\frac{1}{4}\left(1+e^{-\mathsf{s}g_2(t)}\right) \tag{3.25b}$$

$$\implies \quad 4\left(\frac{1}{1+e^{-\mathsf{s}r(t)^2}}\right)\leq 1+e^{-\mathsf{s}g_2(t)} \tag{3.25c}$$

$$\implies \quad 4\left(\frac{1}{1+e^{-\mathsf{s}r(t)^2}}\right)-1\leq e^{-\mathsf{s}g_2(t)} \tag{3.25d}$$

$$\implies \quad \ln\left[4\left(\frac{1}{1+e^{-\mathsf{s}r(t)^2}}\right)-1\right]\leq -\mathsf{s}g_2(t) \tag{3.25e}$$

$$\implies \quad g_2(t)\leq -\frac{1}{\mathsf{s}}\ln\left[4\left(\frac{1}{1+e^{-\mathsf{s}r(t)^2}}\right)-1\right]. \tag{3.25f}$$

That is, if the lateral separation is zero, then the sigmoid ATM separation approximation requires the square of the vertical separation to be at least $\frac{1}{\mathsf{s}}\ln\left[4\left(\frac{1}{1+e^{-\mathsf{s}r(t)^2}}\right)-1\right]$ greater than the square of the minimum allowable vertical separation. Since the actual ATM separation requirement is that if the lateral separation is zero, then the square of the vertical separation must be at least equal to the square of the minimum allowable vertical separation, $\frac{1}{\mathsf{s}}\ln\left[4\left(\frac{1}{1+e^{-\mathsf{s}r(t)^2}}\right)-1\right]$ is the maximum error of the sigmoid ATM separation approximation in the vertical direction.

Note that $\frac{1}{1+e^{-\mathsf{s}r(t)^2}} \to 1$ as $\mathsf{s} \to \infty$, so the maximum error of the sigmoid ATM separation approximation in the vertical direction, denoted $\varepsilon_V(\mathsf{s})$, is bounded by the relationship

$$0 \leq \varepsilon_V(\mathsf{s}) \leq \frac{1}{\mathsf{s}} \ln[3]. \tag{3.26}$$

Similarly, if $z_{\alpha_1}(t) = z_{\alpha_2}(t)$, then $g_2(t) = h^2$ and the sigmoid constraint approximation becomes

$$-\left(2^{-2}\right) + \left(\frac{1}{1+e^{-\mathsf{s}g_1(t)}}\right)\left(\frac{1}{1+e^{-\mathsf{s}h^2}}\right) \leq 0, \tag{3.27a}$$

or equivalently,

$$\left(\frac{1}{1+e^{-\mathsf{s}h^2}}\right) \leq \frac{1}{4}\left(1+e^{-\mathsf{s}g_1(t)}\right) \tag{3.27b}$$

$$\implies \quad 4\left(\frac{1}{1+e^{-\mathsf{s}h^2}}\right) \leq 1+e^{-\mathsf{s}g_1(t)} \tag{3.27c}$$

$$\implies \quad 4\left(\frac{1}{1+e^{-\mathsf{s}h^2}}\right) - 1 \leq e^{-\mathsf{s}g_1(t)} \tag{3.27d}$$

$$\implies \quad \ln\left[4\left(\frac{1}{1+e^{-\mathsf{s}h^2}}\right) - 1\right] \leq -\mathsf{s}g_1(t) \tag{3.27e}$$

$$\implies \quad g_1(t) \leq -\frac{1}{\mathsf{s}} \ln\left[4\left(\frac{1}{1+e^{-\mathsf{s}h^2}}\right) - 1\right]. \tag{3.27f}$$

That is, if the vertical separation is zero, then the sigmoid ATM separation approximation requires the square of the lateral separation to be at least $\frac{1}{\mathsf{s}} \ln\left[4\left(\frac{1}{1+e^{-\mathsf{s}h^2}}\right) - 1\right]$ greater than the square of the minimum allowable lateral separation. Since the actual ATM separation requirement is that if the vertical separation is zero, then the square of the lateral separation must be at least equal to the square of the minimum allowable lateral separation, $\frac{1}{\mathsf{s}} \ln\left[4\left(\frac{1}{1+e^{-\mathsf{s}h^2}}\right) - 1\right]$ is the maximum error of the sigmoid ATM separation approximation in the lateral plane.

Note that $\frac{1}{1+e^{-\mathsf{s}h^2}} \to 1$ as $\mathsf{s} \to \infty$, so the maximum error of the sigmoid ATM separation approximation in the lateral plane, denoted $\varepsilon_L(\mathsf{s})$, is bounded by the relationship

$$0 \leq \varepsilon_L(\mathsf{s}) \leq \frac{1}{\mathsf{s}} \ln[3]. \tag{3.28}$$

Equations (3.26) and (3.28) indicate that increasing the parameter $\mathsf{s} > 0$ should result in more accurate approximations of the ATM separation constraint. However, as $\mathsf{s} \to \infty$, the sigmoid

approximation becomes computationally unstable when evaluated with numerical differentiation methods. Section 3.1.2.5 presents tests constructed to determine appropriate values of `s` for use with the multi-objective HCS optimization problem.

3.1.2.3 p-Norm ATM Separation Constraint Approximation.

From Section 2.3.1.6 equation (2.41), the differentiable p-norm approximation of the ATM separation constraints given in equation (3.15a) are

$$2 - \left[\left(\frac{\left(x_{\alpha_1}(t) - x_{\alpha_2}(t)\right)^2 + \left(y_{\alpha_1}(t) - y_{\alpha_2}(t)\right)^2}{r(t)^2}\right)^p + \left(\frac{\left(z_{\alpha_1}(t) - z_{\alpha_2}(t)\right)^2}{h^2}\right)^p\right] \leq 0. \tag{3.29}$$

Note that if $x_{\alpha_1}(t) = x_{\alpha_2}(t)$ and $y_{\alpha_1}(t) = y_{\alpha_2}(t)$, then the p-norm constraint approximation becomes

$$2 - \left(\frac{\left(z_{\alpha_1}(t) - z_{\alpha_2}(t)\right)^2}{h^2}\right)^p \leq 0, \tag{3.30a}$$

or equivalently,

$$2 \leq \left(\frac{\left(z_{\alpha_1}(t) - z_{\alpha_2}(t)\right)^2}{h^2}\right)^p \tag{3.30b}$$

$$\implies \quad 2^{1/p} \leq \frac{\left(z_{\alpha_1}(t) - z_{\alpha_2}(t)\right)^2}{h^2} \tag{3.30c}$$

$$\implies \quad 2^{1/p}\left(h^2\right) \leq \left(z_{\alpha_1}(t) - z_{\alpha_2}(t)\right)^2. \tag{3.30d}$$

That is, if the lateral separation is zero, then the p-norm ATM separation approximation requires the square of the vertical separation to be at least a factor of $2^{1/p}$ times greater than the square of the minimum allowable vertical separation. Since the actual ATM separation requirement is that if the lateral separation is zero, then the square of the vertical separation must be at least equal to the square of the minimum allowable vertical separation, the maximum error of the p-norm ATM separation approximation in the vertical direction, denoted $\varepsilon_V(p)$ is bounded by the relationship

$$0 \leq \varepsilon_V(p) \leq \left(h^2\right)\left(2^{1/p} - 1\right). \tag{3.31}$$

Similarly, if $z_{\alpha_1}(t) = z_{\alpha_2}(t)$ then the p-norm constraint approximation becomes

$$2 - \left(\frac{\left(x_{\alpha_1}(t) - x_{\alpha_2}(t)\right)^2 + \left(y_{\alpha_1}(t) - y_{\alpha_2}(t)\right)^2}{r(t)^2}\right)^p \leq 0, \tag{3.32a}$$

or equivalently,

$$2 \leq \left(\frac{\left(x_{\alpha_1}(t) - x_{\alpha_2}(t)\right)^2 + \left(y_{\alpha_1}(t) - y_{\alpha_2}(t)\right)^2}{r(t)^2} \right)^p \tag{3.32b}$$

$$\implies \quad 2^{1/p} \leq \frac{\left(x_{\alpha_1}(t) - x_{\alpha_2}(t)\right)^2 + \left(y_{\alpha_1}(t) - y_{\alpha_2}(t)\right)^2}{r(t)^2} \tag{3.32c}$$

$$\implies \quad 2^{1/p}\left(r(t)^2\right) \leq \left(x_{\alpha_1}(t) - x_{\alpha_2}(t)\right)^2 + \left(y_{\alpha_1}(t) - y_{\alpha_2}(t)\right)^2. \tag{3.32d}$$

That is, if the vertical separation is zero, then the p-norm ATM separation approximation requires the square of the lateral separation to be at least $2^{1/p}$ *times* greater than the square of the minimum allowable lateral separation. Since the actual ATM separation requirement is that if the vertical separation is zero, then the square of the lateral separation must be at least equal to the square of the minimum allowable lateral separation, the maximum error of the p-norm ATM separation approximation in the lateral plan, denoted $\varepsilon_L(p)$ is bounded by the relationship

$$0 \leq \varepsilon_L(p) \leq \left(r(t)^2\right)\left(2^{1/p} - 1\right). \tag{3.33}$$

Increasing the parameter $p > 0$ should result in more accurate approximations of the ATM separation constraint. But once again, as $p \to \infty$, the p-norm approximation becomes computationally unstable when evaluated with numerical differentiation methods. Section 3.1.2.5 describes the tests constructed to determine appropriate values of p for use with the multi-objective HCS optimization problem.

3.1.2.4 Exponential p-Norm ATM Separation Constraint Approximation.

Given the non-differentiable constraint

$$\min\{g_1(t), g_2(t), \ldots, g_K(t)\} \leq 0, \tag{3.34}$$

the exponential p-norm constraint approximation given in Section 2.3.1.6 by equation (2.42) was shown to underestimate the true infeasible region. That is, when $g_k(t) = \frac{1}{p}\ln(K)$, for $k = 1, \ldots, K$, then $\min\{g_1(t), g_2(t), \ldots, g_K(t)\} > 0$ so the constraint is violated, but the exponential p-norm constraint approximation is *not* violated. Therefore, a corrected form of the exponential p-norm constraint approximation is needed to ensure the approximate feasible region does not over-estimate the true feasible region.

Suppose the corrected exponential p-norm constraint function is defined as

$$G_p(g_1, g_2, \ldots, g_K) \triangleq -\ln\left[\left(\sum_{k=1}^{K} (e^{-g_k})^p\right)^{1/p}\right] + \frac{1}{p}\ln[K], \tag{3.35}$$

and the corrected exponential p-norm constraint approximation is defined as

$$G_p(g_1, g_2, \ldots, g_K) \leq 0. \tag{3.36}$$

If $g_k(t) > 0$, for all $k = 1, \ldots, K$, then the original constraint (3.34) is violated. Furthermore,

$$e^{-g_k} < e^0 = 1 \tag{3.37a}$$

$$\implies \left(e^{-g_k}\right)^p < \left(1\right)^p = 1 \tag{3.37b}$$

$$\implies \sum_{k=1}^{K}\left(e^{-g_k}\right)^p < \sum_{k=1}^{K} 1 = K \tag{3.37c}$$

$$\implies \left(\sum_{k=1}^{K}\left(e^{-g_k}\right)^p\right)^{1/p} < (K)^{1/p} \tag{3.37d}$$

$$\implies \ln\left[\left(\sum_{k=1}^{K}\left(e^{-g_k}\right)^p\right)^{1/p}\right] < \ln\left[K^{1/p}\right] = \frac{1}{p}\ln[K] \tag{3.37e}$$

$$\implies -\ln\left[\left(\sum_{k=1}^{K}\left(e^{-g_k}\right)^p\right)^{1/p}\right] > -\frac{1}{p}\ln[K] \tag{3.37f}$$

$$\implies -\ln\left[\left(\sum_{k=1}^{K}\left(e^{-g_k}\right)^p\right)^{1/p}\right] + \frac{1}{p}\ln[K] > 0. \tag{3.37g}$$

Therefore, if the original constraint (3.34) is violated, then the corrected exponential p-norm constraint approximation (3.36) is also violated.

If there is some $\hat{k} \in \{1, 2, \ldots, K\}$ such that $-\frac{1}{p}\ln[K] < g_{\hat{k}}(t) \leq 0$, while $g_k(t) > 0$ for all $k \in \{1, \ldots, K\}$ such that $k \neq \hat{k}$, then the original constraint (3.34) is satisfied, since

$\min\{g_1(t), g_2(t), \ldots, g_K(t)\} \leq g_{\hat{k}}(t) \leq 0$. However,

$$e^{-g_{\hat{k}}} < e^{\frac{1}{p}\ln[K]} \tag{3.38a}$$

$$e^{-g_k} < e^0 = 1, \quad \text{if } k \neq \hat{k} \tag{3.38b}$$

$$\implies \sum_{k=1}^{K}\left(e^{-g_k}\right)^p < \left(e^{\frac{1}{p}\ln[K]}\right)^p + \sum_{k\neq\hat{k}}^{K} 1 \tag{3.38c}$$

$$= e^{\ln[K]} + K - 1 \tag{3.38d}$$

$$= K + K - 1 \tag{3.38e}$$

$$= 2K - 1 \tag{3.38f}$$

$$< 2K \tag{3.38g}$$

$$\implies \left(\sum_{k=1}^{K}\left(e^{-g_k}\right)^p\right)^{1/p} < (2K)^{1/p} \tag{3.38h}$$

$$\implies \ln\left[\left(\sum_{k=1}^{K}\left(e^{-g_k}\right)^p\right)^{1/p}\right] < \ln\left[(2K)^{1/p}\right] \tag{3.38i}$$

$$= \frac{1}{p}\ln[K] + \frac{1}{p}\ln[2] \tag{3.38j}$$

$$\implies -\ln\left[\left(\sum_{k=1}^{K}\left(e^{-g_k}\right)^p\right)^{1/p}\right] > -\frac{1}{p}\ln[K] - \frac{1}{p}\ln[2] \tag{3.38k}$$

$$\implies -\ln\left[\left(\sum_{k=1}^{K}\left(e^{-g_k}\right)^p\right)^{1/p}\right] + \frac{1}{p}\ln[K] > -\frac{1}{p}\ln[2]. \tag{3.38l}$$

Therefore, if there is some $\hat{k} \in \{1, 2, \ldots, K\}$ such that $-\frac{1}{p}\ln[K] < g_{\hat{k}}(t) \leq 0$, while $g_k(t) > 0$ for all $k \in \{1, \ldots, K\}$ such that $k \neq \hat{k}$, then the original constraint (3.34) is satisfied, but the corrected exponential p-norm constraint approximation (3.36) is *not necessarily* satisfied.

If there is some $\hat{k} \in \{1, 2, \ldots, K\}$ such that $g_{\hat{k}}(t) \leq -\frac{1}{p} \ln [K]$, then the original constraint (3.34) is satisfied, since $\min \{g_1(t), g_2(t), \ldots, g_K(t)\} \leq g_{\hat{k}}(t) \leq 0$. Furthermore,

$$e^{-g_{\hat{k}}} \geq e^{\frac{1}{p} \ln [K]} \tag{3.39a}$$

$$\implies \left(e^{-g_{\hat{k}}}\right)^p \geq \left(e^{\frac{1}{p} \ln [K]}\right)^p \tag{3.39b}$$

$$= e^{\ln [K]} \tag{3.39c}$$

$$\implies \sum_{k=1}^{K} \left(e^{-g_k}\right)^p \geq e^{\ln [K]} \tag{3.39d}$$

$$\implies \left(\sum_{k=1}^{K} \left(e^{-g_{\hat{k}}}\right)^p\right)^{1/p} \geq \left(e^{\ln [K]}\right)^{1/p} \tag{3.39e}$$

$$= e^{\frac{1}{p} \ln [K]} \tag{3.39f}$$

$$\implies \ln \left[\left(\sum_{k=1}^{K} \left(e^{-g_{\hat{k}}}\right)^p\right)^{1/p}\right] \geq \ln \left[e^{\frac{1}{p} \ln [K]}\right] \tag{3.39g}$$

$$= \frac{1}{p} \ln [K] \tag{3.39h}$$

$$\implies -\ln \left[\left(\sum_{k=1}^{K} \left(e^{-g_k}\right)^p\right)^{1/p}\right] \leq -\frac{1}{p} \ln [K] \tag{3.39i}$$

$$\implies -\ln \left[\left(\sum_{k=1}^{K} \left(e^{-g_k}\right)^p\right)^{1/p}\right] + \frac{1}{p} \ln [K] \leq 0. \tag{3.39j}$$

Therefore, if there is any $\hat{k} \in \{1, 2, \ldots, K\}$ such that $g_{\hat{k}}(t) \leq -\frac{1}{p} \ln [K]$, then the corrected exponential p-norm constraint approximation is satisfied. Thus, $\frac{1}{p} \ln [K]$ is the maximum error of the corrected exponential p-norm constraint approximation.

Setting $K = 2$, the corrected exponential p-norm approximation of the ATM separation constraints given in equation (3.15a) should appear as

$$-\ln \left[\left(\left(e^{-g_1(t)}\right)^p + \left(e^{-g_2(t)}\right)^p\right)^{1/p}\right] + \frac{1}{p} \ln [2] \leq 0, \tag{3.40a}$$

where

$$g_1(t) = r^2 - \left(\left(x_{\alpha_1}(t) - x_{\alpha_2}(t)\right)^2 + \left(y_{\alpha_1}(t) - y_{\alpha_2}(t)\right)^2\right), \tag{3.40b}$$

$$g_2(t) = h^2 - \left(z_{\alpha_1}(t) - z_{\alpha_2}(t)\right)^2. \tag{3.40c}$$

Note that if $x_{\alpha_1}(t) = x_{\alpha_2}(t)$ and $y_{\alpha_1}(t) = y_{\alpha_2}(t)$, then the corrected exponential p-norm constraint approximation becomes

$$-\ln\left[\left(\left(e^{-\left(r(t)^2\right)}\right)^p + \left(e^{-g_2(t)}\right)^p\right)^{1/p}\right] + \frac{1}{p}\ln[2] \leq 0, \tag{3.41a}$$

or equivalently,

$$\ln\left[2^{1/p}\right] \leq \ln\left[\left(\left(e^{-\left(r(t)^2\right)}\right)^p + \left(e^{-g_2(t)}\right)^p\right)^{1/p}\right] \tag{3.41b}$$

$$\implies \quad 2^{1/p} \leq \left(\left(e^{-\left(r(t)^2\right)}\right)^p + \left(e^{-g_2(t)}\right)^p\right)^{1/p} \tag{3.41c}$$

$$\implies \quad 2 \leq \left(e^{-\left(r(t)^2\right)}\right)^p + \left(e^{-g_2(t)}\right)^p \tag{3.41d}$$

$$\implies \quad 2 - \left(e^{-\left(r(t)^2\right)}\right)^p \leq \left(e^{-g_2(t)}\right)^p \tag{3.41e}$$

$$\implies \quad \ln\left[2 - \left(e^{-\left(r(t)^2\right)}\right)^p\right] \leq -p\left(g_2(t)\right) \tag{3.41f}$$

$$\implies \quad -\frac{1}{p}\ln\left[2 - \left(e^{-\left(r(t)^2\right)}\right)^p\right] \geq g_2(t) \tag{3.41g}$$

That is, if the lateral separation is zero, then the exponential p-norm ATM separation approximation requires the square of the vertical separation to be at least $\frac{1}{p}\ln\left[2 - \left(e^{-\left(r(t)^2\right)}\right)^p\right]$ greater than the square of the minimum allowable vertical separation. Since the actual ATM separation requirement is that if the lateral separation is zero, then the square of the vertical separation must be at least equal to the square of the minimum allowable vertical separation, the maximum error of the exponential p-norm ATM separation approximation in the vertical direction, denoted $\varepsilon_{Ve}(p)$, is bounded by the relationship

$$0 \leq \varepsilon_{Ve}(p) \leq \frac{1}{p}\ln\left[2 - \left(e^{-\left(r(t)^2\right)}\right)^p\right]. \tag{3.42}$$

Similarly, if $z_{\alpha_1}(t) = z_{\alpha_2}(t)$, then the corrected exponential p-norm constraint approximation becomes

$$-\ln\left[\left(\left(e^{-g_1(t)}\right)^p + \left(e^{-\left(h^2\right)}\right)^p\right)^{1/p}\right] + \frac{1}{p}\ln[2] \leq 0, \tag{3.43a}$$

or equivalently,

$$\ln\left[2^{1/p}\right] \leq \ln\left[\left(\left(e^{-g_1(t)}\right)^p + \left(e^{-(h^2)}\right)^p\right)^{1/p}\right] \tag{3.43b}$$

$$\implies 2^{1/p} \leq \left(\left(e^{-g_1(t)}\right)^p + \left(e^{-(h^2)}\right)^p\right)^{1/p} \tag{3.43c}$$

$$\implies 2 \leq \left(e^{-g_1(t)}\right)^p + \left(e^{-(h^2)}\right)^p \tag{3.43d}$$

$$\implies 2 - \left(e^{-(h^2)}\right)^p \leq \left(e^{-g_1(t)}\right)^p \tag{3.43e}$$

$$\implies \ln\left[2 - \left(e^{-(h^2)}\right)^p\right] \leq -p\left(g_1(t)\right) \tag{3.43f}$$

$$\implies -\frac{1}{p}\ln\left[2 - \left(e^{-(h^2)}\right)^p\right] \geq g_1(t) \tag{3.43g}$$

That is, if the vertical separation is zero, then the exponential p-norm ATM separation approximation requires the square of the lateral separation to be at least $\frac{1}{p}\ln\left[2 - \left(e^{-(h^2)}\right)^p\right]$ greater than the square of the minimum allowable lateral separation. Since the actual ATM separation requirement is that if the vertical separation is zero, then the square of the lateral separation must be at least equal to the square of the minimum allowable lateral separation, the maximum error of the exponential p-norm ATM separation approximation in the lateral plane, denoted $\varepsilon_{Le}(p)$, is bounded by the relationship

$$0 \leq \varepsilon_{Le}(p) \leq \frac{1}{p}\ln\left[2 + \left(e^{-(h^2)}\right)^p\right]. \tag{3.44}$$

Increasing the parameter $p > 0$ should result in more accurate approximations of the ATM separation constraint. However, as $p \to \infty$, the exponential p-norm approximation becomes computationally unstable when evaluated with numerical differentiation methods. Section 3.1.2.5 describes the tests constructed to determine appropriate values of p for use with the multi-objective HCS optimization problem.

3.1.2.5 ATM Separation Constraint Approximation Testing.

As indicated in Sections 3.1.2.2- 3.1.2.4, the accuracy and computational stability of each ATM separation constraint approximation is determined by a user-defined parameter. This section describes the tests conducted to determine values of each approximation method's parameters that provide accurate estimates without becoming computationally unstable when using numerical methods to evaluate the multi-objective HCS optimization problem.

The first test was designed to determine how well each approximation method estimates the pair-wise state space conflict region, as defined by equation (3.16). However, the airspace geometry of a pair-wise aircraft interaction may affect how well an approximation method estimates the conflict region. Therefore, the following pair-wise aircraft interaction test scenarios were developed:

1. Two constant, co-altitude aircraft whose current path segments intersect. The unitless minimum allowable lateral separation is $r = 0.3$.

2. Two constant, co-altitude aircraft whose current path segments do not intersect

3. Two variable altitude aircraft whose current path segments intersect

4. Two variable altitude aircraft whose current path segments do not intersect

For all scenarios, the unitless minimum allowable lateral separation was set to $r(t) = 0.3$ to reflect the separation value given in [73], and the unitless minimum allowable vertical separation was set to $h = 0.05$ to reflect a realistic ratio of the lateral minimum allowable separation value divided by the vertical minimum allowable separation value. Within each scenario, unique representative aircraft interaction configurations (denoted *treatments*) were generated such that each aircraft's path consisted of two segments, where the unitless length of each path segment was set to 1, giving the total unitless path length for each aircraft as 2. Thus, for each treatment, the state space was defined as

$$\mathcal{X}^{1,2} \triangleq \left\{ (c_1, c_2) \;\middle|\; \begin{array}{ll} 0 \le c_1 \le 2, & \text{(3.45a)} \\ 0 \le c_2 \le 2, & \text{(3.45b)} \end{array} \right\}$$

where c_1 is the roadmap state space coordinate of aircraft 1 and and c_2 is the roadmap state space coordinate of aircraft 2, and the area of the state space for each treatment was $2 \times 2 = 4$. However, the area of the resulting pair-wise conflict region for each treatment was estimated numerically by generating a grid of points within the state space and calculating the proportion of grid points that violated the ATM pair-wise separation constraint given in equation (3.15b). For each treatment, the grid consisted of every combination of points from the set $\Big\{\{0, 0.005, 0.01, \ldots, 1.995, 2\} \times \{0, 0.005, 0.01, \ldots, 1.995, 2\}\Big\}$, for a total of $(401 \times 401) = 160,801$ grid points.

For each treatment, the proportion of grid points that violated the Multiplier Method ATM pairwise separation constraint approximation given in equation (3.17a) was calculated for each value of the Multiplier Method accuracy parameter $\gamma \in \{1, 5, 10, 50, 100, 500\}$, while the priority parameter λ was set to $\left(\sqrt{2} - 1\right)$. This procedure was also applied to the sigmoid, p-norm, and exponential p-norm constraint approximations. Table 3.1 displays the approximation parameter values tested for each treatment.

Table 3.1: Approximation Parameter Values.

Approximation Method	Parameter	Values Tested at Each Treatment					
Multiplier Method	γ	1	5	10	50	100	500
Sigmoid	s	10	50	100	500	1000	5000
p-Norm	p	2	10	20	100	200	1000
Exponential p-Norm	p	2	10	20	100	200	1000

Scenario 1 was tested with the heading angle, $\alpha_{\measuredangle}$, set to 0, ±45 and ±90 degrees for each aircraft approaching the point of intersection and 0, ±45 and ±90 degrees departing the point of intersection. This resulted in 22 reflection- and rotation-unique configurations. Figure 3.1 displays the lateral orientation of the two notional paths for each Scenario 1 test design treatment. Figure 3.2 displays the state space conflict region for each Scenario 1 test design treatment based on the methods developed in Appendix B. Table 3.2 provides the complete test design for Scenario 1.

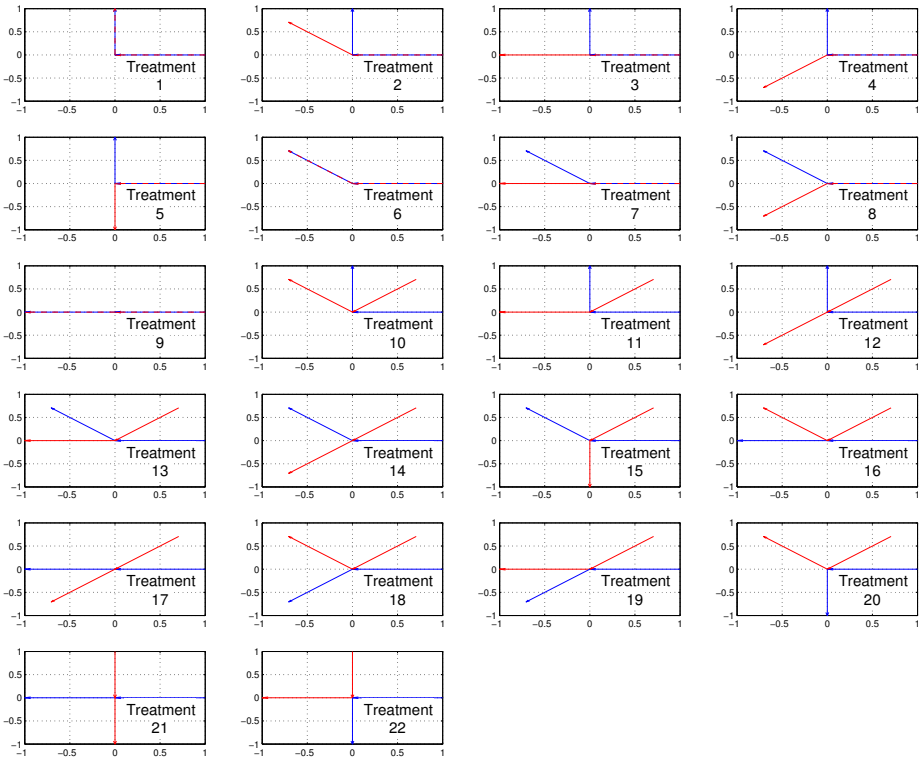

Figure 3.1: Lateral Path Orientations for Scenario 1 Test Design

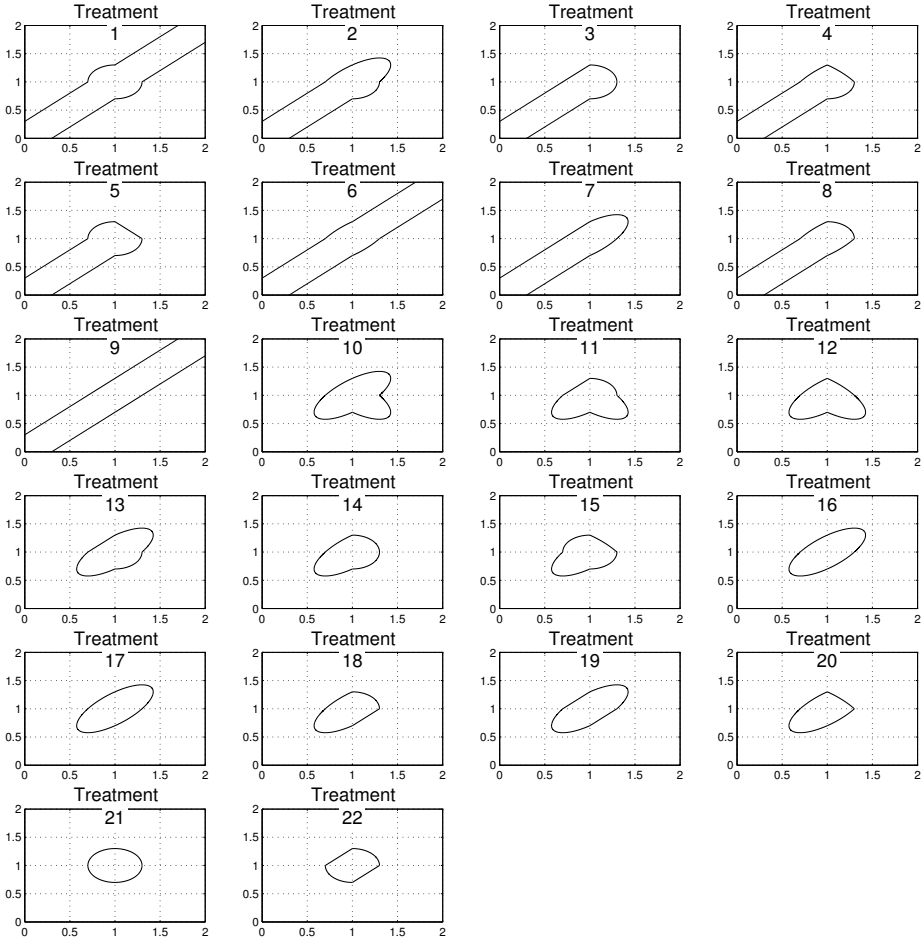

Figure 3.2: State Space Conflict Region Boundaries for Scenario 1 Test Design

Table 3.2: Scenario 1 Test Design.

Treatment	Aircraft 1 Heading (degrees)		Aircraft 2 Heading (degrees)	
	Approach	Departure	Approach	Departure
1	0	90	0	90
2	0	90	0	-45
3	0	90	0	0
4	0	90	0	45
5	0	90	0	-90
6	0	-45	0	-45
7	0	-45	0	0
8	0	-45	0	45
9	0	0	0	0
10	0	90	45	-45
11	0	90	45	0
12	0	90	45	45
13	0	-45	45	0
14	0	-45	45	45
15	0	-45	45	-90
16	0	0	45	-45
17	0	0	45	45
18	0	45	45	-45
19	0	45	45	0
20	0	-90	45	-45
21	0	0	90	-90
22	0	-90	90	0

Scenario 2 was tested with the same path configurations designed for Scenario 1; however, since the paths are not allowed to intersect for Scenario 2, only 14 of the configurations were applicable. For each of these 14 configurations, Scenario 2 was tested with the Minimum Lateral Distance (MLD) between the two aircraft (as defined in Appendix B) set to 10%, 25% and 75% of the notional unitless minimum lateral separation, $r(t) = 0.3$. Figure 3.3 displays the lateral orientation of the two notional paths for each Scenario 2 test design treatment. Figure 3.4 displays the state space conflict region for Scenario 2 test design treatments with MLD set to 25% of the notional unitless minimum lateral separation, based on the methods developed in Appendix B. Table 3.3 provides the complete test design for Scenario 2.

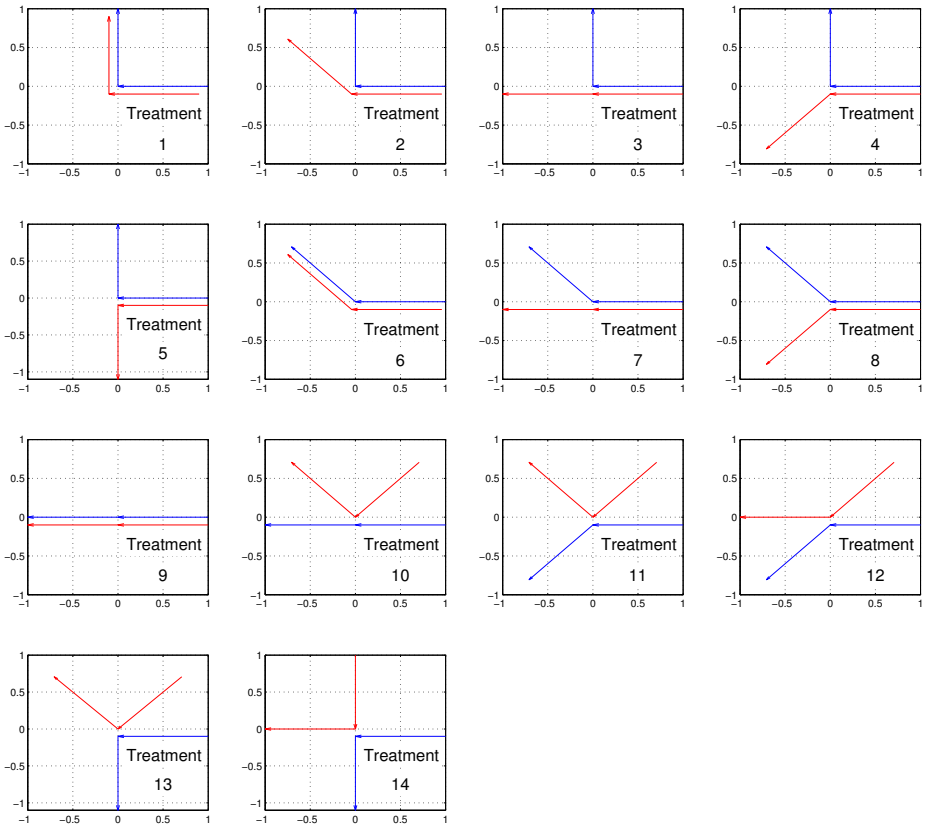

Figure 3.3: Non-Intersecting Lateral Path Orientations for Scenario 2 Test Design

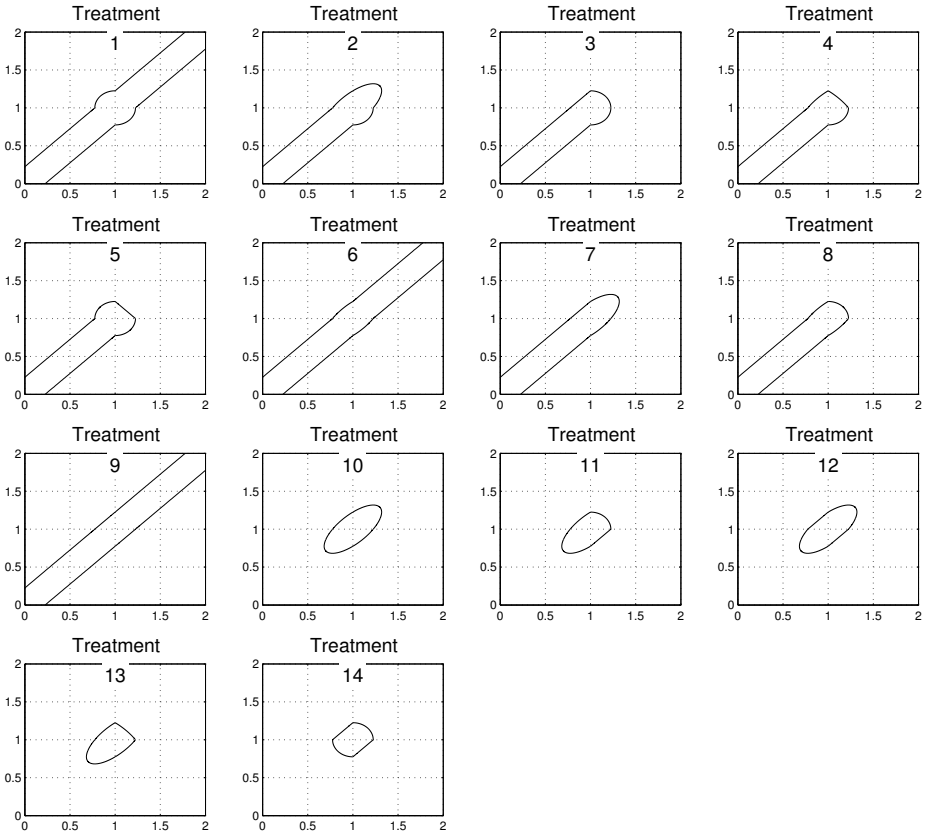

Figure 3.4: State Space Conflict Region Boundaries for Scenario 2 Test Design

Table 3.3: Scenario 2 Test Design.

Treatment			Aircraft 1 Heading (degrees)		Aircraft 2 Heading (degrees)		MLD Distance		
			Approach	Departure	Approach	Departure	(%r)		
1	15	29	0	90	0	90	10	25	75
2	16	30	0	90	0	-45	10	25	75
3	17	31	0	90	0	0	10	25	75
4	18	32	0	90	0	45	10	25	75
5	19	33	0	90	0	-90	10	25	75
6	20	34	0	-45	0	-45	10	25	75
7	21	35	0	-45	0	0	10	25	75
8	22	36	0	-45	0	45	10	25	75
9	23	37	0	0	0	0	10	25	75
10	24	38	0	0	45	-45	10	25	75
11	25	39	0	45	45	-45	10	25	75
12	26	40	0	45	45	0	10	25	75
13	27	41	0	-90	45	-45	10	25	75
14	28	42	0	-90	90	0	10	25	75

Scenario 3 was tested with the same lateral path configurations designed for Scenario 1; however, for each lateral path configuration, each path segment was configured to ascend or descend toward the point of intersection, and ascend or descend away from the point of intersection. The angles of ascent and descent, $\alpha_{\triangleleft}$, were set to ±30 degrees. This resulted in eight (8) rotation- and reflection-unique three-dimensional configurations for each lateral configuration. Figures 3.5 - 3.12 display the state space conflict region for each Scenario 3 test design treatment, based on the three-dimensional intersection methods developed in Appendix B. Tables 3.4 - 3.11 provide the complete test design for Scenario 3.

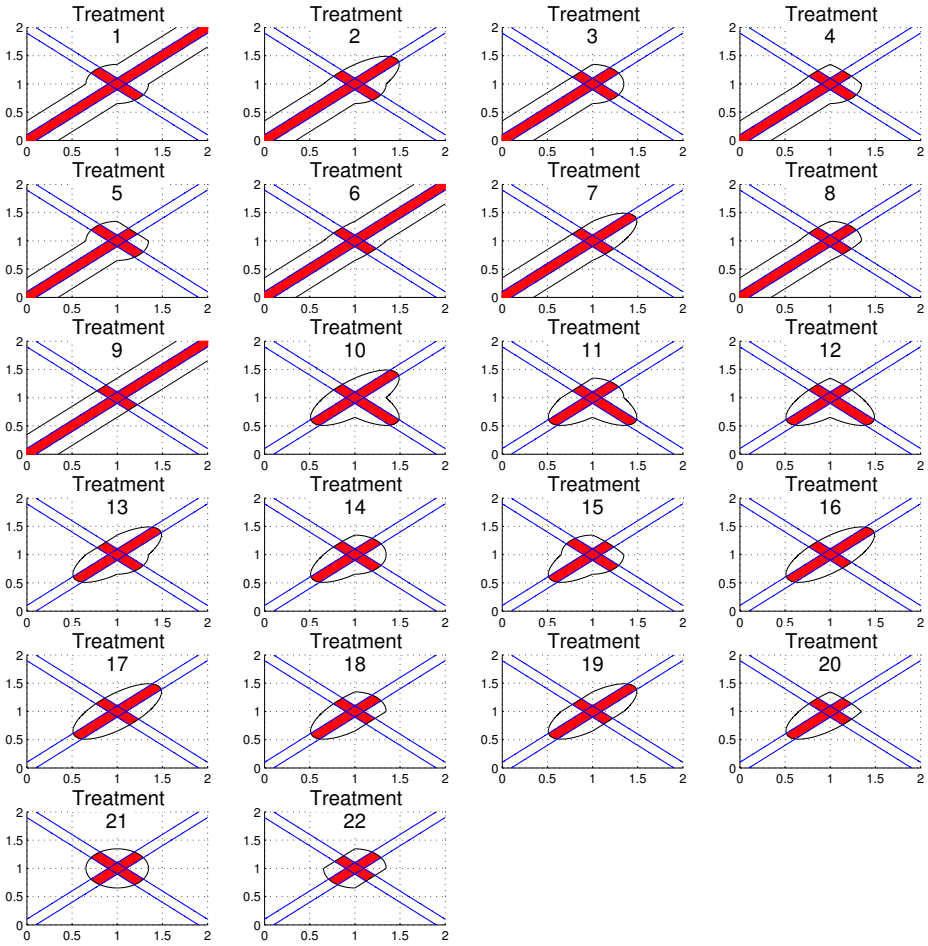

Figure 3.5: State Space Conflict Region (Shaded) for Scenario 3 Test Design: 3-Dimensional Configuration 1

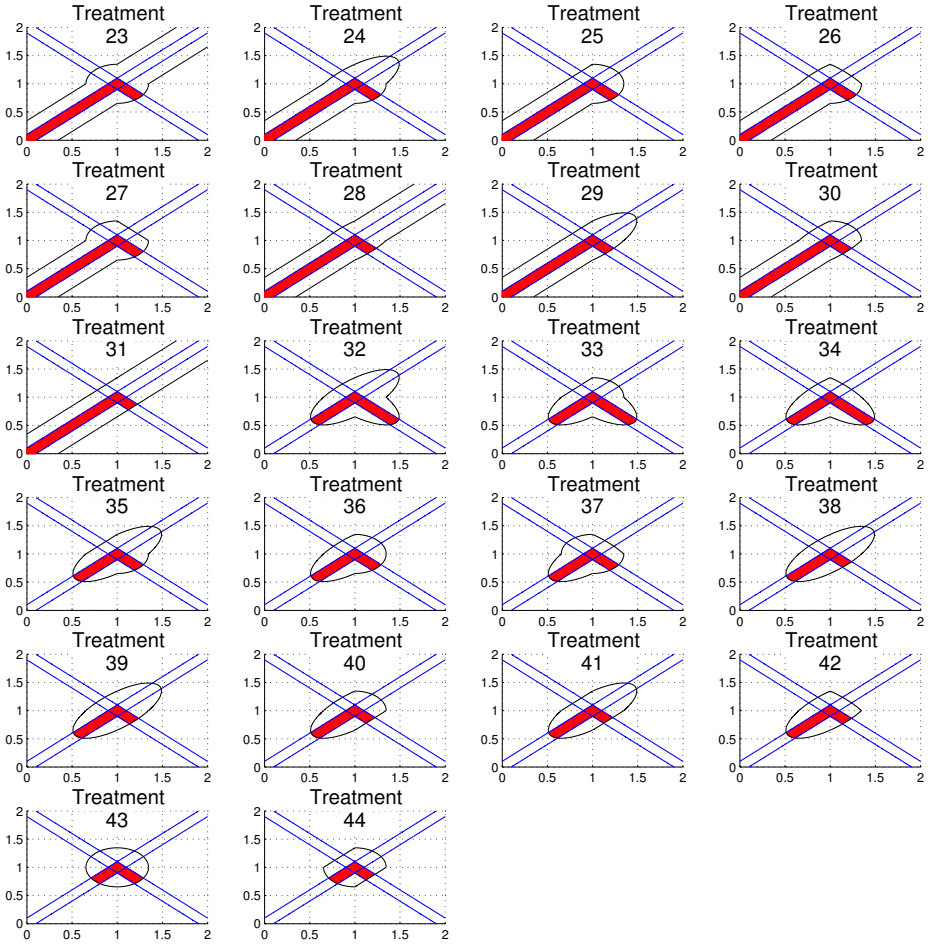

Figure 3.6: State Space Conflict Region (Shaded) for Scenario 3 Test Design: 3-Dimensional Configuration 2

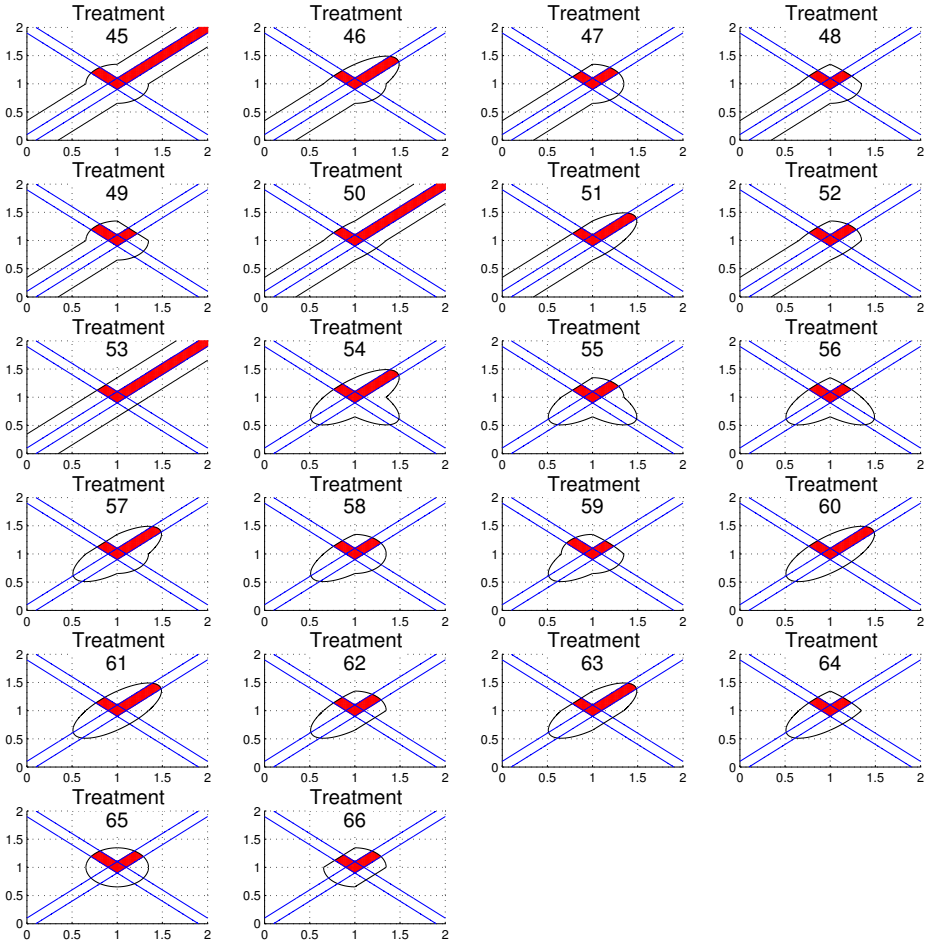

Figure 3.7: State Space Conflict Region (Shaded) for Scenario 3 Test Design: 3-Dimensional Configuration 3

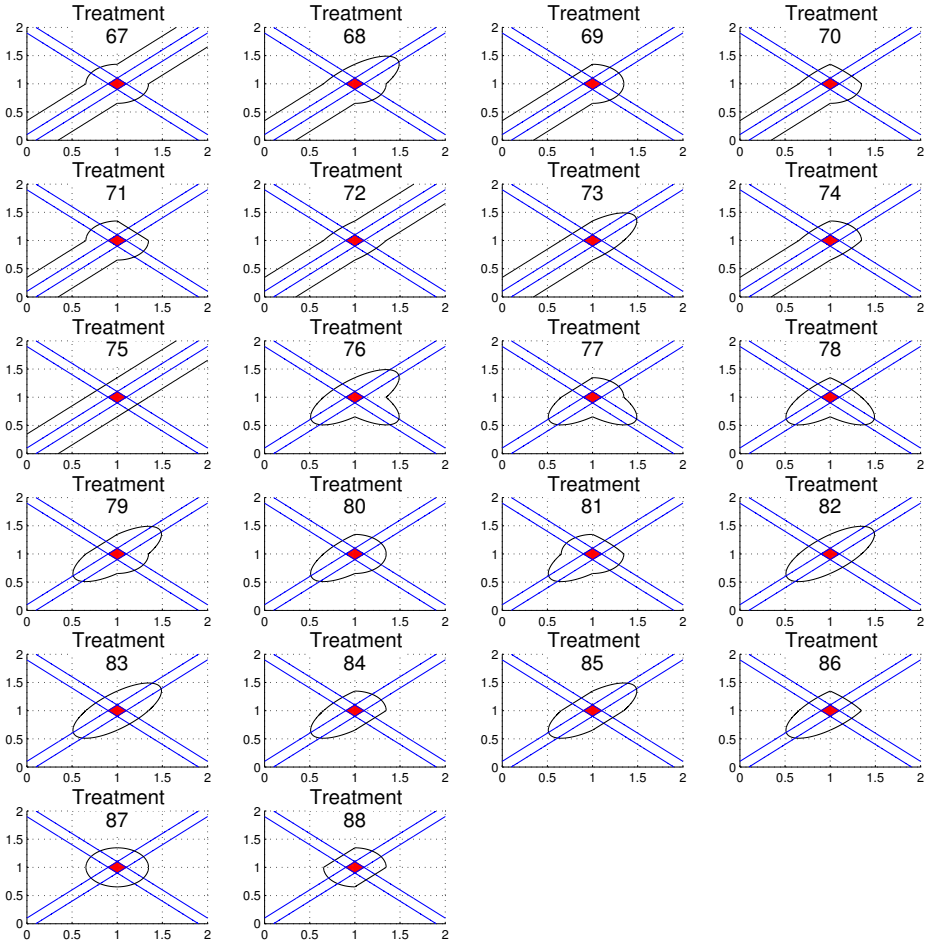

Figure 3.8: State Space Conflict Region (Shaded) for Scenario 3 Test Design: 3-Dimensional Configuration 4

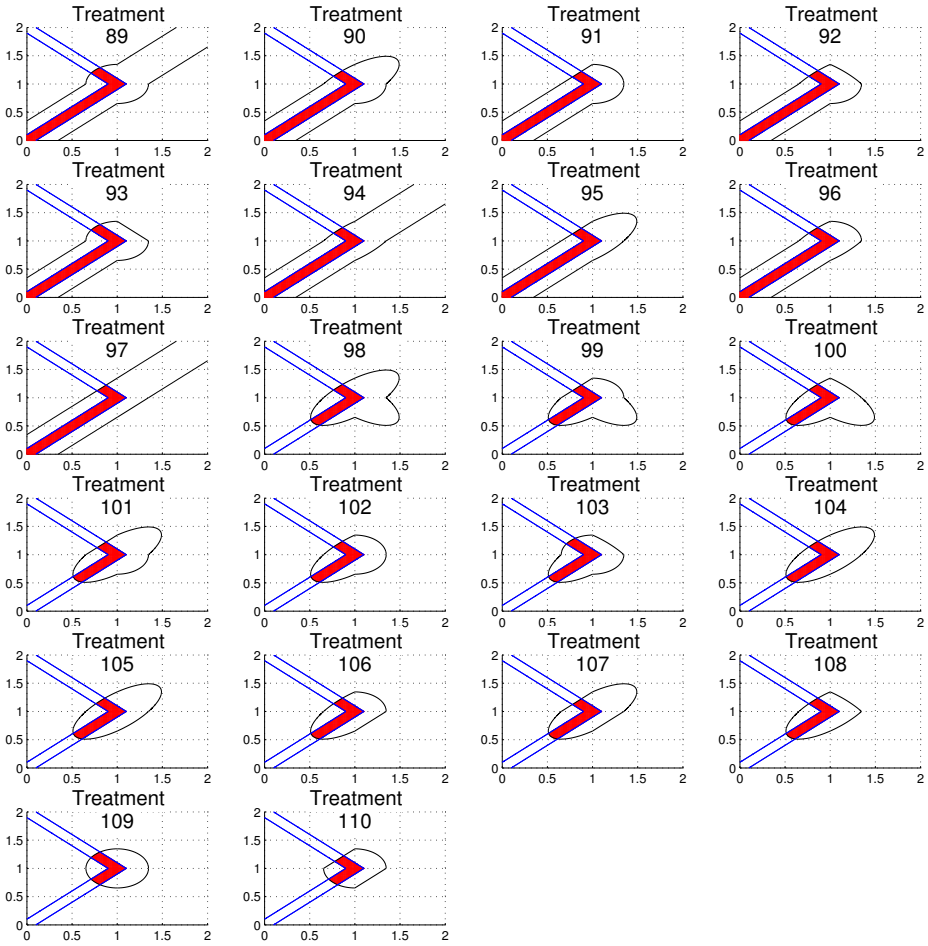

Figure 3.9: State Space Conflict Region (Shaded) for Scenario 3 Test Design: 3-Dimensional Configuration 5

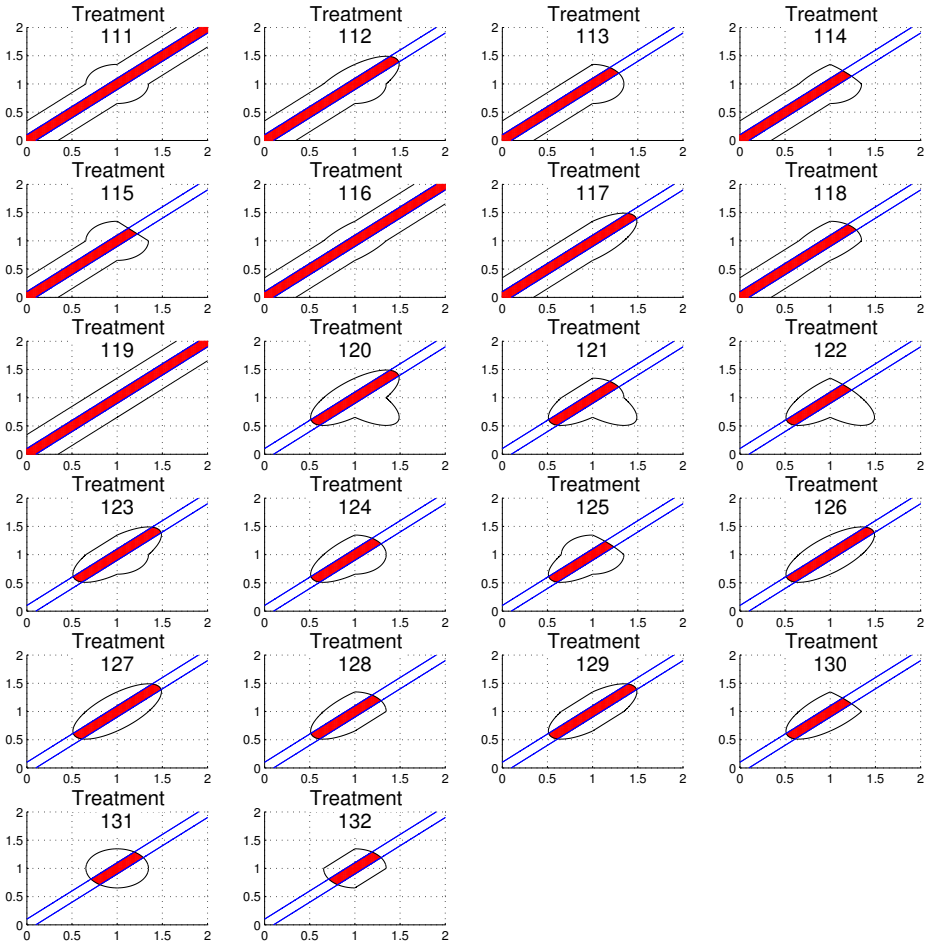

Figure 3.10: State Space Conflict Region (Shaded) for Scenario 3 Test Design: 3-Dimensional Configuration 6

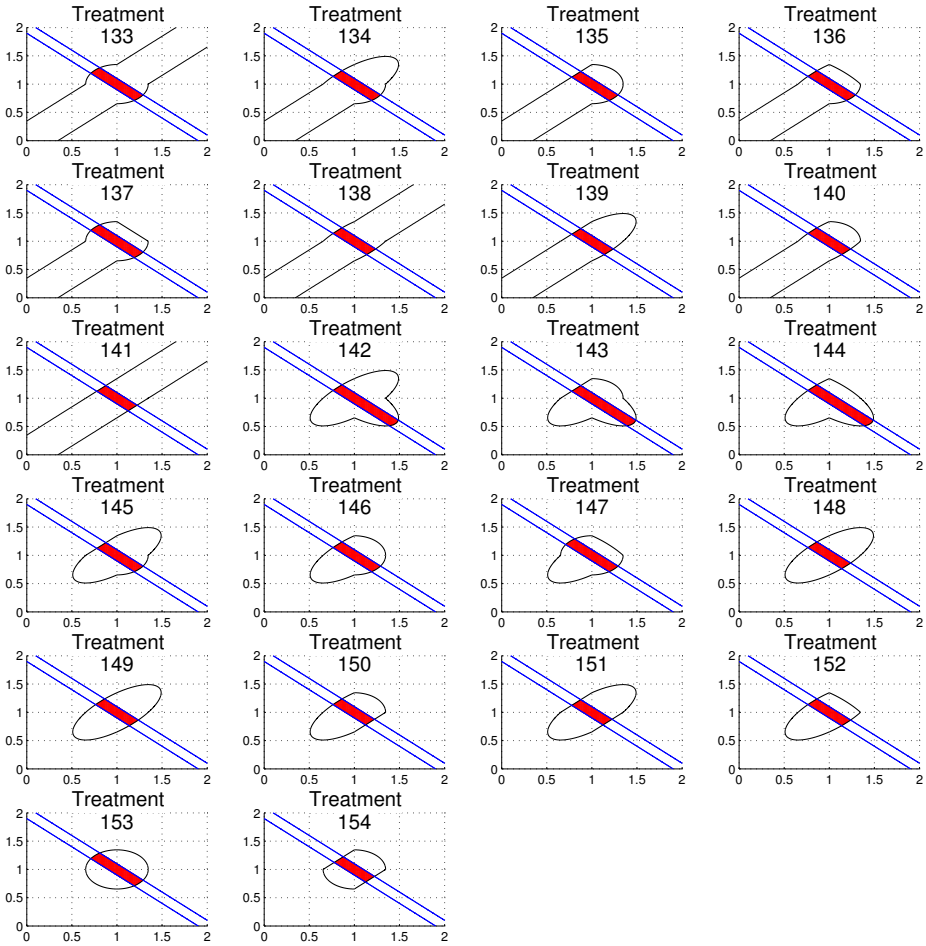

Figure 3.11: State Space Conflict Region (Shaded) for Scenario 3 Test Design: 3-Dimensional Configuration 7

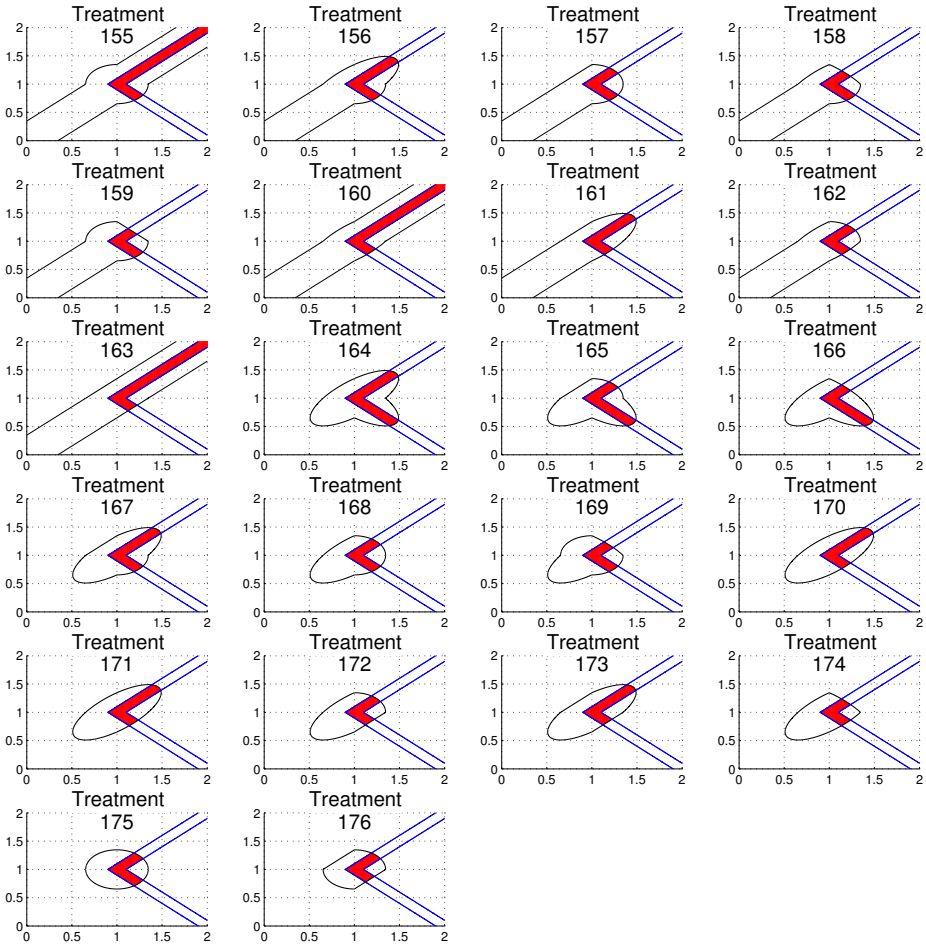

Figure 3.12: State Space Conflict Region (Shaded) for Scenario 3 Test Design: 3-Dimensional Configuration 8

Table 3.4: Scenario 3 Test Design - 3 Dimensional Configuration 1.

Treatment	Aircraft 1 Heading (degrees)				Aircraft 2 Heading (degrees)			
	Approach		Departure		Approach		Departure	
	Lateral	Vertical	Lateral	Vertical	Lateral	Vertical	Lateral	Vertical
1	0	30	90	30	0	30	90	30
2	0	30	90	30	0	30	-45	30
3	0	30	90	30	0	30	0	30
4	0	30	90	30	0	30	45	30
5	0	30	90	30	0	30	-90	30
6	0	30	-45	30	0	30	-45	30
7	0	30	-45	30	0	30	0	30
8	0	30	-45	30	0	30	45	30
9	0	30	0	30	0	30	0	30
10	0	30	90	30	45	30	-45	30
11	0	30	90	30	45	30	0	30
12	0	30	90	30	45	30	45	30
13	0	30	-45	30	45	30	0	30
14	0	30	-45	30	45	30	45	30
15	0	30	-45	30	45	30	-90	30
16	0	30	0	30	45	30	-45	30
17	0	30	0	30	45	30	45	30
18	0	30	45	30	45	30	-45	30
19	0	30	45	30	45	30	0	30
20	0	30	-90	30	45	30	-45	30
21	0	30	0	30	90	30	-90	30
22	0	30	-90	30	90	30	0	30

Table 3.5: Scenario 3 Test Design - 3 Dimensional Configuration 2.

Treatment	Aircraft 1 Heading (degrees)				Aircraft 2 Heading (degrees)			
	Approach		Departure		Approach		Departure	
	Lateral	Vertical	Lateral	Vertical	Lateral	Vertical	Lateral	Vertical
23	0	30	90	30	0	30	90	-30
24	0	30	90	30	0	30	-45	-30
25	0	30	90	30	0	30	0	-30
26	0	30	90	30	0	30	45	-30
27	0	30	90	30	0	30	-90	-30
28	0	30	-45	30	0	30	-45	-30
29	0	30	-45	30	0	30	0	-30
30	0	30	-45	30	0	30	45	-30
31	0	30	0	30	0	30	0	-30
32	0	30	90	30	45	30	-45	-30
33	0	30	90	30	45	30	0	-30
34	0	30	90	30	45	30	45	-30
35	0	30	-45	30	45	30	0	-30
36	0	30	-45	30	45	30	45	-30
37	0	30	-45	30	45	30	-90	-30
38	0	30	0	30	45	30	-45	-30
39	0	30	0	30	45	30	45	-30
40	0	30	45	30	45	30	-45	-30
41	0	30	45	30	45	30	0	-30
42	0	30	-90	30	45	30	-45	-30
43	0	30	0	30	90	30	-90	-30
44	0	30	-90	30	90	30	0	-30

Table 3.6: Scenario 3 Test Design - 3 Dimensional Configuration 3.

Treatment	Aircraft 1 Heading (degrees)				Aircraft 2 Heading (degrees)			
	Approach		Departure		Approach		Departure	
	Lateral	Vertical	Lateral	Vertical	Lateral	Vertical	Lateral	Vertical
45	0	30	90	30	0	-30	90	30
46	0	30	90	30	0	-30	-45	30
47	0	30	90	30	0	-30	0	30
48	0	30	90	30	0	-30	45	30
49	0	30	90	30	0	-30	-90	30
50	0	30	-45	30	0	-30	-45	30
51	0	30	-45	30	0	-30	0	30
52	0	30	-45	30	0	-30	45	30
53	0	30	0	30	0	-30	0	30
54	0	30	90	30	45	-30	-45	30
55	0	30	90	30	45	-30	0	30
56	0	30	90	30	45	-30	45	30
57	0	30	-45	30	45	-30	0	30
58	0	30	-45	30	45	-30	45	30
59	0	30	-45	30	45	-30	-90	30
60	0	30	0	30	45	-30	-45	30
61	0	30	0	30	45	-30	45	30
62	0	30	45	30	45	-30	-45	30
63	0	30	45	30	45	-30	0	30
64	0	30	-90	30	45	-30	-45	30
65	0	30	0	30	90	-30	-90	30
66	0	30	-90	30	90	-30	0	30

Table 3.7: Scenario 3 Test Design - 3 Dimensional Configuration 4.

Treatment	Aircraft 1 Heading (degrees)				Aircraft 2 Heading (degrees)			
	Approach		Departure		Approach		Departure	
	Lateral	Vertical	Lateral	Vertical	Lateral	Vertical	Lateral	Vertical
67	0	30	90	30	0	-30	90	-30
68	0	30	90	30	0	-30	-45	-30
69	0	30	90	30	0	-30	0	-30
70	0	30	90	30	0	-30	45	-30
71	0	30	90	30	0	-30	-90	-30
72	0	30	-45	30	0	-30	-45	-30
73	0	30	-45	30	0	-30	0	-30
74	0	30	-45	30	0	-30	45	-30
75	0	30	0	30	0	-30	0	-30
76	0	30	90	30	45	-30	-45	-30
77	0	30	90	30	45	-30	0	-30
78	0	30	90	30	45	-30	45	-30
79	0	30	-45	30	45	-30	0	-30
80	0	30	-45	30	45	-30	45	-30
81	0	30	-45	30	45	-30	-90	-30
82	0	30	0	30	45	-30	-45	-30
83	0	30	0	30	45	-30	45	-30
84	0	30	45	30	45	-30	-45	-30
85	0	30	45	30	45	-30	0	-30
86	0	30	-90	30	45	-30	-45	-30
87	0	30	0	30	90	-30	-90	-30
88	0	30	-90	30	90	-30	0	-30

Table 3.8: Scenario 3 Test Design - 3 Dimensional Configuration 5.

Treatment	Aircraft 1 Heading (degrees)				Aircraft 2 Heading (degrees)			
	Approach		Departure		Approach		Departure	
	Lateral	Vertical	Lateral	Vertical	Lateral	Vertical	Lateral	Vertical
89	0	30	90	-30	0	30	90	30
90	0	30	90	-30	0	30	-45	30
91	0	30	90	-30	0	30	0	30
92	0	30	90	-30	0	30	45	30
93	0	30	90	-30	0	30	-90	30
94	0	30	-45	-30	0	30	-45	30
95	0	30	-45	-30	0	30	0	30
96	0	30	-45	-30	0	30	45	30
97	0	30	0	-30	0	30	0	30
98	0	30	90	-30	45	30	-45	30
99	0	30	90	-30	45	30	0	30
100	0	30	90	-30	45	30	45	30
101	0	30	-45	-30	45	30	0	30
102	0	30	-45	-30	45	30	45	30
103	0	30	-45	-30	45	30	-90	30
104	0	30	0	-30	45	30	-45	30
105	0	30	0	-30	45	30	45	30
106	0	30	45	-30	45	30	-45	30
107	0	30	45	-30	45	30	0	30
108	0	30	-90	-30	45	30	-45	30
109	0	30	0	-30	90	30	-90	30
110	0	30	-90	-30	90	30	0	30

Table 3.9: Scenario 3 Test Design - 3 Dimensional Configuration 6.

Treatment	Aircraft 1 Heading (degrees)				Aircraft 2 Heading (degrees)			
	Approach		Departure		Approach		Departure	
	Lateral	Vertical	Lateral	Vertical	Lateral	Vertical	Lateral	Vertical
111	0	30	90	-30	0	30	90	-30
112	0	30	90	-30	0	30	-45	-30
113	0	30	90	-30	0	30	0	-30
114	0	30	90	-30	0	30	45	-30
115	0	30	90	-30	0	30	-90	-30
116	0	30	-45	-30	0	30	-45	-30
117	0	30	-45	-30	0	30	0	-30
118	0	30	-45	-30	0	30	45	-30
119	0	30	0	-30	0	30	0	-30
120	0	30	90	-30	45	30	-45	-30
121	0	30	90	-30	45	30	0	-30
122	0	30	90	-30	45	30	45	-30
123	0	30	-45	-30	45	30	0	-30
124	0	30	-45	-30	45	30	45	-30
125	0	30	-45	-30	45	30	-90	-30
126	0	30	0	-30	45	30	-45	-30
127	0	30	0	-30	45	30	45	-30
128	0	30	45	-30	45	30	-45	-30
129	0	30	45	-30	45	30	0	-30
130	0	30	-90	-30	45	30	-45	-30
131	0	30	0	-30	90	30	-90	-30
132	0	30	-90	-30	90	30	0	-30

Table 3.10: Scenario 3 Test Design - 3 Dimensional Configuration 7.

Treatment	Aircraft 1 Heading (degrees)				Aircraft 2 Heading (degrees)			
	Approach		Departure		Approach		Departure	
	Lateral	Vertical	Lateral	Vertical	Lateral	Vertical	Lateral	Vertical
133	0	30	90	-30	0	-30	90	30
134	0	30	90	-30	0	-30	-45	30
135	0	30	90	-30	0	-30	0	30
136	0	30	90	-30	0	-30	45	30
137	0	30	90	-30	0	-30	-90	30
138	0	30	-45	-30	0	-30	-45	30
139	0	30	-45	-30	0	-30	0	30
140	0	30	-45	-30	0	-30	45	30
141	0	30	0	-30	0	-30	0	30
142	0	30	90	-30	45	-30	-45	30
143	0	30	90	-30	45	-30	0	30
144	0	30	90	-30	45	-30	45	30
145	0	30	-45	-30	45	-30	0	30
146	0	30	-45	-30	45	-30	45	30
147	0	30	-45	-30	45	-30	-90	30
148	0	30	0	-30	45	-30	-45	30
149	0	30	0	-30	45	-30	45	30
150	0	30	45	-30	45	-30	-45	30
151	0	30	45	-30	45	-30	0	30
152	0	30	-90	-30	45	-30	-45	30
153	0	30	0	-30	90	-30	-90	30
154	0	30	-90	-30	90	-30	0	30

Table 3.11: Scenario 3 Test Design - 3 Dimensional Configuration 8.

Treatment	Aircraft 1 Heading (degrees)				Aircraft 2 Heading (degrees)			
	Approach		Departure		Approach		Departure	
	Lateral	Vertical	Lateral	Vertical	Lateral	Vertical	Lateral	Vertical
155	0	30	90	-30	0	-30	90	-30
156	0	30	90	-30	0	-30	-45	-30
157	0	30	90	-30	0	-30	0	-30
158	0	30	90	-30	0	-30	45	-30
159	0	30	90	-30	0	-30	-90	-30
160	0	30	-45	-30	0	-30	-45	-30
161	0	30	-45	-30	0	-30	0	-30
162	0	30	-45	-30	0	-30	45	-30
163	0	30	0	-30	0	-30	0	-30
164	0	30	90	-30	45	-30	-45	-30
165	0	30	90	-30	45	-30	0	-30
166	0	30	90	-30	45	-30	45	-30
167	0	30	-45	-30	45	-30	0	-30
168	0	30	-45	-30	45	-30	45	-30
169	0	30	-45	-30	45	-30	-90	-30
170	0	30	0	-30	45	-30	-45	-30
171	0	30	0	-30	45	-30	45	-30
172	0	30	45	-30	45	-30	-45	-30
173	0	30	45	-30	45	-30	0	-30
174	0	30	-90	-30	45	-30	-45	-30
175	0	30	0	-30	90	-30	-90	-30
176	0	30	-90	-30	90	-30	0	-30

Scenario 4 was tested with the same lateral path configurations designed for Scenario 2; however, for each lateral path configuration, the MLD was set to 50% of the notional unitless minimum lateral separation, and each path segment was configured to ascend or descend toward the MLD, and ascend or descend away from the MLD. The angles of ascent and descent, $\alpha_{\triangleleft}$, were set to ±30 degrees. This resulted in eight (8) rotation- and reflection-unique three-dimensional configurations for each lateral configuration. Figures 3.13 - 3.20 display the state space conflict region for Scenario 4 test design treatments with the MLD set to 50% of the notional unitless minimum lateral separation, based on the three-dimensional intersection methods developed in Appendix B. Tables 3.12 - 3.19 provide the complete test design for Scenario 4.

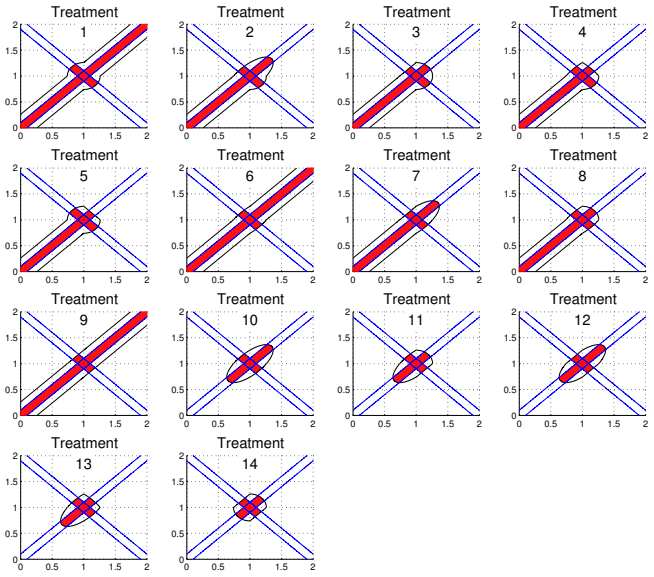

Figure 3.13: State Space Conflict Region (Shaded) for Scenario 4 Test Design: 3-Dimensional Configuration 1

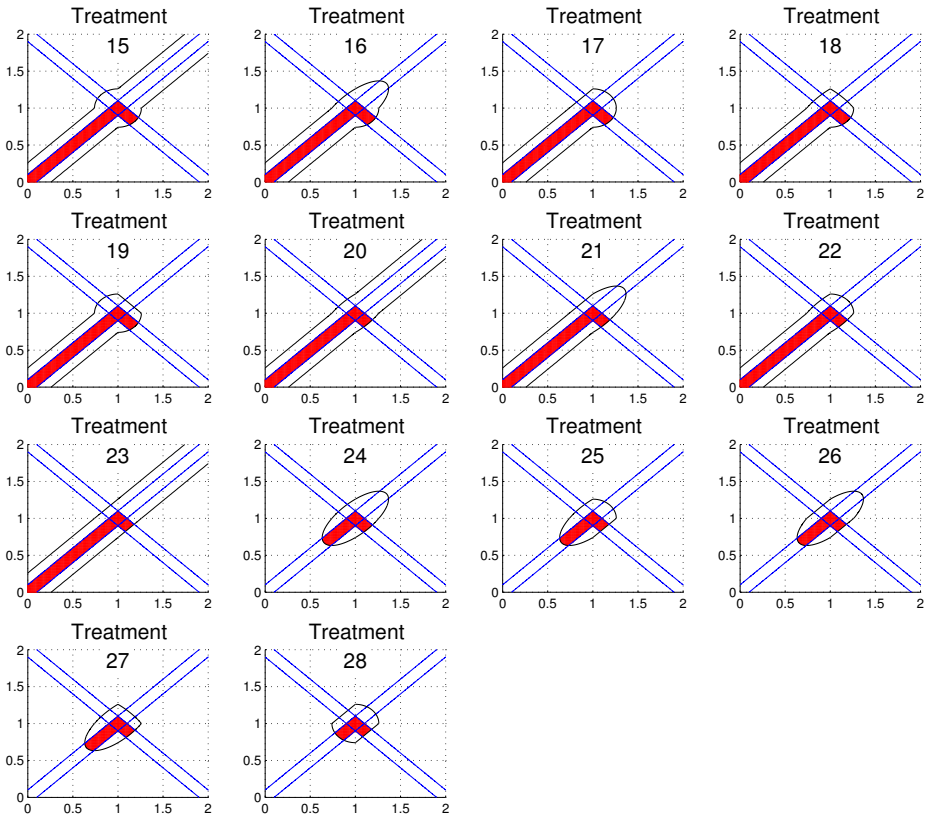

Figure 3.14: State Space Conflict Region (Shaded) for Scenario 4 Test Design: 3-Dimensional Configuration 2

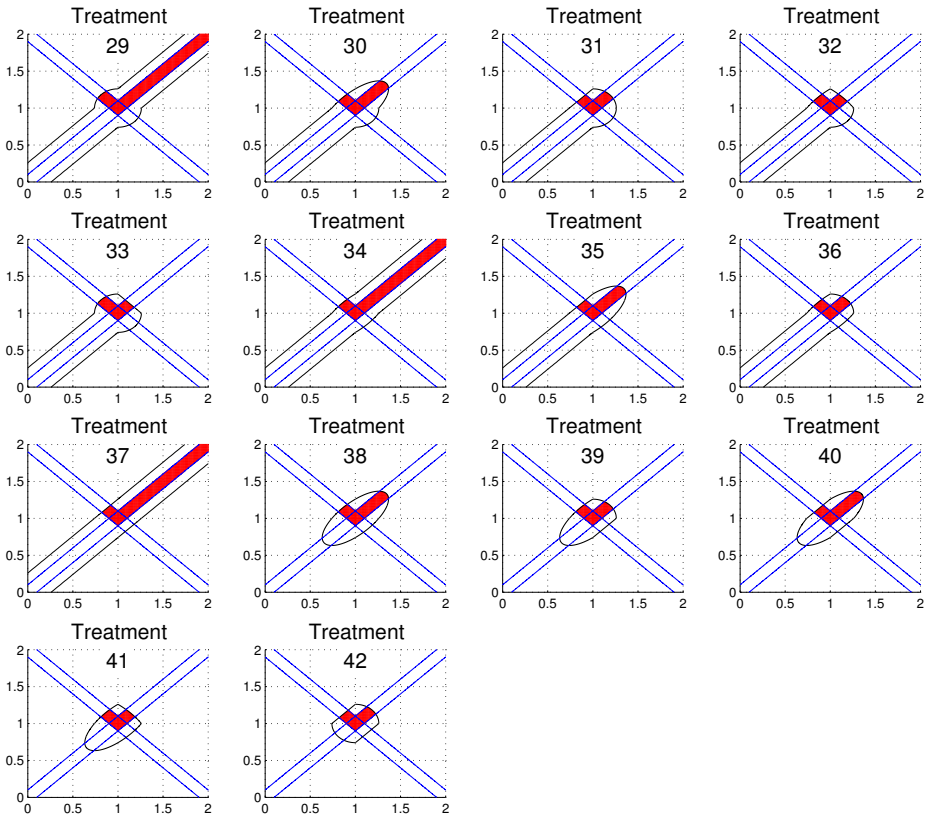

Figure 3.15: State Space Conflict Region (Shaded) for Scenario 4 Test Design: 3-Dimensional Configuration 3

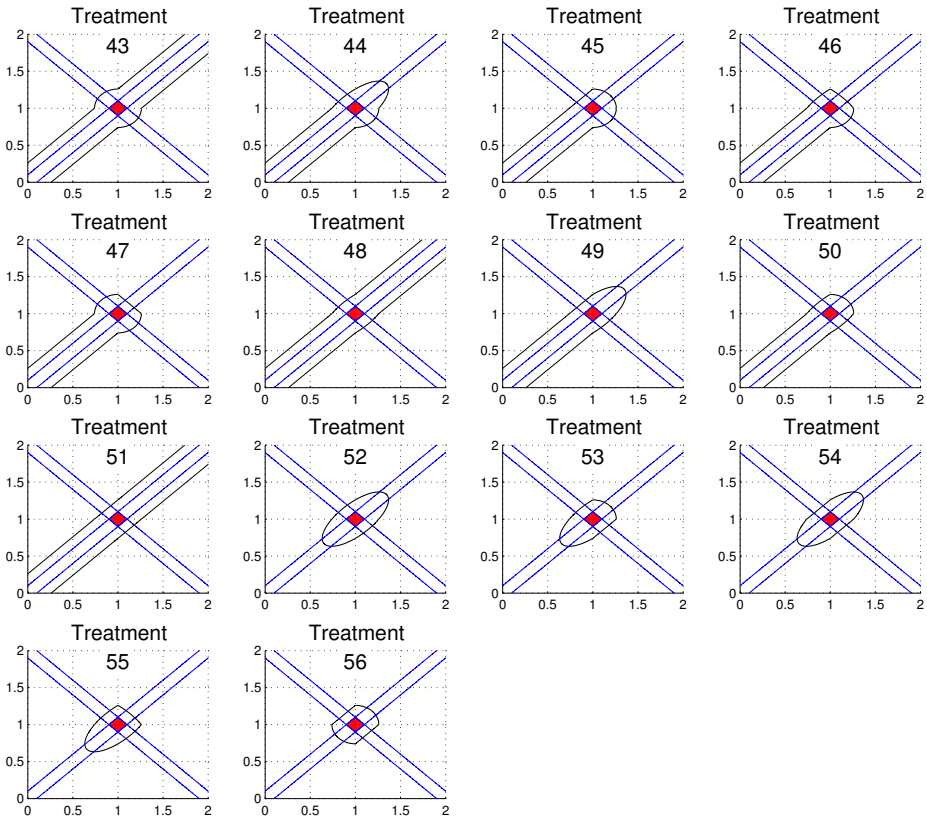

Figure 3.16: State Space Conflict Region (Shaded) for Scenario 4 Test Design: 3-Dimensional Configuration 4

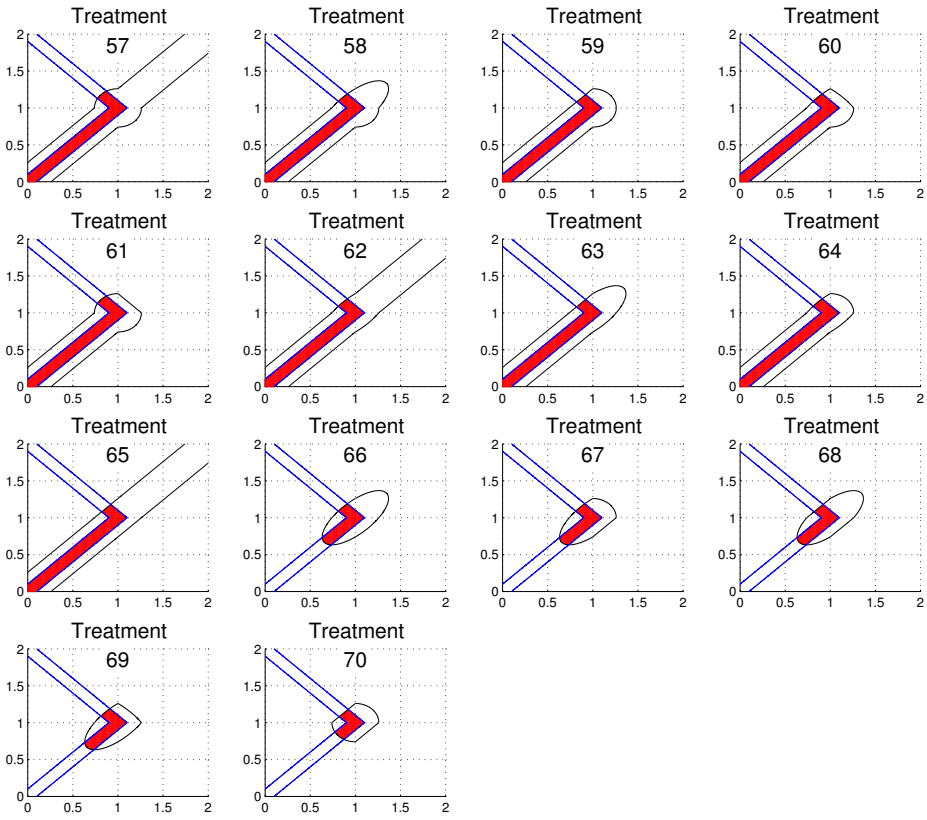

Figure 3.17: State Space Conflict Region (Shaded) for Scenario 4 Test Design: 3-Dimensional Configuration 5

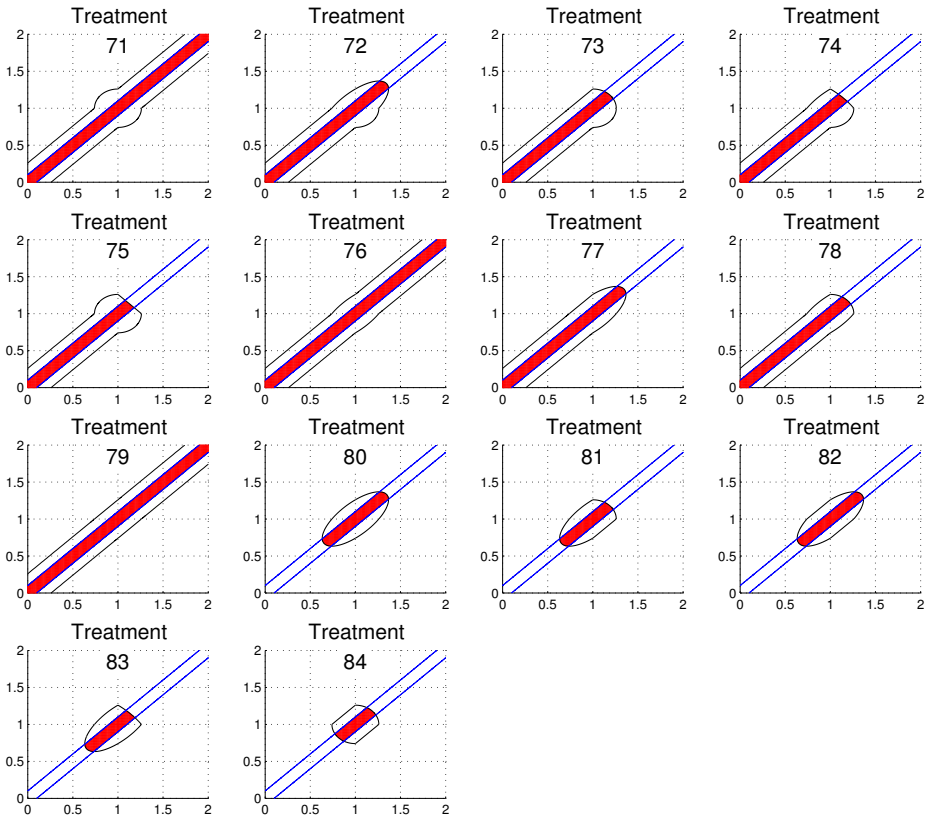

Figure 3.18: State Space Conflict Region (Shaded) for Scenario 4 Test Design: 3-Dimensional Configuration 6

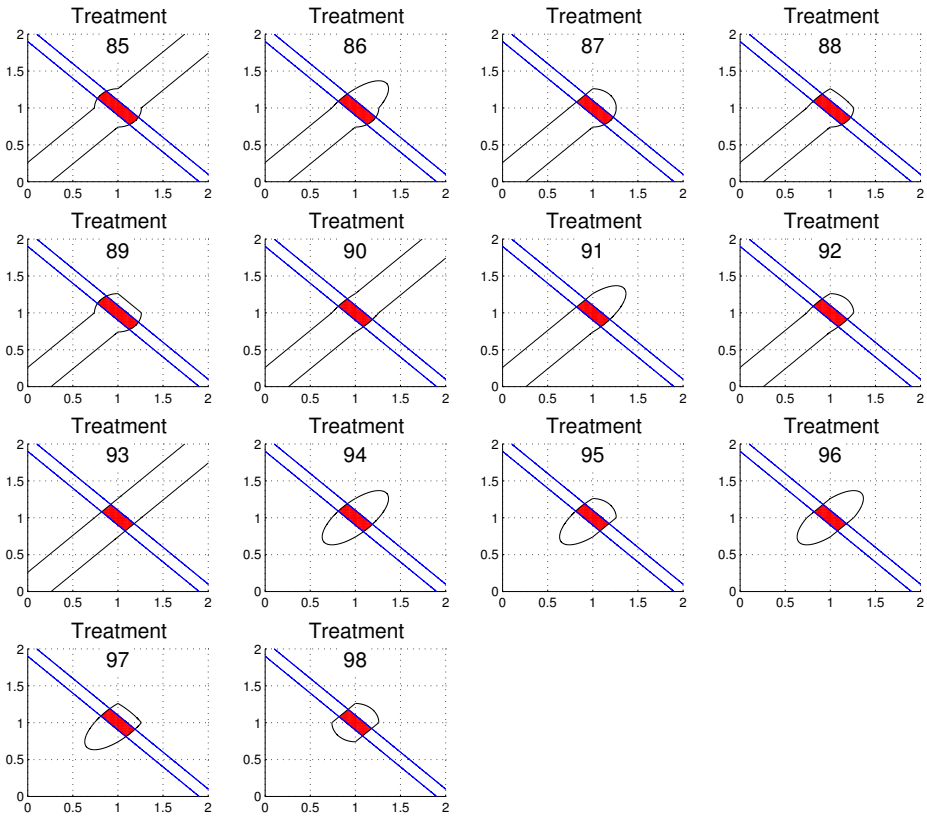

Figure 3.19: State Space Conflict Region (Shaded) for Scenario 4 Test Design: 3-Dimensional Configuration 7

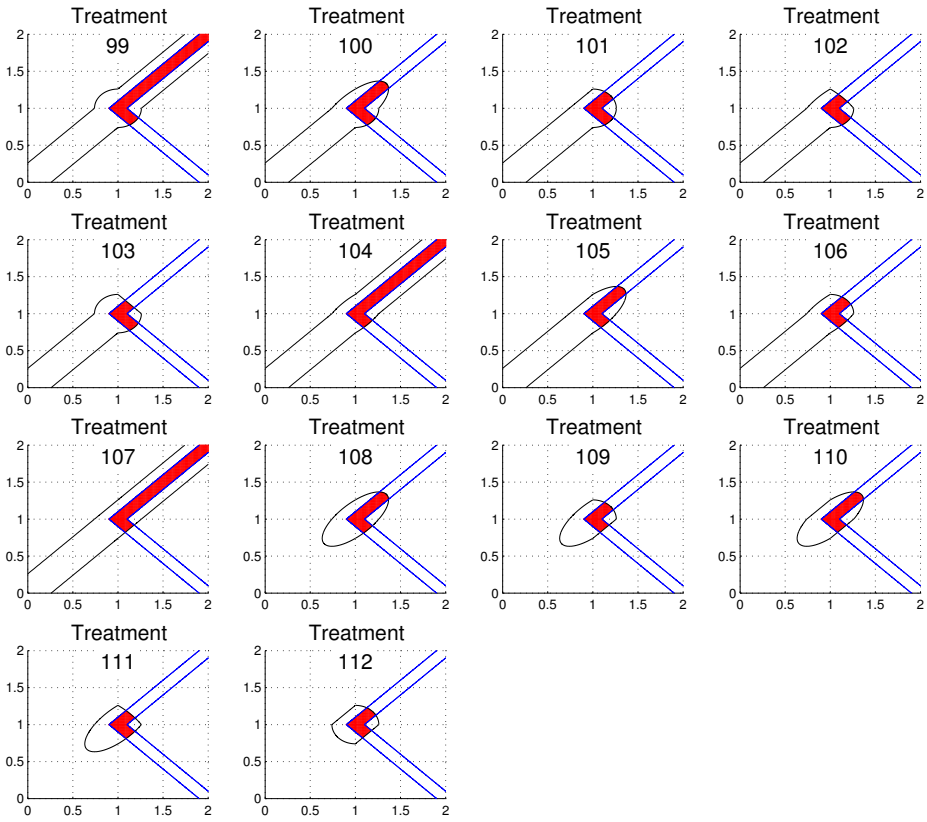

Figure 3.20: State Space Conflict Region (Shaded) for Scenario 4 Test Design: 3-Dimensional Configuration 8

Table 3.12: Scenario 4 Test Design - 3 Dimensional Configuration 1.

Treatment	Aircraft 1 Heading (degrees)				Aircraft 2 Heading (degrees)			
	Approach		Departure		Approach		Departure	
	Lateral	Vertical	Lateral	Vertical	Lateral	Vertical	Lateral	Vertical
1	0	30	90	30	0	30	90	30
2	0	30	90	30	0	30	-45	30
3	0	30	90	30	0	30	0	30
4	0	30	90	30	0	30	45	30
5	0	30	90	30	0	30	-90	30
6	0	30	-45	30	0	30	-45	30
7	0	30	-45	30	0	30	0	30
8	0	30	-45	30	0	30	45	30
9	0	30	0	30	0	30	0	30
10	0	30	0	30	45	30	-45	30
11	0	30	45	30	45	30	-45	30
12	0	30	45	30	45	30	0	30
13	0	30	-90	30	45	30	-45	30
14	0	30	-90	30	90	30	0	30

Table 3.13: Scenario 4 Test Design - 3 Dimensional Configuration 2.

Treatment	Aircraft 1 Heading (degrees)				Aircraft 2 Heading (degrees)			
	Approach		Departure		Approach		Departure	
	Lateral	Vertical	Lateral	Vertical	Lateral	Vertical	Lateral	Vertical
15	0	30	90	30	0	30	90	-30
16	0	30	90	30	0	30	-45	-30
17	0	30	90	30	0	30	0	-30
18	0	30	90	30	0	30	45	-30
19	0	30	90	30	0	30	-90	-30
20	0	30	-45	30	0	30	-45	-30
21	0	30	-45	30	0	30	0	-30
22	0	30	-45	30	0	30	45	-30
23	0	30	0	30	0	30	0	-30
24	0	30	0	30	45	30	-45	-30
25	0	30	45	30	45	30	-45	-30
26	0	30	45	30	45	30	0	-30
27	0	30	-90	30	45	30	-45	-30
28	0	30	-90	30	90	30	0	-30

Table 3.14: Scenario 4 Test Design - 3 Dimensional Configuration 3.

Treatment	Aircraft 1 Heading (degrees)				Aircraft 2 Heading (degrees)			
	Approach		Departure		Approach		Departure	
	Lateral	Vertical	Lateral	Vertical	Lateral	Vertical	Lateral	Vertical
29	0	30	90	30	0	-30	90	30
30	0	30	90	30	0	-30	-45	30
31	0	30	90	30	0	-30	0	30
32	0	30	90	30	0	-30	45	30
33	0	30	90	30	0	-30	-90	30
34	0	30	-45	30	0	-30	-45	30
35	0	30	-45	30	0	-30	0	30
36	0	30	-45	30	0	-30	45	30
37	0	30	0	30	0	-30	0	30
38	0	30	0	30	45	-30	-45	30
39	0	30	45	30	45	-30	-45	30
40	0	30	45	30	45	-30	0	30
41	0	30	-90	30	45	-30	-45	30
42	0	30	-90	30	90	-30	0	30

Table 3.15: Scenario 4 Test Design - 3 Dimensional Configuration 4.

Treatment	Aircraft 1 Heading (degrees)				Aircraft 2 Heading (degrees)			
	Approach		Departure		Approach		Departure	
	Lateral	Vertical	Lateral	Vertical	Lateral	Vertical	Lateral	Vertical
43	0	30	90	30	0	-30	90	-30
44	0	30	90	30	0	-30	-45	-30
45	0	30	90	30	0	-30	0	-30
46	0	30	90	30	0	-30	45	-30
47	0	30	90	30	0	-30	-90	-30
48	0	30	-45	30	0	-30	-45	-30
49	0	30	-45	30	0	-30	0	-30
50	0	30	-45	30	0	-30	45	-30
51	0	30	0	30	0	-30	0	-30
52	0	30	0	30	45	-30	-45	-30
53	0	30	45	30	45	-30	-45	-30
54	0	30	45	30	45	-30	0	-30
55	0	30	-90	30	45	-30	-45	-30
56	0	30	-90	30	90	-30	0	-30

Table 3.16: Scenario 4 Test Design - 3 Dimensional Configuration 5.

Treatment	Aircraft 1 Heading (degrees)				Aircraft 2 Heading (degrees)			
	Approach		Departure		Approach		Departure	
	Lateral	Vertical	Lateral	Vertical	Lateral	Vertical	Lateral	Vertical
57	0	30	90	-30	0	30	90	30
58	0	30	90	-30	0	30	-45	30
59	0	30	90	-30	0	30	0	30
60	0	30	90	-30	0	30	45	30
61	0	30	90	-30	0	30	-90	30
62	0	30	-45	-30	0	30	-45	30
63	0	30	-45	-30	0	30	0	30
64	0	30	-45	-30	0	30	45	30
65	0	30	0	-30	0	30	0	30
66	0	30	0	-30	45	30	-45	30
67	0	30	45	-30	45	30	-45	30
68	0	30	45	-30	45	30	0	30
69	0	30	-90	-30	45	30	-45	30
70	0	30	-90	-30	90	30	0	30

Table 3.17: Scenario 4 Test Design - 3 Dimensional Configuration 6.

Treatment	Aircraft 1 Heading (degrees)				Aircraft 2 Heading (degrees)			
	Approach		Departure		Approach		Departure	
	Lateral	Vertical	Lateral	Vertical	Lateral	Vertical	Lateral	Vertical
71	0	30	90	-30	0	30	90	-30
72	0	30	90	-30	0	30	-45	-30
73	0	30	90	-30	0	30	0	-30
74	0	30	90	-30	0	30	45	-30
75	0	30	90	-30	0	30	-90	-30
76	0	30	-45	-30	0	30	-45	-30
77	0	30	-45	-30	0	30	0	-30
78	0	30	-45	-30	0	30	45	-30
79	0	30	0	-30	0	30	0	-30
80	0	30	0	-30	45	30	-45	-30
81	0	30	45	-30	45	30	-45	-30
82	0	30	45	-30	45	30	0	-30
83	0	30	-90	-30	45	30	-45	-30
84	0	30	-90	-30	90	30	0	-30

Table 3.18: Scenario 4 Test Design - 3 Dimensional Configuration 7.

Treatment	Aircraft 1 Heading (degrees)				Aircraft 2 Heading (degrees)			
	Approach		Departure		Approach		Departure	
	Lateral	Vertical	Lateral	Vertical	Lateral	Vertical	Lateral	Vertical
85	0	30	90	-30	0	-30	90	30
86	0	30	90	-30	0	-30	-45	30
87	0	30	90	-30	0	-30	0	30
88	0	30	90	-30	0	-30	45	30
89	0	30	90	-30	0	-30	-90	30
90	0	30	-45	-30	0	-30	-45	30
91	0	30	-45	-30	0	-30	0	30
92	0	30	-45	-30	0	-30	45	30
93	0	30	0	-30	0	-30	0	30
94	0	30	0	-30	45	-30	-45	30
95	0	30	45	-30	45	-30	-45	30
96	0	30	45	-30	45	-30	0	30
97	0	30	-90	-30	45	-30	-45	30
98	0	30	-90	-30	90	-30	0	30

Table 3.19: Scenario 3 Test Design - 4 Dimensional Configuration 8.

Treatment	Aircraft 1 Heading (degrees)				Aircraft 2 Heading (degrees)			
	Approach		Departure		Approach		Departure	
	Lateral	Vertical	Lateral	Vertical	Lateral	Vertical	Lateral	Vertical
99	0	30	90	-30	0	-30	90	-30
100	0	30	90	-30	0	-30	-45	-30
101	0	30	90	-30	0	-30	0	-30
102	0	30	90	-30	0	-30	45	-30
103	0	30	90	-30	0	-30	-90	-30
104	0	30	-45	-30	0	-30	-45	-30
105	0	30	-45	-30	0	-30	0	-30
106	0	30	-45	-30	0	-30	45	-30
107	0	30	0	-30	0	-30	0	-30
108	0	30	0	-30	45	-30	-45	-30
109	0	30	45	-30	45	-30	-45	-30
110	0	30	45	-30	45	-30	0	-30
111	0	30	-90	-30	45	-30	-45	-30
112	0	30	-90	-30	90	-30	0	-30

The second test was designed to determine the maximum value that each approximation method's parameter can obtain before causing computational difficulties with the numerical methods used to evaluate the multi-objective HCS optimization problem. Thus, for every treatment generated for the accuracy test, the gradient of each constraint approximation method was estimated at every interior point of the state space using Matlab's central difference numerical gradient estimation function.

For each treatment, the proportion of grid points that resulted in a numerical gradient estimator output of "Inf" (infinity), "-Inf" or "NaN" was calculated for each value of the Multiplier Method accuracy parameter $\gamma \in \{1, 5, 10, 50, 100, 500\}$, while the priority parameter λ was set to $\left(\sqrt{2} - 1\right)$. This procedure was also applied to the sigmoid, p-norm, and exponential p-norm constraint approximations. Table 3.1 displays the approximation parameter values tested for each treatment.

3.1.3 Phase and Variable Arrival Sequence Formulation.

The intermediate state, control and ATM separation constraints given by equations (3.76) - (3.16) introduce *phases* to the multi-objective HCS optimization problem, as described in Section 2.4.2. Additionally, equations (3.2) - (3.7) imply that the arrival sequence is *variable*, as described in Section 2.2.3 and Section 2.2.4. This section details a method of formulating the multi-objective HCS optimization problem to account for phases and variable arrival sequences.

3.1.3.1 Shadow Time Overshoot Phase Model.

The *Shadow Time Overshoot Phase (STOP)* model proposes to satisfy the intermediate state, control and ATM separation constraints given by equations (3.76) - (3.16) by transforming the problem into a *fixed final time* problem through the use of a *shadow time* state variable. For the multi-objective HCS ATM problem without inertia, the single shadow time state variable is governed by the dynamic equation

$$\frac{d}{dt}\tau_{[\mu]}(t) = 1, \tag{3.46}$$

where $\tau_{[\mu]}(t)$ is the shadow time state of control mode μ at time t. Since the multi-objective HCS ATM problem assumes arrival times are not necessarily fixed, for each aircraft α the STOP model

defines its arrival time as the continuous decision variable $t_{[f,\alpha]}$, such that

$$t_{[f,\alpha]_{\min}} \leq t_{[f,\alpha]} \leq t_{[f,\alpha]_{\max}}, \quad \forall \alpha \in \{1, 2, \ldots, A\}, \tag{3.47}$$

where $t_{[f,\alpha]_{\min}}$ is the earliest allowable arrival time for aircraft α and $t_{[f,\alpha]_{\max}}$ is the latest allowable arrival time for aircraft α. Constraint (3.47) provides a lower bound for the fixed final time for the problem, so that

$$t_f \geq \left(\max\left\{t_{[f,1]_{\max}}, \ldots, t_{[f,A]_{\max}}\right\}\right), \tag{3.48}$$

which generates the constraints added to impose the intermediate state and control constraints:

$$0 \leq \tau_{[\mu]}(t) \leq t_f, \tag{3.49a}$$

$$\left(l_{[\mu,\alpha]} - c_{[\mu,\alpha]}(t)\right)\left(t - t_{[f,\alpha]}\right) \leq 0, \quad \forall \alpha \in \{1, 2, \ldots, A\}, \tag{3.49b}$$

Constraint (3.49b) guarantees that every feasible solution to the STOP model problem has only on-time arrivals, defined as

$$c_{[\mu,\alpha]}(t_{[f,\alpha]}) = l_{[\mu,\alpha]}. \tag{3.50}$$

For example, suppose $c_{[\mu,\alpha]}(t_{[f,\alpha]}) < l_{[\mu,\alpha]}$, which implies a late arrival. If $\frac{d}{dt}c_{[\mu,\alpha]}(t) > 0$, $\forall t > t_{[0,\alpha]}$, as indicated by equations (3.9) and (3.76), then there exists some $\varepsilon > 0$ such that $t = t_{[f,\alpha]} + \varepsilon$ and $c_{[\mu,\alpha]}(t) < l_{[\mu,\alpha]}$. Therefore,

$$\begin{aligned} & l_{[\mu,\alpha]} - c_{[\mu,\alpha]}(t) > 0, \\ & t - t_{[f,\alpha]} > 0 \\ \implies \quad & \left(l_{[\mu,\alpha]} - c_{[\mu,\alpha]}(t)\right)\left(t - t_{[f,\alpha]}\right) > 0, \end{aligned}$$

so constraint (3.49b) would be violated.

On the other hand, suppose there exists some $\varepsilon > 0$ such that $t = t_{[f,\alpha]} - \varepsilon$ and $c_{[\mu,\alpha]}(t) = l_{[\mu,\alpha]}$, which would imply an early arrival. If $\frac{d}{dt}c_{[\mu,\alpha]}(t) > 0$, $\forall t > t_{[0,\alpha]}$, as indicated by equations (3.9) and (3.76), then there exists some $\hat{\varepsilon} > 0$ such that $\hat{t} = t_{[f,\alpha]} - \varepsilon + \hat{\varepsilon} < t_{[f,\alpha]}$ and $c_{[\mu,\alpha]}(\hat{t}) > l_{[\mu,\alpha]}$. Therefore,

$$\begin{aligned} & l_{[\mu,\alpha]} - c_{[\mu,\alpha]}(\hat{t}) < 0, \\ & \hat{t} - t_{[f,\alpha]} < 0 \\ \implies \quad & \left(l_{[\mu,\alpha]} - c_{[\mu,\alpha]}(\hat{t})\right)\left(\hat{t} - t_{[f,\alpha]}\right) > 0, \end{aligned}$$

so constraint (3.49b) would be violated. Thus, early and late arrivals violate constraint (3.49b).

Suppose $t = t_{[f,\alpha]}$ and $c_{[\mu,\alpha]}(t) = l_{[\mu,\alpha]}$, which defines an on-time arrival. Then,

$$\begin{aligned} l_{[\mu,\alpha]} - c_{[\mu,\alpha]}(t) &= 0, \\ t - t_{[f,\alpha]} &= 0 \\ \implies \quad \Big(l_{[\mu,\alpha]} - c_{[\mu,\alpha]}(t)\Big)\Big(t - t_{[f,\alpha]}\Big) &= 0, \end{aligned}$$

so constraint (3.49b) would be satisfied. Additionally, if $c_{[\mu,\alpha]}(t) = l_{[\mu,\alpha]}$ for $t = t_{[f,\alpha]}$ and $\frac{d}{dt}c_{[\mu,\alpha]}(t) > 0$, $\forall t > t_{[0,\alpha]}$, then there exists some $\hat{t} < t_{[f,\alpha]}$ such that $c_{[\mu,\alpha]}(t) < l_{[\mu,\alpha]}$. Therefore,

$$\begin{aligned} l_{[\mu,\alpha]} - c_{[\mu,\alpha]}(\hat{t}) &> 0, \\ \hat{t} - t_{[f,\alpha]} &< 0 \\ \implies \quad \Big(l_{[\mu,\alpha]} - c_{[\mu,\alpha]}(\hat{t})\Big)\Big(\hat{t} - t_{[f,\alpha]}\Big) &< 0, \end{aligned}$$

so constraint (3.49b) would be satisfied. And, if $c_{[\mu,\alpha]}(t) = l_{[\mu,\alpha]}$ for $t = t_{[f,\alpha]}$ and $\frac{d}{dt}c_{[\mu,\alpha]}(t) > 0$, $\forall t > t_{[0,\alpha]}$, then there exists some $t^* > t_{[f,\alpha]}$ such that $c_{[\mu,\alpha]}(t^*) > l_{[\mu,\alpha]}$. Therefore,

$$\begin{aligned} l_{[\mu,\alpha]} - c_{[\mu,\alpha]}(t^*) &< 0, \\ t^* - t_{[f,\alpha]} &> 0 \\ \implies \quad \Big(l_{[\mu,\alpha]} - c_{[\mu,\alpha]}(t^*)\Big)\Big(t^* - t_{[f,\alpha]}\Big) &< 0, \end{aligned}$$

so constraint (3.49b) would be satisfied.

Since the STOP model does not induce a change in dynamics after an aircraft's arrival time, each aircraft is modeled to continue along its path even after its chosen arrival time. That is, each aircraft is allowed to *overshoot* its destination. Figure 3.21 displays how this overshoot affects constraint (3.49b) (in red) and forces feasible solutions to have aircraft reach their destination precisely at their arrival time.

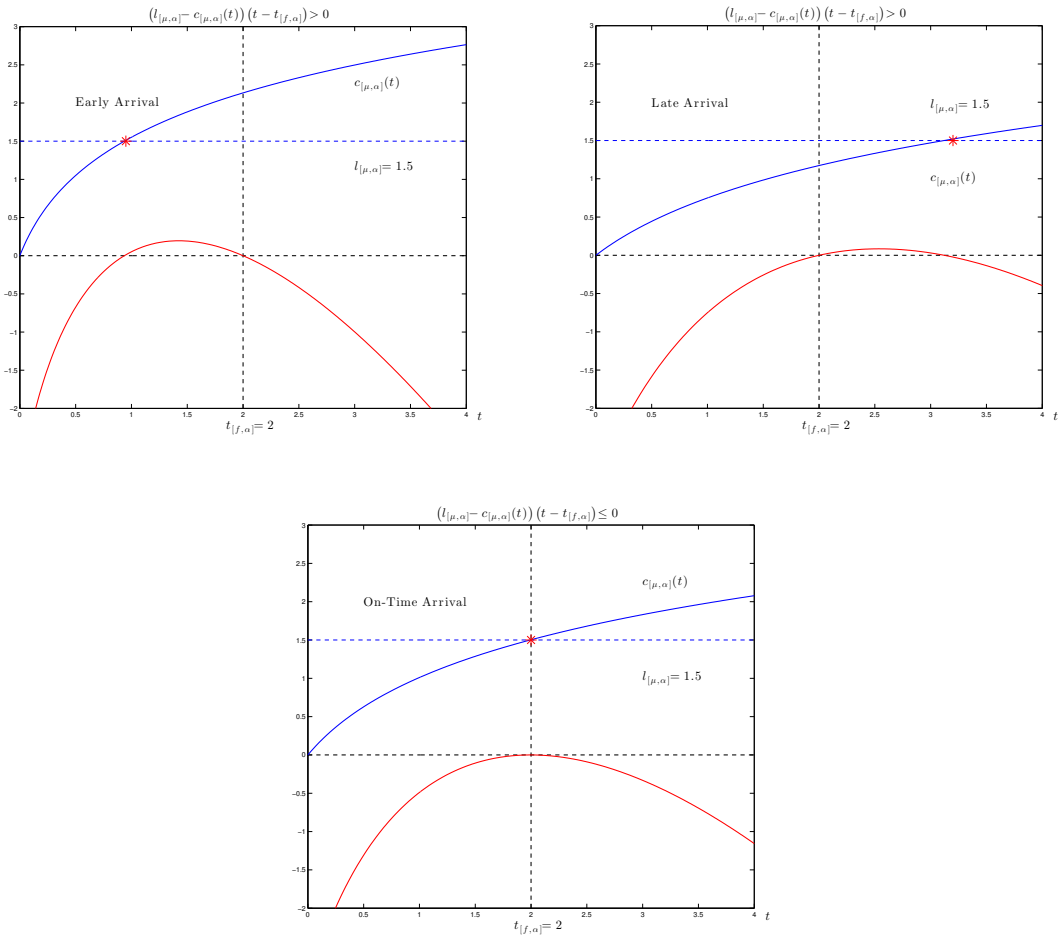

Figure 3.21: Arrival Time Constraint with Overshoot

Nonetheless, due to the overshoot, it is necessary to adjust the intermediate ATM separation constraints for the STOP model. Given equations (3.10) - (3.12) and Algorithm 3.1, for each pair of aircraft (α_1, α_2) such that $\alpha_1 \in \{1, 2, \ldots, A\}$, $\alpha_1 \in \{1, 2, \ldots, A\}$ and $\alpha_1 \neq \alpha_2$, the STOP model ATM separation constraint function is defined as

$$G^{\text{STOP}}_{\alpha_1,\alpha_2}(t) \triangleq \Big(S_{\alpha_1}(t)\Big)\Big(S_{\alpha_2}(t)\Big) - \max\left\{\frac{\Big(x_{\alpha_1}(t) - x_{\alpha_2}(t)\Big)^2 + \Big(y_{\alpha_1}(t) - y_{\alpha_2}(t)\Big)^2}{r(t)^2}, \frac{\Big(z_{\alpha_1}(t) - z_{\alpha_2}(t)\Big)^2}{h^2}\right\}, \tag{3.51}$$

where the indicator functions S_{α_1} and S_{α_2} are defined such that

$$S_{\alpha_1}(t) = \begin{cases} 1 & \text{if } c_{[\mu,\alpha_1]}(t) < l_{[\mu,\alpha_1]}(t), \\ 0 & \text{if } c_{[\mu,\alpha_1]}(t) \geq l_{[\mu,\alpha_1]}(t), \end{cases} \tag{3.52a}$$

and

$$S_{\alpha_2}(t) = \begin{cases} 1 & \text{if } c_{[\mu,\alpha_2]}(t) < l_{[\mu,\alpha_2]}(t), \\ 0 & \text{if } c_{[\mu,\alpha_1]}(t) \geq l_{[\mu,\alpha_1]}(t). \end{cases} \tag{3.52b}$$

However, since constraint (3.49b) guarantees that for feasible solutions

$$c_{[\mu,\alpha_1]}(t) < l_{[\mu,\alpha_1]}(t) \iff t < t_{[f,\alpha]}$$

and

$$c_{[\mu,\alpha_1]}(t) \geq l_{[\mu,\alpha_1]}(t) \iff t \geq t_{[f,\alpha]},$$

the indicator functions may also be defined such that

$$S_{\alpha_1}(t) = \begin{cases} 1 & \text{if } t < t_{[f,\alpha_1]}, \\ 0 & \text{if } t \geq t_{[f,\alpha_1]}, \end{cases} \tag{3.53a}$$

and

$$S_{\alpha_2}(t) = \begin{cases} 1 & \text{if } t < t_{[f,\alpha_2]}, \\ 0 & \text{if } t \geq t_{[f,\alpha_2]}. \end{cases} \tag{3.53b}$$

When the ATM separation constraint is approximated with a sigmoid function, $S_{\alpha_1}(t)$ and $S_{\alpha_2}(t)$ can also be approximated as sigmoid functions defined by the accuracy parameter $\mathsf{s} > 0$,

$$\hat{S}_{\alpha_1}(t) \triangleq \left(1 + e^{\mathsf{s}\left(c_{[\mu,\alpha_1]}(t) - l_{[\mu,\alpha_1]}\right)}\right)^{-1} \tag{3.54a}$$

and

$$\hat{S}_{\alpha_2}(t) \triangleq \left(1 + e^{\mathsf{s}\left(c_{[\mu,\alpha_2]}(t) - l_{[\mu,\alpha_2]}\right)}\right)^{-1}, \tag{3.54b}$$

such that

$$\hat{S}_{\alpha_1}(t) \approx \begin{cases} 1 & \text{if } c_{[\mu,\alpha_1]}(t) < l_{[\mu,\alpha_1]}(t), \\ 0 & \text{if } c_{[\mu,\alpha_1]}(t) \geq l_{[\mu,\alpha_1]}(t), \end{cases} \tag{3.55a}$$

and

$$\hat{S}_{\alpha_2}(t) \approx \begin{cases} 1 & \text{if } c_{[\mu,\alpha_2]}(t) < l_{[\mu,\alpha_2]}(t), \\ 0 & \text{if } c_{[\mu,\alpha_1]}(t) \geq l_{[\mu,\alpha_1]}(t). \end{cases} \tag{3.55b}$$

However, due to constraint (3.49b), $S_{\alpha_1}(t)$ and $S_{\alpha_2}(t)$ may also be approximated by

$$\hat{S}_{\alpha_1}(t) \triangleq \left(1 + e^{\mathsf{s}\left(t - t_{[f,\alpha_1]}\right)}\right)^{-1} \tag{3.56a}$$

and

$$\hat{S}_{\alpha_2}(t) \triangleq \left(1 + e^{\mathsf{s}\left(t - t_{[f,\alpha_2]}\right)}\right)^{-1}, \tag{3.56b}$$

such that

$$\hat{S}_{\alpha_1}(t) \approx \begin{cases} 1 & \text{if } t < t_{[f,\alpha_1]}, \\ 0 & \text{if } t \geq t_{[f,\alpha_1]}, \end{cases} \tag{3.57a}$$

and

$$\hat{S}_{\alpha_2}(t) \approx \begin{cases} 1 & \text{if } t < t_{[f,\alpha_2]}, \\ 0 & \text{if } t \geq t_{[f,\alpha_1]}. \end{cases} \tag{3.57b}$$

Therefore, from the arrival time constraint (3.49b),

$$G^{\text{STOP}}_{\alpha_1,\alpha_2}(t) \approx \begin{cases} G^{\text{ATM}}_{\alpha_1,\alpha_2}(t) & \text{if } t < \min\left\{t_{[f,\alpha_1]}, t_{[f,\alpha_2]}\right\}, \\ 0 & \text{if } t \geq \min\left\{t_{[f,\alpha_1]}, t_{[f,\alpha_2]}\right\}. \end{cases} \tag{3.58}$$

Thus, before an aircraft has reached its destination, it must satisfy the original pair-wise ATM separation constraint, but after it has reached its destination, it can no longer cause ATM separation conflicts.

The inclusion of two additional sigmoid functions into the sigmoid ATM separation constraint approximation would force the constraint approximation to be given as

$$-\left(2^{-4}\right) + \left(\hat{S}_{\alpha_1}(t)\right)\left(\hat{S}_{\alpha_2}(t)\right)\left(\frac{1}{1 + e^{-\mathsf{s}g_1(t)}}\right)\left(\frac{1}{1 + e^{-\mathsf{s}g_2(t)}}\right) \leq 0, \tag{3.59}$$

where

$$g_1(t) = r(t)^2 - \left(\left(x_{\alpha_1}(t) - x_{\alpha_2}(t)\right)^2 + \left(y_{\alpha_1}(t) - y_{\alpha_2}(t)\right)^2\right) \tag{3.60a}$$

and

$$g_2(t) = h^2 - \left(z_{\alpha_1}(t) - z_{\alpha_2}(t)\right)^2. \tag{3.60b}$$

The sigmoid multipliers from equation (3.54) or (3.56) were also included in the STOP model objective function to minimize the effect of each aircraft's overshoot in the optimization problem.

The exact indicator functions from equations (3.52) and (3.53) were not included since they would induce non-differentiability into the objective function. Therefore, given the set of scheduled arrival times,

$$\mathbf{t}_S = \left\{t_{[S,1]}, \ldots, t_{[S,A]}\right\}, \tag{3.61}$$

with minimum allowable arrival times,

$$\mathbf{t}_{[f,\min]} = \left\{t_{[f,1]_{\min}}, \ldots, t_{[f,A]_{\min}}\right\}, \tag{3.62}$$

and maximum allowable arrival times,

$$\mathbf{t}_{[f,\max]} = \left\{t_{[f,1]_{\max}}, \ldots, t_{[f,A]_{\max}}\right\}, \tag{3.63}$$

the STOP model form of the generalized weighted-sum HCS ATM optimization problem without inertia is given as

minimize

$$\lambda_1^{\beta_1}\left(\sum_{\alpha=1}^{A}\left[\int_{t_{[0,\alpha]}}^{t_f}\left[S_\alpha(t)u_{[\mu,\alpha]}(t)\right]^2 dt\right)^{\lambda_1^{1-\beta_1}}\right. \tag{3.64a}$$

$$+\lambda_2^{\beta_2}\left(\kappa_2 + \sum_{\alpha=1}^{A}\left[t_{[f,\alpha]} - t_{[S,\alpha]}\right]^2\right)^{\lambda_2^{1-\beta_2}} \tag{3.64b}$$

$$+\lambda_3^{\beta_3}\left(\kappa_3 + \sum_{\alpha=1}^{A}\left[t_{[f,\alpha]} - t_{[f,\alpha]_{\min}}\right]^2\right)^{\lambda_3^{1-\beta_3}} \tag{3.64c}$$

subject to:

1. The boundary conditions,

$$t_f \geq \max\left\{t_{[f,1]_{\max}}, \ldots, t_{[f,A]_{\max}}\right\}, \tag{3.65a}$$

$$t_{[0,\alpha]} = 0, \quad \forall\alpha \in \{1, 2, \ldots, A\}, \tag{3.65b}$$

$$t_{[f,\alpha]_{\min}} \leq t_{[f,\alpha]} \leq t_{[f,\alpha]_{\max}}, \quad \forall\alpha \in \{1, 2, \ldots, A\}, \tag{3.65c}$$

$$c_{[\mu,\alpha]}\left(t_{[0,\alpha]}\right) = c_{[\min,\alpha]}, \quad \forall\alpha \in \{1, 2, \ldots, A\}, \tag{3.65d}$$

$$c_{[\mu,\alpha]}\left(t_{[f,\alpha]}\right) = l_{[\mu,\alpha]}, \quad \forall\alpha \in \{1, 2, \ldots, A\}, \tag{3.65e}$$

2. The dynamic equations,

$$\frac{d}{dt}\tau_{[\mu]}(t) = 1, \tag{3.66a}$$

$$\frac{d}{dt}c_{[\mu,\alpha]}(t) = u_{[\mu,\alpha]}(t), \quad \forall\alpha \in \{1, 2, \ldots, A\}, \tag{3.66b}$$

$$u_{[\min,\alpha]} \leq u_{[\mu,\alpha]}(t) \leq u_{[\max,\alpha]}, \quad \forall\alpha \in \{1, 2, \ldots, A\}, \tag{3.66c}$$

3. The STOP form of the intermediate constraints,

$$0 \leq \tau_{[\mu]}(t) \leq t_f, \tag{3.67a}$$

$$\Big(l_{[\mu,\alpha]} - c_{[\mu,\alpha]}(t)\Big)\Big(t - t_{[f,\alpha]}\Big) \leq 0, \quad \forall\alpha \in \{1, 2, \ldots, A\}, \tag{3.67b}$$

4. The STOP form of the ATM separation constraints,

$$\Big(S_{\alpha_1}(t)\Big)\Big(S_{\alpha_2}(t)\Big) - \max\left\{\frac{\Big(x_{\alpha_1}(t)-x_{\alpha_2}(t)\Big)^2+\Big(y_{\alpha_1}(t)-y_{\alpha_2}(t)\Big)^2}{r(t)^2}, \frac{\Big(z_{\alpha_1}(t)-z_{\alpha_2}(t)\Big)^2}{h^2}\right\} \leq 0, \tag{3.68}$$

for each pair of aircraft (α_1, α_2) such that $\alpha_1 \in \{1, 2, \ldots, A\}$, $\alpha_1 \in \{1, 2, \ldots, A\}$ and $\alpha_1 \neq \alpha_2$, which may be approximated with any method described in Section 3.1.2.

3.1.4 Multi-Objective Implementation and Testing.

This section describes notional example multi-objective HCS ATM problems, and details how they were evaluated using the STOP method described in Section 3.1.3.1 to demonstrate the ability of the STOP method to generate feasible control strategies.

3.1.4.1 Notional Air Traffic Test Cases.

This section details the three notional air traffic test cases that were evaluated as multi-objective HCS ATM problems using the STOP method. These test cases are based on the example problems presented in [74].

1. The first test case is defined as three aircraft flying in the plane with no change in altitude. Table 3.20 defines the three-dimensional position of each airspace waypoint as a node in the airspace graph, and Table 3.21 provides the graph's node adjacency matrix, so that the graph arcs represent airspace path segments. Figure 3.22 displays the resulting airspace paths, while Table 3.22 defines the air traffic control mode for the test case; that is, it defines the

path selected for each aircraft, as well as the initial path length coordinate of each aircraft's *origination* and the final path length coordinate of each aircraft's *destination*. Table 3.23 provides the schedule and control constraints for the first test case. The unitless minimum allowable lateral separation for the first test case was set to $r(t) = 0.3$, and the unitless minimum allowable vertical separation for the first test case was set to $h = 0.02$. Figure 3.23 displays the resulting state space conflict region.

Table 3.20: Test Case 1 Notional Airspace Graph Nodes (No Units).

Waypoint	Coordinate Value		
	x	y	z
v_1	-1	0	0
v_2	-1	-1	0
v_3	0	1	0
v_4	1	0	0
v_5	1	-1	0

Table 3.21: Test Case 1 Graph Adjacency Matrix.

	v_1	v_2	v_3	v_4	v_5
v_1	0	0	0	1	0
v_2	0	0	1	0	0
v_3	0	0	0	0	0
v_4	0	0	0	0	0
v_5	0	0	1	0	0

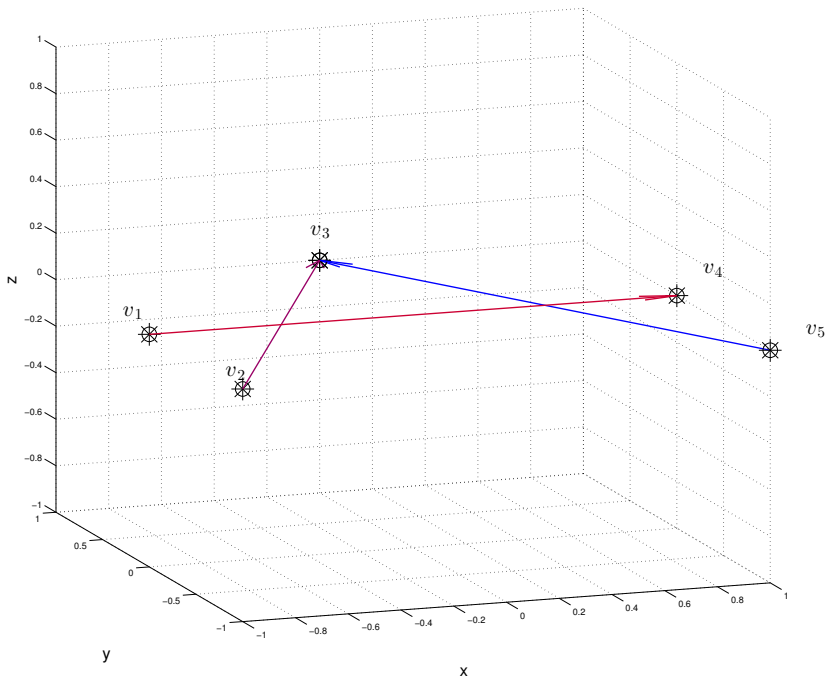

Figure 3.22: Notional Airspace Paths for Test Case 1

Table 3.22: Test Case 1 Notional Air Traffic Paths (No Units).

Aircraft (α)	Path $\left(P_{\mu,\alpha}\right)$	Origination $\left(c_{[\mu,\alpha]}(0)\right)$	Destination $\left(l_{[\mu,\alpha]}\right)$
1	(v_2, v_3)	0	$\sqrt{5}$
2	(v_5, v_3)	0	$\sqrt{5}$
3	(v_1, v_4)	0	2

Table 3.23: Test Case 1 Notional Air Traffic Constraints (No Units).

Aircraft (α)	Minimum Speed ($u_{[\min,\alpha]}$)	Maximum Speed ($u_{[\max,\alpha]}$)	Departure Time ($t_{[0,\alpha]}$)	Scheduled Arrival ($t_{[S,\alpha]}$)	Earliest Arrival $\left(t_{[f,\alpha]_{\min}}\right)$	Latest Arrival $\left(t_{[f,\alpha]_{\max}}\right)$
1	0.3	1.5	0	2	1	3
2	0.3	0.8	0	3	2	4
3	0.4	0.9	0	4	3	5

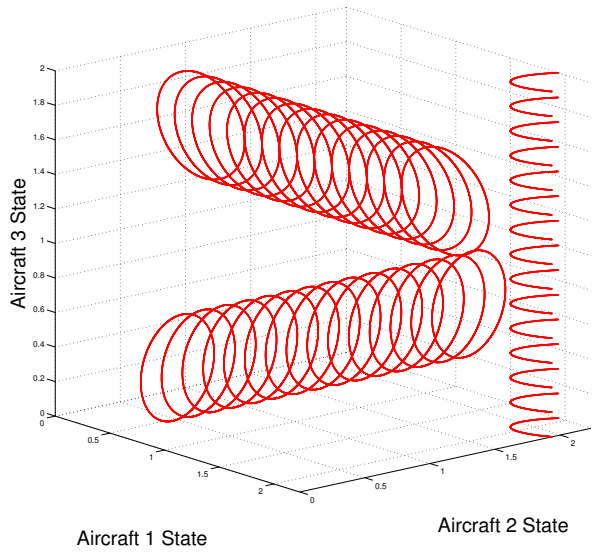

Figure 3.23: Notional State Space Conflict Regions for Test Case 1

2. The second test case is defined as three aircraft flying in the plane with no change in altitude for only Aircraft 3. Table 3.24 defines the three-dimensional position of each airspace waypoint as a node in the airspace graph, and Table 3.25 provides the graph's node adjacency matrix, so that the graph arcs represent airspace path segments. Figure 3.24 displays the resulting airspace paths, while Table 3.26 defines the control mode for the test case; that is,

it defines the path selected for each aircraft, as well as the initial path length coordinate of each aircraft's *origination* and the final path length coordinate of each aircraft's *destination*. Table 3.27 provides the schedule and control constraints for the second test case. The unitless minimum allowable lateral separation for the second test case was set to $r(t) = 0.3$, and the unitless minimum allowable vertical separation for the second test case was set to $h = 0.02$. Figure 3.25 displays the resulting state space conflict region.

Table 3.24: Test Case 2 Notional Airspace Graph Nodes (No Units).

Waypoint	Coordinate Value		
	x	y	z
v_1	-1	0	0
v_2	-1	-1	0.025
v_3	0	1	0
v_4	1	0	0.025
v_5	1	-1	0

Table 3.25: Test Case 2 Graph Adjacency Matrix.

	v_1	v_2	v_3	v_4	v_5
v_1	0	0	0	1	0
v_2	0	0	1	0	0
v_3	0	0	0	0	0
v_4	0	0	0	0	0
v_5	0	0	1	0	0

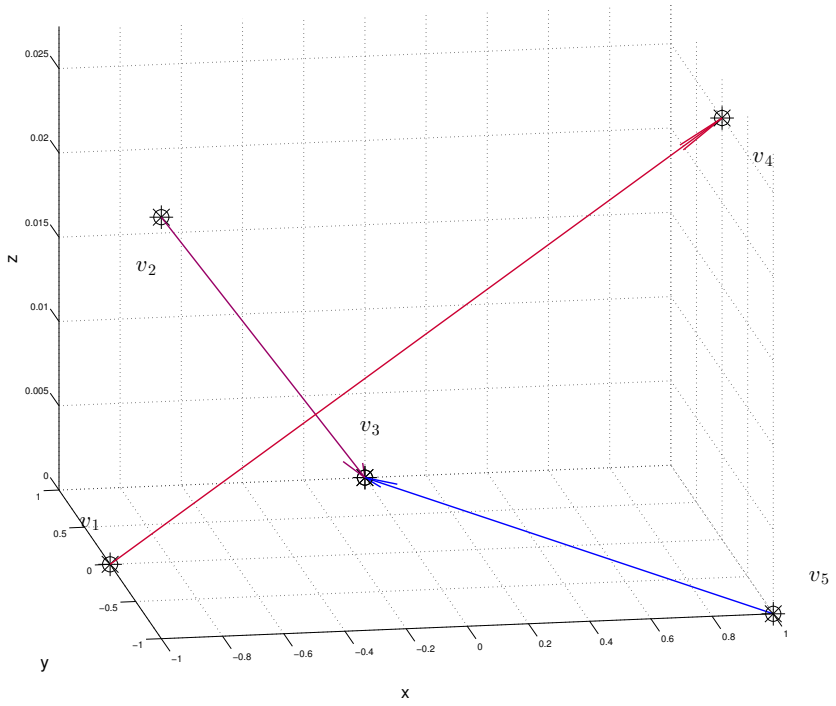

Figure 3.24: Notional Airspace Paths for Test Case 2

Table 3.26: Test Case 2 Notional Air Traffic Paths (No Units).

Aircraft (α)	Path $\left(P_{\mu,\alpha}\right)$	Origination $\left(c_{[\mu,\alpha]}(0)\right)$	Destination $\left(l_{[\mu,\alpha]}\right)$
1	(v_2, v_3)	0	2.2362
2	(v_5, v_3)	0	$\sqrt{5}$
3	(v_1, v_4)	0	2.0002

Table 3.27: Test Case 2 Notional Air Traffic Constraints (No Units).

Aircraft (α)	Minimum Speed ($u_{[\min,\alpha]}$)	Maximum Speed ($u_{[\max,\alpha]}$)	Departure Time ($t_{[0,\alpha]}$)	Scheduled Arrival ($t_{[S,\alpha]}$)	Earliest Arrival $\left(t_{[f,\alpha]_{\min}}\right)$	Latest Arrival $\left(t_{[f,\alpha]_{\max}}\right)$
1	0.3	1.5	0	2	1	3
2	0.3	0.8	0	3	2	4
3	0.4	0.9	0	4	3	5

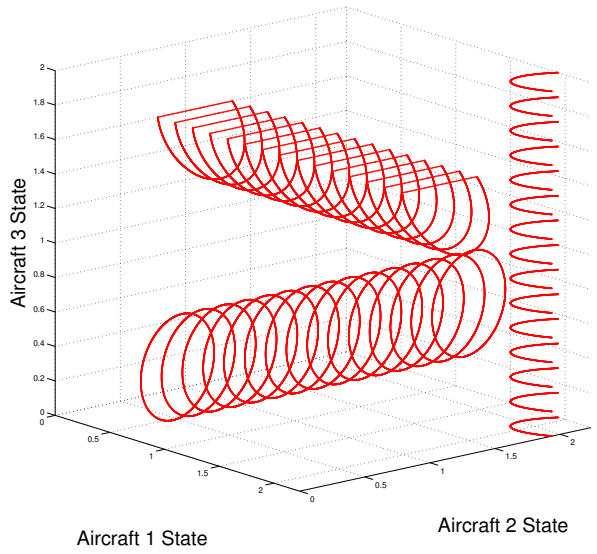

Figure 3.25: Notional State Space Conflict Regions for Test Case 2

3. The third test case is defined as three aircraft flying in the plane with no change in altitude for only Aircraft 3. Table 3.28 defines the three-dimensional position of each airspace waypoint as a node in the airspace graph, and Table 3.29 provides the graph's node adjacency matrix, so that the graph arcs represent airspace path segments. Figure 3.26 displays the resulting airspace paths, while Table 3.30 defines the control mode for the test case; that is, it defines

the path selected for each aircraft, as well as the initial path length coordinate of each aircraft's *origination*) and the final path length coordinate of each aircraft's *destination*. Table 3.31 provides the schedule and control constraints for the third test case. The unitless minimum allowable lateral separation for the third test case was set to $r(t) = 0.3$, and the unitless minimum allowable vertical separation for the third test case was set to $h = 0.02$. Figure 3.27 displays the resulting state space conflict region.

Table 3.28: Test Case 3 Notional Airspace Graph Nodes (No Units).

Waypoint	Coordinate Value		
	x	y	z
v_1	-1	0	0
v_2	-1	-1	0.025
v_3	0	1	0
v_4	1	0	0.025
v_5	1	-1	0.025
v_6	0	2	-0.025

Table 3.29: Test Case 3 Graph Adjacency Matrix.

	v_1	v_2	v_3	v_4	v_5	v_6
v_1	0	0	0	1	0	0
v_2	0	0	1	0	0	0
v_3	0	0	0	0	0	1
v_4	0	0	0	0	0	0
v_5	0	0	1	0	0	0
v_6	0	0	0	0	0	0

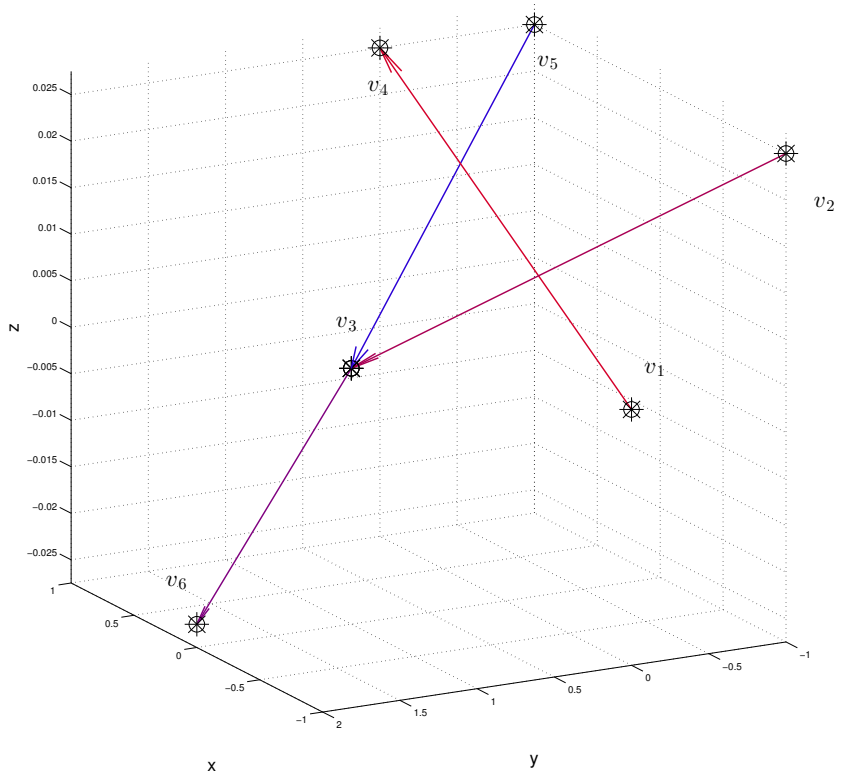

Figure 3.26: Notional Airspace Paths for Test Case 3

Table 3.30: Test Case 3 Notional Air Traffic Paths (No Units).

Aircraft (α)	Path $\left(P_{\mu,\alpha}\right)$	Origination $\left(c_{[\mu,\alpha]}(0)\right)$	Destination $\left(l_{[\mu,\alpha]}\right)$
1	(v_2, v_3, v_6)	0	3.2365
2	(v_5, v_3, v_6)	0	3.2365
3	(v_1, v_4)	0	2.0002

Table 3.31: Test Case 3 Notional Air Traffic Constraints (No Units).

Aircraft (α)	Minimum Speed ($u_{[\min,\alpha]}$)	Maximum Speed ($u_{[\max,\alpha]}$)	Departure Time ($t_{[0,\alpha]}$)	Scheduled Arrival ($t_{[S,\alpha]}$)	Earliest Arrival $\left(t_{[f,\alpha]_{\min}}\right)$	Latest Arrival $\left(t_{[f,\alpha]_{\max}}\right)$
1	0.3	1.5	0	3	2	4
2	0.3	0.8	0	4	3	5
3	0.4	0.9	0	4	3	5

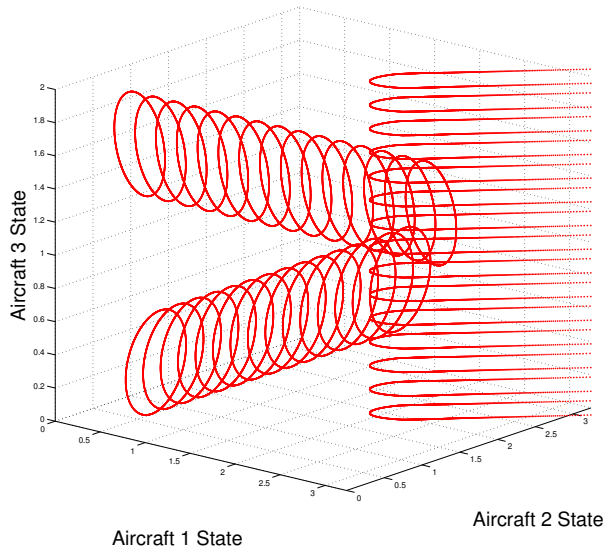

Figure 3.27: Notional State Space Conflict Regions for Test Case 3

3.1.4.2 Test Case Evaluation.

Each test case defined in Section 3.1.4.1 was evaluated using the STOP formulation of the generalized weighted-sum representation of the multi-objective HCS ATM problem using both the arrival time and final state forms of the adjusted ATM separation constraint. Analysis of the initial screening tests on the parameters of the generalized weighted-sum objective given in equation (3.64)

indicated that setting $t_f = 1.2 \times \max\left\{t_{[f,1]_{\max}}, \ldots, t_{[f,A]_{\max}}\right\}$, with $\kappa_2 = \kappa_3 = \min\left(t_{[f,\alpha]_{\min}}\right)$ and varying the values of λ_1, λ_2, and λ_3 according to the values given in Table 3.32 was most likely to generate locally optimal solutions. Therefore, Table 3.32 displays the unique combinations (or *treatments*) of λ_1, λ_2, λ_3 that were evaluated with each ATM separation constraint approximation. For each treatment, the STOP generalized weighted-sum objective function, defined in equation (3.64), was minimized using the GPOPS-II Matlab optimization package running on Mac OS 10.9.4 with a 2.8 GHz Intel Core i5 processor and 8GB of RAM. The GPOPS-II settings that were used for the optimization are detailed in Appendix C. For each treatment, the control strategies, state trajectories and arrival times that satisfied the GPOPS-II local optimality conditions were recorded. The time required to generate each treatment's locally optimal solution, as well as the total deviation from scheduled arrival time, makespan, and the total control cost associated with each treatment's locally optimal solution were also recorded.

Table 3.32: Generalized weighted-sum Parameter Design for Notional ATM Cases.

Treatment	λ_1	β_1	λ_2	β_2	λ_3	β_3
1	5.5	1	10	0	10	0
2	5.5	1	10	0	0.1	0
3	5.5	1	10	0	0	0
4	5.5	1	0.1	0	10	0
5	5.5	1	0.1	0	0.1	0
6	5.5	1	0.1	0	0	0
7	5.5	1	0	0	10	0
8	5.5	1	0	0	0.1	0
9	5.5	1	0	0	0	0
10	5	1	10	0	10	0
11	5	1	10	0	0.1	0
12	5	1	10	0	0	0
13	5	1	0.1	0	10	0
14	5	1	0.1	0	0.1	0
15	5	1	0.1	0	0	0
16	5	1	0	0	10	0
17	5	1	0	0	0.1	0
18	5	1	0	0	0	0

3.2 Control Mode Modifications

This section describes how the effects of modifications to the current control mode, including the addition of new waypoints, were investigated.

3.2.1 Additional Waypoints.

The conflict region of a three-dimensional control mode can be reduced if the vertical separation between pre-defined paths is increased. For example, Test Case 2 from Section 3.1.4.1 is

nearly identical to Test Case 1 from Section 3.1.4.1, except that the z-coordinate value of waypoints v_2 and v_4 of Test Case 2 is 0.025, while the z-coordinate value of waypoints v_2 and v_4 of Test Case 1 is 0. Nonetheless, these small changes in the waypoint definitions result in a reduction in the conflict region and an increase in the path length, as observed in a comparison between Figure 3.23 and Figure 3.25. However, the small physical differences between Test Case 1 and Test Case 2 reflect a fundamental difference between the two cases, since the *origination* of aircraft 1 of Test Case 1 differs from the origination of aircraft 1 of Test Case 2, and the *destination* of aircraft 3 of Test Case 1 is differs from the destination of aircraft 3 of Test Case 2. This is due to the fact that neither graph from Test Case 1 nor Test Case 2 includes an *intermediate* waypoint; all waypoints in both test cases are either originations or destinations. However, Test Case 3 from Section 3.1.4.1 includes an intermediate waypoint, v_3. Therefore, it was selected to study the impact of additional waypoints on feasible and optimal control strategies.

3.2.1.1 Modified Notional Air Traffic Test Cases.

This section details the two modified notional air traffic test cases that were evaluated as multi-objective HCS ATM problems using the STOP method to compare to the original Test Case 3 from Section 3.1.4.1.

1. The first test case is defined identically to the *third* test case from Section 3.1.4.1, except that a new waypoint is included above waypoint v_3 as a replacement waypoint for aircraft 1. Table 3.33 defines the three-dimensional position of each airspace waypoint as a node in the airspace graph, and Table 3.34 provides the graph's node adjacency matrix, so that the graph arcs represent airspace path segments. Figure 3.28 displays the resulting airspace paths, while Table 3.35 defines the air traffic control mode for the test case; that is, it defines the path selected for each aircraft, as well as the initial path length coordinate of each aircraft's *origination* and the final path length coordinate of each aircraft's *destination*. Table 3.36 provides the schedule and control constraints for the first test case. The unitless minimum allowable lateral separation for the first test case was set to $r(t) = 0.3$, and the unitless minimum allowable vertical separation for the first test case was set to $h = 0.02$. Figure 3.29 displays the resulting state space conflict region.

Table 3.33: Test Case 3 Modification 1 Notional Airspace Graph Nodes (No Units).

Waypoint	Coordinate Value		
	x	y	z
v_1	-1	0	0
v_2	-1	-1	0.025
v_3	0	1	0
v_4	0	1	0.020
v_5	1	0	0.025
v_6	1	-1	0.025
v_7	0	2	-0.025

Table 3.34: Test Case 3 Modification 1 Graph Adjacency Matrix.

	v_1	v_2	v_3	v_4	v_5	v_6	v_7
v_1	0	0	0	0	1	0	0
v_2	0	0	0	1	0	0	0
v_3	0	0	0	0	0	0	1
v_4	0	0	0	0	0	0	1
v_5	0	0	0	0	0	0	0
v_6	0	0	1	0	0	0	0
v_7	0	0	0	0	0	0	0

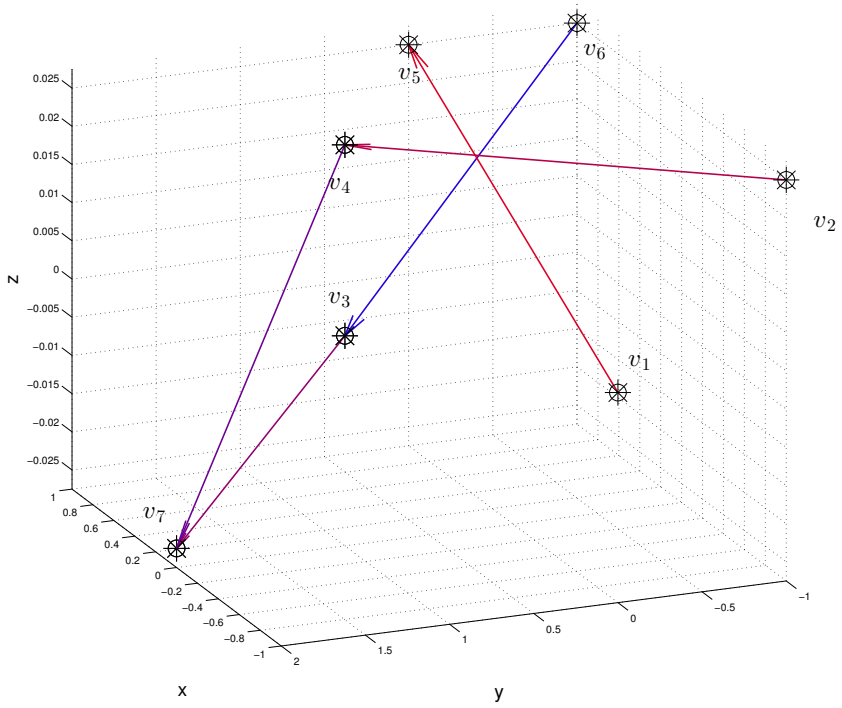

Figure 3.28: Notional Airspace Paths for Test Case 3 Modification 1

Table 3.35: Test Case 3 Modification 1 Notional Air Traffic Paths (No Units).

Aircraft (α)	Path $\left(P_{\mu,\alpha}\right)$	Origination $\left(c_{[\mu,\alpha]}(0)\right)$	Destination $\left(l_{[\mu,\alpha]}\right)$
1	(v_2, v_4, v_7)	0	3.2373
2	(v_6, v_3, v_7)	0	3.2365
3	(v_1, v_5)	0	2.0002

Table 3.36: Test Case 3 Modification 1 Notional Air Traffic Constraints (No Units).

Aircraft (α)	Minimum Speed ($u_{[\min,\alpha]}$)	Maximum Speed ($u_{[\max,\alpha]}$)	Departure Time ($t_{[0,\alpha]}$)	Scheduled Arrival ($t_{[S,\alpha]}$)	Earliest Arrival $\left(t_{[f,\alpha]_{\min}}\right)$	Latest Arrival $\left(t_{[f,\alpha]_{\max}}\right)$
1	0.3	1.5	0	3	2	4
2	0.3	0.8	0	4	3	5
3	0.4	0.9	0	4	3	5

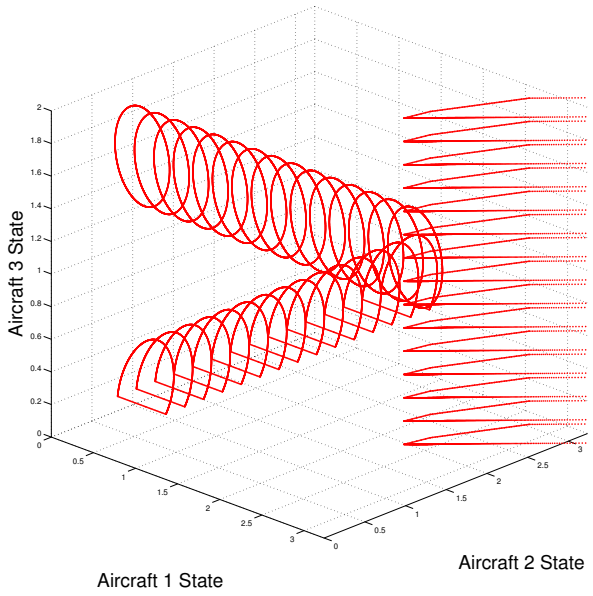

Figure 3.29: Notional State Space Conflict Regions for Test Case 3 Modification 1

2. The second test case is defined identically to the *third* test case from Section 3.1.4.1, except that a new waypoint is included above waypoint v_3 as a replacement waypoint for aircraft 2. Table 3.37 defines the three-dimensional position of each airspace waypoint as a node in the airspace graph, and Table 3.38 provides the graph's node adjacency matrix, so that the

graph arcs represent airspace path segments. Figure 3.30 displays the resulting airspace paths, while Table 3.39 defines the air traffic control mode for the test case; that is, it defines the path selected for each aircraft, as well as the initial path length coordinate of each aircraft's *origination* and the final path length coordinate of each aircraft's *destination*. Table 3.40 provides the schedule and control constraints for the second test case. The unitless minimum allowable lateral separation for the second test case was set to $r(t) = 0.3$, and the unitless minimum allowable vertical separation for the second test case was set to $h = 0.02$. Figure 3.31 displays the resulting state space conflict region.

Table 3.37: Test Case 3 Modification 2 Notional Airspace Graph Nodes (No Units).

Waypoint	Coordinate Value		
	x	y	z
v_1	-1	0	0
v_2	-1	-1	0.025
v_3	0	1	0
v_4	0	1	0.025
v_5	1	0	0.025
v_6	1	-1	0.025
v_7	0	2	-0.025

Table 3.38: Test Case 3 Modification 2 Graph Adjacency Matrix.

	v_1	v_2	v_3	v_4	v_5	v_6	v_7
v_1	0	0	0	0	1	0	0
v_2	0	0	1	0	0	0	0
v_3	0	0	0	0	0	0	1
v_4	0	0	0	0	0	0	1
v_5	0	0	0	0	0	0	0
v_6	0	0	0	1	0	0	0
v_7	0	0	0	0	0	0	0

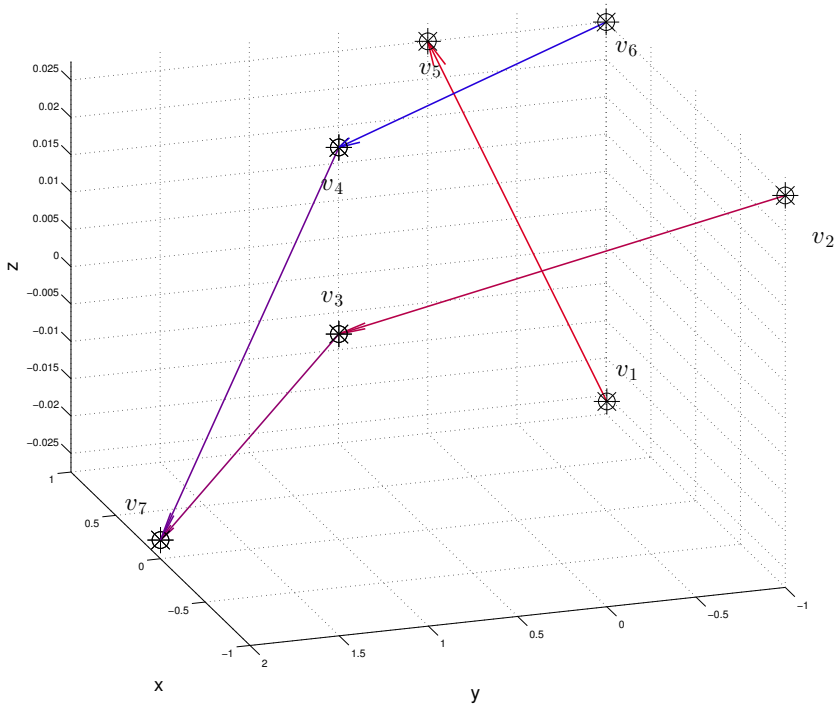

Figure 3.30: Notional Airspace Paths for Test Case 3 Modification 2

Table 3.39: Test Case 3 Modification 2 Notional Air Traffic Paths (No Units).

Aircraft (α)	Path $\left(P_{\mu,\alpha}\right)$	Origination $\left(c_{[\mu,\alpha]}(0)\right)$	Destination $\left(l_{[\mu,\alpha]}\right)$
1	(v_2, v_3, v_7)	0	3.2365
2	(v_6, v_4, v_7)	0	3.2373
3	(v_1, v_5)	0	2.0002

Table 3.40: Test Case 3 Modification 2 Notional Air Traffic Constraints (No Units).

Aircraft (α)	Minimum Speed $(u_{[\min,\alpha]})$	Maximum Speed $(u_{[\max,\alpha]})$	Departure Time $(t_{[0,\alpha]})$	Scheduled Arrival $(t_{[S,\alpha]})$	Earliest Arrival $\left(t_{[f,\alpha]_{\min}}\right)$	Latest Arrival $\left(t_{[f,\alpha]_{\max}}\right)$
1	0.3	1.5	0	3	2	4
2	0.3	0.8	0	4	3	5
3	0.4	0.9	0	4	3	5

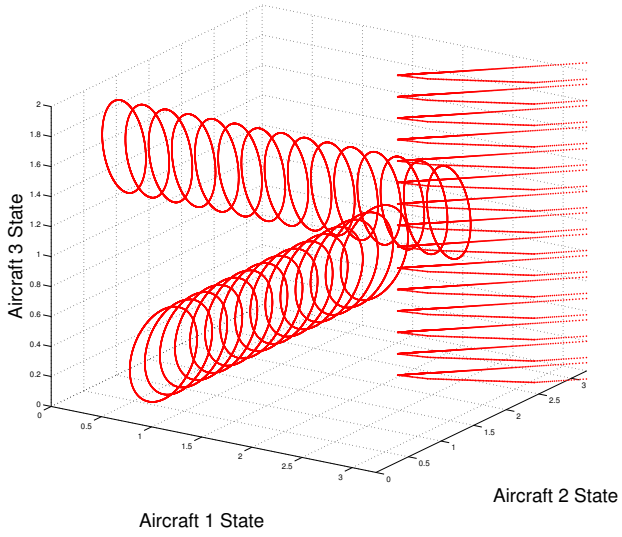

Figure 3.31: Notional State Space Conflict Regions for Test Case 3 Modification 2

3.2.1.2 Test Case Evaluation.

Each test case defined in Section 3.2.1.1 was evaluated using the STOP formulation of the generalized weighted-sum representation of the multi-objective HCS ATM problem using both the arrival time and final state forms of the adjusted ATM separation constraint, with $t_f = 1.2 \times \max\left\{t_{[f,1]_{\max}}, \ldots, t_{[f,A]_{\max}}\right\}$, $\kappa_2 = \kappa_3 = \min\left(t_{[f,\alpha]_{\min}}\right)$, with varying values for λ_1, λ_2, and λ_3, as well as different ATM separation constraint approximations. Table 3.32 displays the unique combinations (or *treatments*) of λ_1, λ_2, λ_3 that were evaluated with each ATM separation constraint approximation. For each treatment, the STOP generalized weighted-sum objective function, defined in equation (3.64), was minimized using the GPOPS-II Matlab optimization package running on Mac OS 10.9.4 with a 2.8 GHz Intel Core i5 processor and 8GB of RAM. The GPOPS-II settings that were used for the optimization are detailed in Appendix C. For each treatment, the control strategies, state trajectories and arrival times that satisfied the GPOPS-II local optimality conditions were recorded. The time required to generate each treatment's locally optimal solution, as well as the total deviation from scheduled arrival time, makespan, and the total control cost associated with each treatment's locally optimal solution were also recorded.

3.3 Incorporation of Inertia

Incorporating inertia into the multi-objective HCS ATM optimization problem involves adding an additional vector of control variables, denoted $\mathbf{u}_a$, to represent the acceleration control of each aircraft, and defining the speed or velocity of each aircraft as a vector of state variables, denoted $\mathbf{v}$. This section details the methods used to incorporate inertia into the multi-objective HCS ATM optimization problem from Section 3.1 to define the kinodynamic multi-objective HCS ATM optimization problem.

3.3.1 Kinodynamic Mutli-Objective Formulation.

The kinodynamic multi-objective HCS ATM problem is formulated as the generalized weighted-sum of the fuel consumption measure, the deviation from scheduled arrival time measure and the makespan measure. Thus, the problem is given as

$$\text{minimize} \quad F \triangleq \left(\lambda_1{}^{\beta_1}\right) F_1{}^{\left(\lambda_1{}^{1-\beta_1}\right)} + \left(\lambda_2{}^{\beta_2}\right) F_2{}^{\left(\lambda_2{}^{1-\beta_2}\right)} + \left(\lambda_3{}^{\beta_3}\right) F_3{}^{\left(\lambda_3{}^{1-\beta_3}\right)} \tag{3.69}$$

where $\lambda_1 \geq 0$ is the scalar that represents the relative importance of the fuel consumption measure, F_1, $\lambda_2 \geq 0$ is the scalar that represents the relative importance of the schedule deviation measure, F_2, $\lambda_3 \geq 0$ is the scalar that represents the relative importance of the total time measure, F_3, and each $\beta_k \in \{0, 1\}$ is a binary term for $k \in \{1, 2, 3\}$ that controls how each measure is weighted. That is, if $\beta_k = 1$, then F_k is weighted on a linear scale, but if $\beta_k = 0$, then F_k is weighted exponentially..

Furthermore, the measure of fuel consumption, F_1, is given by

$$F_1(\mu, \mathbf{u}_a, \mathbf{t}_0, \mathbf{t}_f, t) = \sum_{\alpha=1}^{A} \left[\int_{t_{[0,\alpha]}}^{t_{[f,\alpha]}} \left[u_{a[\mu,\alpha]}(t) \right]^2 dt \right], \tag{3.70}$$

where μ is the selected control mode which designates the pre-defined set of paths for each aircraft $\alpha \in \{1, 2, \ldots, A\}$, $\mathbf{u}_a = [u_{a[\mu,1]}, u_{a[\mu,2]}, \ldots, u_{a[\mu,A]}]$ is a feasible vector of acceleration control strategies, $\mathbf{t}_0 = [t_{[0,1]}, t_{[0,2]}, \ldots, t_{[0,A]}]$ is the vector of initial times for each aircraft, and $\mathbf{t}_f = [t_{[f,1]}, t_{[f,2]}, \ldots, t_{[f,A]}]$ is vector set of final (or actual arrival) times for each aircraft.

F_2 is the measure of deviation from scheduled arrival time given by

$$F_2(\mu, \kappa_2, \mathbf{t}_f, \mathbf{t}_S) = \kappa_2 + \sum_{\alpha=1}^{A} \left[t_{[f,\alpha]} - t_{[S,\alpha]} \right]^2, \tag{3.71}$$

where $\mathbf{t}_S = [t_{[S,1]}, t_{[S,2]}, \ldots, t_{[S,A]}]$ is the vector of scheduled arrival times for each aircraft and $\kappa_2 \geq 1$ is a scalar term added to ensure ${F_2}^{\lambda_2} \geq 1$.

F_3 is the measure of total time (or makespan) given by

$$\hat{F}_3(\mu, \kappa_3, \mathbf{t}_f, \mathbf{t}_{f_{\min}}) = \kappa_3 + \sum_{\alpha=1}^{A} \left[t_{[f,\alpha]} - t_{[f,\alpha]_{\min}} \right]^2, \tag{3.72}$$

where $\mathbf{t}_{f_{\min}} = [t_{[f,1]_{\min}}, t_{[f,2]_{\min}}, \ldots, t_{[f,A]_{\min}}]$ is the vector of earliest allowable arrival times for each aircraft and $\kappa_3 \geq 1$ is a scalar term added to ensure ${F_3}^{\lambda_3} \geq 1$.

An acceleration control strategy $u_{a[\mu,\alpha]}$ is feasible if and only if it satisfies the problem's dynamic equations, boundary conditions, and its intermediate state, control and ATM separation constraints. Using roadmap coordination space notation, the kinodynamic equations of the HCS problem with inertia are given by

$$\frac{d}{dt} c_{[\mu,\alpha]}(t) = v_{[\mu,\alpha]}(t), \quad \forall \alpha \in \{1, 2, \ldots, A\}, \tag{3.73}$$

$$\frac{d}{dt} v_{[\mu,\alpha]}(t) = u_{a[\mu,\alpha]}(t), \quad \forall \alpha \in \{1, 2, \ldots, A\}, \tag{3.74}$$

where $c_{[\mu,\alpha]}(t)$ is the path-length parameterized position at time t of aircraft α along its route defined by control mode μ, and $v_{[\mu,\alpha]}(t)$ is the speed or velocity at time t of aircraft α. Thus, $u_{a[\mu,\alpha]}(t)$ indirectly controls the instantaneous change in position of aircraft α along its route.

The boundary conditions and intermediate constraints for the kinodynamic HCS ATM problem are defined similarly to the boundary conditions and intermediate constraints for the HCS ATM problem without inertia. That is, given equations (3.10) - (3.12), the boundary conditions of the kinodynamic HCS ATM problem are given by

$$t_{[0,\alpha]} = 0, \quad \forall \alpha \in \{1, 2, \ldots, A\}, \tag{3.75a}$$

$$c_{[\mu,\alpha]}\left(t_{[0,\alpha]}\right) = c_{[\min,\alpha]}, \quad \forall \alpha \in \{1, 2, \ldots, A\}, \tag{3.75b}$$

$$c_{[\mu,\alpha]}\left(t_{[f,\alpha]}\right) = l_{[\mu,\alpha]}, \quad \forall \alpha \in \{1, 2, \ldots, A\}, \tag{3.75c}$$

where $l_{[\mu,\alpha]}$ is the path length of the route defined by control mode μ for aircraft α. That is, all aircraft are assumed to enter the problem at the same initial time, $t = 0$, at some distance $c_{[\min,\alpha]}$ along their path, and they are required to travel the remaining distance, $l_{[\mu,\alpha]} - c_{[\min,\alpha]}$, of their path defined by the control mode μ.

Given equations (3.10) - (3.12), the intermediate state and control constraints for all aircraft $\alpha \in \{1, 2, \ldots, A\}$ are given by

$$c_{[\min,\alpha]} \leq c_{[\mu,\alpha]}(t) \leq l_{[\mu,\alpha]}, \tag{3.76a}$$

$$v_{[\min,\alpha]} \leq v_{[\mu,\alpha]}(t) \leq v_{[\max,\alpha]}, \tag{3.76b}$$

$$u_{a[\min,\alpha]} \leq u_{a[\mu,\alpha]}(t) \leq u_{a[\max,\alpha]}, \tag{3.76c}$$

for all intermediate time $0 \leq t \leq t_{[f,\alpha]}$, where $v_{[\min,\alpha]}$ is the minimum allowable speed value for aircraft α, $v_{[\max,\alpha]}$ is the maximum allowable speed value for aircraft α, $u_{a[\min,\alpha]}$ is the minimum allowable acceleration value for aircraft α and $u_{a[\max,\alpha]}$ is the maximum allowable acceleration value for aircraft α.

Given equations (3.10) - (3.12) and Algorithm 3.1, for each pair of aircraft (α_1, α_2) such that $\alpha_1 \in \{1, 2, \ldots, A\}$, $\alpha_1 \in \{1, 2, \ldots, A\}$ and $\alpha_1 \neq \alpha_2$, the intermediate ATM separation constraint function is given by equation (3.15). The ATM separation constraint is thus,

$$G^{\text{ATM}}_{[\alpha_1,\alpha_2]}(t) \leq 0 \tag{3.77}$$

for all intermediate time $0 \leq t \leq \min\left\{t_{[f,\alpha_1]}, t_{[f,\alpha_2]}\right\}$. Therefore, the pair-wise ATM separation constraint is only defined until aircraft α_1 or aircraft α_2 reaches its destination.

3.3.2 Kinodynamic Implementation and Testing.

This section describes notional example multi-objective HCS ATM problems, and details how they were evaluated using the STOP method described in Section 3.1.3.1.

3.3.2.1 Notional Air Traffic Test Cases.

This section details the notional air traffic test case that was evaluated as a kinodynamic multi-objective HCS ATM problem using the STOP method.

The kinodynamic notional test case is defined identically to the *third* test case from Section 3.1.4.1. However, Table 3.41 provides the adjusted schedule and control constraints for the first test case. The unitless minimum allowable lateral separation for the first test case was set to $r(t) = 0.3$, and the unitless minimum allowable vertical separation for the first test case was set to $h = 0.02$.

Table 3.41: Test Case 1 Notional Air Traffic Constraints (No Units).

Aircraft (α)	Minimum Acceleration ($u_{a[\min,\alpha]}$)	Maximum Acceleration ($u_{a[\max,\alpha]}$)	Minimum Speed ($v_{[\min,\alpha]}$)	Maximum Speed ($v_{[\max,\alpha]}$)	Initial Speed ($v_{[0,\alpha]}$)	Departure Time ($t_{[0,\alpha]}$)	Scheduled Arrival ($t_{[S,\alpha]}$)	Earliest Arrival $\left(t_{[f,\alpha]_{\min}}\right)$	Latest Arrival $\left(t_{[f,\alpha]_{\max}}\right)$
1	−5	5	0.3	1.5	0.3	0	3	2	4
2	−5	5	0.3	0.8	0.3	0	4	3	5
3	−5	5	0.4	0.9	0.4	0	4	3	5

3.3.2.2 Test Case Evaluation.

The test case defined in Section 3.3.2.1 was evaluated using the STOP formulation of the generalized weighted-sum representation of the multi-objective HCS ATM problem using both the arrival time and final state forms of the adjusted ATM separation constraint, with $t_f = 1.2 \times \max\left\{t_{[f,1]_{\max}}, \ldots, t_{[f,A]_{\max}}\right\}$, $\kappa_2 = \kappa_3 = \min\left(t_{[f,\alpha]_{\min}}\right)$, with varying values for λ_1, λ_2, and λ_3, as well as different ATM separation constraint approximations. Table 3.32 in Section 3.1.4.2 displays the unique combinations (or *treatments*) of λ_1, λ_2, λ_3 that were evaluated with each ATM separation constraint approximation. For each treatment, the STOP generalized weighted-sum objective function, defined in equation (3.64), was minimized using the GPOPS-II Matlab optimization package running on Mac OS 10.9.4 with a 2.8 GHz Intel Core i5 processor and 8GB of RAM. The GPOPS-II settings that were used for the optimization are detailed in Appendix C. For each treatment, the control strategies, state trajectories and arrival times that satisfied the GPOPS-II local optimality conditions were recorded. The time required to generate each treatment's locally optimal solution, as well as the total deviation from scheduled arrival time, makespan, and the total control cost associated with each treatment's locally optimal solution were also recorded.

3.4 Incorporation of Stochastic Components

As described in Section 2.6, various physical and human factors may result in uncertainty in the speed and position of an aircraft. Therefore, this section details the methods used to incorporate uncertainty (or *stochastic components*) into the multi-objective HCS ATM optimization problem.

3.4.1 Probability Ellipsoid.

As described in Section 2.6, a common way of accounting for the uncertainty in the position of an aircraft is to model its position as a three-dimensional ellipsoid, centered at the expected position of the aircraft, with radii based on the level of uncertainty in each direction of motion. For the HCS roadmap framework, the uncertainty in the path-length parameterized position of aircraft α along its current path segment, p_k, was modeled as a normal random variable, with mean of zero and standard deviation denoted $\sigma_{[p_k,\alpha]}$. Thus, for each aircraft α, the $(1-\rho)\times 100\%$ confidence interval for its path-length parameterized coordinate at time t is given by,

$$c_{[\mu,\alpha]}(t) - \left(z_{1-\frac{\rho}{2}}\right)\sigma_{[p_k,\alpha]} \leq c_{[\mu,\alpha]}(t) \leq c_{[\mu,\alpha]}(t) + \left(z_{1-\frac{\rho}{2}}\right)\sigma_{[p_k,\alpha]}, \tag{3.78}$$

where $c_{[\mu,\alpha]}(t)$ is the expected path-length coordinate of the aircraft at time t, p_k is the current path segment, and $z_{1-\frac{\rho}{2}}$ is the *critical value* such that

$$\int_{-\infty}^{z_{1-\frac{\rho}{2}}} \frac{1}{\sqrt{2\pi}} e^{-(\frac{1}{2})(t^2)} dt = 1 - \frac{\rho}{2}. \tag{3.79}$$

That is, the probability of a standard-normal random variable being less than $z_{1-\frac{\rho}{2}}$ is $\left(1-\frac{\rho}{2}\right)$.

Furthermore, while the HCS roadmap ATM model assumes each aircraft α follows its pre-defined path exactly, in operation, aircraft may deviate from these paths due to wind or weather. Therefore, an aircraft's path-oriented lateral deviation (parallel to the ground and perpendicular to the current path segment p_k) was modeled as a normal random variable, with mean of zero and standard deviation denoted $\sigma_{\perp[p_k,\alpha]}$. Similarly, an aircraft's path-oriented vertical deviation (perpendicular to the current path segment p_k and perpendicular to the lateral direction) was modeled as a normal random variable, with mean of zero and standard deviation denoted $\sigma_{\uparrow[p_k,\alpha]}$.

Thus, if the uncertainty in each airspace dimension (oriented in the direction of the current path segment) is modeled as a normal random variable centered at the position given by the expected path-length coordinate, each aircraft α can be expected to be located with probability $(1-\rho)$ at time t within the three-dimensional ellipsoid centered at the position given by $c_{[\mu,\alpha]}(t)$ and oriented in the direction of the current path segment, with radius

$$R_{[p_k,\alpha]} \triangleq \left(z_{\sqrt[3]{1-\frac{\rho}{2}}}\right)\sigma_{[p_k,\alpha]} \tag{3.80}$$

in the direction of the current path segment, radius

$$R_{L[p_k,\alpha]} \triangleq \left(z \sqrt[3]{1-\frac{\rho}{2}}\right)\sigma_{\perp[p_k,\alpha]} \tag{3.81}$$

in the path-oriented lateral direction (or *lateral cross-path*), parallel to the ground and perpendicular to the current path segment, and radius

$$R_{V[p_k,\alpha]} \triangleq \left(z \sqrt[3]{1-\frac{\rho}{2}}\right)\sigma_{\uparrow[p_k,\alpha]} \tag{3.82}$$

in the path-oriented vertical direction (or *vertical cross-path*), perpendicular to the current path segment and perpendicular to the lateral cross-path direction. Figure 3.32 depicts a notional $1-\rho$ probability position ellipsoid.

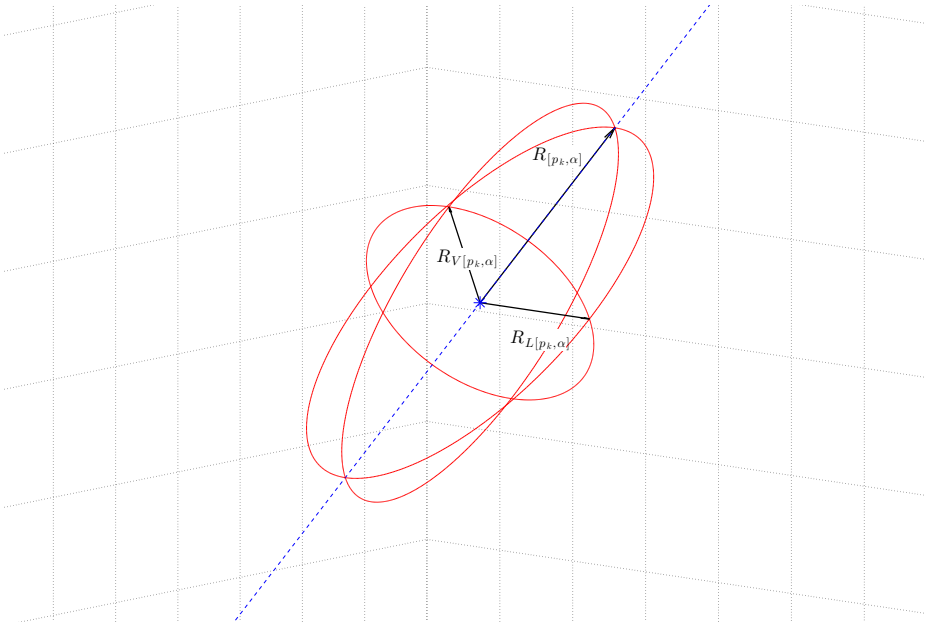

Figure 3.32: Notional Probability Position Ellipsoid

3.4.2 Lateral Separation Estimate.

If the position of each aircraft is modeled as a three-dimensional ellipsoid, then the minimum lateral separation between any pair of aircraft, α_1 and α_2, is estimated as the minimum distance between the probability ellipsoid of aircraft α_1 projected onto the horizontal plane parallel to the

ground, denoted $\mathbb{H}$, and the probability ellipsoid of aircraft α_2 projected onto the same plane, $\mathbb{H}$. For each aircraft α, the projection of its probability ellipsoid onto $\mathbb{H}$ is a two-dimensional ellipse, centered on the projection of the position given by $c_{[\mu,\alpha]}(t)$ onto $\mathbb{H}$, with radius

$$r_{[p_k,\alpha]} \triangleq \max\left\{\left(\sigma_{[p_k,\alpha]}\right)\cos\left(\phi_{[p_k,\alpha]}\right), \left(\sigma_{\uparrow[p_k,\alpha]}\right)\cos\left(\phi_{[p_k,\alpha]} + \tfrac{\pi}{2}\right)\right\} \tag{3.83}$$

in the direction of the projection of the current path segment onto $\mathbb{H}$, where $\cos\left(\phi_{[p_k,\alpha]}\right)$ is the cosine of the angle of ascent or descent of the current path segment, denoted $\phi_{[p_k,\alpha]}$, and $\cos\left(\phi_{[p_k,\alpha]} + \frac{\pi}{2}\right)$ is the cosine of the angle of the vertical cross-path direction. The radius of the two-dimensional projected ellipse in the direction of the projection of lateral cross-path direction is $R_{L[p_k,\alpha]}$, since the lateral cross-path direction is defined as parallel $\mathbb{H}$. Thus, the value of the *semi-major axis* of the two-dimensional projected probability ellipse for the current path segment, p_k, is defined as

$$a_{[p_k,\alpha]} \triangleq \max\left\{r_{[p_k,\alpha]}, R_{L[p_k,\alpha]}\right\}, \tag{3.84}$$

where $a_{[p_k,\alpha]}$ denotes the semi-major axis value. Since the unit vector in the direction of the semi-major axis is dependent on the relationship between $r_{[p_k,\alpha]}$ and $R_{L[p_k,\alpha]}$, the unit vector in the direction of the semi-major axis is given as

$$d_{[\mu,\alpha]} \triangleq \begin{cases} \left[\cos\left(\theta_{[p_k,\alpha]}\right), \sin\left(\theta_{[p_k,\alpha]}\right)\right] & \text{if } r_{[p_k,\alpha]} \geq R_{L[p_k,\alpha]}, \\ \left[\cos\left(\theta_{[p_k,\alpha]} + \frac{\pi}{2}\right), \sin\left(\theta_{[p_k,\alpha]} + \frac{\pi}{2}\right)\right] & \text{if } r_{[p_k,\alpha]} < R_{L[p_k,\alpha]}, \end{cases} \tag{3.85}$$

where $\theta_{[p_k,\alpha]}$ is the angle between the x-axis and the projection of the current path segment onto $\mathbb{H}$, so that

$$\theta_{[p_k,\alpha]} \triangleq \arccos\left(\frac{x_\alpha(t)}{\sqrt{(x_\alpha(t))^2 + (y_\alpha(t))^2}}\right), \tag{3.86}$$

where $x_\alpha(t)$ and $y_\alpha(t)$ are determined from $c_{[\mu,\alpha]}(t)$ and Algorithm 3.1.

Therefore, if control mode μ assigns to each aircraft α a set of path segments,

$$\mathbf{P}_\alpha \triangleq \{p_{[1,\alpha]}, p_{[2,\alpha]}, \ldots, p_{[k_\alpha,\alpha]}\}, \tag{3.87}$$

with individual segment lengths

$$\mathbf{L}_\alpha \triangleq \{l_{[1,\alpha]}, l_{[2,\alpha]}, \ldots, l_{[k_\alpha,\alpha]}\}, \tag{3.88}$$

lateral headings

$$\mathbf{A}_{[L,\alpha]} \triangleq \{\theta_{[1,\alpha]}, \theta_{[2,\alpha]}, \ldots, \theta_{[k_\alpha,\alpha]}\} \tag{3.89}$$

and angles of ascent (or descent)

$$\mathbf{A}_{[V,\alpha]} \triangleq \{\phi_{[1,\alpha]}, \phi_{[2,\alpha]}, \ldots, \phi_{[k_\alpha,\alpha]}\}, \tag{3.90}$$

then given a set of uncertainty parameters in the direction of each segment,

$$\mathbf{\Sigma} \triangleq \{\sigma_{[1,\alpha]}, \sigma_{[2,\alpha]}, \ldots, \sigma_{[k_\alpha,\alpha]}\}, \tag{3.91}$$

in the segment-oriented lateral direction,

$$\mathbf{\Sigma}_{\perp} \triangleq \{\sigma_{\perp[1,\alpha]}, \sigma_{\perp[2,\alpha]}, \ldots, \sigma_{\perp[k_\alpha,\alpha]}\} \tag{3.92}$$

and in the segment-oriented vertical direction,

$$\mathbf{\Sigma}_{\uparrow} \triangleq \{\sigma_{\uparrow[1,\alpha]}, \sigma_{\uparrow[2,\alpha]}, \ldots, \sigma_{\uparrow[k_\alpha,\alpha]}\}. \tag{3.93}$$

Algorithm 3.2 can be used to define the values of the semi-major axis, semi-minor axis, and orientation of the two-dimensional projection of the $1-\rho$ probability ellipsoid for any expected coordinate $c_{[\mu,\alpha]}(t)$, and Algorithm 3.1 can be used to define the center of the two-dimensional projection of the $1-\rho$ probability ellipsoid for any expected coordinate $c_{[\mu,\alpha]}(t)$

Given the values of the semi-major axes, semi-minor axes, orientations and centers of a pair of two-dimensional ellipses in the plane, the minimum distance between the pair of ellipses can be calculated from the closed-form solution of Zheng and Palffy-Muhoray [87]. Therefore, after obtaining the following values from Algorithms 3.1, 3.2, and 3.3,

- $[x_{\alpha_1}(t), y_{\alpha_1}(t), z_{\alpha_1}(t)]$
- $a_{[\mu,\alpha_1]}(t)$, $b_{[\mu,\alpha_1]}(t)$ and $d_{[\mu,\alpha_1]}(t)$
- $[x_{\alpha_2}(t), y_{\alpha_2}(t), z_{\alpha_2}(t)]$
- $a_{[\mu,\alpha_2]}(t)$, $b_{[\mu,\alpha_2]}(t)$ and $d_{[\mu,\alpha_2]}(t)$

- $d_{C[\alpha_1,\alpha_2]}(t)$,

the minimum *lateral* distance between aircraft α_1 and aircraft α_2, denoted $D_{L[\alpha_1,\alpha_2]}(t)$, is estimated as the minimum distance between ellipse α_1 and ellipse α_2 using the closed-form method of Zheng and Palffy-Muhoray [87] with the following input:

- Ellipse α_1 is centered at $(x_{\alpha_1}(t), y_{\alpha_1}(t))$. Its semi-major axis is $a_{[\mu,\alpha_1]}(t)$ oriented in the direction of vector $d_{[\mu,\alpha_1]}(t)$, and its semi-minor axis is $b_{[\mu,\alpha_1]}(t)$.

- Ellipse α_2 is centered at $(x_{\alpha_2}(t), y_{\alpha_2}(t))$. Its semi-major axis is $a_{[\mu,\alpha_2]}(t)$ oriented in the direction of vector $d_{[\mu,\alpha_2]}(t)$, and its semi-minor axis is $b_{[\mu,\alpha_1]}(t)$

- The vector that connects the center of ellipse α_1 to the center of ellipse α_2 is given by $d_{C[\alpha_1,\alpha_2]}(t)$.

Therefore, the minimum lateral separation between aircraft α_1 and aircraft α_2 is estimated to be greater than or equal to r with probability at least $(1-\rho)^2$ if

$$D_{L[\alpha_1,\alpha_2]}(t) \geq r. \tag{3.94}$$

3.4.3 Vertical Separation Estimate.

If the position of each aircraft is modeled as a three-dimensional ellipsoid, then the minimum vertical separation between any pair of aircraft, α_1 and α_2, is estimated as the minimum distance between their probability ellipsoids. The minimum vertical distance between two ellipsoids can be evaluated by the following cases, defined without loss of generality:

1. **No Overlap.** The minimum vertical value of ellipsoid α_1 is greater than the maximum vertical value of ellipsoid α_2.

2. **Coincidence.** The minimum vertical value of ellipsoid α_1 is equal to the maximum vertical value of ellipsoid α_2.

3. **Partial Overlap.** The maximum vertical value of ellipsoid α_1 is greater than the maximum vertical value of ellipsoid α_2, the minimum vertical value of ellipsoid α_1 is less than the

Algorithm 3.2 Obtain Probability Ellipse Components given roadmap state $c_{[\mu,\alpha]}(t)$

$\mathbf{L}_\alpha = [l_{[p_1,\alpha]}, l_{[p_2,\alpha]}, \ldots, l_{[p_{k_\alpha},\alpha]}]$

$\mathbf{A}_{[L,\alpha]} = [\theta_{[p_1,\alpha]}, \theta_{[p_2,\alpha]}, \ldots, \theta_{[p_{k_\alpha},\alpha]}]$

$\mathbf{A}_{[V,\alpha]} = [\phi_{[p_1,\alpha]}, \phi_{[p_2,\alpha]}, \ldots, \phi_{[p_{k_\alpha},\alpha]}]$

$\mathbf{\Sigma}_{[\mu,\alpha]} = \left(z\sqrt[3]{1-\frac{\rho}{2}}\right)[\sigma_{[p_1,\alpha]}, \sigma_{[p_2,\alpha]}, \ldots, \sigma_{[p_{k_\alpha},\alpha]}]$

$\mathbf{\Sigma}_{\perp[\mu,\alpha]} = \left(z\sqrt[3]{1-\frac{\rho}{2}}\right)[\sigma_{\perp[p_1,\alpha]}, \sigma_{\perp[p_2,\alpha]}, \ldots, \sigma_{\perp[p_{k_\alpha},\alpha]}]$

$\mathbf{\Sigma}_{\uparrow[\mu,\alpha]} = \left(z\sqrt[3]{1-\frac{\rho}{2}}\right)[\sigma_{\uparrow[p_1,\alpha]}, \sigma_{\uparrow[p_2,\alpha]}, \ldots, \sigma_{\uparrow[p_{k_\alpha},\alpha]}]$

$\theta_{[\mu,\alpha]} = \mathbf{A}_{[L,\alpha]}[1]$

$\phi_{[\mu,\alpha]} = \mathbf{A}_{[V,\alpha]}[1]$

$\sigma_{[\mu,\alpha]} = \left[\mathbf{\Sigma}_{[\mu,\alpha]}[1], \mathbf{\Sigma}_{\perp[\mu,\alpha]}[1], \mathbf{\Sigma}_{\uparrow[\mu,\alpha]}[1]\right]$

for $i = 1$ **to** $k_\alpha - 1$ **do**

  if $c_{[\mu,\alpha]}(t) > \mathbf{L}_\alpha(i)$ **then**

    $\theta_{[\mu,\alpha]} = \mathbf{A}_{[L,\alpha]}[i+1]$

    $\phi_{[\mu,\alpha]} = \mathbf{A}_{[V,\alpha]}[i+1)]$

    $\sigma_{[\mu,\alpha]} = \left[\mathbf{\Sigma}_{[\mu,\alpha]}[i+1], \mathbf{\Sigma}_{\perp[\mu,\alpha]}[i+1], \mathbf{\Sigma}_{\uparrow[\mu,\alpha]}[i+1]\right]$

  end if

end for

$R_{L[\mu,\alpha]} = \sigma_{[\mu,\alpha]}[2]$

$r_{[\mu,\alpha]} = \max\left\{\left(\sigma_{[\mu,\alpha]}[1]\right)\cos(\phi_\alpha), \left(\sigma_{[\mu,\alpha]}[3]\right)\cos\left(\phi_\alpha + \frac{\pi}{2}\right)\right\}$

$a_{[\mu,\alpha]}(t) = r_{[\mu,\alpha]}$

$b_{[\mu,\alpha]}(t) = r_{\perp[\mu,\alpha]}$

$d_{[\mu,\alpha]}(t) = \left[\cos\left(\theta_{[\mu,\alpha]}\right), \sin\left(\theta_{[\mu,\alpha]}\right)\right]$

if $r_{\perp[\mu,\alpha]} > r_{[\mu,\alpha]}$ **then**

  $a_{[\mu,\alpha]}(t) = r_{\perp[\mu,\alpha]}$

  $b_{[\mu,\alpha]}(t) = r_{[\mu,\alpha]}$

  $d_{[\mu,\alpha]}(t) = \left[\cos\left(\theta_{[\mu,\alpha]} + \frac{\pi}{2}\right), \sin\left(\theta_{[\mu,\alpha]} + \frac{\pi}{2}\right)\right]$

end if

$H_{[\mu,\alpha]}(t) = \max\left\{\left(\sigma_{[\mu,\alpha]}[1]\right)\sin(\phi_\alpha), \left(\sigma_{[\mu,\alpha]}[3]\right)\sin\left(\phi_\alpha + \frac{\pi}{2}\right)\right\}$

Algorithm 3.3 Obtain Inputs for Lateral Separation Estimate given roadmap states $c_{[\mu,\alpha_1]}(t)$ and $c_{[\mu,\alpha_2]}(t)$

Obtain $[x_{\alpha_1}(t), y_{\alpha_1}(t), z_{\alpha_1}(t)]$ from Algorithm 3.1 with input $c_{[\mu,\alpha_1]}(t)$

Obtain $a_{[\mu,\alpha_1]}(t)$, $b_{[\mu,\alpha_1]}(t)$ and $d_{[\mu,\alpha_1]}(t)$ from Algorithm 3.2

Obtain $[x_{\alpha_2}(t), y_{\alpha_2}(t), z_{\alpha_2}(t)]$ from Algorithm 3.1 with input $c_{[\mu,\alpha_2]}(t)$

Obtain $a_{[\mu,\alpha_2]}(t)$, $b_{[\mu,\alpha_2]}(t)$ and $d_{[\mu,\alpha_2]}(t)$ from Algorithm 3.2

$d_{C[\alpha_1,\alpha_2]}(t) = [x_{\alpha_2}(t), y_{\alpha_2}(t)] - [x_{\alpha_1}(t), y_{\alpha_1}(t)]$

maximum vertical value of ellipsoid α_2 and the minimum vertical value of ellipsoid α_1 is greater than the minimum vertical value of ellipsoid α_2.

4. **Total Overlap.** The maximum vertical value of ellipsoid α_1 is greater than the maximum vertical value of ellipsoid α_2 and the minimum vertical value of ellipsoid α_1 is less than the minimum vertical value of ellipsoid α_2.

The minimum vertical distance between two ellipsoids is only positive for Case 1, **No Overlap**. After obtaining the altitudes $z_{\alpha_1}(t)$ and $z_{\alpha_2}(t)$ from Algorithm 3.1, and $H_{[\mu,\alpha_1]}(t)$ and $H_{[\mu,\alpha_2]}(t)$ from Algorithm 3.2, the minimum vertical value of ellipsoid α_1 is given by

$$z_{\alpha_1}(t) - H_{[\mu,\alpha_1]}(t), \tag{3.95}$$

the maximum vertical value of ellipsoid α_1 is given by

$$z_{\alpha_1}(t) + H_{[\mu,\alpha_1]}(t), \tag{3.96}$$

the minimum vertical value of ellipsoid α_2 is given by

$$z_{\alpha_2}(t) - H_{[\mu,\alpha_2]}(t), \tag{3.97}$$

and the maximum vertical value of ellipsoid α_2 is given by

$$z_{\alpha_2}(t) + H_{[\mu,\alpha_2]}(t). \tag{3.98}$$

Therefore, Case 1, **No Overlap**, is achieved if

$$z_{\alpha_1}(t) - H_{[\mu,\alpha_1]}(t) \geq z_{\alpha_2}(t) + H_{[\mu,\alpha_2]}(t) \tag{3.99a}$$

$$\implies z_{\alpha_1}(t) - z_{\alpha_2}(t) \geq H_{[\mu,\alpha_1]}(t) + H_{[\mu,\alpha_2]}(t) \tag{3.99b}$$

or if

$$z_{\alpha_2}(t) - H_{[\mu,\alpha_2]}(t) \geq z_{\alpha_1}(t) - H_{[\mu,\alpha_1]}(t) \tag{3.100}$$

$$\implies z_{\alpha_2}(t) - z_{\alpha_1}(t) \geq H_{[\mu,\alpha_1]}(t) + H_{[\mu,\alpha_2]}(t). \tag{3.101}$$

Thus, if there is no overlap between ellipsoids α_1 and α_2, the minimum vertical distance between ellipsoids α_1 and α_2 is positive if

$$\left|z_{\alpha_1}(t) - z_{\alpha_2}(t)\right| \geq H_{[\mu,\alpha_1]}(t) + H_{[\mu,\alpha_2]}(t), \tag{3.102}$$

and the minimum vertical distance between α_1 and α_2 is estimated to be greater than or equal to h with probability at least $(1-\rho)^2$ if

$$\left|z_{\alpha_1}(t) - z_{\alpha_2}(t)\right| \geq H_{[\mu,\alpha_1]}(t) + H_{[\mu,\alpha_2]}(t) + h. \tag{3.103}$$

Furthermore, if Case 2, **Coincidence**, occurs, with $H_{[\mu,\alpha_1]}(t) > 0$, $H_{[\mu,\alpha_2]}(t) > 0$ and $h > 0$. Then

$$z_{\alpha_1}(t) - H_{[\mu,\alpha_1]}(t) = z_{\alpha_2}(t) + H_{[\mu,\alpha_2]}(t)$$

$$\implies \quad z_{\alpha_1}(t) - z_{\alpha_2}(t) = H_{[\mu,\alpha_1]}(t) + H_{[\mu,\alpha_2]}(t)$$

$$\implies \quad \left|z_{\alpha_1}(t) - z_{\alpha_2}(t)\right| = \left|H_{[\mu,\alpha_1]}(t) + H_{[\mu,\alpha_2]}(t)\right|$$

However, $H_{[\mu,\alpha_1]}(t) > 0$, $H_{[\mu,\alpha_2]}(t) > 0$ and $h > 0$, so

$$\left|H_{[\mu,\alpha_1]}(t) + H_{[\mu,\alpha_2]}(t)\right| = H_{[\mu,\alpha_1]}(t) + H_{[\mu,\alpha_2]}(t)$$

and

$$H_{[\mu,\alpha_1]}(t) + H_{[\mu,\alpha_2]}(t) < H_{[\mu,\alpha_1]}(t) + H_{[\mu,\alpha_2]}(t) + h.$$

Therefore, if Case 2, **Coincidence**, occurs, with $H_{[\mu,\alpha_1]}(t) > 0$, $H_{[\mu,\alpha_2]}(t) > 0$ and $h > 0$, then

$$\left|z_{\alpha_1}(t) - z_{\alpha_2}(t)\right| < H_{[\mu,\alpha_1]}(t) + H_{[\mu,\alpha_2]}(t) + h,$$

so constraint (3.103) cannot be satisfied.

If Case 3, **Partial Overlap**, occurs, with $H_{[\mu,\alpha_1]}(t) > 0$, $H_{[\mu,\alpha_2]}(t) > 0$ and $h > 0$, then

$$z_{\alpha_1}(t) - H_{[\mu,\alpha_1]}(t) \leq z_{\alpha_2}(t) + H_{[\mu,\alpha_2]}(t) \tag{3.104a}$$

and

$$z_{\alpha_1}(t) - H_{[\mu,\alpha_1]}(t) \geq z_{\alpha_2}(t) - H_{[\mu,\alpha_2]}(t). \tag{3.104b}$$

Now, suppose $\left|z_{\alpha_1}(t) - z_{\alpha_2}(t)\right| \geq H_{[\mu,\alpha_1]}(t) + H_{[\mu,\alpha_2]}(t) + h$. If $z_{\alpha_1} > z_{\alpha_2}$, then

$$\begin{aligned} & z_{\alpha_1}(t) - z_{\alpha_2}(t) \geq H_{[\mu,\alpha_1]}(t) + H_{[\mu,\alpha_2]}(t) + h \\ \implies \quad & z_{\alpha_1}(t) - H_{[\mu,\alpha_1]}(t) \geq z_{\alpha_2}(t) + H_{[\mu,\alpha_2]}(t) + h \\ \implies \quad & z_{\alpha_1}(t) - H_{[\mu,\alpha_1]}(t) > z_{\alpha_2}(t) + H_{[\mu,\alpha_2]}(t), \end{aligned}$$

which contradicts equation (3.104a). On the other hand, if $z_{\alpha_1} < z_{\alpha_2}$, then

$$\begin{aligned} & z_{\alpha_2}(t) - z_{\alpha_1}(t) \geq H_{[\mu,\alpha_1]}(t) + H_{[\mu,\alpha_2]}(t) + h \\ \implies \quad & z_{\alpha_2}(t) - H_{[\mu,\alpha_2]}(t) \geq z_{\alpha_1}(t) + H_{[\mu,\alpha_1]}(t) + h \\ \implies \quad & z_{\alpha_2}(t) - H_{[\mu,\alpha_2]}(t) > z_{\alpha_1}(t) - H_{[\mu,\alpha_1]}(t), \end{aligned}$$

which contradicts equation (3.104b). Thus, if Case 3, **Partial Overlap**, occurs, with $H_{[\mu,\alpha_1]}(t) > 0$, $H_{[\mu,\alpha_2]}(t) > 0$ and $h > 0$, then constraint (3.103) cannot be satisfied.

If Case 4, **Total Overlap**, occurs, with $H_{[\mu,\alpha_1]}(t) > 0$, $H_{[\mu,\alpha_2]}(t) > 0$ and $h > 0$, then

$$z_{\alpha_1}(t) - H_{[\mu,\alpha_1]}(t) \geq z_{\alpha_2}(t) + H_{[\mu,\alpha_2]}(t) \tag{3.105a}$$

and

$$z_{\alpha_1}(t) - H_{[\mu,\alpha_1]}(t) \leq z_{\alpha_2}(t) - H_{[\mu,\alpha_2]}(t). \tag{3.105b}$$

Now, suppose $\left|z_{\alpha_1}(t) - z_{\alpha_2}(t)\right| \geq H_{[\mu,\alpha_1]}(t) + H_{[\mu,\alpha_2]}(t) + h$. If $z_{\alpha_1} > z_{\alpha_2}$, then

$$z_{\alpha_1}(t) - z_{\alpha_2}(t) \geq H_{[\mu,\alpha_1]}(t) + H_{[\mu,\alpha_2]}(t) + h$$

$$\implies \quad z_{\alpha_1}(t) - H_{[\mu,\alpha_1]}(t) \geq z_{\alpha_2}(t) + H_{[\mu,\alpha_2]}(t) + h$$

$$\implies \quad z_{\alpha_1}(t) - H_{[\mu,\alpha_1]}(t) > z_{\alpha_2}(t) - H_{[\mu,\alpha_2]}(t),$$

which contradicts equation (3.105b). On the other hand, if $z_{\alpha_1} < z_{\alpha_2}$, then

$$z_{\alpha_2}(t) - z_{\alpha_1}(t) \geq H_{[\mu,\alpha_1]}(t) + H_{[\mu,\alpha_2]}(t) + h$$

$$\implies \quad z_{\alpha_2}(t) - H_{[\mu,\alpha_2]}(t) \geq z_{\alpha_1}(t) + H_{[\mu,\alpha_1]}(t) + h.$$

However, $z_{\alpha_2}(t) + H_{[\mu,\alpha_2]}(t) > z_{\alpha_2}(t) - H_{[\mu,\alpha_2]}(t)$ and $z_{\alpha_1}(t) + H_{[\mu,\alpha_1]}(t) + h > z_{\alpha_1}(t) + H_{[\mu,\alpha_1]}(t)$. So,

$$z_{\alpha_2}(t) - z_{\alpha_1}(t) \geq H_{[\mu,\alpha_1]}(t) + H_{[\mu,\alpha_2]}(t) + h$$

$$\implies \quad z_{\alpha_2}(t) - H_{[\mu,\alpha_2]}(t) > z_{\alpha_1}(t) - H_{[\mu,\alpha_1]}(t),$$

which contradicts equation (3.105a). Thus, if Case 4, **Total Overlap**, occurs, with $H_{[\mu,\alpha_1]}(t) > 0$, $H_{[\mu,\alpha_2]}(t) > 0$ and $h > 0$, then constraint (3.103) cannot be satisfied.

Therefore, constraint (3.103) is satisfied if and only if the minimum vertical separation between ellipsoid α_1 and ellipsoid α_2 is at least h.

3.4.4 ATM Separation Constraint with Uncertainty.

Given equations (3.94) - (3.103), Algorithms 3.1, 3.2, and 3.3 , for each pair of aircraft (α_1, α_2) such that $\alpha_1 \in \{1, 2, \ldots, A\}$, $\alpha_1 \in \{1, 2, \ldots, A\}$ and $\alpha_1 \neq \alpha_2$, the intermediate ATM separation constraint function with uncertainty is given by

$$G^{\Sigma\text{ATM}}_{[\alpha_1,\alpha_2]}(t) \triangleq 1 - \max\left\{\frac{\left(D_{L[\alpha_1,\alpha_2]}(t)\right)^2}{r(t)^2}, \frac{\left(z_{\alpha_1}(t) - z_{\alpha_2}(t)\right)^2}{\left(H_{[\mu,\alpha_1]}(t) + H_{[\mu,\alpha_2]}(t) + h\right)^2}\right\}, \tag{3.106a}$$

or equivalently,

$$G^{\Sigma\text{ATM}}_{[\alpha_1,\alpha_2]}(t) \triangleq \min\left\{r(t)^2 - \left(D_{L[\alpha_1,\alpha_2]}(t)\right)^2, \left(H_{[\mu,\alpha_1]}(t) + H_{[\mu,\alpha_2]}(t) + h\right)^2 - \left(z_{\alpha_1}(t) - z_{\alpha_2}(t)\right)^2\right\}. \tag{3.106b}$$

Therefore, the intermediate ATM separation constraint in the presence of uncertainty is defined as

$$G^{\Sigma\text{ATM}}_{[\alpha_1,\alpha_2]}(t) \leq 0. \tag{3.107}$$

3.4.5 Stochastic Components Implementation and Testing.

This section describes a notional example multi-objective HCS ATM problem with stochastic components, and details how it was evaluated using the STOP method described in Sections 3.1.3.1, replacing the deterministic ATM separation constraint (3.15) with the probabilistic ATM separation constraint (3.107).

3.4.5.1 Notional Air Traffic Test Case.

This section details the notional air traffic test case that was evaluated as a kinodynamic multi-objective HCS ATM problem with uncertainty using the STOP method.

The kinodynamic test case with uncertainty is defined identically to the first test case from Section 3.3.2.1. However, Table 3.42 provides the uncertainty parameter values for the first test case.

Table 3.42: Test Case 1 Notional Air Traffic Uncertainty Values (No Units).

Segment	Along Path	Cross Path	
		Lateral	Vertical
(v_i, v_j)	(σ_μ)	$(\sigma_{\perp\mu})$	$(\sigma_{\uparrow\mu})$
(v_2, v_3)	0.015	0.0075	0.0035
(v_5, v_3)	0.015	0.0075	0.0035
(v_1, v_4)	0.007	0.0035	0.0020
(v_3, v_6)	0.010	0.0050	0.0050

3.4.5.2 Test Case Evaluation.

The test case defined in Section 3.4.5.1 was evaluated with the STOP formulation of the generalized weighted-sum representation of the multi-objective HCS ATM problem using both the arrival time and final state forms of the adjusted probabilistic ATM separation constraint for $(1-\rho) = 0.75$, $(1-\rho) = 0.85$ and $(1-\rho) = 0.95$. For each value of $(1-\rho)^2$, the test case was evaluated with $t_f = 1.2 \times \max\left\{t_{[f,1]_{\max}}, \ldots, t_{[f,A]_{\max}}\right\}$, $\kappa_2 = \kappa_3 = \min\left(t_{[f,\alpha]_{\min}}\right)$, and $\lambda_1 = 5.5$, $\lambda_2 = 10$, and $\lambda_3 = 0.1$ using the sigmoid ATM separation constraint approximation method. For each treatment, the STOP generalized weighted-sum objective function, defined in equation (3.64),

was minimized using the GPOPS-II Matlab optimization package running on Mac OS 10.9.4 with a 2.8 GHz Intel Core i5 processor and 8GB of RAM. The GPOPS-II settings that were used for the optimization are detailed in Appendix C. For each treatment, the control strategies, state trajectories and arrival times that satisfied the GPOPS-II local optimality conditions were recorded. The time required to generate each treatment's locally optimal solution, as well as the total deviation from scheduled arrival time, makespan, and the total control cost associated with each treatment's locally optimal solution were also recorded.

3.5 Asymmetric Lateral Separation

This section describes the methods developed to account for *asymmetric* lateral separation. Asymmetric lateral separation in ATM refers to cases in which policy or operational procedures dictate that the lateral separation between two aircraft is dependent on their *lead-trail weight class* configuration; that is, the minimum allowable lateral separation between two aircraft should be greater if a lighter aircraft is following behind a heavier aircraft [74].

3.5.1 Lead-Trail Definition.

For the purposes of this research, aircraft α_1 is considered to trail aircraft α_2 if and only if

$$\left\langle \Delta_{\alpha_2} xy(t), \Delta_{[\alpha_2,\alpha_1]} xy(t) \right\rangle < 0, \tag{3.108}$$

where $\Delta_{\alpha_2} xy(t)$ is the vector given by the lateral heading of aircraft α_2 at time t and $\Delta_{[\alpha_2,\alpha_1]} xy(t)$ is the vector given by the difference in the lateral position of aircraft α_1 and the lateral position of aircraft α_2, such that

$$\Delta_{[\alpha_2,\alpha_1]} xy(t) \triangleq \left[x_{\alpha_1}(t) - x_{\alpha_2}(t), y_{\alpha_1}(t) - y_{\alpha_2}(t) \right]. \tag{3.109}$$

That is, if the lateral heading from aircraft α_2 to aircraft α_1 is greater than 90 degrees from the current lateral heading of aircraft α_2, then aircraft α_1 is considered to trail aircraft α_2.

Therefore, given $c_{[\mu,\alpha_1]}(t)$ and $c_{[\mu,\alpha_2]}(t)$, $\Delta_{[\alpha_2,\alpha_1]} xy(t)$ can be determined using Algorithm 3.1. However, the lateral heading vector of each aircraft α, denoted $\Delta_\alpha xy(t)$, is determined by the lateral airspace heading of the current path segment for aircraft α. As detailed in Section 3.1.1, in control mode μ, each aircraft $\alpha \in \{1, 2, \ldots, A\}$ is assigned a set of n_α way-points in the three-dimensional

airspace that must be visited in order. The set of way-points is given as

$$WP_{[\mu,\alpha]} = \{(x_{[1,\alpha]}, y_{[1,\alpha]}, z_{[1,\alpha]}), (x_{[2,\alpha]}, y_{[2,\alpha]}, z_{[2,\alpha]}), \ldots, (x_{[n_\alpha,\alpha]}, y_{[n_\alpha,\alpha]}, z_{[n_\alpha,\alpha]})\}, \tag{3.110}$$

so the route of aircraft α is partitioned into a set of $(n_\alpha - 1)$ route segments (or *arcs*) defined by the airspace way-points. Thus, the total path-length for the route of aircraft α in control mode μ, denoted $l_{[\mu,\alpha]}$, is given by

$$l_{[\mu,\alpha]} = \sum_{i=0}^{n_\alpha - 1} \left\| \mathbf{a}_{[i,\alpha]} \right\|, \tag{3.111a}$$

where

$$\mathbf{a}_{[i,\alpha]} \triangleq \begin{cases} [0,0,0] & \text{if } i = 0, \\ [x_{[i+1,\alpha]}, y_{[i+1,\alpha]}, z_{[i+1,\alpha]}] - [x_{[i,\alpha]}, y_{[i,\alpha]}, z_{[i,\alpha]}] & \text{if } i \geq 1, \end{cases} \tag{3.111b}$$

is a vector representation of the route segment that connects way-point i to way-point $(i + 1)$. Thus, the roadmap state $c_{[\mu,\alpha]}(t) \in [0, l_{[\mu,\alpha]}]$ in control mode μ is related to the lateral heading vector of aircraft α, denoted $\Delta_\alpha xy(t)$ by the following relationship:

$$\Delta_{\alpha_2} xy(t) \triangleq (\mathbf{a}_{[\hat{n}_\alpha,\alpha]} - \mathbf{a}_{[\hat{n}_\alpha - 1,\alpha]}) \begin{bmatrix} 1 & 0 & 0 \\ 0 & 1 & 0 \\ 0 & 0 & 0 \end{bmatrix}, \tag{3.112a}$$

where

$$\sum_{i=0}^{\hat{n}_\alpha - 1} \left\| \mathbf{a}_{[i,\alpha]} \right\| \leq c_{[\mu,\alpha]}(t) \leq \sum_{i=0}^{\hat{n}_\alpha} \left\| \mathbf{a}_{[i,\alpha]} \right\|. \tag{3.112b}$$

Alternatively, the lateral airspace heading vector of aircraft α at time t in control mode μ, denoted $\Delta_\alpha xy(t)$, can be determined using Algorithm 3.4.

3.5.2 Minimum Lateral Separation Update.

Given the lead-trail criterion in equation (3.108), Algorithms 3.1 and 3.4 for aircraft α_1 and aircraft α_2, the trail indicator functions q_{α_1} and q_{α_2}, are given by

$$q_{\alpha_1}(t) = \begin{cases} 1 & \text{if } \left\langle \Delta_{\alpha_2} xy(t), \Delta_{[\alpha_2,\alpha_1]} xy(t) \right\rangle < 0, \\ 0 & \text{if } \left\langle \Delta_{\alpha_2} xy(t), \Delta_{[\alpha_2,\alpha_1]} xy(t) \right\rangle \geq 0, \end{cases} \tag{3.113}$$

Algorithm 3.4 Calculate lateral heading given roadmap state $c_{[\mu,\alpha]}(t)$

$\mathbf{a}_\alpha = [0, 0, 0]$

$l_\alpha = 0$

$\hat{n}_\alpha = 1$

while $l_\alpha + \|\mathbf{a}_{[\hat{n}_\alpha,\alpha]}\| \leq c_{[\mu,\alpha]}(t)$ **do**

$\mathbf{a}_\alpha = \mathbf{a}_\alpha + \mathbf{a}_{[\hat{n}_\alpha,\alpha]}$

$l_\alpha = l_\alpha + \|\mathbf{a}_{[\hat{n}_\alpha,\alpha]}\|$

$\hat{n}_\alpha = \hat{n}_\alpha + 1$

end while

$$\Delta_{\alpha_2} xy(t) = (\mathbf{a}_{[\hat{n}_\alpha,\alpha]} - \mathbf{a}_\alpha) \begin{bmatrix} 1 & 0 & 0 \\ 0 & 1 & 0 \\ 0 & 0 & 0 \end{bmatrix}$$

and

$$q_{\alpha_2}(t) = \begin{cases} 1 & \text{if } \left\langle \Delta_{\alpha_1} xy(t), \Delta_{[\alpha_1,\alpha_2]} xy(t) \right\rangle < 0, \\ 0 & \text{if } \left\langle \Delta_{\alpha_1} xy(t), \Delta_{[\alpha_1,\alpha_2]} xy(t) \right\rangle \geq 0. \end{cases} \tag{3.114}$$

That is, $q_{\alpha_1}(t)$ is equal to 1 if and only if aircraft α_1 is considered to trail aircraft α_2, and it is equal to 0 otherwise, while $q_{\alpha_2}(t)$ is equal to 1 if and only if aircraft α_2 is considered to trail aircraft α_1, and it is equal to 0 otherwise.

Furthermore, suppose the current control mode defines an increase to r, the baseline lateral separation requirement, if aircraft α_1 is considered to trail aircraft α_2, or if aircraft α_2 is considered to trail aircraft α_1. If aircraft α_1 is considered to trail aircraft α_2, denote this increase $\Delta r_{[\alpha_1,\alpha_2]}$. If aircraft α_2 is considered to trail aircraft α_1, denote this increase $\Delta r_{[\alpha_2,\alpha_1]}$. Then the updated lateral separation requirement would be $r + \Delta r_{[\alpha_1,\alpha_2]}$ if aircraft α_1 is considered to trail aircraft α_2 and aircraft α_2 is *not* considered to trail aircraft α_1. Similarly, the updated lateral separation requirement would be $r + \Delta r_{[\alpha_2,\alpha_1]}$ if aircraft α_2 is considered to trail aircraft α_1 and aircraft α_1 is *not* considered to trail aircraft α_2. However, if both aircraft are considered to trail each other, then the updated lateral separation requirement should be $r + \max\{\Delta r_{[\alpha_1,\alpha_2]}, \Delta r_{[\alpha_2,\alpha_1]}\}$.

Therefore, the asymmetric minimum allowable lateral separation is given by

$$\hat{r}(t) = r + \max\left\{\left(q_{\alpha_1}(t)\right)\Delta r_{[\alpha_1,\alpha_2]}, \left(q_{\alpha_2}(t)\right)\Delta r_{[\alpha_2,\alpha_1]}\right\}. \tag{3.115}$$

Note that to improve differentiability of the asymmetric minimum allowable lateral separation requirement given by equation (3.115), it can be approximated using the Multiplier Method described in Section 2.3.1.4 to approximate the value of $\max\left\{\left(q_{\alpha_1}(t)\right)\Delta r_{[\alpha_1,\alpha_2]}, \left(q_{\alpha_2}\right)\Delta r_{[\alpha_2,\alpha_1]}\right\}$ and the Sigmoid Method described in Section 2.3.1.7 to approximate the indicator functions $q_{\alpha_1}(t)$ and $q_{\alpha_2}(t)$.

3.5.3 Asymmetric Lateral Separation Implementation and Testing.

This section describes a notional example multi-objective HCS ATM problem with asymmetric lateral separation requirements, and details how it was evaluated using the STOP method described in Sections 3.1.3.1, replacing the asymmetric minimum allowable lateral separation equation (3.115) with the combined Multiplier and Sigmoid Method approximation.

3.5.3.1 Notional Air Traffic Test Cases.

This section details the notional air traffic test case that was evaluated as a multi-objective HCS ATM problem with asymmetric lateral separation requirements using the STOP method.

The kinodynamic test case with uncertainty and asymmetric lateral separation is defined identically to the test case from Section 3.4.5.1. However, Table 3.43 provides the changes in the baseline lateral separation requirement for the given lead-trail configuration.

Table 3.43: Test Case 1 Notional Air Traffic Lateral Separation Update Values (No Units).

Trail Aircraft (α_1)	Lead Aircraft (α_2)	Lateral Separation Update ($\Delta_{[\alpha_1,\alpha_2]}r$)
1	2	0
1	3	0
2	1	0.01
2	3	0
3	1	0.01
3	2	0

3.5.3.2 Test Case Evaluation.

The test case defined in Section 3.5.3.1 was evaluated using the STOP formulation of the generalized weighted-sum representation of the multi-objective HCS ATM problem using both the arrival time and final state forms of the adjusted ATM separation constraint, with $t_f = 1.2 \times \max\left\{t_{[f,1]_{\max}}, \ldots, t_{[f,A]_{\max}}\right\}$, $\kappa_2 = \kappa_3 = \min\left(t_{[f,\alpha]_{\min}}\right)$, with varying values for λ_1, λ_2, and λ_3, as well as different ATM separation constraint approximations. Table 3.32 displays the unique combinations (or *treatments*) of λ_1, λ_2, λ_3 that were evaluated with each ATM separation constraint approximation. For each treatment, the STOP generalized weighted-sum objective function, defined in equation (3.64), was minimized using the GPOPS-II Matlab optimization package running on Mac OS 10.9.4 with a 2.8 GHz Intel Core i5 processor and 8GB of RAM. The GPOPS-II settings that were used for the optimization are detailed in Appendix C. For each treatment, the control strategies, state trajectories and arrival times that satisfied the GPOPS-II local optimality conditions were recorded. The time required to generate each treatment's locally optimal solution, as well as the total deviation from scheduled arrival time, makespan, and the total control cost associated with each treatment's locally optimal solution were also recorded.

IV. Results

This chapter presents the results of the evaluations and test cases described in Chapter 3. The results of evaluating the suitability of each constraint approximation are presented in Sections 4.1 and 4.2. The results from the notional air traffic test cases are presented in Sections 4.3, 4.4, 4.5, 4.6, and 4.7.

4.1 Approximation Method Accuracy

This section presents the results from testing the accuracy of the four constraint approximation methods described in Section 3.1.2, namely:

1. Multiplier Method
2. Sigmoid Method
3. p-Norm Method
4. Exponential p-Norm Method

The accuracy of each approximation method was measured for each treatment described in Section 3.1.2 as the ratio of the number of grid points that the approximation method classified as within the conflict region divided by the number of grid points that were actually within the conflict region defined for that treatment. If the ratio is greater than 1, then the approximation method overestimated the conflict region. Thus, the larger the over-estimation error, the less accurate the approximation. Tables 4.1, 4.3, 4.5 and 4.7 provide a summary of this accuracy measure for each approximation method listed. However, the impact of the over-estimation error is dependent on how the over-estimation affects the approximated coordination space regions. Therefore, Tables 4.2, 4.4, 4.6 and 4.8 provide a summary of the ratio of the number of grid points for each treatment that the approximation method classified as inside the coordination space region divided by the number of grid points that were actually inside the coordination space region defined for that treatment.

Table 4.1: Overall Multiplier Method Conflict Region Approximation Results.

	Approximated Area Mean over-estimation (%)					
Scenario	With $\gamma = 1$	With $\gamma = 5$	With $\gamma = 10$	With $\gamma = 50$	With $\gamma = 100$	With $\gamma = 500$
1	1.6659	1.6428	1.5961	1.2412	1.0699	0.642
2-1	1.8241	1.795	1.7394	1.4988	0.5248	0.229
2-2	1.1932	1.1784	1.0335	0.7893	0.5715	0.2476
2-3	3.6545	3.5381	3.3626	2.9675	2.7308	0.4006
3-1	126.1271	121.9973	112.5275	43.1572	23.2539	6.0593
3-2	198.8302	179.493	151.6155	48.4733	25.1526	5.9761
3-3	249.8132	202.2906	157.6691	50.186	26.4099	6.8777
3-4	1354.5289	1001.2095	667.1159	126.1239	58.0802	12.3937
3-5	208.9381	185.1516	153.4082	48.5747	25.1761	5.9674
3-6	188.9029	175.4869	151.1669	49.0261	25.6813	6.4472
3-7	289.356	218.2315	161.1938	50.4616	26.4802	6.8458
3-8	230.8356	191.9769	154.4456	49.9637	26.3343	6.8695
4-1	133.9663	128.5548	117.2222	45.7147	26.1145	5.9373
4-2	206.54	186.9667	158.8222	52.5693	29.1917	6.5564
4-3	245.2401	199.8242	157.3218	52.5367	29.3749	6.3412
4-4	1339.3193	991.8396	674.8337	138.2168	68.5412	13.3969
4-5	208.1514	188.1624	159.4579	52.7251	29.2654	6.5378
4-6	187.7376	177.0491	155.1966	52.1736	29.075	6.5258
4-7	308.1269	228.3853	165.9364	53.621	29.7546	6.3725
4-8	241.1679	197.6338	157.2165	52.5499	29.3614	6.398
Mean	292.49	234.02	176.61	49.3	25.77	5.97

Table 4.1 indicates that the Multiplier Approximation Method, described in Section 3.1.2.1, was largely inaccurate for values of γ less than 100, but its accuracy improved dramatically for values of γ greater than 100.

Table 4.2: Overall Multiplier Method Coordination Space Approximation Results.

	Approximated Area Mean Estimation (%)					
Scenario	With $\gamma = 1$	With $\gamma = 5$	With $\gamma = 10$	With $\gamma = 50$	With $\gamma = 100$	With $\gamma = 500$
1	99.7555	99.7581	99.7637	99.8055	99.826	99.8765
2-1	99.6777	99.6811	99.6877	99.7171	99.9383	99.9733
2-2	99.875	99.8762	99.8948	99.9194	99.9457	99.9768
2-3	99.7516	99.7537	99.7578	99.7688	99.7739	99.9895
3-1	90.0361	90.3791	91.1864	96.7329	98.2477	99.5457
3-2	90.5727	91.4708	92.7672	97.7156	98.8169	99.7201
3-3	92.6243	93.9339	95.1901	98.471	99.1947	99.7884
3-4	93.0317	94.8493	96.5681	99.3512	99.7012	99.9362
3-5	90.6903	91.708	93.089	97.844	98.8853	99.7372
3-6	89.3997	90.0841	91.4156	97.2667	98.5714	99.6415
3-7	93.692	95.2025	96.4289	98.8739	99.4085	99.8469
3-8	92.5105	93.7031	94.8759	98.3446	99.1267	99.7704
4-1	88.828	89.3164	90.3504	96.3611	97.9303	99.5304
4-2	89.7836	90.7416	92.1081	97.4096	98.5628	99.6768
4-3	92.445	93.755	95.0352	98.3527	99.08	99.7998
4-4	93.2342	94.9723	96.5695	99.297	99.6514	99.932
4-5	89.7925	90.7721	92.1689	97.4315	98.5745	99.6808
4-6	88.0874	88.7923	90.2439	96.7652	98.1993	99.5956
4-7	94.0143	95.5632	96.7679	98.9533	99.419	99.8754
4-8	92.4391	93.7286	94.9795	98.3325	99.0692	99.796
Mean	92.9031	93.8105	94.8698	98.3217	99.0942	99.78

Table 4.1 indicates that the Multiplier Approximation Method, described in Section 3.1.2.1, consistently identified over 90% of the coordination space, and, on average, accurately identified more than 98% of the coordination space for values of γ greater than 50.

Table 4.3: Overall Sigmoid Conflict Region Approximation Results.

	Approximated Area Mean over-estimation (%)					
Scenario	With s = 10	With s = 50	With s = 100	With s = 500	With s = 1000	With s = 5000
1	2.0627	1.9991	1.9167	1.503	1.1502	0.4937
2-1	2.1559	2.0805	2.0331	1.6889	1.3433	0.1642
2-2	1.5126	1.4536	1.3944	0.9779	0.669	0.1767
2-3	4.6913	4.365	4.2372	3.2951	2.7771	0.2347
3-1	120.6186	111.0778	91.9257	31.3762	14.8918	1.5975
3-2	183.4356	153.8348	115.4797	34.5318	15.6952	1.1302
3-3	219.8828	164.5489	118.5298	35.9343	16.8156	1.9199
3-4	1142.7372	736.5625	425.5164	83.8396	34.2649	2.1871
3-5	191.2189	156.7663	116.2702	34.5789	15.7093	1.115
3-6	176.4756	152.3398	115.7471	35.0905	16.2023	1.5916
3-7	247.5416	171.5944	119.845	36.0373	16.8361	1.846
3-8	205.4167	159.2545	117.1048	35.8142	16.761	1.9277
4-1	127.4832	116.8376	95.142	32.2579	17.7842	4.0667
4-2	190.3742	161.6825	120.7332	36.3907	19.6476	4.5327
4-3	216.0067	164.6904	119.1718	35.9358	19.8347	4.3543
4-4	1126.5377	742.7563	435.9948	86.4837	43.8908	9.4387
4-5	191.6488	162.4427	121.421	36.5286	19.7005	4.5496
4-6	176.1753	156.3338	119.0395	36.0291	19.5902	4.4064
4-7	261.4138	178.71	123.2585	36.8785	20.0709	4.6416
4-8	212.9536	163.7766	118.9728	36.0775	19.8432	4.3922
Mean	255.45	186.78	126.57	34.17	16.63	2.49

Table 4.3 indicates that the Sigmoid Approximation Method, described in Section 3.1.2.2, was largely inaccurate for values of s less than 1000, but its accuracy improved dramatically for values of s greater than 1000.

Table 4.4: Overall Sigmoid Coordination Space Approximation Results.

	Approximated Area Mean Estimation (%)					
Scenario	With s = 10	With s = 50	With s = 100	With s = 500	With s = 1000	With s = 5000
1	99.7084	99.7159	99.7255	99.7745	99.8164	99.8944
2-1	99.6383	99.6471	99.653	99.6944	99.7389	99.9811
2-2	99.8442	99.8502	99.8564	99.9002	99.9364	99.9839
2-3	99.7209	99.7358	99.7391	99.7594	99.7728	99.9934
3-1	90.467	91.2788	92.8844	97.6306	98.881	99.8814
3-2	91.2798	92.6689	94.5045	98.374	99.2632	99.9482
3-3	93.4585	95.0093	96.3751	98.9046	99.4869	99.9389
3-4	94.1212	96.2108	97.8109	99.5687	99.8237	99.9887
3-5	91.4458	92.9489	94.7778	98.467	99.3061	99.9522
3-6	90.0433	91.3578	93.4535	98.0459	99.1003	99.9113
3-7	94.5862	96.2097	97.3362	99.1952	99.6238	99.9585
3-8	93.2973	94.7361	96.1078	98.8126	99.4437	99.9336
4-1	89.3819	90.3415	92.2517	97.4433	98.5946	99.6819
4-2	90.5712	91.9713	93.999	98.2063	99.0339	99.7786
4-3	93.2961	94.8123	96.2334	98.8721	99.3794	99.8646
4-4	94.3021	96.2288	97.783	99.5604	99.7768	99.952
4-5	90.5883	92.0158	94.0439	98.2261	99.0421	99.7814
4-6	88.8164	90.1297	92.5342	97.7685	98.7887	99.7304
4-7	94.9217	96.5231	97.5965	99.28	99.6081	99.9095
4-8	93.2822	94.7722	96.1926	98.8537	99.3717	99.8621
Mean	93.5399	94.7369	96.0904	98.8037	99.3949	99.904

Table 4.4 indicates that the Sigmoid Approximation Method, described in Section 3.1.2.2, consistently identified over 93% of the coordination space, and, on average, accurately identified more than 98% of the coordination space for values of s greater than 100.

Table 4.5: Overall p-Norm Conflict Region Approximation Results.

	Approximated Area Mean over-estimation (%)					
Scenario	With p = 2	With p = 10	With p = 20	With p = 100	With p = 200	With p = 1000
1	33.209	6.1527	3.2932	0.9442	0.5846	0.425
2-1	30.0171	5.1813	2.6019	0.3773	0.2101	0.0828
2-2	32.0988	5.6519	2.861	0.4228	0.216	0.1154
2-3	79.4627	13.0887	7.1702	2.3905	0.3427	0.093
3-1	24.8961	4.1511	2.8841	1.7577	1.6364	1.4762
3-2	24.0591	3.264	2.1829	1.2522	1.1597	1.0377
3-3	27.9557	4.7639	3.3978	2.1215	1.9692	1.7676
3-4	34.2649	2.1871	2.1871	2.1871	2.1871	2.1871
3-5	23.9846	3.2127	2.1706	1.2434	1.1506	1.0222
3-6	24.4476	3.7118	2.6311	1.7156	1.6222	1.4982
3-7	29.3636	5.0106	3.5132	2.0696	1.8993	1.6758
3-8	27.9243	4.798	3.3802	2.1142	1.966	1.7795
4-1	24.1592	5.3777	2.5113	0.4851	0.2825	0.0396
4-2	24.1922	5.4118	2.4951	0.4379	0.2479	0.0339
4-3	28.5445	6.1775	2.7326	0.574	0.3224	0.0493
4-4	42.3441	8.6739	3.1034	0.3435	0.0623	0.0186
4-5	24.121	5.4079	2.4329	0.4283	0.2374	0.0281
4-6	23.7686	5.1368	2.4146	0.4792	0.2583	0.0314
4-7	31.1086	7.1513	3.0227	0.4851	0.2949	0.054
4-8	28.6188	6.2921	2.8414	0.5509	0.3141	0.0548
Mean	30.29	5.25	2.96	1.24	1.00	0.83

Table 4.5 indicates that the p-Norm Approximation Method, described in Section 3.1.2.3, was very inaccurate for all values of p greater than 2, but its accuracy improved dramatically for values of p greater than 100.

Table 4.6: Overall p-Norm Coordination Space Approximation Results.

	Approximated Area Mean Estimation (%)					
Scenario	With p = 2	With p = 10	With p = 20	With p = 100	With p = 200	With p = 1000
1	95.2388	99.0775	99.4895	99.8409	99.8834	99.9027
2-1	95.1687	99.1654	99.5809	99.9547	99.9756	99.9905
2-2	95.5998	99.2116	99.6025	99.9589	99.98	99.9898
2-3	95.5851	99.1972	99.5081	99.7871	99.9908	99.9967
3-1	98.2437	99.7188	99.7993	99.8711	99.8788	99.8891
3-2	98.9402	99.8656	99.9074	99.9434	99.947	99.9519
3-3	99.1922	99.8638	99.9002	99.9337	99.9376	99.9427
3-4	99.8237	99.9887	99.9887	99.9887	99.9887	99.9887
3-5	99.0179	99.8792	99.9153	99.9477	99.9509	99.9555
3-6	98.7635	99.825	99.8691	99.9064	99.91	99.915
3-7	99.3434	99.8874	99.9213	99.9535	99.9573	99.9623
3-8	99.1147	99.8491	99.8911	99.9282	99.9324	99.9377
4-1	98.2246	99.6142	99.8177	99.9641	99.9797	99.9973
4-2	98.8922	99.757	99.8871	99.9805	99.9893	99.9986
4-3	99.1712	99.8246	99.9206	99.9831	99.9908	99.9987
4-4	99.7846	99.9558	99.9844	99.9983	99.9997	99.9999
4-5	98.9065	99.7636	99.8911	99.9798	99.9892	99.9987
4-6	98.6569	99.7187	99.8656	99.9727	99.9857	99.9983
4-7	99.3925	99.8605	99.9408	99.9905	99.9943	99.999
4-8	99.1575	99.8183	99.9167	99.9837	99.991	99.9985
Mean	98.3763	99.7086	99.8347	99.9393	99.9563	99.964

Table 4.6 indicates that the p-Norm Approximation Method, described in Section 3.1.2.3, consistently identified over 98% of the coordination space, and, on average, accurately identified more than 99.9% of the coordination space for values of p greater than 100.

Table 4.7: Overall Exponential p-Norm Conflict Region Approximation Results.

	Approximated Area Mean over-estimation (%)					
Scenario	With p = 2	With p = 10	With p = 20	With p = 100	With p = 200	With p = 1000
1	2.0742	2.0229	1.9991	1.7923	1.6428	0.9681
2-1	2.1603	2.1329	2.0943	1.9171	1.7638	0.3923
2-2	1.527	1.4827	1.4642	1.2948	1.1637	0.4418
2-3	4.7416	4.432	4.3971	3.966	3.4392	2.4312
3-1	121.1744	118.8144	114.6925	70.0137	42.9274	10.5007
3-2	186.8957	176.8178	164.0581	83.1589	48.2968	10.8417
3-3	229.9908	205.5197	181.5915	85.3386	49.8985	11.8492
3-4	1216.9557	1036.7502	861.6923	260.2673	126.1239	23.0863
3-5	195.6001	183.3087	168.473	83.4962	48.3969	10.8419
3-6	178.5655	171.4982	161.0933	83.6738	48.8724	11.3296
3-7	263.2968	226.7387	193.9368	85.9189	50.0907	11.8451
3-8	213.6878	193.5498	173.5504	84.7067	49.6841	11.8221
4-1	128.6556	125.4268	120.6546	73.2687	45.7356	11.926
4-2	194.4927	184.0439	171.2774	88.6511	52.6648	13.2458
4-3	226.3101	202.6069	180.3625	87.7441	52.5274	12.8986
4-4	1204.3189	1025.8954	859.2546	277.6885	138.9621	28.183
4-5	195.9776	185.3032	172.2955	89.0194	52.8142	13.3018
4-6	178.5003	172.4341	163.4481	87.8365	52.3216	12.9713
4-7	279.2979	238.3523	202.8109	89.6713	53.4408	13.5585
4-8	222.782	200.0428	178.7477	87.663	52.5569	13.0202
Mean	267.97	237.84	208.12	87.74	49.3	11.31

Table 4.7 indicates that the Exponential p-Norm Approximation Method, described in Section 3.1.2.4, was very inaccurate for all values of p less than 200, but its accuracy improved dramatically for values of p greater than 200.

Table 4.8: Overall Exponential p-Norm Coordination Space Approximation Results.

	Approximated Area Mean Estimation (%)					
Scenario	With p = 2	With p = 10	With p = 20	With p = 100	With p = 200	With p = 1000
1	99.7071	99.7132	99.7159	99.7405	99.7581	99.8381
2-1	99.6378	99.6408	99.6454	99.6662	99.6845	99.9529
2-2	99.8429	99.8468	99.849	99.8654	99.8775	99.9566
2-3	99.7198	99.7343	99.7353	99.7451	99.7554	99.7859
3-1	90.4315	90.6222	90.966	94.6421	96.7475	99.2117
3-2	91.1256	91.5921	92.1857	96.0608	97.7224	99.4914
3-3	93.1841	93.8588	94.5265	97.3937	98.4784	99.6376
3-4	93.7394	94.6665	95.5671	98.6611	99.3512	99.8812
3-5	91.2661	91.7911	92.4326	96.2709	97.8503	99.5215
3-6	89.9528	90.311	90.8693	95.3003	97.2727	99.3707
3-7	94.2522	95.0288	95.7307	98.0857	98.882	99.7352
3-8	93.0478	93.6652	94.2859	97.1878	98.3524	99.6069
4-1	89.2791	89.5662	89.9947	94.0926	96.3539	99.063
4-2	90.3648	90.879	91.501	95.6078	97.4016	99.3494
4-3	93.0013	93.6868	94.3431	97.2327	98.35	99.5981
4-4	93.9134	94.8059	95.6429	98.5877	99.2932	99.8567
4-5	90.3778	90.9029	91.5368	95.6415	97.4239	99.3588
4-6	88.6673	89.0641	89.6541	94.5152	96.7505	99.2018
4-7	94.5732	95.3694	96.0573	98.2503	98.9568	99.7353
4-8	92.9914	93.6666	94.3113	97.2019	98.3294	99.5893
Mean	93.3543	93.8288	94.3464	97.1569	98.317	99.5873

Table 4.8 indicates that the Exponential p-Norm Approximation Method, described in Section 3.1.2.4, consistently identified over 93% of the coordination space, and, on average, accurately identified more than 98% of the coordination space for values of p greater than 200.

4.1.1 Summary.

These results indicate that all four of the approximation methods tested can achieve accuracy suitable for estimating the roadmap-based ATM conflict regions. However, the Multiplier and

Exponential p-Norm Approximation Methods generated the least accurate estimates for the parameter values tested, while the p-Norm Approximation Method generated the most accurate estimates for the parameter values tested.

4.2 Approximation Method Computational Stability

This section presents the results from testing the computational stability of the four constraint approximation methods described in Section 3.1.2, namely:

1. Multiplier Method
2. Sigmoid Method
3. p-Norm Method
4. Exponential p-Norm Method

The computational stability of each approximation method was measured for each treatment described in Section 3.1.2 as the ratio of the number of grid points for which the Matlab *gradient* function failed to estimate a gradient value based on the grid of the approximation method's function value divided by the total number of grid points that were defined for that treatment. Tables 4.9- 4.12 provide a summary of this computational stability measure for each approximation method listed. Figures 4.1 - 4.4 present typical surface plot for each constraint approximation method described in Section 3.1.2 to visualize the function's computational stability. Note the similarity between the Multiplier Method constraint function surface and the Exponential p-Norm Method constraint function surface.

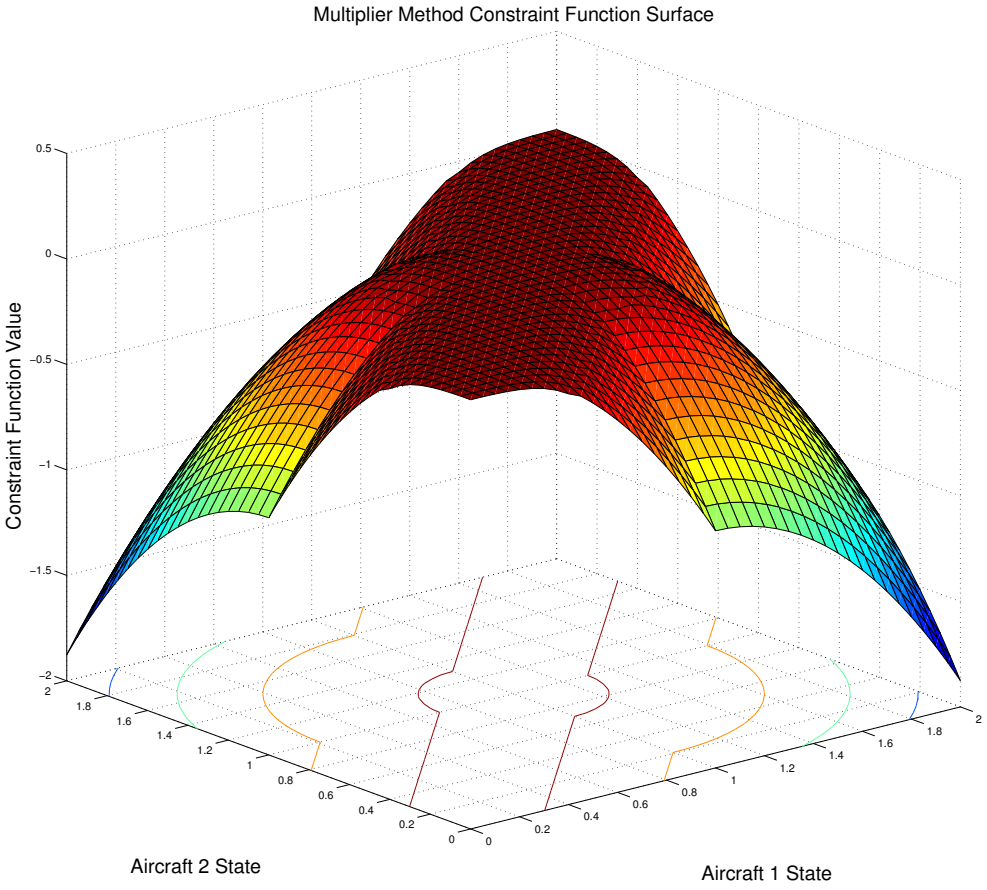

Figure 4.1: Multiplier Method Constraint Function Surface

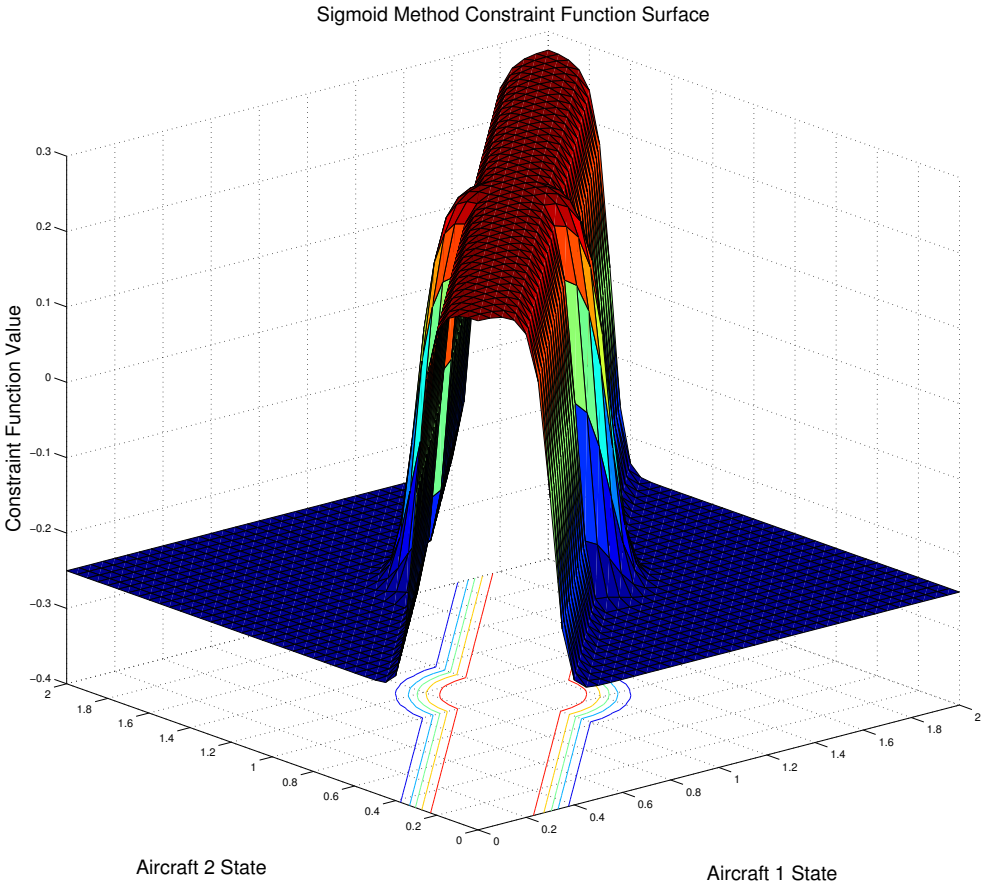

Figure 4.2: Sigmoid Method Constraint Function Surface

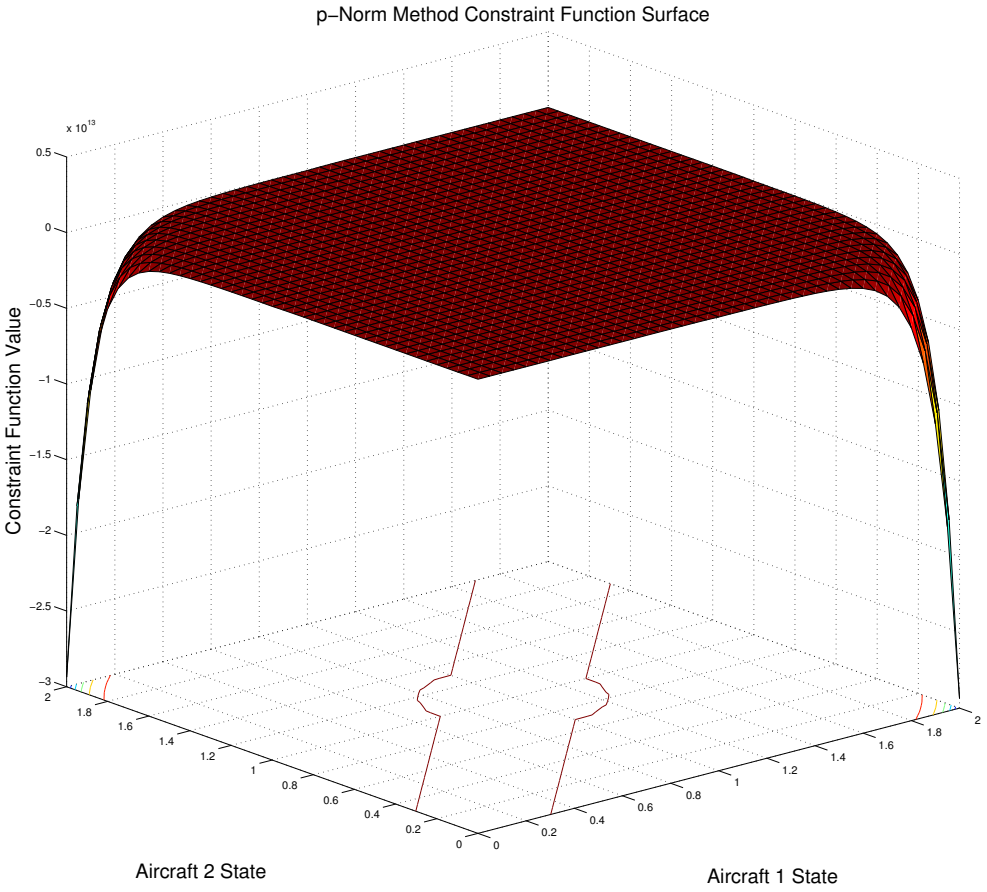

Figure 4.3: *p*-Norm Method Constraint Function Surface

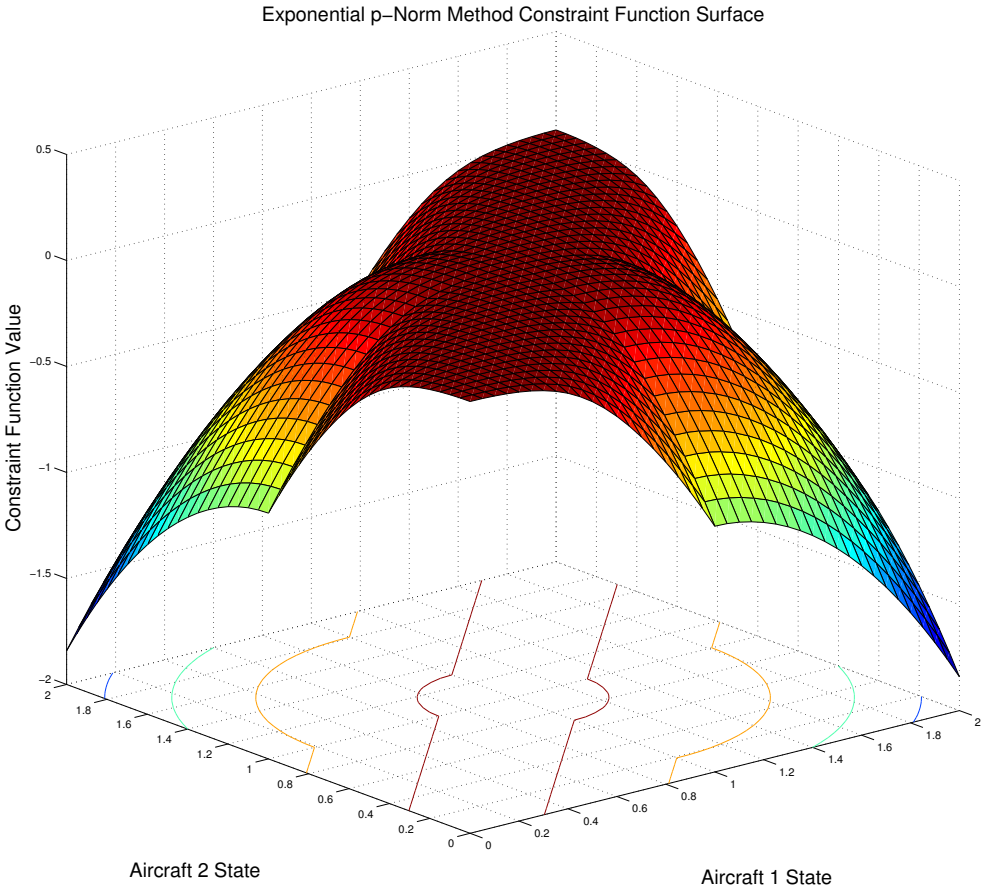

Figure 4.4: Exponential p-Norm Method Constraint Function Surface

Table 4.9: Overall Multiplier Method Computational Stability Results.

	Proportion of Grid Points where Gradient Estimate Failed (%)					
Scenario	With $\gamma = 1$	With $\gamma = 5$	With $\gamma = 10$	With $\gamma = 50$	With $\gamma = 100$	With $\gamma = 500$
1	0	0	0	0	0	0
2-1	0	0	0	0	0	0
2-2	0	0	0	0	0	0
2-3	0	0	0	0	0	0
3-1	0	0	0	0	0	0
3-2	0	0	0	0	0	0
3-3	0	0	0	0	0	0
3-4	0	0	0	0	0	0
3-5	0	0	0	0	0	0
3-6	0	0	0	0	0	0
3-7	0	0	0	0	0	0
3-8	0	0	0	0	0	0
4-1	0	0	0	0	0	0
4-2	0	0	0	0	0	0
4-3	0	0	0	0	0	0
4-4	0	0	0	0	0	0
4-5	0	0	0	0	0	0
4-6	0	0	0	0	0	0
4-7	0	0	0	0	0	0
4-8	0	0	0	0	0	0
Mean	0	0	0	0	0	0

Table 4.9 indicates that the Matlab *gradient* function successfully estimated a gradient for the Multiplier Approximation Method, described in Section 3.1.2.1, at all grid points, for all values of γ.

Table 4.10: Overall Sigmoid Computational Stability Results.

	Proportion of Grid Points where Gradient Estimate Failed (%)					
Scenario	With s = 10	With s = 50	With s = 100	With s = 500	With s = 1000	With s = 5000
1	0	0	0	0	0	0
2-1	0	0	0	0	0	0
2-2	0	0	0	0	0	0
2-3	0	0	0	0	0	0
3-1	0	0	0	0	0	0
3-2	0	0	0	0	0	0
3-3	0	0	0	0	0	0
3-4	0	0	0	0	0	0
3-5	0	0	0	0	0	0
3-6	0	0	0	0	0	0
3-7	0	0	0	0	0	0
3-8	0	0	0	0	0	0
4-1	0	0	0	0	0	0
4-2	0	0	0	0	0	0
4-3	0	0	0	0	0	0
4-4	0	0	0	0	0	0
4-5	0	0	0	0	0	0
4-6	0	0	0	0	0	0
4-7	0	0	0	0	0	0
4-8	0	0	0	0	0	0
Mean	0	0	0	0	0	0

Table 4.10 indicates that the Matlab *gradient* function successfully estimated a gradient for the Sigmoid Approximation Method, described in Section 3.1.2.2, at all grid points, for all values of s.

Table 4.11: Overall p-Norm Computational Stability Results.

	Proportion of Grid Points where Gradient Estimate Failed (%)					
Scenario	With p = 2	With p = 10	With p = 20	With p = 100	With p = 200	With p = 1000
1	0	0	0	0	0.6313	76.8115
2-1	0	0	0	0	0.8765	75.3927
2-2	0	0	0	0	1.0505	76.9243
2-3	0	0	0	0	1.9492	83.254
3-1	0	0	0	0	17.9725	88.2095
3-2	0	0	0	0	50.69	92.5623
3-3	0	0	0	0	50.69	94.7062
3-4	0	0	0	0	83.4074	99.0591
3-5	0	0	0	0	50.69	93.0499
3-6	0	0	0	0	50.69	91.4762
3-7	0	0	0	0	50.69	95.7923
3-8	0	0	0	0	50.69	94.2187
4-1	0	0	0	0	17.7739	88.389
4-2	0	0	0	0	50.6967	92.7034
4-3	0	0	0	0	50.1895	94.7414
4-4	0	0	0	0	83.1123	99.0558
4-5	0	0	0	0	50.3675	92.78
4-6	0	0	0	0	50.4431	91.1497
4-7	0	0	0	0	50.4431	96.2951
4-8	0	0	0	0	50.5187	94.6648
Mean	0	0	0	0	41.5887	90.8079

Table 4.11 indicates that the Matlab *gradient* function successfully estimated a gradient for the p-Norm Approximation Method, described in Section 3.1.2.3, at all grid points, for all values of p less than 200, but consistently failed to estimate a gradient at over 40% of grid points, for all values of p greater than or equal to 200.

Table 4.12: Overall Exponential p-Norm Computational Stability Results.

	Proportion of Grid Points where Gradient Estimate Failed (%)					
Scenario	With p = 2	With p = 10	With p = 20	With p = 100	With p = 200	With p = 1000
1	0	0	0	0	0.0712	31.8931
2-1	0	0	0	0	0.1138	34.6914
2-2	0	0	0	0	0.1573	36.3494
2-3	0	0	0	0	0.5016	44.0194
3-1	0	0	0	0	0	20.966
3-2	0	0	0	0	0	21.554
3-3	0	0	0	0	0	22.3184
3-4	0	0	0	0	0	22.9063
3-5	0	0	0	0	0	21.7304
3-6	0	0	0	0	0	21.1424
3-7	0	0	0	0	0	22.7299
3-8	0	0	0	0	0	22.142
4-1	0	0	0	0	0	24.5294
4-2	0	0	0	0	0	25.3494
4-3	0	0	0	0	0	25.7124
4-4	0	0	0	0	0	26.5324
4-5	0	0	0	0	0	25.3494
4-6	0	0	0	0	0	24.5294
4-7	0	0	0	0	0	26.5324
4-8	0	0	0	0	0	25.7124
Mean	0	0	0	0	0.0352	25.6611

Table 4.12 indicates that the Matlab *gradient* function successfully estimated a gradient for the Exponential p-Norm Approximation Method, described in Section 3.1.2.3, at all grid points, for all values of p less than 200, but consistently failed to estimate a gradient at over 25% of grid points, for all values of p equal to 1000.

4.2.1 Summary.

These results indicate that the Exponential p-Norm Approximation Method is unsuitable for use in defining the roadmap-based ATM conflict regions. Additionally, the non-exponential p-Norm Approximation Method is unsuitable for use in defining the roadmap-based ATM conflict regions when its accuracy parameter, p, is greater than 200. However, the Multiplier and Sigmoid Approximation methods appear suitable for use in defining the roadmap-based ATM conflict regions for all values of the accuracy parameters tested.

4.3 Shadow Time Overshoot Phase Model Results without Inertia

This section presents the results of evaluating the three test cases described in Section 3.1.4.1 using the STOP model implementation of the multi-objective HCS ATM optimization problem.

4.3.1 Viability of the Arrival Time Constraint.

The STOP method relies on the arrival time constraint to guarantee that each aircraft is modeled to arrive at its destination at its chosen arrival time. The constraint is defined in equation (3.49b) as

$$\Big(l_{[\mu,\alpha]} - c_{[\mu,\alpha]}(t)\Big)\Big(t - t_{[f,\alpha]}\Big) \leq 0, \quad \forall \alpha \in \{1, 2, \ldots, A\},$$

where control mode μ defines the path for each aircraft $\alpha \in \{1, 2, \ldots, A\}$, $l_{[\mu,\alpha]}$ is the path length for the path of aircraft α, $c_{[\mu,\alpha]}(t)$ is the path-length parameterized coordinate of aircraft α at time t, and $t_{[f,\alpha]}$ is the chosen arrival time of aircraft α. This section displays how well the various implementations of the STOP model were able to satisfy the arrival time constraint.

4.3.1.1 Multiplier Method Implementation Results.

Tables 4.13 - 4.18 display the maximum value of the arrival time constraint function (3.49b) for each of the Test Cases described in Section 3.1.4.1 evaluated in GPOPS-II using the STOP model with the Multiplier Method constraint approximation method with accuracy parameter set to $\gamma = 500$. For each treatment, either a time-based or state-based indicator function was used to adjust the ATM separation constraint, as detailed in Section 3.1.3.1. The results shown are only for treatments that satisfied the GPOPS-II optimality or feasibility criteria (detailed in Appendix C). Figures 4.5 - 4.7 plot the arrival time constraint function values for each treatment of Test Case 3

that satisfied the GPOPS-II optimality or feasibility criteria using the Multiplier Method constraint approximation with a state-based indicator function to adjust the ATM separation constraint.

Table 4.13: Test Case 1 Multiplier Method Maximum Arrival Time Constraint Violation.

Using Time-based Arrival Indicator			
Treatment	Aircraft 1	Aircraft 2	Aircraft 3
1	0	0	0
2	0	0.0003	0.0002
3	0	0	0
4	0	0	0
5	0	0	0
6	0	0	0
7	0	0	0
8	0	0	0
9	0.0004	0	0.0048
10	0	0	0
11	0	0	0
12	0	0.0003	0
13	0	0	0
14	0	0	0
15	0	0	0
16	0	0	0.0051
17	0	0	0
18	0.0004	0	0.0005
Max	0.0004	0.0003	0.0051
Mean	0	0	0.0006

Table 4.14: Test Case 2 Multiplier Method Maximum Arrival Time Constraint Violation.

Using Time-based Arrival Indicator			
Treatment	Aircraft 1	Aircraft 2	Aircraft 3
2	0	0.0003	0.0002
4	0	0	0
6	0	0	0
7	0	0	0
9	0.0003	0	0.0002
10	0	0	0.0032
12	0	0.0003	0
13	0	0	0.0003
16	0	0	0.0037
Max	0.0003	0.0003	0.0037
Mean	0	0.0001	0.0008

Table 4.15: Test Case 3 Multiplier Method Maximum Arrival Time Constraint Violation.

Using Time-based Arrival Indicator			
Treatment	Aircraft 1	Aircraft 2	Aircraft 3
1	0	0	0.0017
2	0.0003	0	0
3	0	0	0
4	0	0	0.0079
5	0	0	0
6	0	0	0
7	0	0	0.0051
8	0	0	0
10	0	0	0.0003
11	0	0	0
12	0	0	0.0002
13	0	0	0.0059
14	0	0	0
15	0	0	0
16	0	0	0.0001
17	0	0	0
18	0	0.0003	0.0015
Max	0.0003	0.0003	0.0079
Mean	0	0	0.0013

Table 4.16: Test Case 1 Multiplier Method Maximum Arrival Time Constraint Violation.

Using State-based Arrival Indicator			
Treatment	Aircraft 1	Aircraft 2	Aircraft 3
1	0	0	0
2	0	0.0003	0.0002
3	0	0	0
4	0	0	0
5	0	0	0
6	0	0	0
7	0	0	0
8	0	0	0
9	0.0001	0	0.0054
10	0	0	0.0006
11	0	0	0.0003
12	0	0.0003	0.0002
13	0	0	0
14	0	0	0
15	0	0	0
16	0	0	0.0011
17	0	0	0
18	0.0058	0	0
Max	0.0058	0.0003	0.0054
Mean	0.0003	0	0.0004

Table 4.17: Test Case 2 Multiplier Method Maximum Arrival Time Constraint Violation.

Using State-based Arrival Indicator			
Treatment	Aircraft 1	Aircraft 2	Aircraft 3
1	0	0	0
2	0	0.0003	0
3	0	0	0
4	0	0	0.0029
5	0	0	0
6	0	0	0
7	0	0	0
8	0	0	0
9	0.0001	0	0.0048
10	0	0	0
11	0	0	0
12	0	0.0003	0
13	0	0	0.0011
14	0	0	0
15	0	0	0
16	0	0	0.0028
17	0	0	0
18	0.0004	0	0
Max	0.0004	0.0003	0.0048
Mean	0	0	0.0006

Table 4.18: Test Case 3 Multiplier Method Maximum Arrival Time Constraint Violation.

Using State-based Arrival Indicator			
Treatment	Aircraft 1	Aircraft 2	Aircraft 3
1	0	0	0
2	0.0003	0	0
3	0	0	0
4	0	0	0.0024
5	0	0	0
6	0	0	0
7	0	0	0
8	0	0	0
9	0.0001	0.0025	0.0001
10	0	0	0
11	0	0	0
12	0.0061	0	0.0003
13	0	0	0.0003
14	0	0	0
16	0	0	0.0003
17	0	0	0
18	0.0004	0.0041	0.0006
Max	0.0061	0.0041	0.0024
Mean	0.0004	0.0004	0.0002

Tables 4.13 - 4.18 indicate that the Multiplier Method implementation of the STOP model consistently satisfied the arrival time constraint (3.49b), with a maximum violation of 0.008 observed when using the time-based indicator function.

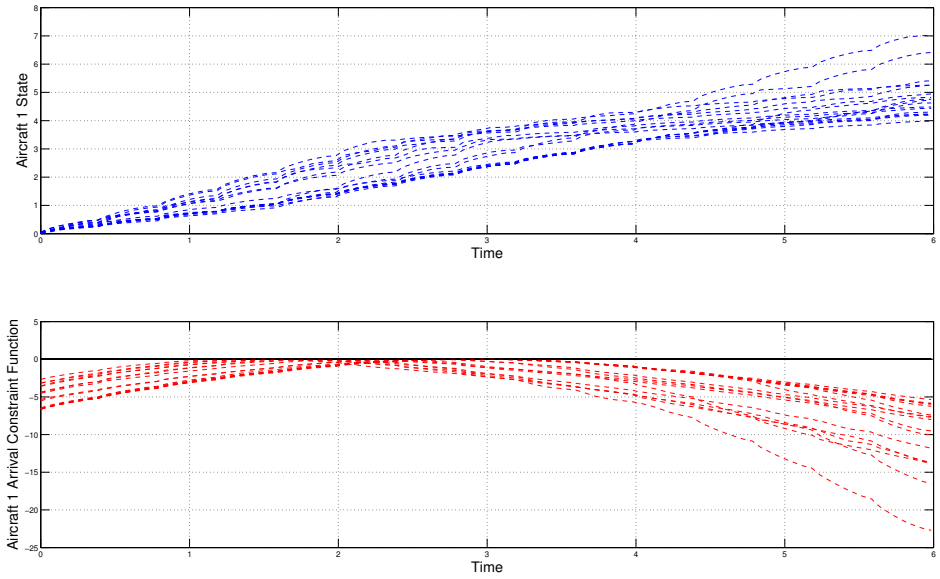

Figure 4.5: Multiplier Method Aircraft 1 Arrival Time Constraint Function Values

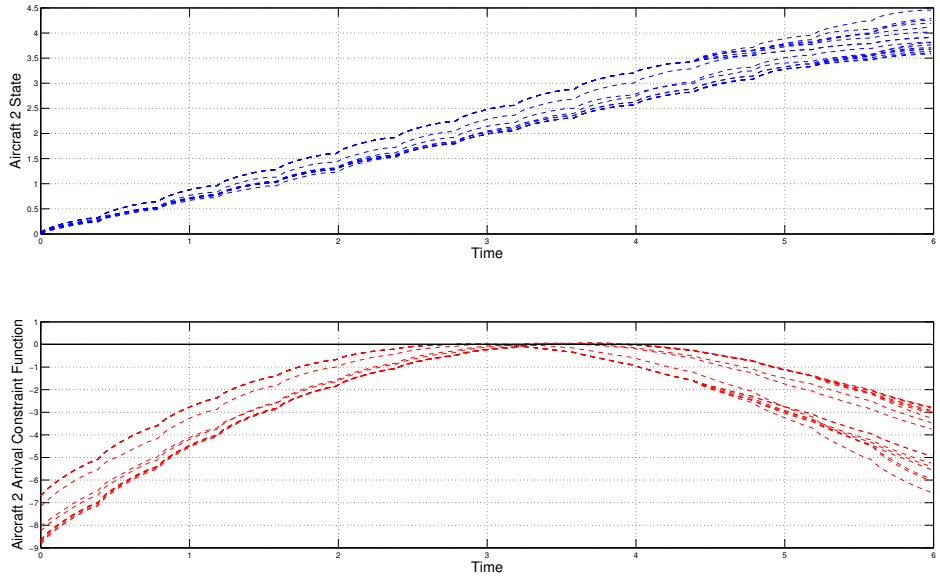

Figure 4.6: Multiplier Method Aircraft 2 Arrival Time Constraint Function Values

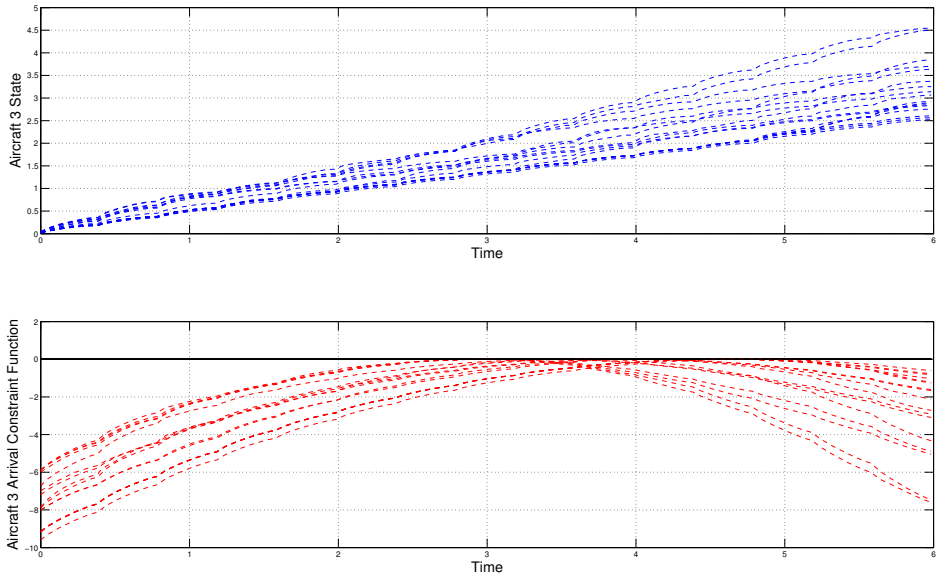

Figure 4.7: Multiplier Method Aircraft 3 Arrival Time Constraint Function Values

4.3.1.2 Sigmoid Method Implementation Results.

Tables 4.19 - 4.30 display the maximum value of the arrival time constraint function (3.49b) for each of the Test Cases described in Section 3.1.4.1 evaluated in GPOPS-II using the STOP model with the Sigmoid constraint approximation method with accuracy parameter set to $s = 200$. For each treatment, either a time-based or state-based indicator function or sigmoid was used to adjust the ATM separation constraint, as detailed in Section 3.1.3.1. The results shown are only for treatments that satisfied the GPOPS-II optimality or feasibility criteria (detailed in Appendix C). Figures 4.8 - 4.10 plot the arrival time constraint function values for each treatment of Test Case 3 that satisfied the GPOPS-II optimality or feasibility criteria using the sigmoid constraint approximation with a state-based indicator function to adjust the ATM separation constraint.

Table 4.19: Test Case 1 Sigmoid Method Maximum Arrival Time Constraint Violation.

Using Time-based Arrival Indicator			
Treatment	Aircraft 1	Aircraft 2	Aircraft 3
1	0	0	0
2	0	0	0.0071
3	0.0019	0	0.0058
5	0	0	0
8	0	0	0
9	0.0007	0	0.0055
11	0	0	0
12	0	0	0.0013
14	0	0	0
15	0	0	0
16	0	0	0
17	0	0	0
18	0.0068	0	0.0001
Max	0.0068	0	0.0071
Mean	0.0007	0	0.0015

Table 4.20: Test Case 2 Sigmoid Method Maximum Arrival Time Constraint Violation.

Using Time-based Arrival Indicator			
Treatment	Aircraft 1	Aircraft 2	Aircraft 3
1	0	0	0
3	0	0	0.002
5	0	0	0
6	0	0	0
8	0	0	0
9	0.0007	0	0.0054
10	0	0	0.0006
11	0	0	0
14	0	0	0
15	0	0	0
16	0	0	0
17	0	0	0
18	0.0069	0	0.0006
Max	0.0069	0	0.0054
Mean	0.0006	0	0.0007

Table 4.21: Test Case 3 Sigmoid Method Maximum Arrival Time Constraint Violation.

Using Time-based Arrival Indicator			
Treatment	Aircraft 1	Aircraft 2	Aircraft 3
1	0	0	0
2	0.0006	0	0
3	0	0	0
5	0	0	0
6	0	0	0
8	0	0	0
9	0	0.0004	0.0034
10	0	0	0
11	0	0	0
12	0.0006	0	0
13	0	0	0
14	0	0	0
15	0	0	0
18	0	0.0004	0
Max	0.0006	0.0004	0.0034
Mean	0.0001	0.0001	0.0002

Table 4.22: Test Case 1 Sigmoid Method Maximum Arrival Time Constraint Violation.

Using State-based Arrival Indicator			
Treatment	Aircraft 1	Aircraft 2	Aircraft 3
1	0	0	0
2	0	0.0041	0
3	0	0	0.0043
4	0	0	0
5	0	0	0
6	0	0	0
7	0	0	0
8	0	0	0
9	0.0005	0	0.0013
10	0	0	0
11	0	0	0
12	0	0.0004	0
13	0	0	0
14	0	0	0
15	0	0	0
16	0	0	0.0007
17	0	0	0
18	0.0002	0	0.0002
Max	0.0005	0.0041	0.0043
Mean	0	0.0002	0.0004

Table 4.23: Test Case 2 Sigmoid Method Maximum Arrival Time Constraint Violation.

Using State-based Arrival Indicator			
Treatment	Aircraft 1	Aircraft 2	Aircraft 3
1	0	0	0
2	0	0.0004	0
3	0	0	0
4	0	0	0
5	0	0	0
6	0	0	0
7	0	0	0.0004
8	0	0	0
9	0.0007	0	0.0058
10	0	0	0.0004
11	0	0	0.0042
12	0	0.0041	0
14	0	0	0
15	0	0	0
17	0	0	0
18	0.0007	0	0.0048
Max	0.0007	0.0041	0.0058
Mean	0.0001	0.0003	0.001

Table 4.24: Test Case 3 Sigmoid Method Maximum Arrival Time Constraint Violation.

Using State-based Arrival Indicator			
Treatment	Aircraft 1	Aircraft 2	Aircraft 3
1	0	0	0.0002
3	0	0	0.0031
4	0	0	0.0005
5	0	0	0
6	0	0	0
7	0	0.0023	0.0075
8	0	0	0
9	0	0.0004	0.0055
10	0	0	0.0035
11	0	0	0.0038
14	0	0	0
15	0	0	0
17	0	0	0
18	0	0.0003	0.0001
Max	0	0.0023	0.0075
Mean	0	0.0002	0.0017

Table 4.25: Test Case 1 Sigmoid Method Maximum Arrival Time Constraint Violation.

Using Time-based Arrival Sigmoid			
Treatment	Aircraft 1	Aircraft 2	Aircraft 3
2	0	0	0.0008
3	0	0.0046	0.0052
5	0	0	0
6	0	0	0
8	0	0	0
9	0.0005	0	0.0055
10	0	0	0
12	0	0	0.0004
15	0	0	0
17	0	0	0
Max	0.0005	0.0046	0.0055
Mean	0.0001	0.0005	0.0012

Table 4.26: Test Case 2 Sigmoid Method Maximum Arrival Time Constraint Violation.

Using Time-based Arrival Sigmoid			
Treatment	Aircraft 1	Aircraft 2	Aircraft 3
2	0	0	0.0011
3	0	0.0047	0
5	0	0	0
6	0	0	0
8	0	0	0
9	0.0005	0	0.0044
10	0	0	0
11	0	0	0
12	0	0	0.0007
14	0	0	0
15	0	0	0
17	0	0	0
18	0.0007	0	0.0013
Max	0.0007	0.0047	0.0044
Mean	0.0001	0.0004	0.0006

Table 4.27: Test Case 3 Sigmoid Method Maximum Arrival Time Constraint Violation.

Using Time-based Arrival Sigmoid			
Treatment	Aircraft 1	Aircraft 2	Aircraft 3
1	0	0	0
2	0.0006	0	0
3	0	0	0
4	0	0	0
5	0	0	0
6	0	0	0
7	0	0	0
8	0	0	0
9	0	0.0003	0
10	0.0002	0	0
11	0	0	0
12	0.0006	0	0.0003
13	0	0	0.0033
14	0	0	0
15	0	0	0
16	0	0	0.0033
17	0	0	0
18	0	0.0004	0.0008
Max	0.0006	0.0004	0.0033
Mean	0.0001	0	0.0004

Table 4.28: Test Case 1 Sigmoid Method Maximum Arrival Time Constraint Violation.

Using State-based Arrival Sigmoid			
Treatment	Aircraft 1	Aircraft 2	Aircraft 3
1	0	0	0.0006
2	0	0.0004	0.0002
3	0	0	0
4	0	0	0.0075
6	0	0	0
7	0	0	0.0005
8	0	0	0
9	0.0002	0	0.0055
11	0	0	0
12	0	0.0004	0
13	0	0	0.001
14	0	0	0
15	0	0	0
17	0	0	0
18	0.0006	0.0001	0.0055
Max	0.0006	0.0004	0.0075
Mean	0.0001	0.0001	0.0014

Table 4.29: Test Case 2 Sigmoid Method Maximum Arrival Time Constraint Violation.

Using State-based Arrival Sigmoid			
Treatment	Aircraft 1	Aircraft 2	Aircraft 3
1	0	0	0
2	0	0.0004	0
3	0	0	0.0001
4	0	0	0
6	0	0	0
7	0	0	0
9	0.0007	0.0003	0.0045
11	0	0	0
12	0	0.0004	0
13	0	0	0
14	0	0	0
15	0	0	0
17	0	0	0
18	0.0006	0	0.0002
Max	0.0007	0.0004	0.0045
Mean	0.0001	0.0001	0.0003

Table 4.30: Test Case 3 Sigmoid Method Maximum Arrival Time Constraint Violation.

Using State-based Arrival Sigmoid			
Treatment	Aircraft 1	Aircraft 2	Aircraft 3
1	0	0	0.0003
2	0.0007	0	0.0003
3	0	0	0
5	0	0	0
6	0	0	0
7	0	0	0.0032
8	0	0	0
9	0.0043	0.0002	0.0055
10	0	0	0
11	0	0	0.0024
12	0.0006	0	0
14	0	0	0
15	0	0	0
16	0	0	0.0032
17	0	0	0
18	0	0.0004	0.0007
Max	0.0043	0.0004	0.0055
Mean	0.0003	0	0.001

Tables 4.19 - 4.30 indicate that the Sigmoid implementation of the STOP model consistently satisfied the arrival time constraint (3.49b), with a maximum violation of 0.0075 observed when using the state-based indicator function or sigmoid.

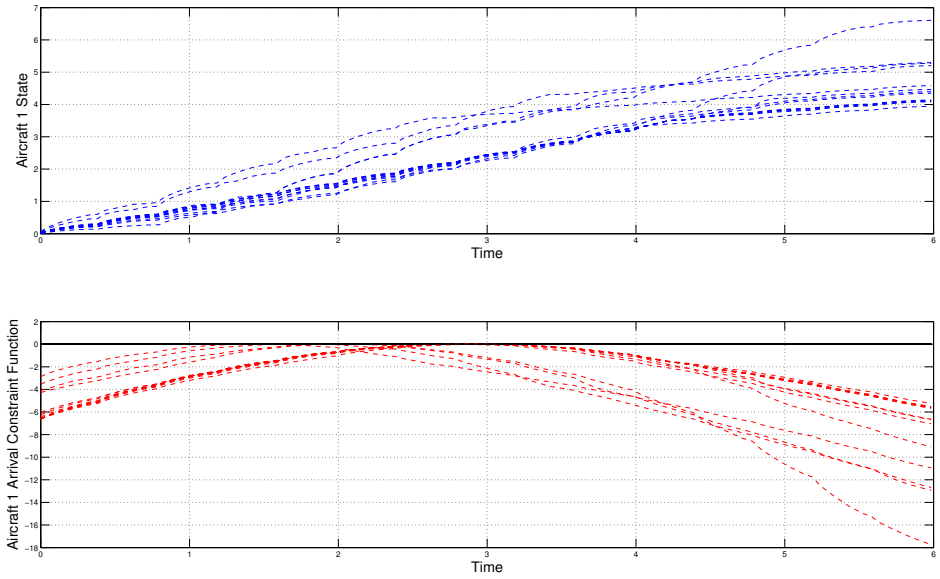

Figure 4.8: Sigmoid Method Aircraft 1 Arrival Time Constraint Function Values

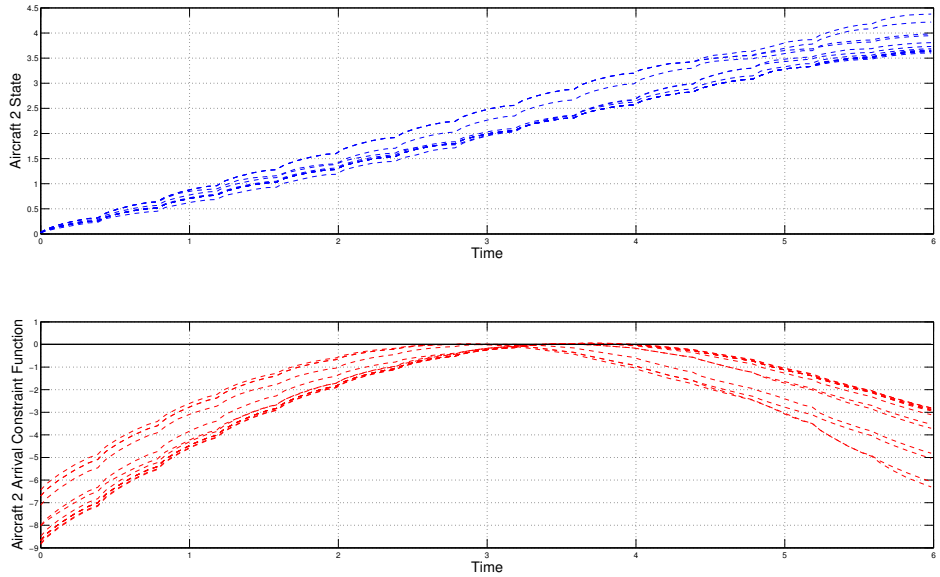

Figure 4.9: Sigmoid Method Aircraft 2 Arrival Time Constraint Function Values

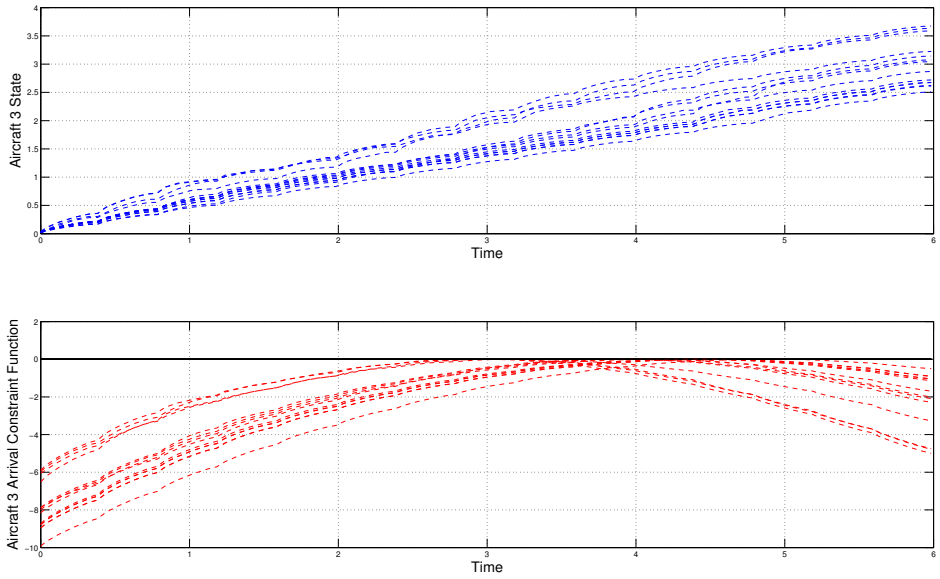

Figure 4.10: Sigmoid Method Aircraft 3 Arrival Time Constraint Function Values

4.3.1.3 p-Norm Method Implementation Results.

Tables 4.31 - 4.34 display the maximum value of the arrival time constraint function (3.49b) for each of the Test Cases described in Section 3.1.4.1 evaluated in GPOPS-II using the STOP model with the p-Norm constraint approximation method with accuracy parameter set to $p = 20$. For each treatment, either a time-based or state-based indicator function was used to adjust the ATM separation constraint, as detailed in Section 3.1.3.1. The results shown are only for treatments that satisfied the GPOPS-II optimality or feasibility criteria (detailed in Appendix C). Figures 4.11 - 4.13 plot the arrival time constraint function values for each treatment of Test Case 2 that satisfied the GPOPS-II optimality or feasibility criteria using the p-Norm constraint approximation with a state-based indicator function to adjust the ATM separation constraint. Note that the p-Norm method failed to complete treatments from Test Case 3 since the constraint approximation values became computationally unstable for these scenarios.

Table 4.31: Test Case 1 p-Norm Method Maximum Arrival Time Constraint Violation.

Using Time-based Arrival Indicator			
Treatment	Aircraft 1	Aircraft 2	Aircraft 3
1	0	0	0
2	0	0.0004	0.0002
3	0	0	0
4	0	0	0
5	0	0	0
6	0	0	0
7	0	0	0
8	0	0	0
9	0	0	0.0048
10	0	0	0.002
11	0	0	0
12	0	0.0004	0.0002
13	0	0	0.0004
14	0	0	0
15	0	0	0
16	0	0	0.0076
17	0	0	0
18	0.0004	0	0.0048
Max	0.0004	0.0004	0.0076
Mean	0	0	0.0011

Table 4.32: Test Case 2 p-Norm Method Maximum Arrival Time Constraint Violation.

Using Time-based Arrival Indicator			
Treatment	Aircraft 1	Aircraft 2	Aircraft 3
1	0	0	0
2	0	0.0004	0.0002
3	0	0	0
4	0	0	0
5	0	0	0
6	0	0	0
7	0	0	0
8	0	0	0
9	0.0003	0	0.0009
11	0	0	0
12	0	0.0004	0.0002
13	0	0	0
14	0	0	0
15	0	0	0
16	0	0	0
17	0	0	0
18	0.0005	0	0.0048
Max	0.0005	0.0004	0.0048
Mean	0	0	0.0004

Table 4.33: Test Case 1 p-Norm Method Maximum Arrival Time Constraint Violation.

Using State-based Arrival Indicator			
Treatment	Aircraft 1	Aircraft 2	Aircraft 3
1	0	0	0
2	0	0.0004	0.0002
3	0	0	0
4	0	0	0
5	0	0	0
6	0.0006	0	0
7	0	0	0.0005
8	0	0	0
9	0.0007	0.0002	0.0055
10	0	0	0.0032
11	0	0	0
12	0	0.0004	0.0002
13	0	0	0
14	0	0	0
15	0	0	0
16	0	0	0.0057
17	0	0	0
18	0.0004	0	0.0048
Max	0.0007	0.0004	0.0057
Mean	0.0001	0.0001	0.0011

Table 4.34: Test Case 2 p-Norm Method Maximum Arrival Time Constraint Violation.

Using State-based Arrival Indicator			
Treatment	Aircraft 1	Aircraft 2	Aircraft 3
1	0	0	0.0094
2	0	0.0004	0.0002
3	0	0	0
4	0	0	0.0002
5	0	0	0
6	0	0	0
7	0	0	0
8	0	0	0
9	0.0001	0	0.0004
10	0	0	0.0002
11	0	0	0
12	0	0.0004	0.0002
13	0	0	0.0053
14	0	0	0
15	0	0	0
16	0	0	0.0002
17	0	0	0
18	0.0006	0	0.0055
Max	0.0006	0.0004	0.0094
Mean	0	0	0.0012

Tables 4.31 - 4.34 indicate that the p-Norm implementation of the STOP model consistently satisfied the arrival time constraint (3.49b), with a maximum violation of 0.0094 observed when using the state-based indicator function.

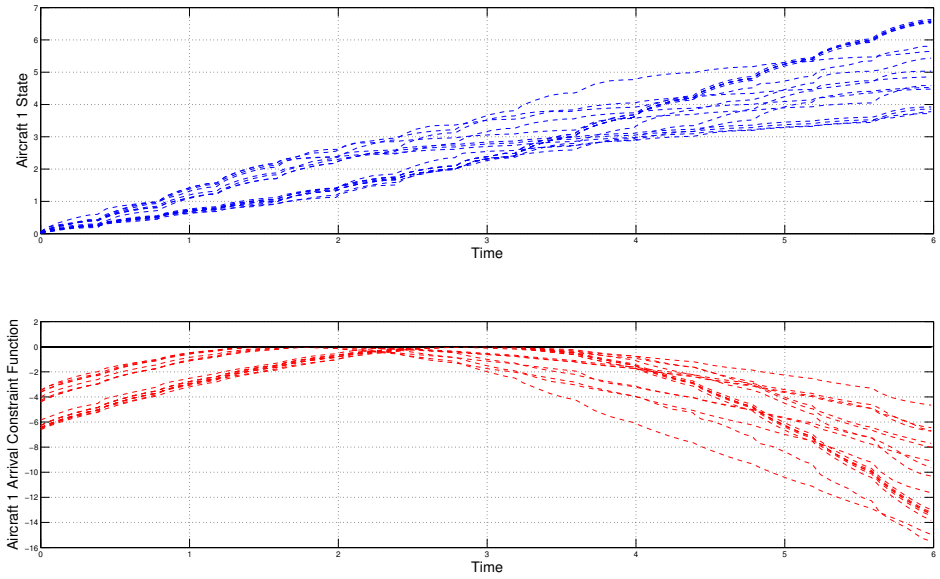

Figure 4.11: *p*-Norm Method Aircraft 1 Arrival Time Constraint Function Values

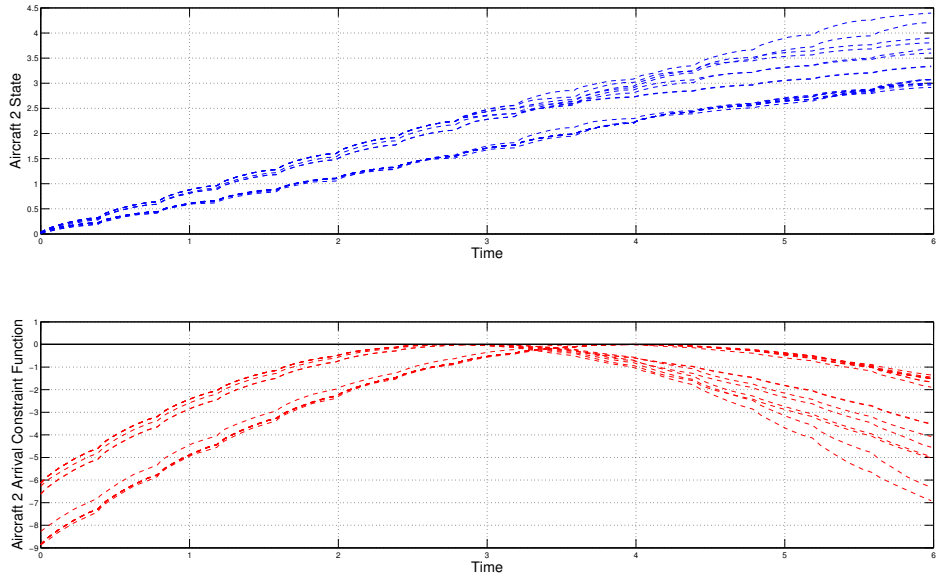

Figure 4.12: *p*-Norm Method Aircraft 2 Arrival Time Constraint Function Values

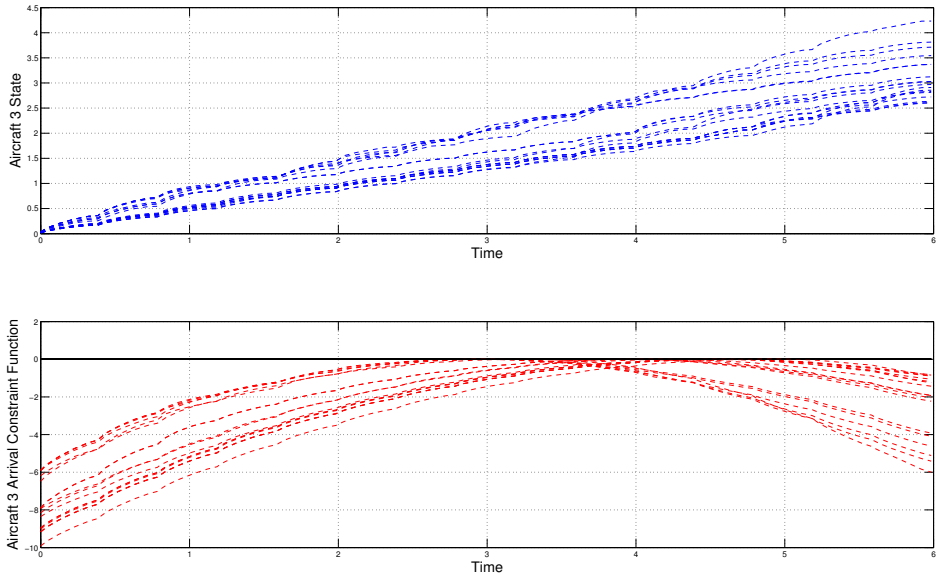

Figure 4.13: *p*-Norm Method Aircraft 3 Arrival Time Constraint Function Values

4.3.2 Multi-Objective Optimization Results without Inertia.

This section provides the results of the multi-objective test case evaluation described in Section 3.1.4.2, and compares the results of different implementation of the STOP model without inertia.

4.3.2.1 Multiplier Method Implementation Performance.

Tables 4.35 - 4.37 display the minimum measures of total deviation from schedule, total time (*makespan*) and fuel consumption achieved across all successfully completed treatments of the test cases described in Section 3.1.4.2, evaluated using the Multiplier Method constraint implementation of the STOP model in GPOPS-II. Tables 4.35 - 4.37 also indicate the average successful completion rate and the average time required to evaluate each treatment. Figures 4.14-4.16 provide scatter plots of the measure of total deviation from schedule, total time and fuel consumption achieved for all treatment evaluations that completed successfully.

Table 4.35: Test Case1 Multiplier Method Implementation Summary Results.

	Minimum Value Achieved			Average Value Achieved	
Indicator Function	Fuel Measure	Schedule Deviation	Total Time	Success Rate	Seconds To Completion
Time-based	3.6616	0	7.3841	1	24.2407
State-based	3.6549	0	7.3841	1	24.3057

Table 4.35 indicates both arrival indicator implementation types achieved nearly identical fuel, schedule deviation, and makespan minima for the Multiplier Method STOP model of Test Case 1.

Table 4.36: Test Case 2 Multiplier Method Implementation Summary Results.

	Minimum Value Achieved			Average Value Achieved	
Indicator Function	Fuel Measure	Schedule Deviation	Total Time	Success Rate	Seconds To Completion
Time-based	3.6739	0	7.3841	0.5	42.6122
State-based	3.6553	0	7.3841	1	77.1687

Table 4.36 indicates the state-based arrival indicator implementation achieved the lowest overall fuel measure and highest average success rate for the Multiplier Method STOP model of Test Case 2. However, it also had the longest average time to completion.

Table 4.37: Test Case 3 Multiplier Method Implementation Summary Results.

	Minimum Value Achieved			Average Value Achieved	
Indicator Function	Fuel Measure	Schedule Deviation	Total Time	Success Rate	Seconds To Completion
Time-based	5.4954	0.0394	9.2642	0.9444	16.5383
State-based	5.5079	0.0394	9.2642	0.9444	44.7151

Table 4.37 indicates both arrival indicator implementation types achieved similar minimum overall fuel measure, schedule deviation measure and makespan for the Multiplier Method STOP

model of Test Case 3. However, the time-based arrival indicator implementation had the lowest average time to completion.

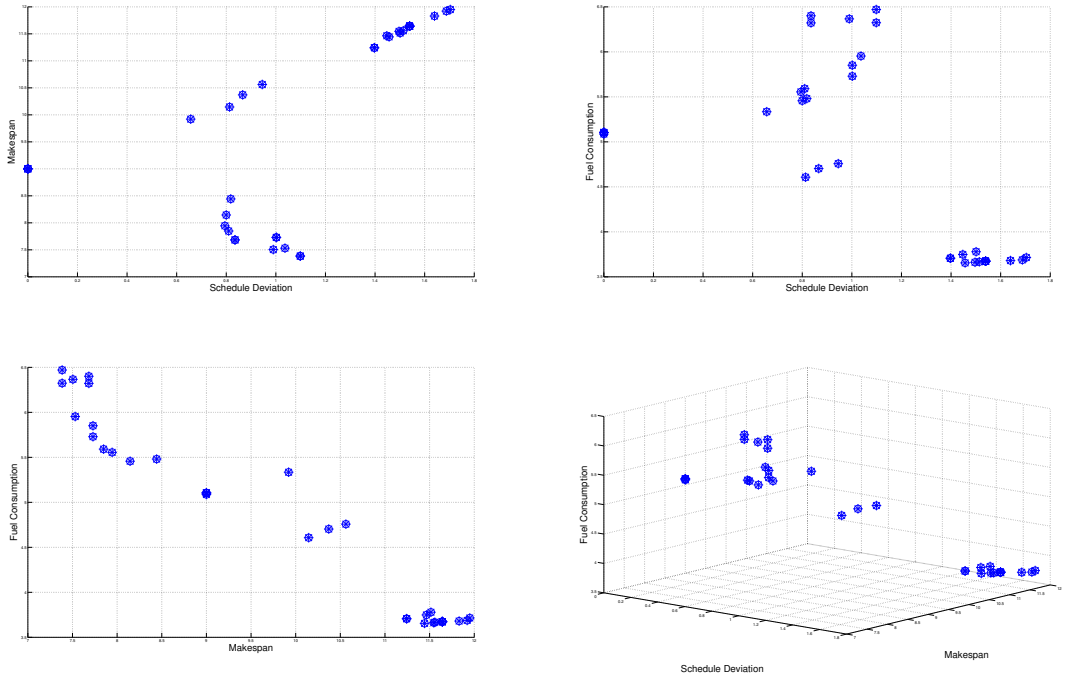

Figure 4.14: Test Case 1 Multiplier Method Objective Plots

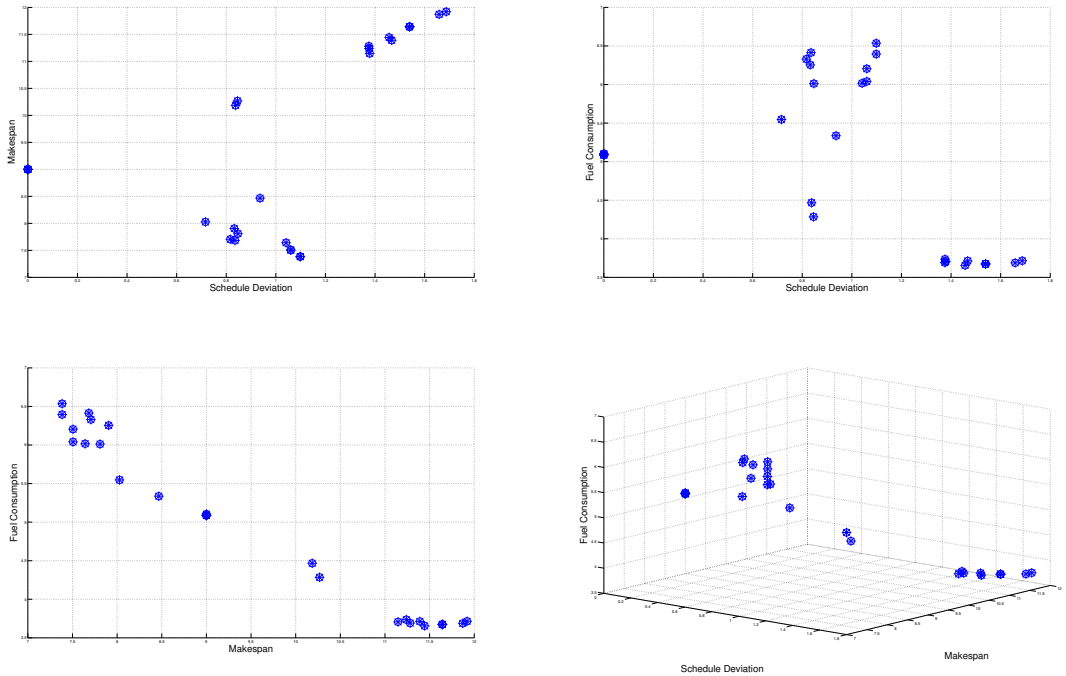

Figure 4.15: Test Case 2 Multiplier Method Objective Plots

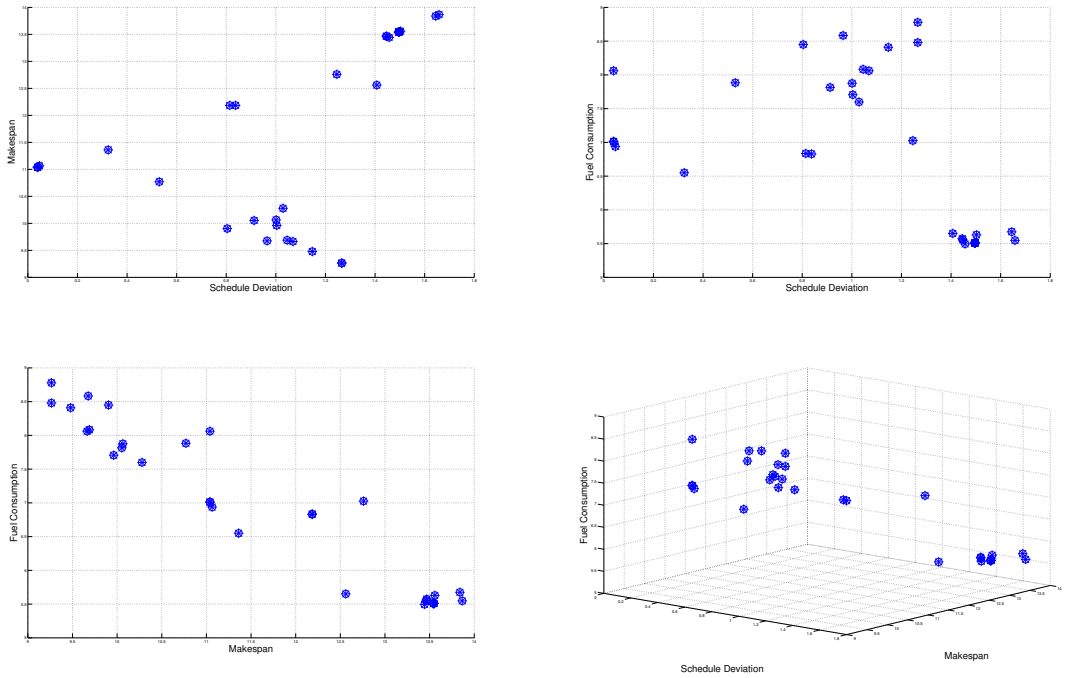

Figure 4.16: Test Case 3 Multiplier Method Objective Plots

Figures 4.14 - 4.16 indicate the Multiplier Method STOP model evaluation of all treatments resulted in multiple gaps in the multi-objective minimization surface.

4.3.2.2 Sigmoid Implementation Performance.

Tables 4.38 - 4.40 display the minimum measures of total deviation from schedule, total time (*makespan*) and fuel consumption achieved across all successfully completed treatments of the test cases described in Section 3.1.4.2, evaluated using the Sigmoid constraint implementation of the STOP model in GPOPS-II. Tables 4.38 - 4.40 also indicate the average successful completion rate and the average time required to evaluate each treatment. Figures 4.14-4.16 provide scatter plots of the measure of total deviation from schedule, total time, and fuel consumption achieved for all treatment evaluations that completed successfully.

Table 4.38: Test Case1 Sigmoid Implementation Summary Results.

	Minimum Value Achieved			Average Value Achieved	
Indicator Function	Fuel Measure	Schedule Deviation	Total Time	Success Rate	Seconds To Completion
Time-based	3.6771	0.4801	7.4483	0.7222	17.5508
State-based	3.6718	0	7.3841	1	52.0399
Time-based Sigmoid	3.6799	0.1958	7.8483	0.5556	31.6178
State-based Sigmoid	3.6799	0	7.5059	0.8333	16.6409

Table 4.38 indicates the state-based arrival indicator implementation achieved the lowest overall fuel measure, schedule deviation measure, and makespan for the sigmoid STOP model of Test Case 1. It also achieved the highest success rate, but had the longest average time to completion.

Table 4.39: Test Case 2 Sigmoid Method Implementation Summary Results.

	Minimum Value Achieved			Average Value Achieved	
Indicator Function	Fuel Measure	Schedule Deviation	Total Time	Success Rate	Seconds To Completion
Time-based	3.6721	0.4185	7.6509	0.7222	12.7943
State-based	3.6774	0	7.6089	0.8889	22.527
Time-based Sigmoid	3.6802	0.2282	7.7453	0.7222	40.5692
State-based Sigmoid	3.69	0	7.4483	0.7778	13.4506

Table 4.39 indicates all arrival indicator implementation types achieved similar results for the sigmoid STOP model of Test Case 2.

Table 4.40: Test Case 3 Sigmoid Method Implementation Summary Results.

	Minimum Value Achieved			Average Value Achieved	
Indicator Function	Fuel Measure	Schedule Deviation	Total Time	Success Rate	Seconds To Completion
Time-based	5.5114	0.0029	9.2642	0.7778	88.0253
State-based	5.5111	0.9548	9.6642	0.7778	37.9908
Time-based Sigmoid	5.5243	0.0394	9.2642	1	10.5476
State-based Sigmoid	5.5198	0.0028	9.2642	0.8889	61.6865

Table 4.40 indicates the time-based sigmoid arrival indicator implementation types achieved the overall highest success rate and lowest average completion time for the sigmoid STOP model of Test Case 3.

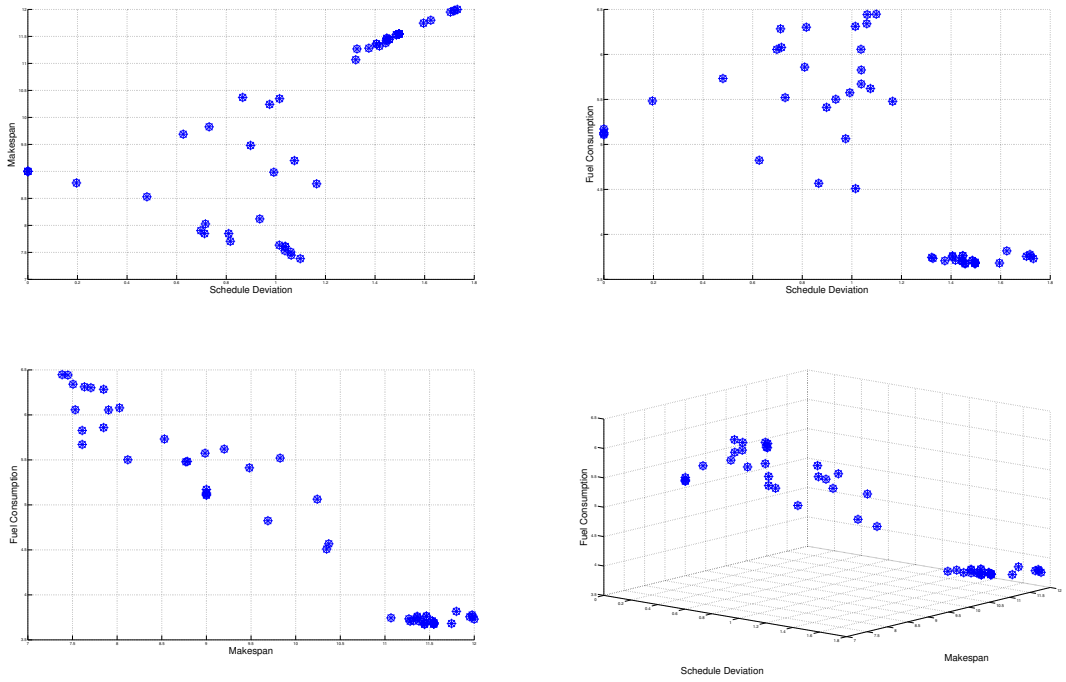

Figure 4.17: Test Case 1 Sigmoid Method Objective Plots

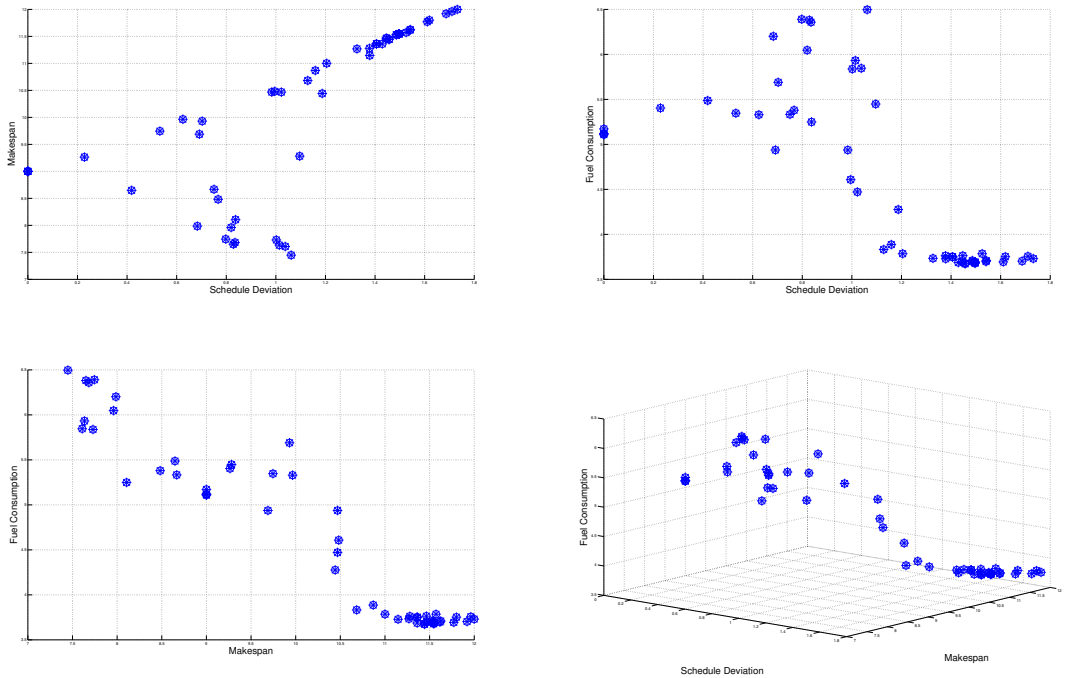

Figure 4.18: Test Case 2 Sigmoid Method Objective Plots

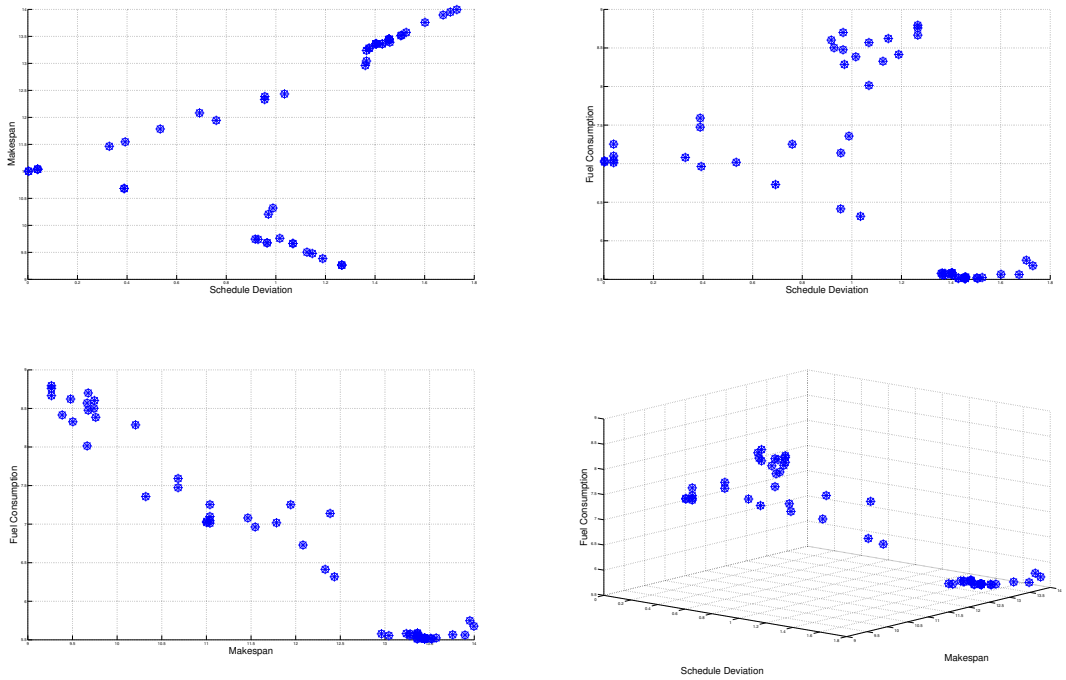

Figure 4.19: Test Case 3 Sigmoid Method Objective Plots

Figures 4.17 - 4.19 indicate the sigmoid STOP model evaluation of all treatments resulted in few gaps in the multi-objective minimization surface.

4.3.2.3 p-Norm Implementation Performance.

Tables 4.41 and 4.42 display the minimum measures of total deviation from schedule, total time (*makespan*), and fuel consumption achieved across all successfully completed treatments of the test cases described in Section 3.1.4.2, evaluated using the *p*-Norm constraint implementation of the STOP model in GPOPS-II. Tables 4.41 and 4.42 also indicate the average successful completion rate and the average time required to evaluate each treatment. Figures 4.20-4.21 provide scatter plots of the measure of total deviation from schedule, total time and fuel consumption achieved for all treatment evaluations that completed successfully.

Table 4.41: Test Case1 p-Norm Implementation Summary Results.

	Minimum Value Achieved			Average Value Achieved	
Indicator Function	Fuel Measure	Schedule Deviation	Total Time	Success Rate	Seconds To Completion
Time-based	3.6741	0	7.3841	1	15.6913
State-based	3.6807	0	7.3208	1	35.5346

Table 4.41 indicates both arrival indicator implementation types achieved similar minimum overall fuel measure, schedule deviation measure, makespan, and success rate for the p-Norm STOP model of Test Case 1. However, the time-based arrival indicator implementation had the lowest average time to completion.

Table 4.42: Test Case 2 p-Norm Implementation Summary Results.

	Minimum Value Achieved			Average Value Achieved	
Indicator Function	Fuel Measure	Schedule Deviation	Total Time	Success Rate	Seconds To Completion
Time-based	3.681	0	7.4089	0.9444	18.4806
State-based	3.681	0	7.3841	1	98.4673

Table 4.42 indicates both arrival indicator implementation types achieved similar minimum overall fuel measure, schedule deviation measure, makespan, and success rate for the p-Norm STOP model of Test Case 2. However, the time-based arrival indicator implementation had the lowest average time to completion.

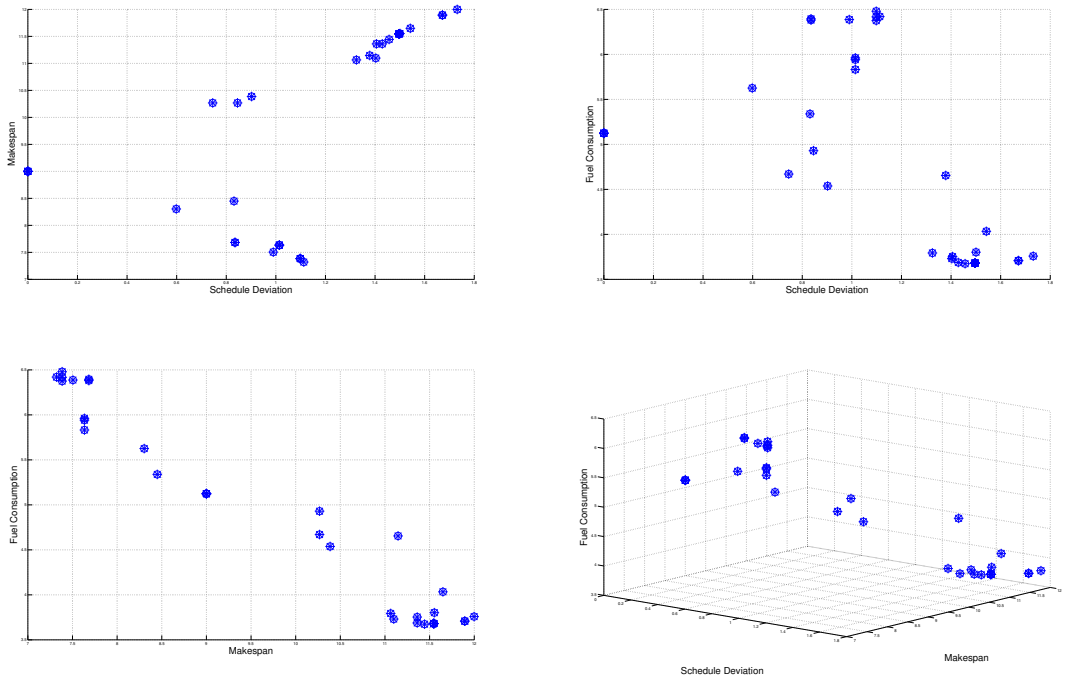

Figure 4.20: Test Case 1 p-Norm Method Objective Plots

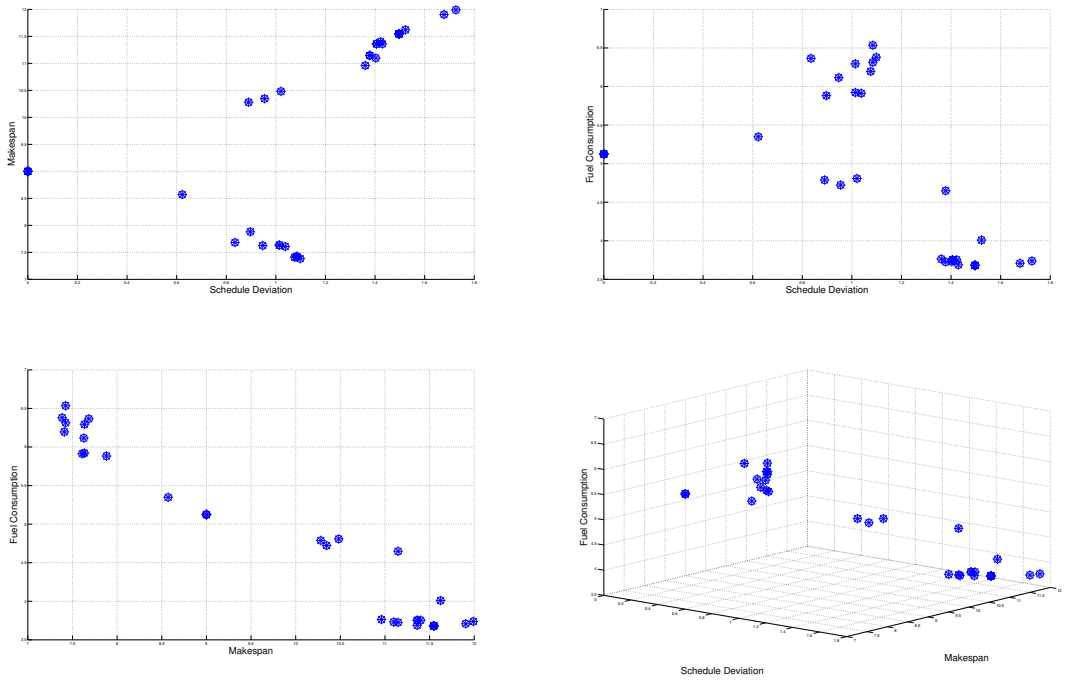

Figure 4.21: Test Case 2 p-Norm Method Objective Plots

Figures 4.20 - 4.21 indicate the p-Norm STOP model evaluation of all treatments resulted in multiple gaps in the multi-objective minimization surface.

4.3.2.4 Conflict Region Avoidance.

This section presents the state space trajectories associated with each successful constraint approximation implementation of the STOP model.

1. Multiplier Method Implementation Trajectories

   Figures 4.22 - 4.24 display all the state-space trajectories obtained from successful treatment evaluations using the Multiplier Method constraint approximation with time- or state-based arrival indicator functions, with three-dimensional conflict regions in red, and pair-wise conflict regions in solid black. These trajectories indicate that the Multiplier Method constraint approximation successfully implemented the ATM separation restrictions, and in at least one instance of Test Case 3, generated a solution that required a change in the nominal

arrival sequence. Note that since the on-time arrival constraint was satisfied, each aircraft's state is plotted as the final state after the aircraft's arrival time.

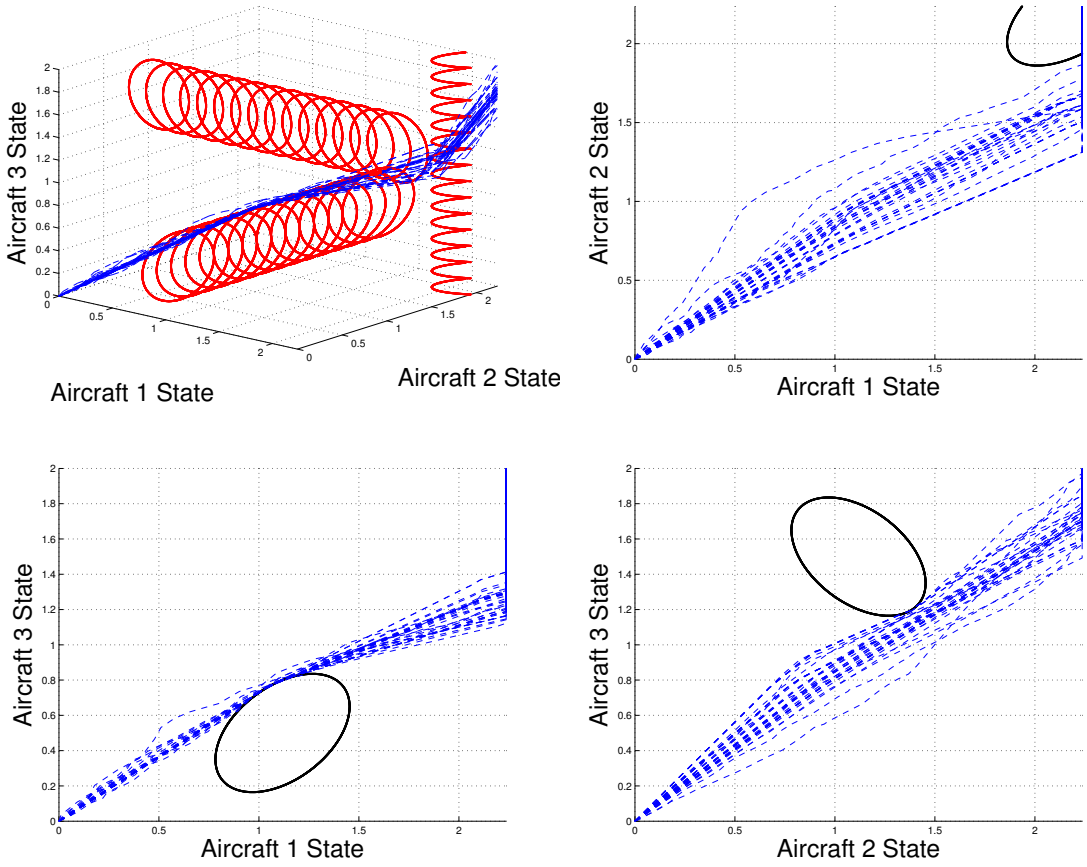

Figure 4.22: Test Case 1 Multiplier Method State Space Trajectories

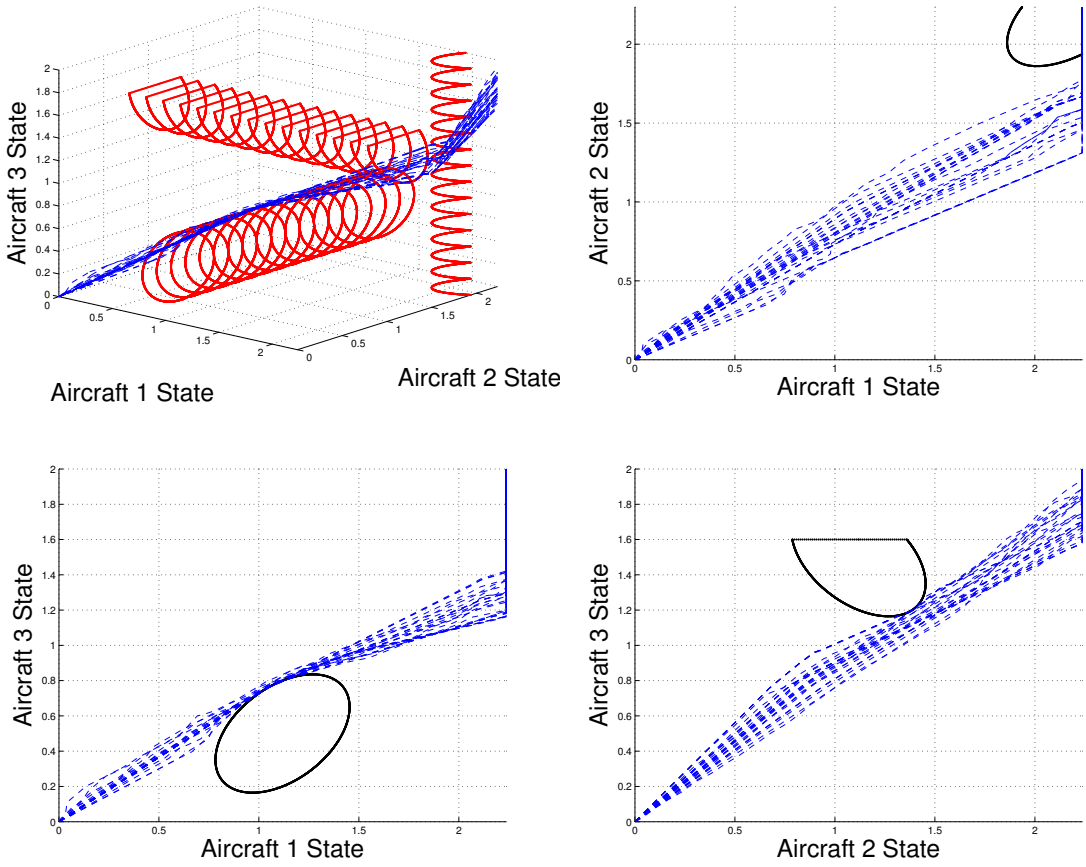

Figure 4.23: Test Case 2 Multiplier Method State Space Trajectories

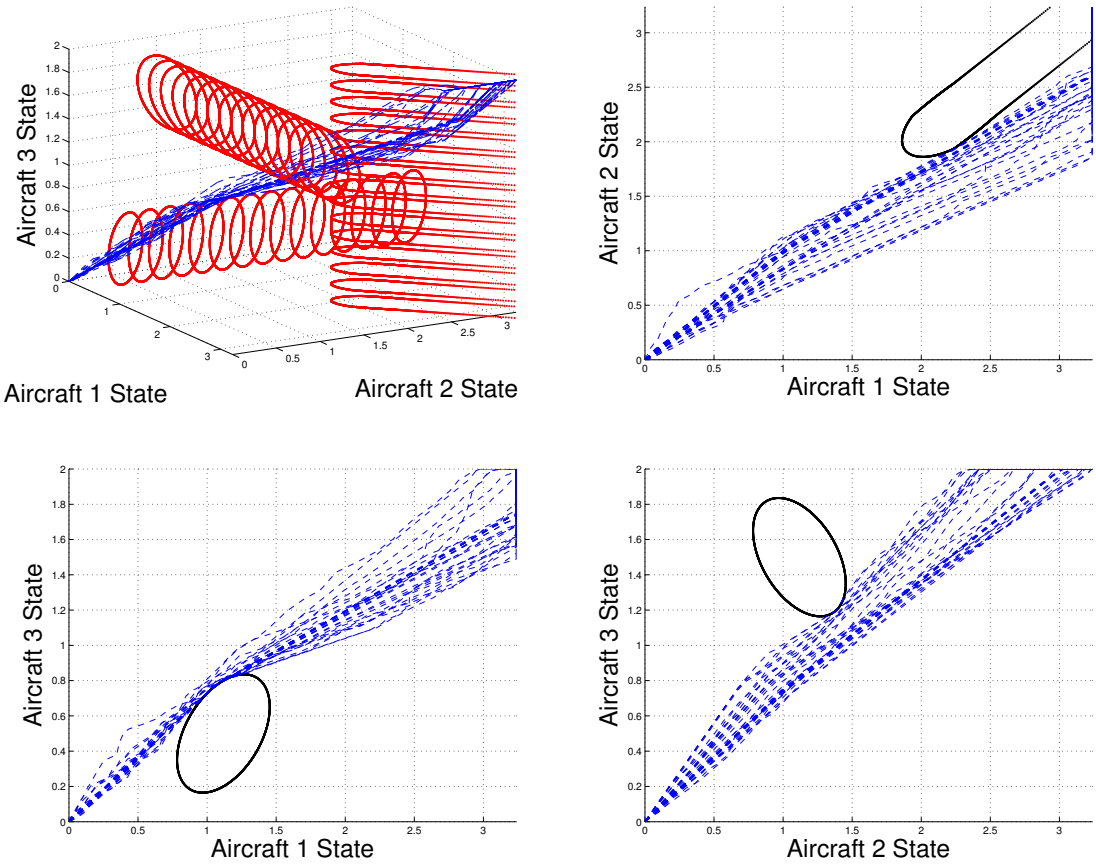

Figure 4.24: Test Case 3 Multiplier Method State Space Trajectories

2. Sigmoid Implementation Trajectories

Figures 4.25 - 4.27 display all the state-space trajectories obtained from successful treatment evaluations using the Sigmoid constraint approximation with time- or state-based arrival indicator and sigmoid functions, with three-dimensional conflict regions in red, and pair-wise conflict regions in solid black. These trajectories indicate that the Sigmoid constraint approximation method successfully implemented the ATM separation restrictions, and in at least one instance of Test Case 2, generated a solution that required a change in the nominal arrival sequence. Note that since the on-time arrival constraint was satisfied, each aircraft's state is plotted as the final state after the aircraft's arrival time.

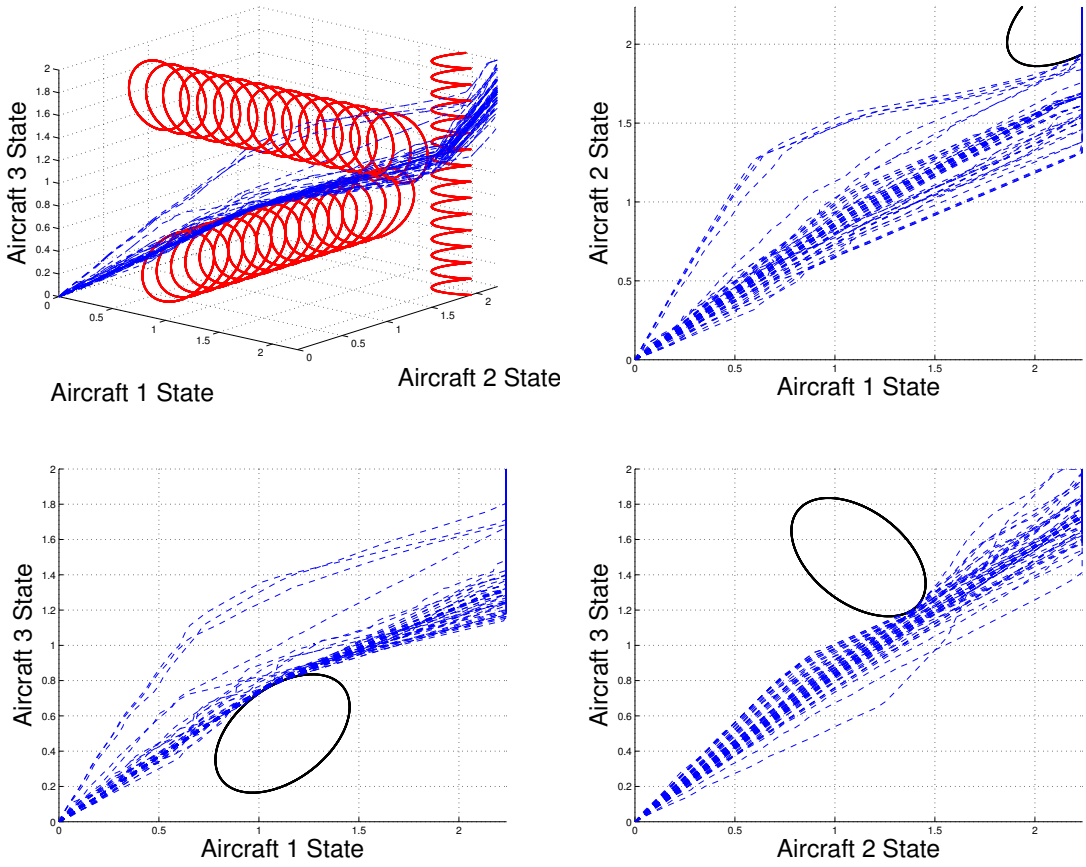

Figure 4.25: Test Case 1 Sigmoid Method State Space Trajectories

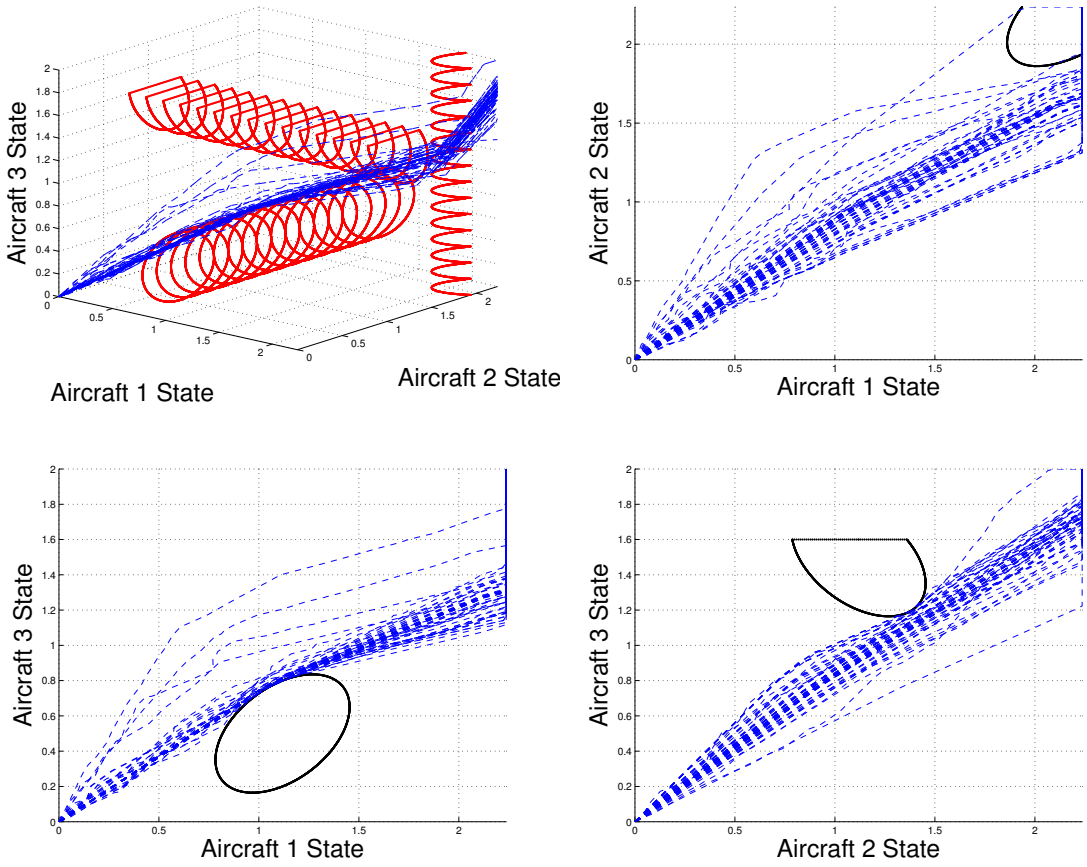

Figure 4.26: Test Case 2 Sigmoid Method State Space Trajectories

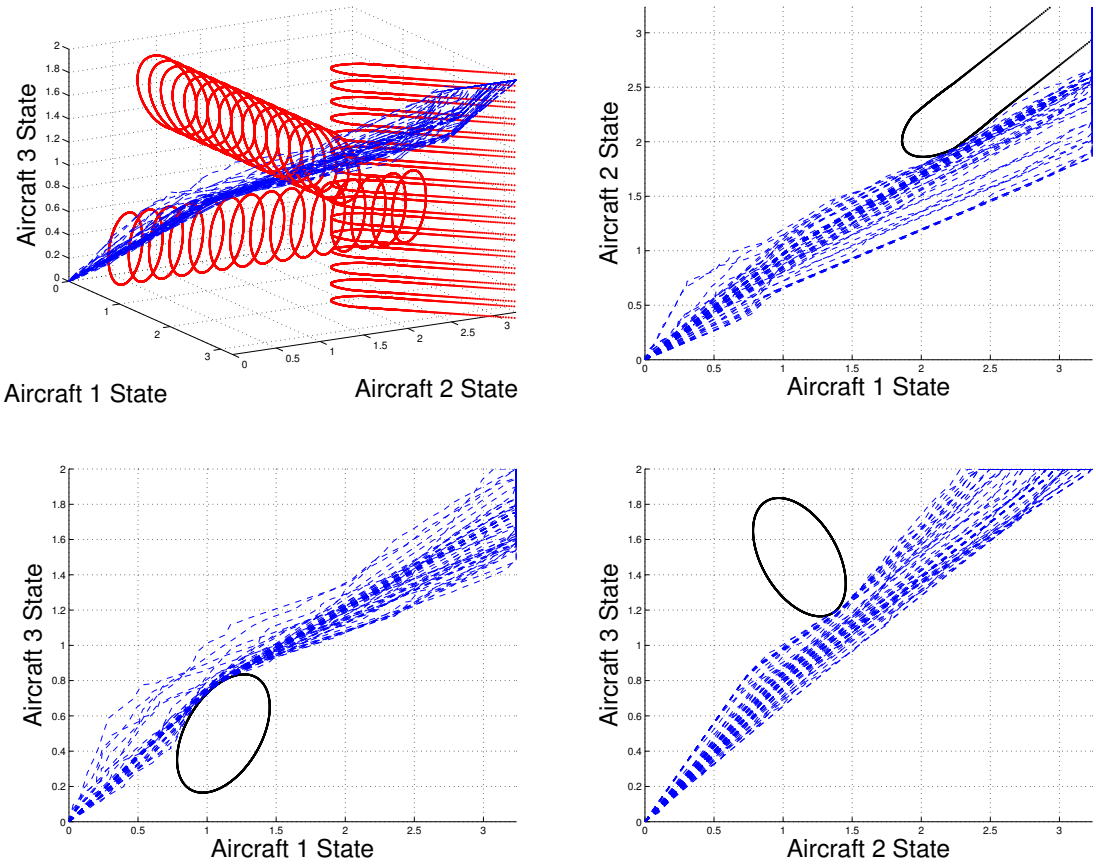

Figure 4.27: Test Case 3 Sigmoid Method State Space Trajectories

3. p-Norm Implementation Trajectories

Figures 4.28 and 4.29 display all the state-space trajectories obtained from successful treatment evaluations using the p-Norm constraint approximation with time- or state-based arrival indicator functions, with three-dimensional conflict regions in red, and pair-wise conflict regions in solid black. These trajectories indicate that the p-Norm constraint approximation method successfully implemented the ATM separation restrictions. Note that since the on-time arrival constraint was satisfied, each aircraft's state is plotted as the final state after the aircraft's arrival time.

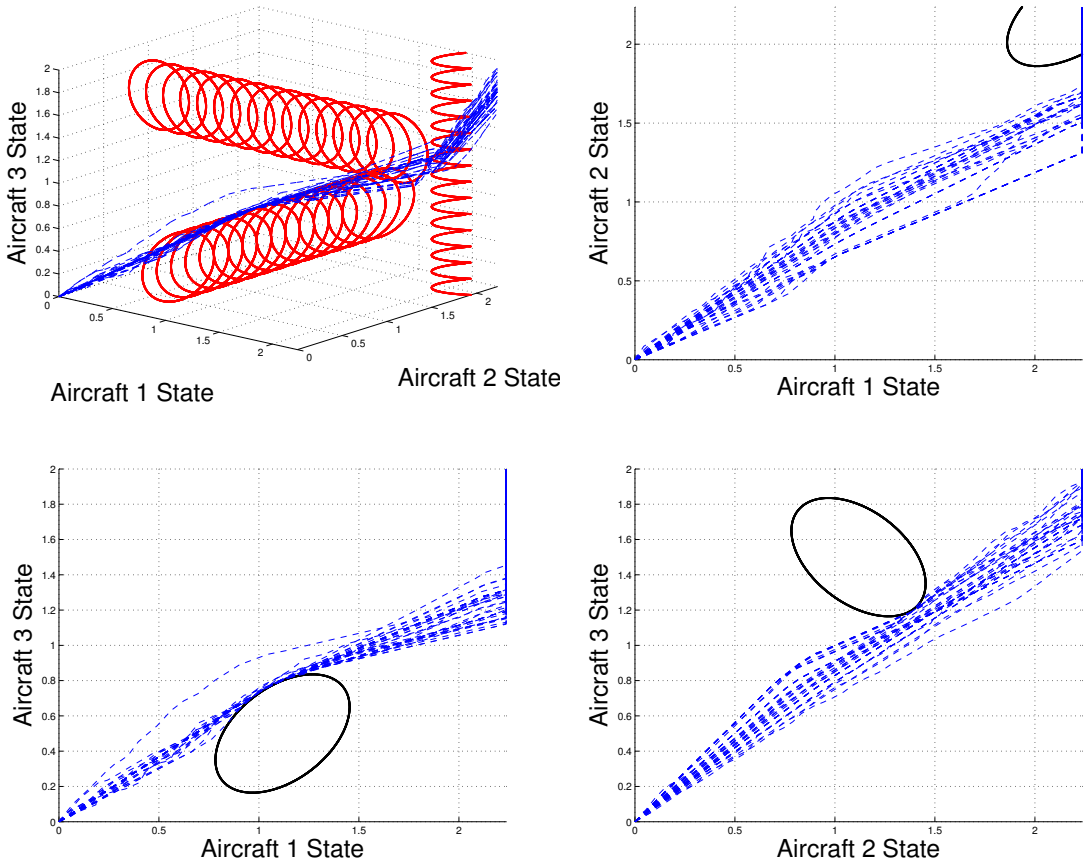

Figure 4.28: Test Case 1 p-Norm Method State Space Trajectories

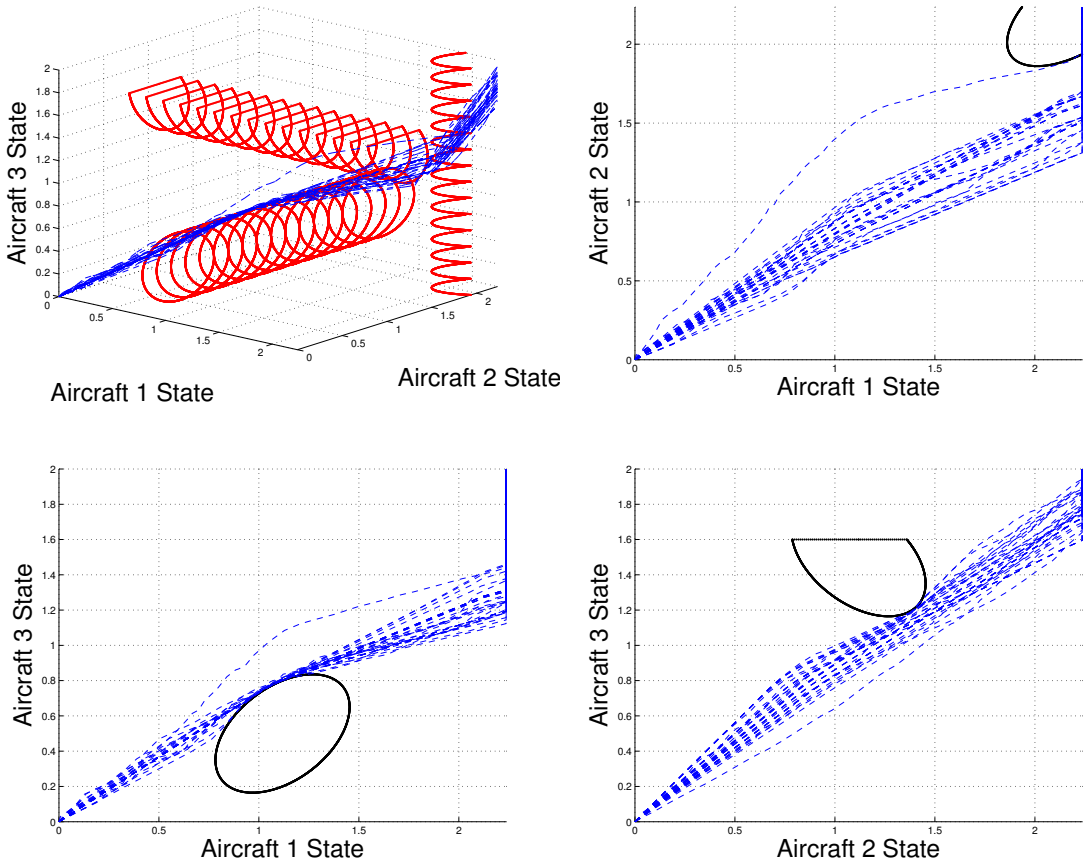

Figure 4.29: Test Case 2 p-Norm Method State Space Trajectories

4.3.3 Summary.

These results successfully demonstrate that the STOP optimization model is suitable for generating safe separation compliant trajectories without inertia that allow for variable arrival sequences. Additionally, the time required to generate feasible control strategies using this approach indicates the efficiency of this method is dependent upon the method used to define a differentiable approximation of the anisotropic separation requirement, and upon the method used to define the STOP optimization model's on-time arrival constraint. For example, the time-based on-time arrival constraint formulations consistently required less time to generate feasible control strategies than the state-based on-time arrival constraint formulations, while the p-norm separation constraint approximation method was unable to generate feasible control strategies for the third test case.

Therefore, state-based on-time arrival constraint formulations and the p-norm separation constraint approximation method appear unsuitable for use with the STOP model of the multi-objective HCS ATM optimization problem.

4.4 STOP Model Results with Modified Graph

This section presents the results from evaluating the two test cases from Section 3.2, which were modifications of Test Case 3 from Section 3.1.4.1.

1. **Alternate Way-point for Aircraft 1.** The first test case involved defining an alternate way-point for Aircraft 1 of Test Case 3 from Section 3.1.4.1. The p-Norm implementation was not used to evaluate the test case since the p-Norm constraint approximation function became computationally unstable in certain regions when evaluated with GPOPS-II. Out of the 18 treatments, this test case resulted in *no successful* treatment evaluations using the time-based arrival indicator implementation of the the Multiplier Method STOP model and only one successful treatment evaluation using the state-based arrival indicator.

   Table 4.43 presents the results obtained using the time- and state-based arrival indicator and sigmoid function implementations of the the Sigmoid STOP model.

Table 4.43: Aircraft 1 Alternate Way-Point with Sigmoid Implementation Summary Results.

	Minimum Value Achieved			Value Achieved	
Indicator Function	Fuel Measure	Schedule Deviation	Total Time	Success Rate	Seconds To Completion
Time-based	5.5123	0.0394	9.3602	0.4706	21.8563
State-based	8.7127	0.917	9.7453	0.0588	100.5522
Time-based Sigmoid	5.5211	0.0394	9.2642	0.8824	14.1679
State-based Sigmoid	8.7127	0.917	9.7453	0.0588	100.5522

Table 4.43 indicates modifying the path of Aircraft 1 of Test Case 3 from Section 3.1.4.1 resulted in worse performance when compared to the results from the original configuration given in Table 4.40.

2. **Alternate Way-point for Aircraft 2.** The second test case involved defining an alternate way-point for Aircraft 2 of Test Case 3 from Section 3.1.4.1. Table 4.44 presents the results obtained using the time- and state-based arrival indicator implementations of the Multiplier Method STOP model.

Table 4.44: Aircraft 2 Alternate Way-Point with Multiplier Method Implementation Summary Results.

	Minimum Value Achieved			Value Achieved	
Indicator Function	Fuel Measure	Schedule Deviation	Total Time	Success Rate	Seconds To Completion
Time-based	5.4964	0.0466	9.2642	0.9412	119.1458
State-based	5.4964	0.0394	9.2642	1	50.7816

Table 4.44 indicates modifying the path of Aircraft 2 of Test Case 3 from Section 3.1.4.1 resulted in similar performance when compared to the results from the original configuration given in Table 4.37. However, modifying the path of Aircraft 2 of Test Case 3 from Section 3.1.4.1 resulted in improved average success rate and time to completion for the Multiplier Method STOP model.

Table 4.45 presents the results obtained using the time- and state-based arrival indicator and sigmoid function implementations of the Sigmoid STOP model.

Table 4.45: Aircraft 2 Alternate Way-Point with Sigmoid Implementation Summary Results.

	Minimum Value Achieved			Value Achieved	
Indicator Function	Fuel Measure	Schedule Deviation	Total Time	Success Rate	Seconds To Completion
Time-based	5.5125	0.0394	9.2642	0.7647	33.3854
State-based	5.5266	0.0394	9.2642	0.8824	62.4298
Time-based Sigmoid	5.5254	0.0394	9.2642	1	48.3197
State-based Sigmoid	5.5266	0.0394	9.2642	0.8824	62.4298

Table 4.45 indicates modifying the path of Aircraft 2 of Test Case 3 from Section 3.1.4.1 resulted in similar performance when compared to the results from the original configuration given in Table 4.40. However, modifying the path of Aircraft 2 of Test Case 3 resulted in improved average success rate and overall minimum schedule deviation measure improved, but increased average time to completion for the Sigmoid STOP model.

4.4.1 Summary.

These results suggest that modifying the path of the aircraft with a later scheduled arrival time may be more beneficial than modifying the path of the aircraft with the earlier scheduled arrival time. Therefore, further research may determine a heuristic or rule for modifying each aircraft's path in order to improve the efficiency of finding feasible control strategies for the current control mode.

4.5 Kinodynamic STOP Model Results

This section presents the results of evaluating the test case from Section 3.3.2.1 at all 18 treatments in GPOPS-II using the STOP model of the multi-objective HCS ATM problem with inertia and the sigmoid constraint approximation. Table 4.46 summarizes the objective function values obtained from the evaluation as well as the time required to evaluate the test case. Figures 4.30 - 4.32 plot the arrival constraint function values that resulted. Figures 4.33-4.35 plot the speed and acceleration profiles that resulted from the second treatment for each aircraft . Figure 4.36 presents the state space trajectory that resulted from the speed and acceleration profiles.

Table 4.46: Test Case with Inertia Sigmoid Method Implementation Summary Results.

	Minimum Value Achieved			Value Achieved	
Indicator Function	Fuel Measure	Schedule Deviation	Total Time	Success Rate	Seconds To Completion
Time-based	0.2611	0.0394	9.3049	0.6667	135.2069
State-based	0.2594	0.0394	9.7385	0.6667	73.235
Time-based Sigmoid	0.2593	0.0394	9.3602	0.8333	103.9952
State-based Sigmoid	0.2591	0.0394	9.3602	0.8333	123.9584

Table 4.46 indicates that all implementations achieved similar minimum fuel and deviation from schedule measures. The sigmoid arrival indicator implementations had the highest success rates, but the state-based arrival indicator implementation had the shortest average time to completion. However, the state-based arrival indicator implementation also had the worst minimum achieved total time.

The time required to evaluate the test case with inertia is between two and ten times greater than the time required to evaluate the test case without inertia. Therefore, it may be useful to generate a solution to the test case without inertia and provide that trajectory as an initial guess for evaluating the test case with inertia.

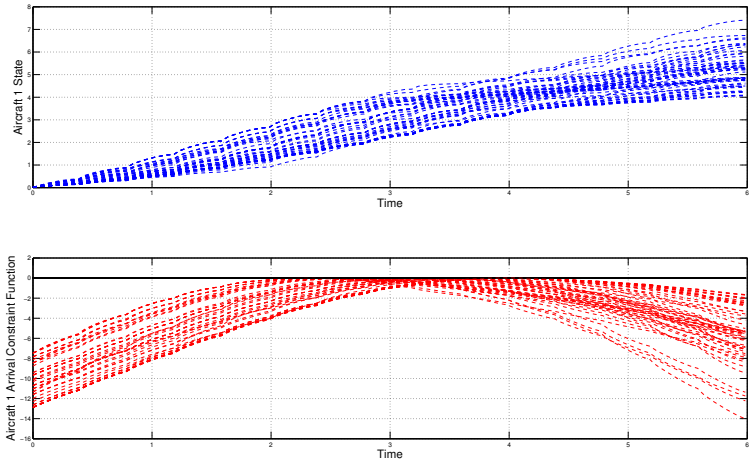

Figure 4.30: Sigmoid Method Aircraft 1 Arrival Time Constraint Function Values

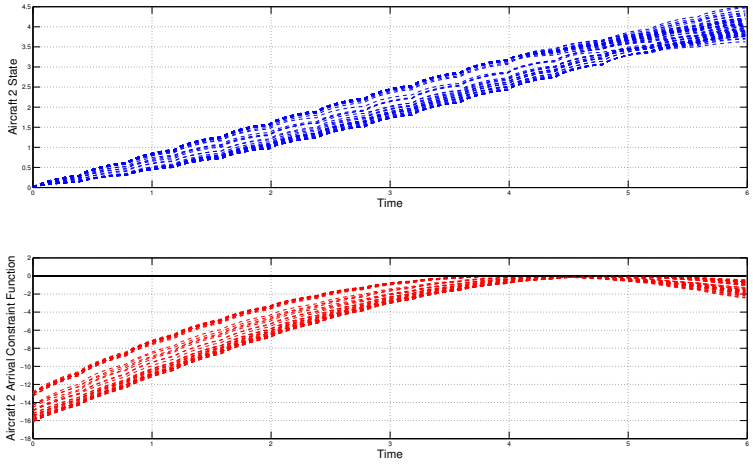

Figure 4.31: Sigmoid Method Aircraft 2 Arrival Time Constraint Function Values

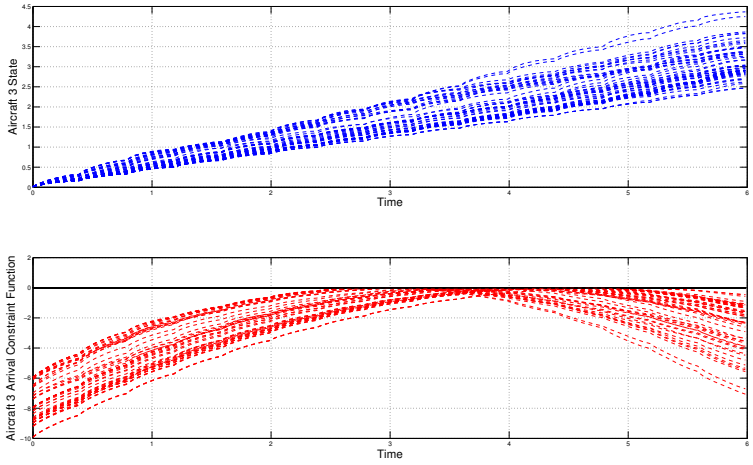

Figure 4.32: Sigmoid Method Aircraft 3 Arrival Time Constraint Function Values

Figures 4.30 - 4.32 indicate the all the arrival indicator implementations successfully satisfied the on-time arrival constraint.

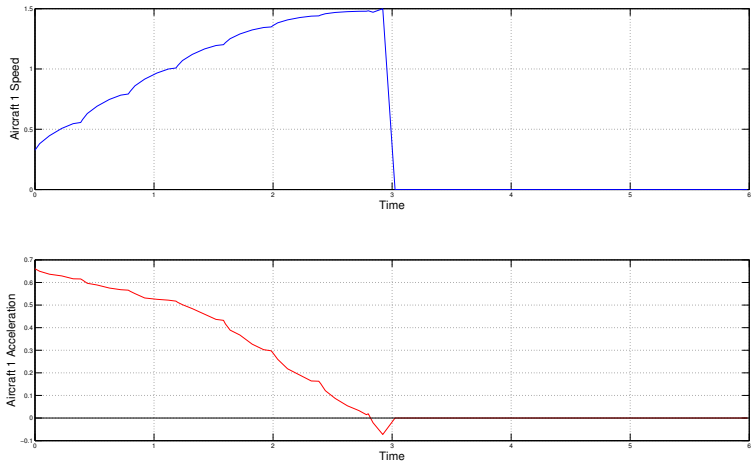

Figure 4.33: Sigmoid Method Aircraft 1 Speed and Acceleration

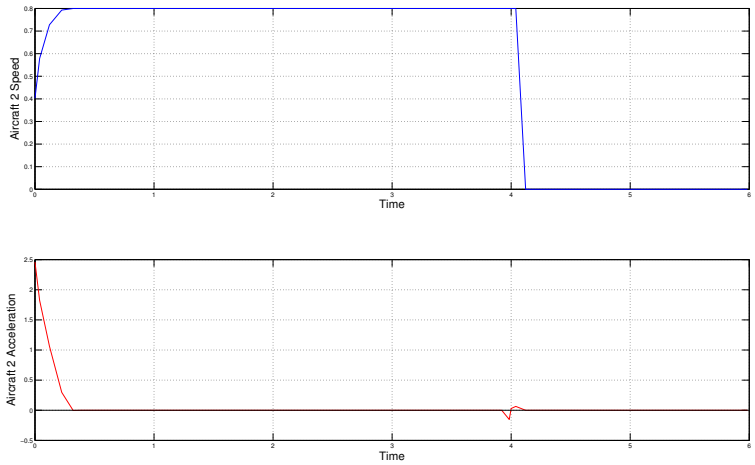

Figure 4.34: Sigmoid Method Aircraft 2 Speed and Acceleration

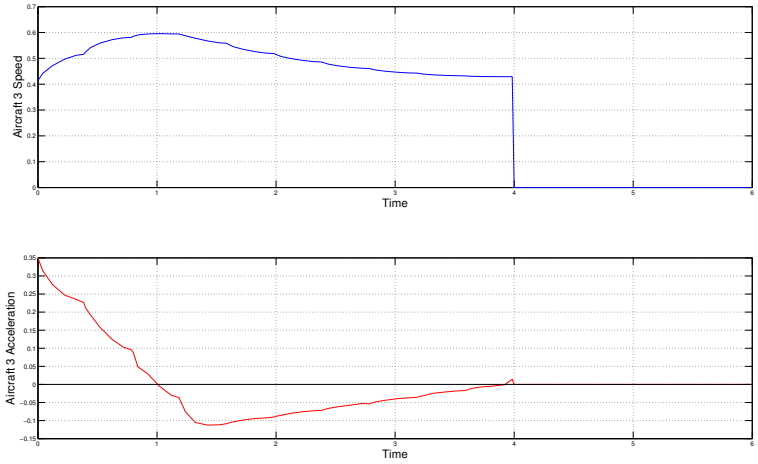

Figure 4.35: Sigmoid Method Aircraft 3 Speed and Acceleration

Since the on-time arrival constraint was satisfied, Figures 4.33 - 4.35 plot all speed and acceleration after the arrival time as zero (0).

Figure 4.36 displays all the state-space trajectories obtained from successful treatment evaluations using the Sigmoid constraint approximation with time- or state-based arrival indicator and sigmoid functions, with three-dimensional conflict regions in red, and pair-wise conflict regions in solid black. These trajectories indicate that the Sigmoid constraint approximation method successfully implemented the ATM separation restrictions with inertia. Note that since the on-time arrival constraint was satisfied, each aircraft's state is plotted as the final state after the aircraft's arrival time.

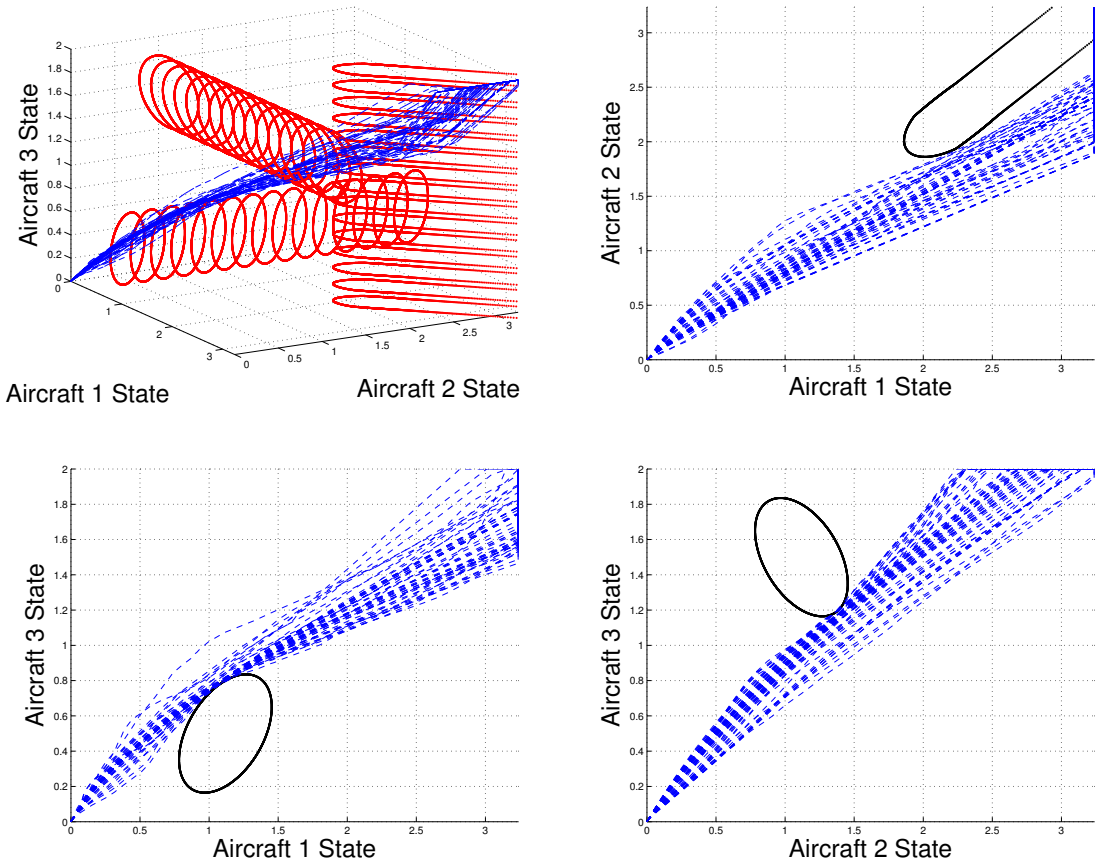

Figure 4.36: Test Case with Inertia Sigmoid Method State Space Trajectories

4.5.1 Summary.

These results successfully demonstrate that aircraft inertia can be incorporated into the roadmap coordination space, and that the STOP optimization model is suitable for generating safe separation compliant trajectories that allow for variable arrival sequences. However, the time required to generate feasible control strategies using this approach indicates that the efficiency of this method is dependent upon the weightings assigned to each objective. Therefore, further research is required to determine how the weighting scheme of the objective function affects the efficiency of the STOP optimization model, and whether or not an optimal weighting scheme exists.

4.6 Kinodynamic STOP Model Results with Uncertainty

This section presents the results of evaluating the test case from Section 3.4.5.1 at Treatment 2 of Table 3.32 in GPOPS-II using the STOP model of the multi-objective HCS ATM problem with kinodynamic and stochastic elements and the sigmoid constraint approximation and state-based sigmoid arrival constraint. The solution to the kinodynamic problem with uncertainty was generated by first evaluating the kinodynamic problem without uncertainty, then using the solution to the simplified problem as the initial guess to the kinodynamic problem with uncertainty. Table 4.47 presents the objective function values obtained from the evaluation with $(1-\rho) = 0.75$, $(1-\rho) = 0.85$ and $(1-\rho) = 0.95$, as well as the time required to evaluate the test case, including the time required to generate solutions to the simplified problem without uncertainty. Figures 4.37 - 4.39 plot the arrival constraint function values that resulted. Figures 4.40-4.42 plot the speed and acceleration profiles that resulted for each aircraft. Figures 4.43-4.43 present the state space trajectories that resulted from the speed and acceleration profiles.

Table 4.47: Kinodynamic Test Case with Uncertainty Sigmoid Implementation Summary Results.

	Minimum Value Achieved			Value Achieved	
Precision $(1-\rho)$	Fuel Measure	Schedule Deviation	Total Time	Success Rate	Seconds To Completion
0.75	1.5946	0.0394	11.0394	1	52.1963
0.85	1.5984	0.0394	11.0394	1	45.9576
0.95	1.6056	0.0394	11.0394	1	62.1744

Table 4.47 indicates that while the measures of schedule deviation and total time are similar for each value of $(1-\rho)$, the measure of fuel consumption increases as $(1-\rho)$ increases, but the time to completion decreases then increases as $(1-\rho)$ increases. The process of supplying the solution of the simpler problem without uncertainty as an initial guess to the problem with uncertainty resulted in faster run times.

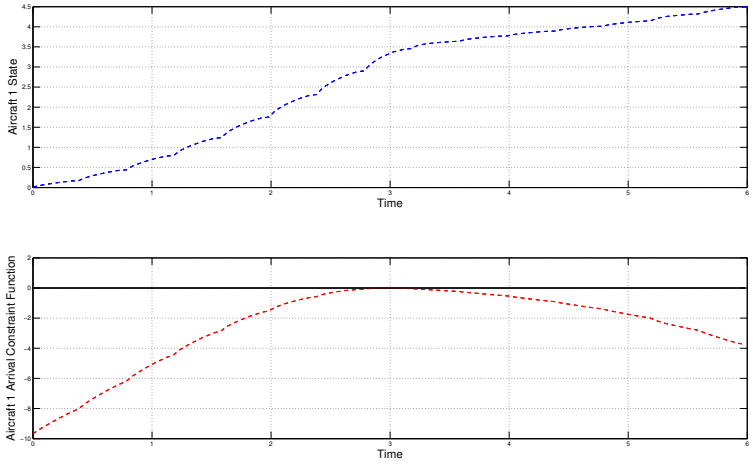

Figure 4.37: Aircraft 1 Arrival Time Constraint Function Values

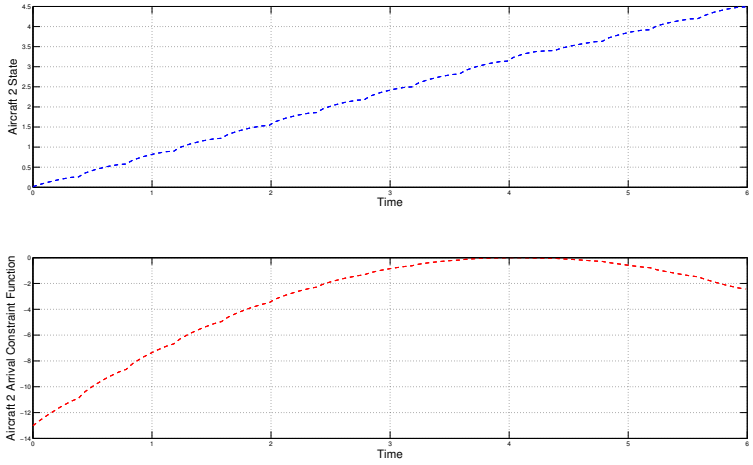

Figure 4.38: Aircraft 2 Arrival Time Constraint Function Values

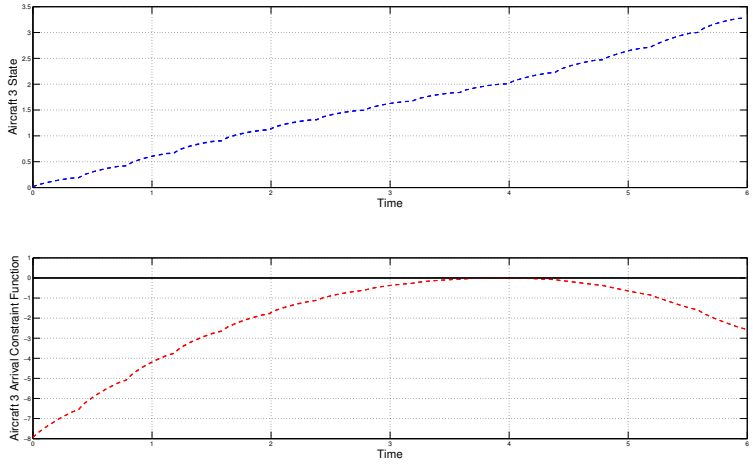

Figure 4.39: Aircraft 3 Arrival Time Constraint Function Values

Figures 4.37 - 4.39 indicate the on-time arrival constraint was satisfied for all values of $(1-\rho)$.

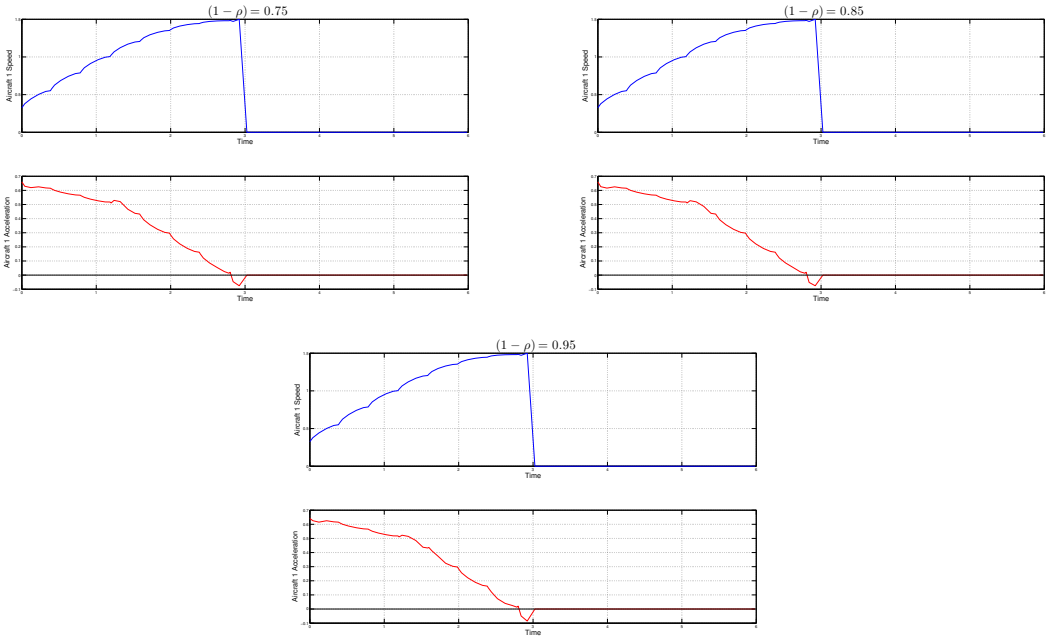

Figure 4.40: Aircraft 1 Speed and Acceleration with $(1-\rho) = 0.75, 0.85, 0.95$

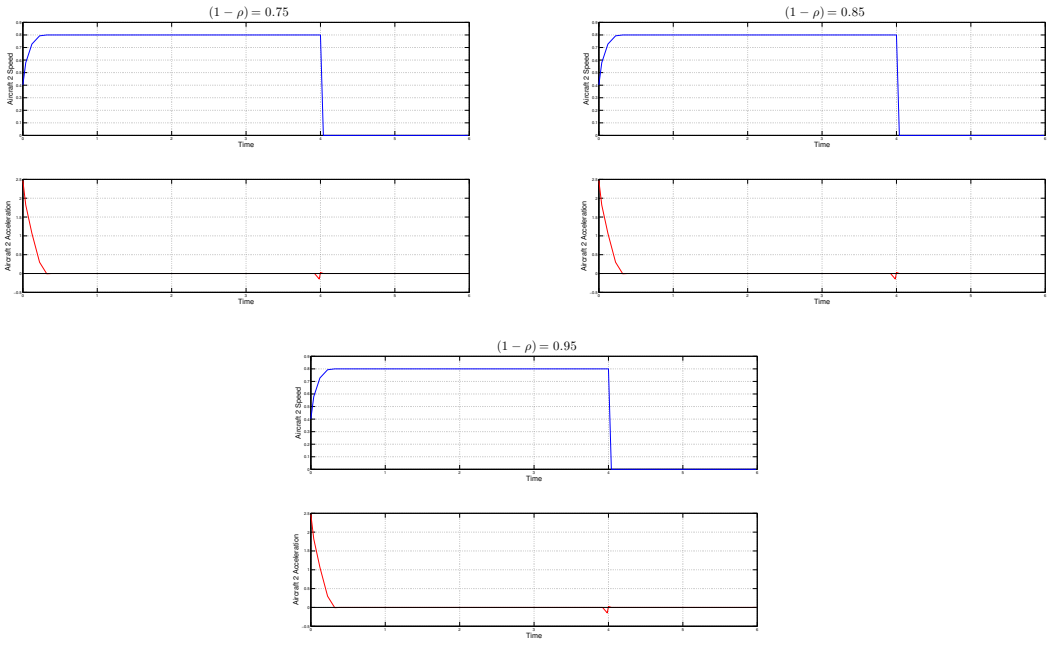

Figure 4.41: Aircraft 2 Speed and Acceleration with $(1-\rho) = 0.75, 0.85, 0.95$

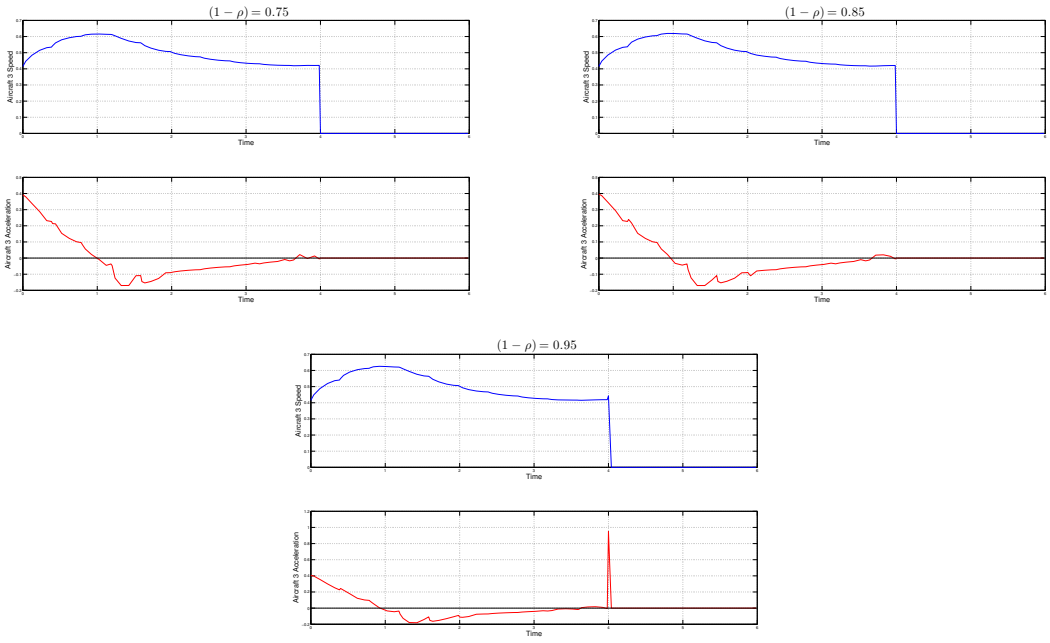

Figure 4.42: Aircraft 3 Speed and Acceleration with $(1-\rho) = 0.75, 0.85, 0.95$

Figures 4.40 and 4.42 indicate slight increases in control effort were apparently required for Aircraft 3 as $(1-\rho)$ increased from 0.75 to 0.95, while no change in control effort is noticeable for Aircraft 1 or Aircraft 2. Note that since the on-time arrival constraint was satisfied, Figures 4.40 - 4.42 plot all speed and acceleration after the arrival time as zero (0).

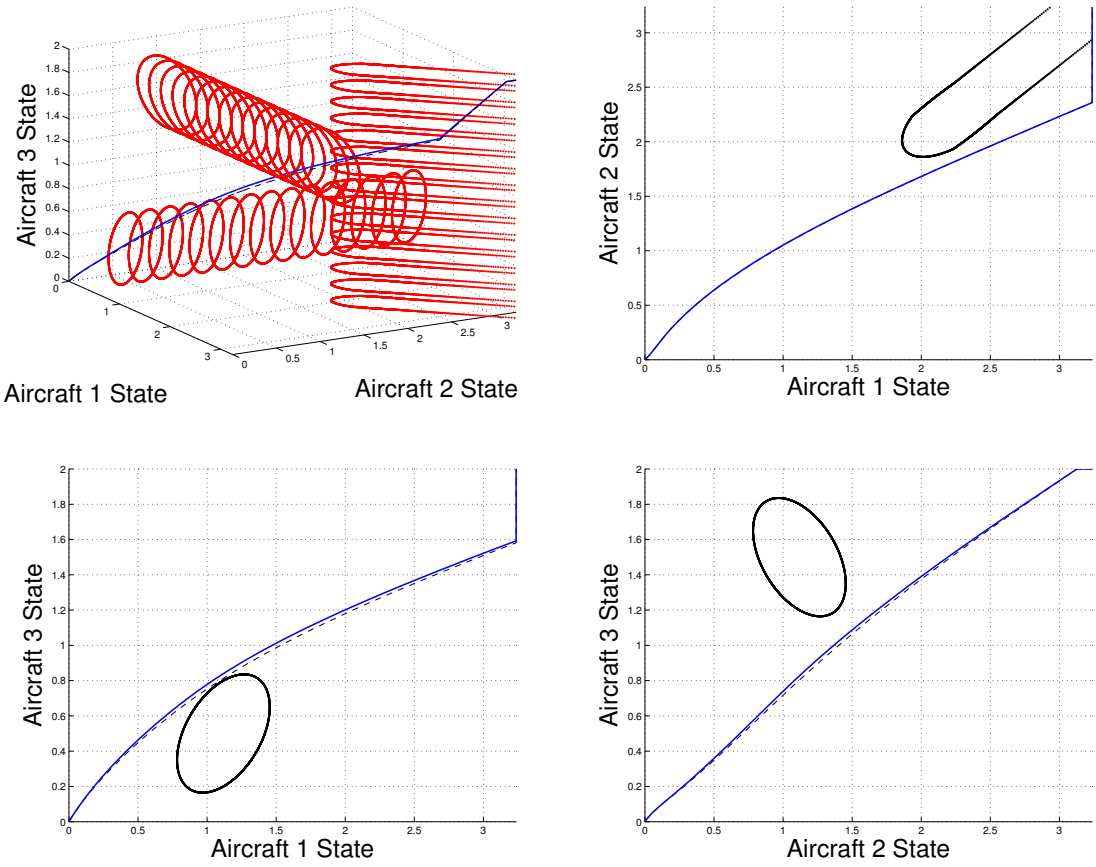

Figure 4.43: Kinodynamic State Space Trajectories with $(1-\rho) = 0.75$

Figure 4.43 indicates the trajectory that resulted from setting $(1-\rho)$ to 0.75 (in blue) differed most from the trajectory with no uncertainty (dashed) when avoiding the conflict region between Aircraft 1 and Aircraft 3.

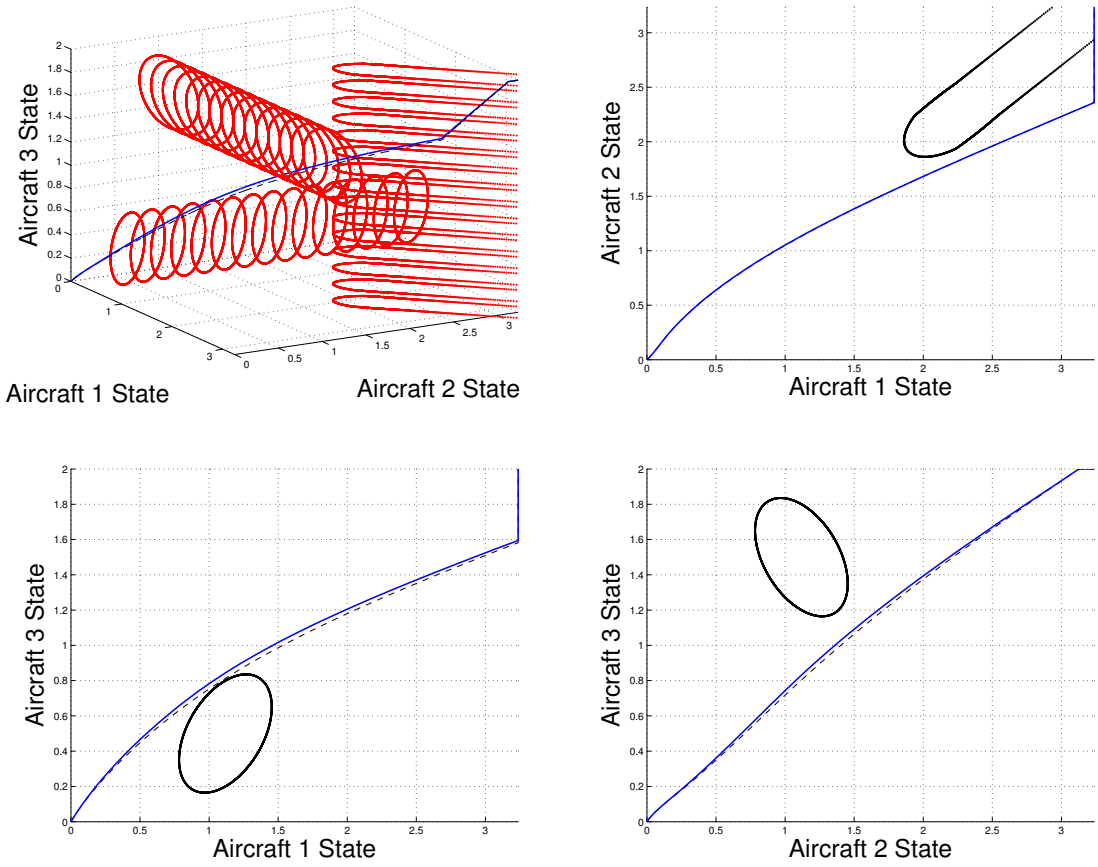

Figure 4.44: Kinodynamic State Space Trajectories with $(1-\rho) = 0.85$

Figure 4.44 indicates the trajectory that resulted from setting $(1-\rho)$ to 0.85 (in blue) differed most from the trajectory with no uncertainty (dashed) when avoiding the conflict region between Aircraft 1 and Aircraft 3, and by slightly more than the difference that resulted from setting $(1-\rho)$ to 0.75

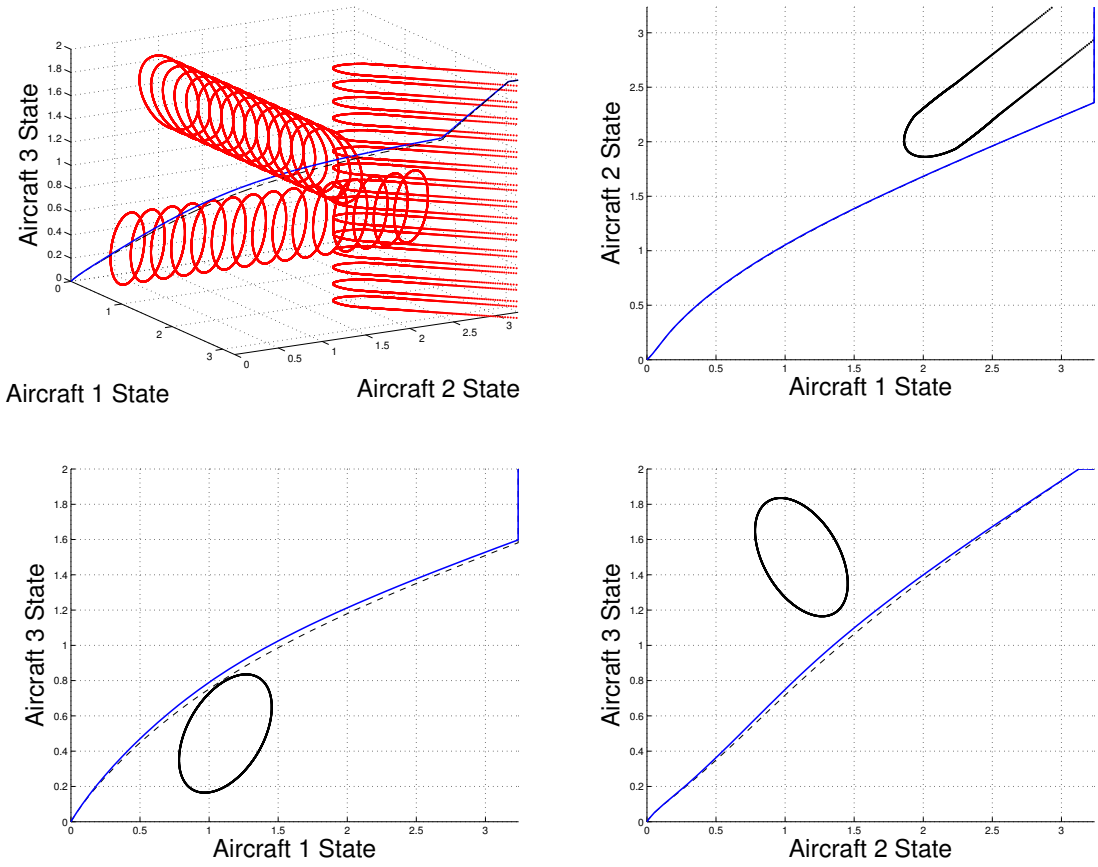

Figure 4.45: Kinodynamic State Space Trajectories with $(1-\rho) = 0.95$

Figure 4.45 indicates the trajectory that resulted from setting $(1-\rho)$ to 0.95 (in blue) differed most from the trajectory with no uncertainty (dashed) when avoiding the conflict region between Aircraft 1 and Aircraft 3, and by slightly more than the difference that resulted from setting $(1-\rho)$ to 0.75 or 0.85.

4.6.1 Summary.

These results successfully demonstrate that stochastic effects can be modeled in the roadmap coordination space by defining an ellipsoid to represent the likely position of each aircraft and projecting the ellipsoid in the lateral plane and vertical axis. Additionally, the time required to generate feasible control strategies using this approach indicates that calculating the distance between projected ellipsoids does not render this method unsuitable for practical applications.

Nonetheless, further research is required to compare the exact ellipsoid distance calculation method used in this research to less accurate estimates of the distance between each aircraft's position ellipsoid.

4.7 Kinodynamic STOP Model Results with Uncertainty and Asymmetric Lateral Separation

This section presents the results of evaluating the test case from Section 3.4.5.1 at Treatment 2 of Table 3.32 in GPOPS-II using the STOP model of the multi-objective HCS ATM problem with kinodynamic and stochastic elements, as well as asymmetric lateral separation constraints. This test case was evaluated using the sigmoid constraint approximation and state-based sigmoid arrival constraint. Additionally, a sigmoid with $\mathtt{s} = 100$ was used to indicate when one aircraft trailed another, while a Multiplier Method with $\lambda = \sqrt{2} - 1$ and $\gamma = 200$ was used to approximate the adjusted minimum allowable lateral separation due to the indicated lead-trail configuration. Furthermore, the solution to the kinodynamic problem with uncertainty and asymmetric lateral separation constraints was generated by first evaluating the kinodynamic problem with asymmetric lateral separation constraints, but no uncertainty, then using the solution to the simplified problem as the initial guess to the kinodynamic problem with asymmetric lateral separation constraints and uncertainty. Table 4.48 presents the objective function values obtained from the evaluation with $(1-\rho) = 0.75$, $(1-\rho) = 0.85$ and $(1-\rho) = 0.95$, as well as the time required to evaluate the test case, including the time required to generate solutions to the simplified problem with no uncertainty. Figures 4.46 - 4.48 plot the arrival constraint function values that resulted. Figures 4.49-4.51 plot the speed and acceleration profiles that resulted for each aircraft. Figures 4.52-4.52 present the state space trajectories that resulted from the speed and acceleration profiles.

Table 4.48: Kinodynamic Test Case with Uncertainty and Asymmetry Sigmoid Implementation Summary Results.

	Minimum Value Achieved			Value Achieved	
Precision $(1-\rho)$	Fuel Measure	Schedule Deviation	Total Time	Success Rate	Seconds To Completion
0.75	1.6753	0.0394	11.0394	1	156.5112
0.85	1.759	0.0394	11.0394	1	158.3588
0.95	1.8221	0.0394	11.0394	1	345.8033

Table 4.48 indicates that while the measures of deviation from schedule and total time are similar for each value of $(1-\rho)$, the measure of fuel consumption increases as $(1-\rho)$ increases as expected. Additionally, while the time to completion is similar for $(1-\rho) = 0.75$ and 0.85, the time to completion more than doubles for $(1-\rho) = 0.95$. Furthermore, the process of providing the solution to the simpler problem without uncertainty as an initial guess to the problem with uncertainty did not decrease the run time by a practically significant amount.

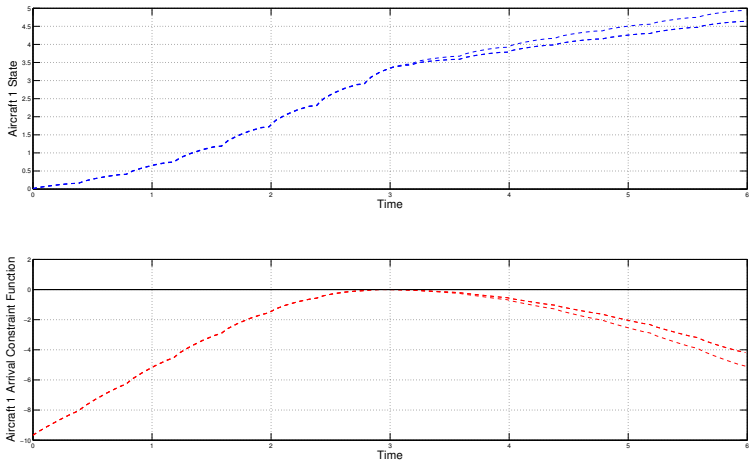

Figure 4.46: Aircraft 1 Arrival Time Constraint Function Values

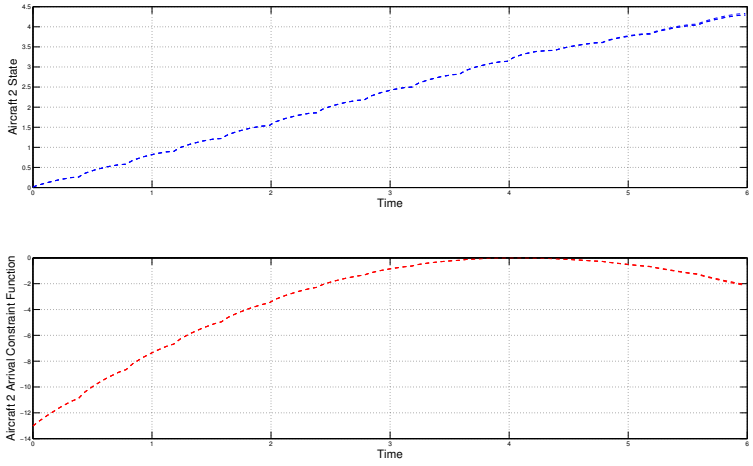

Figure 4.47: Aircraft 2 Arrival Time Constraint Function Values

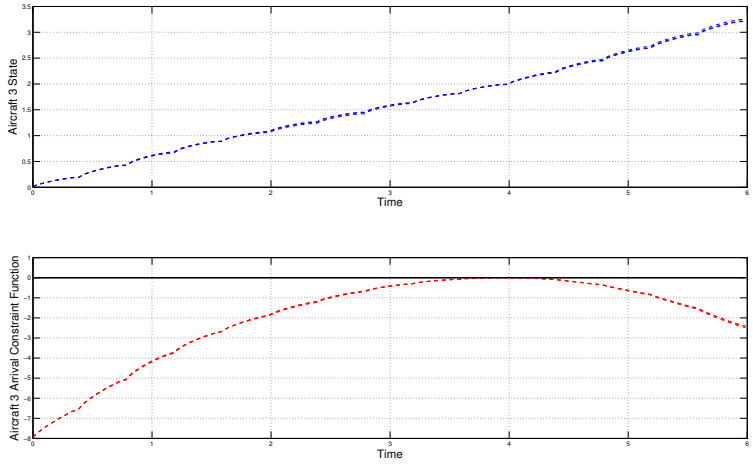

Figure 4.48: Aircraft 3 Arrival Time Constraint Function Values

Figures 4.46 - 4.48 indicate the on-time arrival constraint was satisfied for all values of $(1-\rho)$.

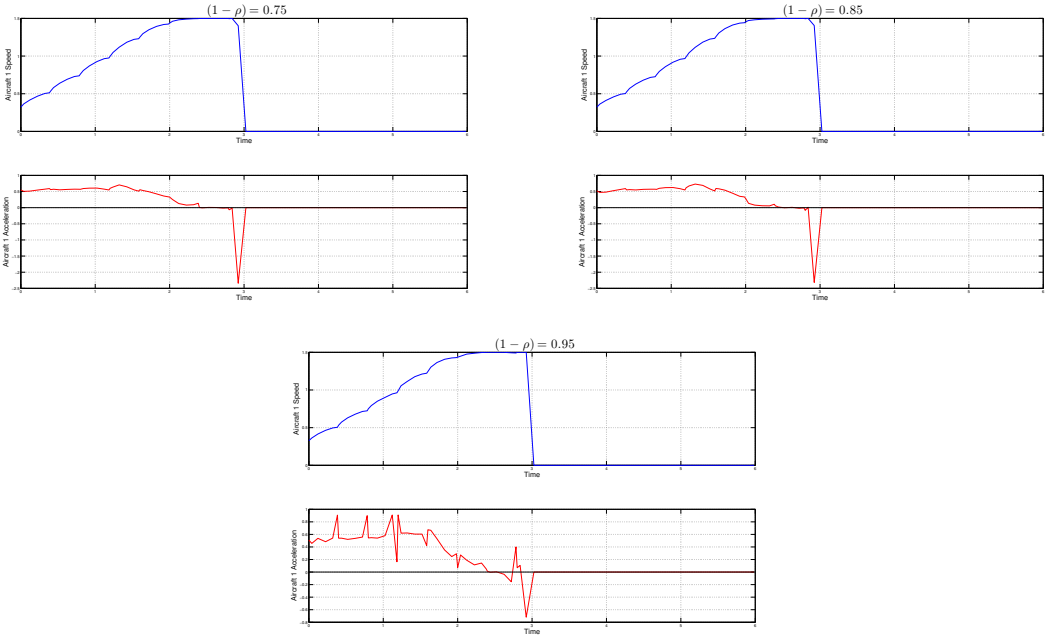

Figure 4.49: Aircraft 1 Speed and Acceleration with $(1 - \rho) = 0.75, 0.85, 0.95$

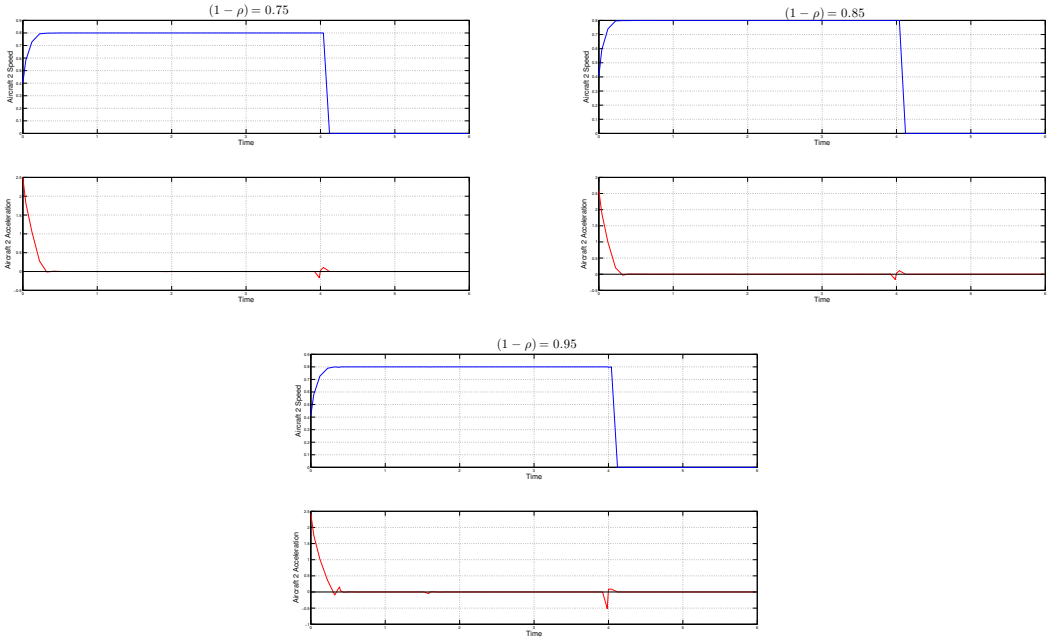

Figure 4.50: Aircraft 2 Speed and Acceleration with $(1-\rho) = 0.75, 0.85, 0.95$

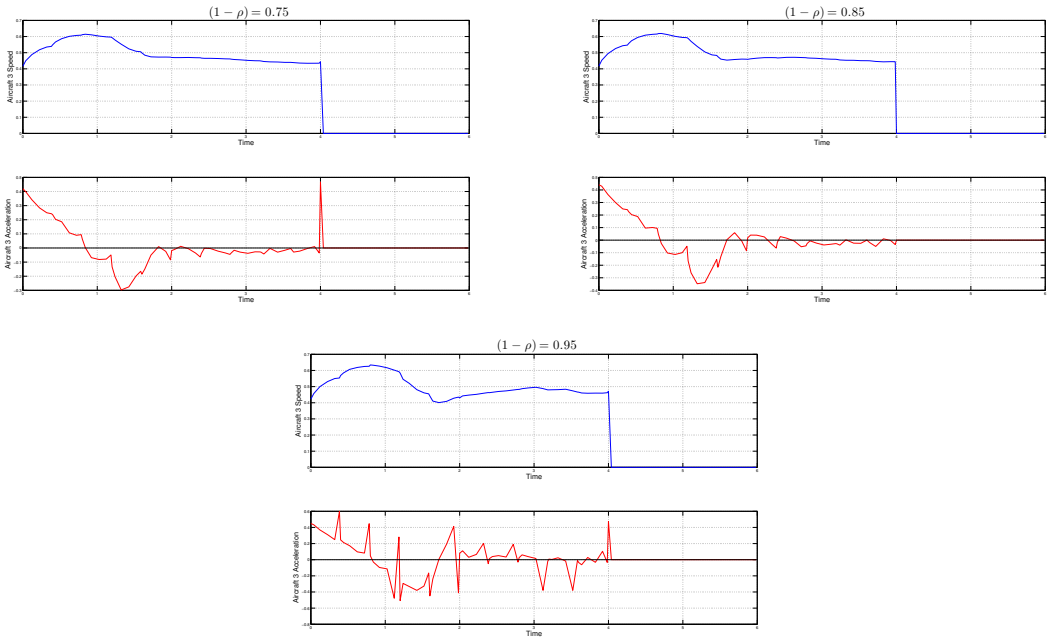

Figure 4.51: Aircraft 3 Speed and Acceleration with $(1-\rho) = 0.75, 0.85, 0.95$

Figures 4.49 and 4.51 indicate the asymmetric lateral separation implementation resulted in increased control effort and a loss of smoothness in the acceleration profile for Aircraft 1 and Aircraft 3. This loss of smoothness was most apparent for $(1-\rho) = 0.95$. Note that since the on-time arrival constraint was satisfied, Figures 4.49 - 4.51 plot all speed and acceleration after the arrival time as zero (0).

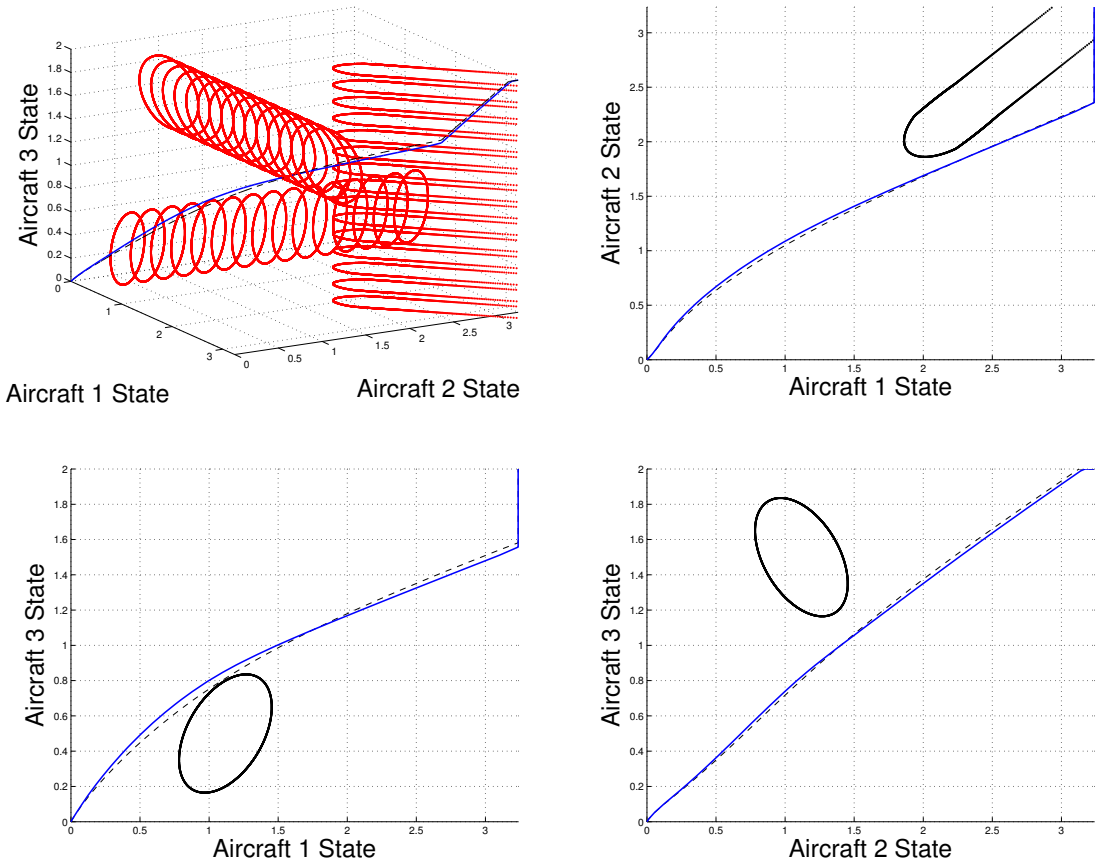

Figure 4.52: Asymmetric State Space Trajectories with $(1 - \rho) = 0.75$

Figure 4.52 indicates the trajectory that resulted from setting $(1 - \rho)$ to 0.75 (in blue) differed most from the trajectory with no uncertainty (dashed) when avoiding the conflict region between Aircraft 1 and Aircraft 2 and the conflict region between Aircraft 1 and Aircraft 3. This should be expected since the asymmetric lateral separation applies when Aircraft 2 or Aircraft 3 is considered to trail Aircraft 1.

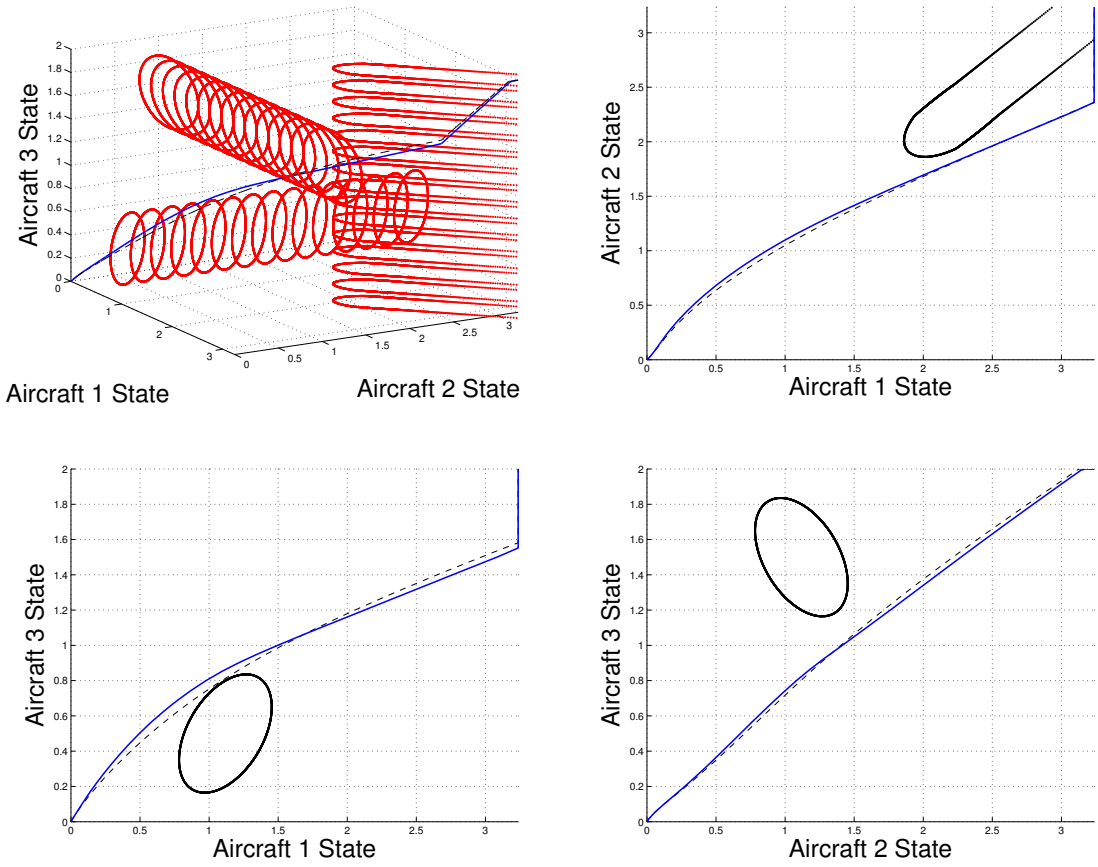

Figure 4.53: Asymmetric State Space Trajectories with $(1 - \rho) = 0.85$

Figure 4.53 indicates the trajectory that resulted from setting $(1 - \rho)$ to 0.85 (in blue) differed most from the trajectory with no uncertainty (dashed) when avoiding the conflict region between Aircraft 1 and Aircraft 2 and the conflict region between Aircraft 1 and Aircraft 3. This should be expected since the asymmetric lateral separation applies when Aircraft 2 or Aircraft 3 is considered to trail Aircraft 1.

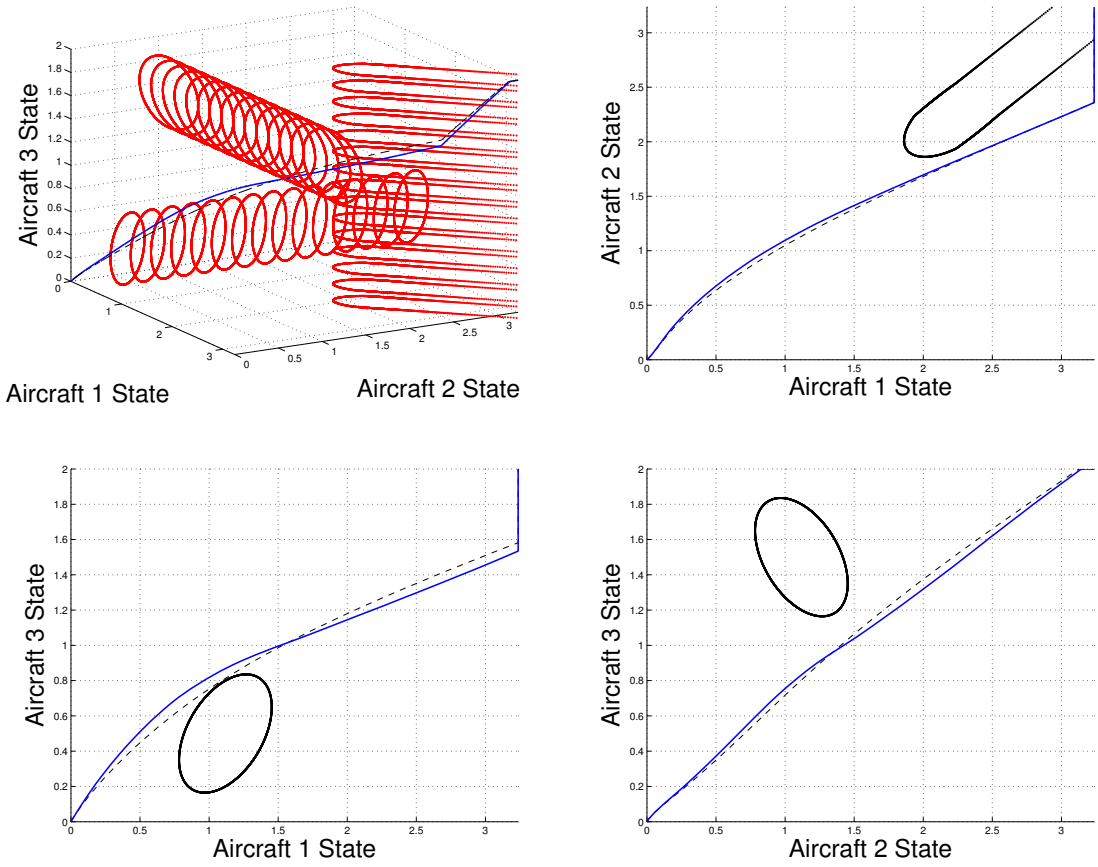

Figure 4.54: Asymmetric State Space Trajectories with $(1 - \rho) = 0.95$

Figure 4.54 indicates the trajectory that resulted from setting $(1 - \rho)$ to 0.95 (in blue) differed most from the trajectory with no uncertainty (dashed) when avoiding the conflict region between Aircraft 1 and Aircraft 2 and the conflict region between Aircraft 1 and Aircraft 3, and by noticeably more than the difference that resulted from setting $(1 - \rho)$ to 0.75 or 0.85.

4.7.1 Summary.

These results successfully demonstrate that the asymmetric lateral separation constraint can be approximated using a sigmoid method to indicate *if* the minimum allowable separation value should be updated, then a Multiplier Method to select *how* it should be updated. However, the time required to generate solutions using this hybrid approach appears impractical. Therefore, further research is required to determine more efficient methods of incorporating asymmetric separation constraints.

4.8 Summary of Results

This chapter demonstrated that the differentiable constraint approximation methods and variable arrival sequence models developed in Chapter 3 are suitable for generating feasible control strategies for ATM optimization problems that incorporate aircraft inertia and realistic safe separation constraints. However, the efficiency of the methods developed to evaluate the ATM optimization problems appears to decrease as the complexity and realism of the ATM model increases. Therefore, further research is required to address the loss of efficiency and improve the applicability of the methods developed in Chapter 3.

V. Conclusion

This chapter provides a summary of the research presented and suggests topics for further study. The original contributions of this research are outlined in Section 5.1, and a brief overview of the motivation, derivation, and demonstration of each contribution is presented. Areas for analytical and experimental extensions of this research are presented in Section 5.2.

5.1 Summary

This section summarizes the research and results presented. The first section summarizes the development of differentiable Air Traffic Management separation constraint approximation methods, and the second section describes the techniques developed to incorporate the differentiable separation constraint approximation into a novel multi-objective optimization framework. The third and fourth sections describe how this research incorporated stochastic effects and asymmetric separation constraints into the new optimization framework.

5.1.1 Differentiable Constraint Approximations.

While the relevant literature provides theoretically differentiable approximations to non-differentiable constraints, this research developed generalized error bounds for the classic Multiplier Method constraint approximation, a sigmoid-based constraint approximation method, and two p-Norm-based constraint approximation techniques. Formulations for each of these methods were also developed to guarantee that the approximate feasible region is a subset of the true feasible region, so that no infeasible solutions are mistakenly considered feasible when using any of the approximation methods.

This research also generated extensive pair-wise aircraft conflict scenarios to test the practicality of implementing these suggested approximation methods when evaluating the non-differentiable Air Traffic Management separation constraint using a gradient-based numerical optimizer. The results of these tests indicated that although the p-Norm-based constraint approximations can estimate the infeasible region with great accuracy, the Multiplier Method and

Sigmoid approximation techniques are more likely to retain computational stability when evaluated with gradient-based numerical solvers.

5.1.2 Multi-objective Air Traffic Optimization.

Given the competing goals of reducing fuel consumption, reducing total time in flight and achieving on-time arrivals, this research developed a roadmap-based formulation of a multi-objective Air Traffic Management problem that takes advantage of the fact that aircraft speeds are assumed to be positive to define a continuous on-time arrival constraint. This on-time arrival constraint allowed the formulation to optimize different weightings of the fuel consumption, total time in flight and deviation from scheduled arrival time measures, without having to explicitly define an arrival sequence. A generalized weighted-sum representation of the multi-objective optimization problem was first defined for notional air traffic problems that model aircraft speed as the direct control of the system, while ignoring inertia or acceleration. It was then tested using the Sigmoid and Multiplier Method approximations of notional air traffic safe separation constraints. Path modifications to one of the test cases were evaluated to provide insight into how these modifications could affect the optimization problem.

Results from these tests suggested that the optimization problem's sensitivity to path modifications was related to the problem's sensitivity to scheduled arrival times. When these tests indicated that the formulation could adequately solve these simplified models, the method was extended to include problems that used acceleration as the aircraft control. Tests on this kinodynamic formulation indicated that gradient-based numerical solvers can quickly generate locally optimal solutions that satisfy the safe-separation requirements. Thus, the on-time arrival constraint-based optimization model was demonstrated to be a viable method for evaluating competing Air Traffic Management goals.

5.1.3 Stochastic Effects.

While the roadmap-based approach used to define the multi-objective Air Traffic optimization problem is efficient, it assumes that aircraft stay precisely on their pre-defined paths and are able to transition from one path segment to another instantaneously. Therefore, this research adopted the standard practice of estimating an aircraft's position with a three-dimensional ellipsoid whose radii

are based on the uncertainty in the aircraft's position in that direction. These probability ellipsoids were then projected into the lateral and vertical planes to estimate the minimum lateral and vertical separation between each pair of aircraft. In the lateral plane, the separation between two aircraft was estimated using a closed-form calculation of the minimum distance between a pair of two-dimensional ellipses developed by Zheng and Palffy-Muhoray [87]. This lateral separation estimate therefore provided a buffer based on the uncertainty in the position of each aircraft, so the roadmap-based approach to Air Traffic Management no longer needs to assume that aircraft stay exactly on their pre-defined paths, but only that their expected position is on the pre-defined path. Tests of this method indicated that the trajectories based on the separation of probability ellipsoids were able to achieve similar objective function values to those obtained assuming no uncertainty; however, the incorporation of stochastic effects resulted in the gradient-based numerical solver requiring more time to find locally optimal solutions that satisfied the safe separation requirements.

5.1.4 Asymmetric Separation Constraints.

The differentiable constraint approximation methods developed in this research were based on constant minimum allowable lateral and vertical air traffic separation values. However, regulations can induce variability in the minimum allowable lateral separation. For instance, if a designated *small* aircraft is trailing behind a designated *heavy* aircraft, the small aircraft may be required to maintain a much greater lateral distance from the heavy aircraft. This change in separation value may be discontinuous and therefore cause gradient-based numerical solvers to fail to find locally optimal or feasible solutions.

This research developed a differentiable approximation of the asymmetric lateral separation constraint by incorporating sigmoid functions to indicate if a relevant lead-trail configuration has occurred, and then adjusting the baseline lateral separation using a Multiplier Method formulation to choose the correct minimum allowable separation value. Tests of this method indicated that the on-time arrival constraint-based optimization model could successfully incorporate asymmetric separation constraints and generate conflict free trajectories. However, the control strategies required to maintain safe-separation when the lateral separation constraint was asymmetric took

much longer to generate and appeared much less smooth than the control strategies that resulted when the constraints were symmetric.

5.2 Suggestions for Further Research

This section discusses potential extensions to this research, including defining conditions that indicate whether or not a given airspace configuration admits a feasible solution, and research into realistic values for use with the methods developed.

5.2.1 Control Mode Feasibility Conditions.

The control mode defines the given configuration of paths in the airspace, and analytical techniques for generating the state space conflict regions that result for the given control mode based on the lateral and vertical separation requirements are provided in Appendix B. These methods defined the boundary of each conflict region as a function of the state variable for each aircraft. Therefore, given the minimum and maximum allowable instantaneous change in state (or *speed*) of each aircraft, it should be possible to calculate the boundary of the set of attainable states for each aircraft. If the boundary of the set of attainable states cannot intersect the boundary of the state space without also intersecting the boundary of the conflict region, then it should be impossible for the aircraft to reach its destination without violating the lateral and vertical separation requirement. Thus, a promising extension of this research is to derive the conditions that indicate when the given airspace configuration admits no feasible solution for at least one aircraft. Furthermore, it may be possible to use the infeasibility condition to derive changes to the control mode's airspace graph that would be necessary to admit a feasible trajectory for all aircraft.

5.2.2 Arrival of New Aircraft.

This research did not model the arrival of new aircraft into the airspace. Therefore, a possible extension of this research is to study methods of incorporating the scheduled or unscheduled arrival of new aircraft. For example, if control mode feasibility conditions can be derived, it may be possible to define new paths for the control mode that are not used by any of the aircraft and are guaranteed not to affect the feasibility of the current system. These paths could then be reserved and assigned to new aircraft that enter the system.

5.2.3 Realistic Uncertainty Parameters.

While this research demonstrated that estimating the position of each aircraft with an ellipsoid can result in robust roadmap-based trajectories that satisfy the ATM separation requirements, the test cases that were evaluated only used notional values for the uncertainty in each aircraft's position. Therefore, another extension of this research is to determine realistic values for the uncertainty parameters involved in estimating an aircraft's position, and to test how well the framework is able to perform given real-world data.

Appendix A: Parameter Screening

This section provides the results of the initial screening tests used to determine suitable parameter values for the generalized weighted-sum objective given in equation (3.2) and the final time parameter, t_f, of the Shadow Time Overshoot Phase (STOP) model detailed in Section 3.1.3.1.

The generalized weighted-sum objective consists of two types of parameters: the binary weight-type indicator variables, β_k, and the non-negative priority weights, λ_k. For each $k \in \{1, 2, 3\}$, $\beta_k = 1$ indicates objective F_k receives a linear scaling, and is multiplied by the priority weight, λ_k, while $\beta_k = 0$ indicates objective F_k receives an exponential scaling, and is raised to the power of λ_k. For three objectives, there are eight possible combinations of the binary weight-type indicator variables. These combinations are given in Table A.1.

Table A.1: Combinations of Weight-Type Indicator Variables.

Combination	β_1	β_2	β_3
1	0	0	0
2	1	0	0
3	0	1	0
4	0	0	1
5	1	1	0
6	1	0	1
7	0	1	1
8	1	1	1

However, the number of possible combinations of the three non-negative priority weights is uncountable. Therefore, the priority weights were tested at varying orders of magnitude to represent the possibility of widely disparate priorities. Each priority weight was tested at a value of 0.0, 0.1, 1.0, and 10. That is, the three priority weights were tested at four levels each for a total of $4^3 = 64$

possible treatment combinations. However, the treatment that corresponds to all priority weights set to 0 was not tested, since this would result in a constant weighted-sum equal to zero.

The STOP fixed final time, t_f, is defined by the constraint $t_f \geq \left(\max\left\{t_{[f,1]_{\max}}, \ldots, t_{[f,A]_{\max}}\right\}\right)$. Therefore, t_f can be parameterized by the equation $t_f = \delta \times \left(\max\left\{t_{[f,1]_{\max}}, \ldots, t_{[f,A]_{\max}}\right\}\right)$, where $\delta \geq 1$. However, as the parameter δ increases, the discretization of the optimization problem becomes less accurate, since a decreasing proportion of discretized time steps are allocated within the time range relevant to the problem (*i.e.*, before the aircraft have reached their destinations). Therefore, the STOP fixed final time parameter δ was tested at values of 1.00, 1.05, 1.10, 1.15, 1.20 and 1.25.

Thus, the initial screening tests were conducted by evaluating Test Case 1 of Section 3.1.4.1 using normalized objectives (detailed in Section 3.1.1), the sigmoid constraint approximation method (detailed in Section 3.1.2.2) and the time-based sigmoid arrival indicator (detailed in Section 3.1.3.1), with all eight combinations of the binary weighting-type indicator variables, β_1, β_2 and β_3, at all six varying values of δ and all 63 combinations of the priority weights, λ_1, λ_2 and λ_3. Tables A.2 - A.9 display the summary results obtained by averaging all 63 combinations of priority weights for a given combination of binary weighting-type indicator variables and t_f parameter, δ.

Table A.2: Summary Results for Weight-Type Indicator Combination 1.

		Minimum Value Achieved			Value Achieved		
	t_f Parameter	Fuel	Schedule	Total	Success	Mean Seconds	Std Dev of Sec.
Treatment	(δ)	Measure	Deviation	Time	Rate	To Completion	To Completion
1	1.00	1.92	0.51	7.32	0.71	37.30	92.07
2	1.05	1.93	0.50	7.69	0.70	18.03	28.56
3	1.10	1.95	0.08	7.66	0.60	53.44	139.12
4	1.15	1.91	0.14	6.73	0.65	70.12	195.93
5	1.20	1.99	0.06	7.14	0.60	25.01	45.96
6	1.25	1.96	0.04	6.78	0.52	21.97	34.47
Minimum		1.91	0.04	6.73	0.52	18.03	28.56
Maximum		1.99	0.51	7.69	0.71	70.12	195.93
Mean		1.94	0.22	7.22	0.63	37.64	89.35

Table A.2 indicates that when all objectives are given exponential weighting, a minimum schedule deviation less than 0.10 can be achieved for values of the t_f parameter, δ, of 1.10, 1.20

and 1.25. However, the range of minimum achieved schedule deviation varies from 0.04 to 0.51, and the average run time was 37.63 seconds.

Table A.3: Summary Results for Weight-Type Indicator Combination 2.

		Minimum Value Achieved			Value Achieved		
	t_f Parameter	Fuel	Schedule	Total	Success	Mean Seconds	Std Dev of Sec.
Treatment	(δ)	Measure	Deviation	Time	Rate	To Completion	To Completion
7	1.00	1.97	0.75	7.23	0.68	33.02	85.47
8	1.05	1.93	0.49	7.12	0.65	44.18	108.38
9	1.10	1.95	0.08	7.09	0.67	45.03	96.97
10	1.15	1.98	0.13	6.90	0.60	60.62	149.51
11	1.20	2.00	0.08	7.14	0.70	29.23	45.98
12	1.25	1.96	0.04	7.39	0.52	49.03	170.45
Minimum		1.93	0.04	6.90	0.52	29.23	45.98
Maximum		2.00	0.75	7.39	0.70	60.62	170.45
Mean		1.97	0.26	7.14	0.64	43.52	109.46

Table A.3 indicates that when only the schedule deviation objective is given a linear weighting, a minimum schedule deviation less than 0.10 can be achieved for values of the t_f parameter, δ, of 1.10, 1.20 and 1.25. However, the range of minimum achieved schedule deviation varies from 0.04 to 0.75, and the average run time was 43.52 seconds.

Table A.4: Summary Results for Weight-Type Indicator Combination 3.

		Minimum Value Achieved			Value Achieved		
	t_f Parameter	Fuel	Schedule	Total	Success	Mean Seconds	Std Dev of Sec.
Treatment	(δ)	Measure	Deviation	Time	Rate	To Completion	To Completion
13	1.00	1.97	0.71	7.30	0.71	39.84	98.60
14	1.05	1.93	0.71	7.69	0.57	45.33	125.33
15	1.10	1.95	0.08	7.21	0.70	56.38	138.40
16	1.15	1.97	0.14	7.52	0.57	25.99	50.77
17	1.20	2.00	0.06	7.31	0.65	23.90	38.00
18	1.25	1.97	0.05	7.06	0.65	35.71	104.20
Minimum		1.93	0.05	7.06	0.57	23.90	38.00
Maximum		2.00	0.71	7.69	0.71	56.38	138.40
Mean		1.97	0.29	7.35	0.64	37.86	92.55

Table A.4 indicates that when only the makespan objective is given a linear weighting, a minimum schedule deviation less than 0.10 can be achieved for values of the t_f parameter, δ, of

1.10, 1.20 and 1.25. However, the range of minimum achieved schedule deviation varies from 0.05 to 0.71, and the average run time was 37.86 seconds.

Table A.5: Summary Results for Weight-Type Indicator Combination 4.

		Minimum Value Achieved			Value Achieved		
	t_f Parameter	Fuel	Schedule	Total	Success	Mean Seconds	Std Dev of Sec.
Treatment	(δ)	Measure	Deviation	Time	Rate	To Completion	To Completion
19	1.00	1.98	0.69	7.32	0.65	43.90	124.78
20	1.05	1.93	0.35	7.61	0.63	52.47	131.13
21	1.10	1.96	0.08	7.66	0.68	59.28	168.61
22	1.15	1.96	0.11	6.73	0.71	39.95	124.59
23	1.20	1.96	0.06	7.34	0.65	35.93	72.55
24	1.25	1.97	0.06	6.78	0.60	28.15	46.91
Minimum		1.93	0.06	6.73	0.60	28.15	46.91
Maximum		1.98	0.69	7.66	0.71	59.28	168.61
Mean		1.96	0.22	7.24	0.66	43.28	111.43

Table A.5 indicates that when only the fuel consumption objective is given a linear weighting, a minimum schedule deviation less than 0.10 can be achieved for values of the t_f parameter, δ, of 1.10, 1.20 and 1.25. However, the range of minimum achieved schedule deviation varies from 0.06 to 0.69, and the average run time was 43.28 seconds.

Table A.6: Summary Results for Weight-Type Indicator Combination 5.

		Minimum Value Achieved			Value Achieved		
	t_f Parameter	Fuel	Schedule	Total	Success	Mean Seconds	Std Dev of Sec.
Treatment	(δ)	Measure	Deviation	Time	Rate	To Completion	To Completion
25	1.00	1.98	0.71	7.22	0.75	24.69	39.77
26	1.05	1.99	0.75	7.30	0.62	37.64	74.14
27	1.10	1.95	0.08	7.21	0.67	50.61	95.70
28	1.15	1.91	0.17	7.58	0.65	46.55	86.98
29	1.20	1.99	0.09	7.17	0.73	35.43	63.96
30	1.25	1.97	0.05	7.04	0.71	26.27	58.83
Minimum		1.91	0.05	7.04	0.62	24.69	39.77
Maximum		1.99	0.75	7.58	0.75	50.61	95.70
Mean		1.97	0.31	7.25	0.69	36.86	69.90

Table A.6 indicates that when only the fuel consumption objective is given an exponential weighting, a minimum schedule deviation less than 0.10 can be achieved for values of the t_f

parameter, δ, of 1.10, 1.20 and 1.25. However, the range of minimum achieved schedule deviation varies from 0.05 to 0.75, and the average run time was 36.86 seconds.

Table A.7: Summary Results for Weight-Type Indicator Combination 6.

		Minimum Value Achieved			Value Achieved		
	t_f Parameter	Fuel	Schedule	Total	Success	Mean Seconds	Std Dev of Sec.
Treatment	(δ)	Measure	Deviation	Time	Rate	To Completion	To Completion
31	1.00	2.00	0.75	7.14	0.68	27.51	56.85
32	1.05	2.00	0.71	7.12	0.67	46.41	82.38
33	1.10	1.96	0.14	7.21	0.67	44.67	156.00
34	1.15	1.98	0.15	6.90	0.67	51.98	141.04
35	1.20	1.99	0.04	7.12	0.79	32.67	48.77
36	1.25	1.96	0.09	7.01	0.56	27.80	43.02
Minimum		1.96	0.04	6.90	0.56	27.51	43.02
Maximum		2.00	0.75	7.21	0.79	51.98	156.00
Mean		1.98	0.31	7.08	0.67	38.51	88.01

Table A.7 indicates that when only the makespan objective is given an exponential weighting, a minimum schedule deviation less than 0.10 can be achieved for values of the t_f parameter, δ, of 1.20 and 1.25. However, the range of minimum achieved schedule deviation varies from 0.04 to 0.75, and the average run time was 38.51 seconds.

Table A.8: Summary Results for Weight-Type Indicator Combination 7.

		Minimum Value Achieved			Value Achieved		
	t_f Parameter	Fuel	Schedule	Total	Success	Mean Seconds	Std Dev of Sec.
Treatment	(δ)	Measure	Deviation	Time	Rate	To Completion	To Completion
37	1.00	1.99	0.32	7.37	0.62	57.10	156.51
38	1.05	1.98	0.71	7.47	0.59	30.91	80.38
39	1.10	1.96	0.08	7.21	0.67	57.26	170.50
40	1.15	1.98	0.14	7.52	0.63	33.42	73.13
41	1.20	1.99	0.01	7.31	0.62	51.05	99.25
42	1.25	1.97	0.06	7.15	0.68	30.09	46.84
Minimum		1.96	0.01	7.15	0.59	30.09	46.84
Maximum		1.99	0.71	7.52	0.68	57.26	170.50
Mean		1.98	0.22	7.34	0.63	43.31	104.44

Table A.8 indicates that when only the schedule deviation objective is given an exponential weighting, a minimum schedule deviation less than 0.10 can be achieved for values of the t_f

parameter, δ, of 1.10, 1.20 and 1.25. However, the range of minimum achieved schedule deviation varies from 0.01 to 0.71, and the average run time was 43.31 seconds.

Table A.9: Summary Results for Weight-Type Indicator Combination 8.

		Minimum Value Achieved			Value Achieved		
	t_f Parameter	Fuel	Schedule	Total	Success	Mean Seconds	Std Dev of Sec.
Treatment	(δ)	Measure	Deviation	Time	Rate	To Completion	To Completion
43	1.00	1.98	0.32	7.14	0.68	26.59	43.58
44	1.05	2.00	0.77	7.30	0.60	42.83	103.32
45	1.10	1.97	0.14	7.21	0.71	37.58	120.30
46	1.15	1.96	0.17	7.58	0.62	44.05	93.43
47	1.20	1.96	0.04	7.14	0.76	35.83	56.70
48	1.25	1.97	0.09	7.56	0.67	33.23	68.44
Minimum		1.96	0.04	7.14	0.60	26.59	43.58
Maximum		2.00	0.77	7.58	0.76	44.05	120.30
Mean		1.97	0.26	7.32	0.67	36.69	80.96

Table A.9 indicates that when all objectives are given a linear weighting, a minimum schedule deviation less than 0.10 can be achieved for values of the t_f parameter, δ, of 1.20 and 1.25. However, the range of minimum achieved schedule deviation varies from 0.04 to 0.77, and the average run time was 36.69 seconds.

These results indicate that the t_f parameter, δ, should be set to a value near 1.20 and 1.25. However, since increasing the value of δ will likely decrease the accuracy of the discretized optimization problem, the t_f parameter, δ, should be set to a value near 1.20.

Figure A.1 plots the minimum achieved fuel, schedule deviation and makespan values for all 48 summary treatments. It indicates that treatments from Weight-Type Indicator Combinations 1 and 2 are most suitable for minimizing all three objectives. That is, exponential weightings appear more suitable for the schedule deviation and makespan measures than linear weightings.

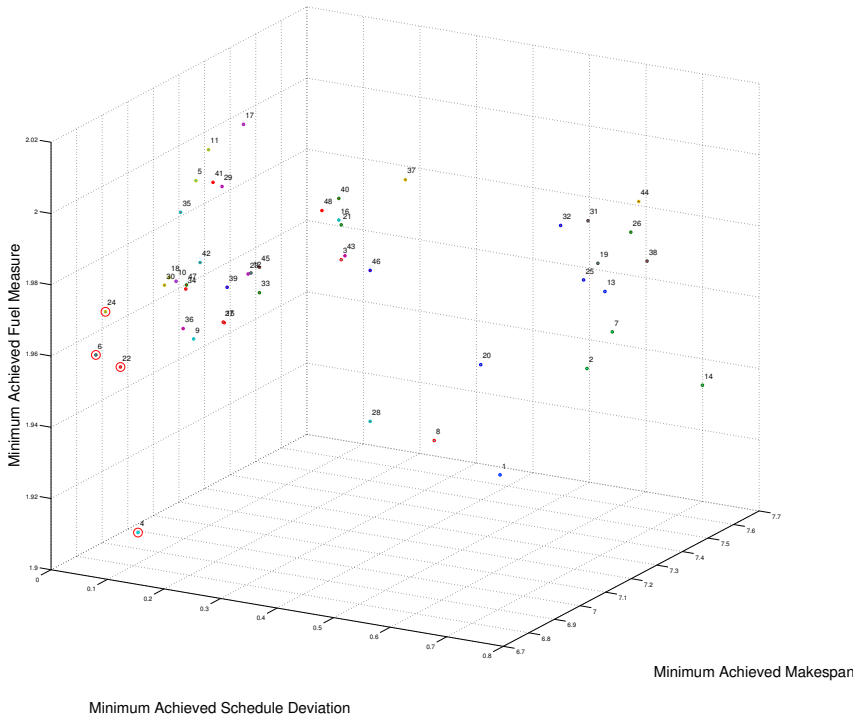

Figure A.1: Minimum Achieved Objective Values

Therefore, this research will focus on formulating the generalized weighted-sum representation of the multi-objective Air Traffic Management optimization problem using exponential weightings for the schedule deviation and makespan objectives, and define the STOP fixed final time, t_f, as

$$t_f = 1.2 \times \left(\max \left\{ t_{[f,1]_{\max}}, \ldots, t_{[f,A]_{\max}} \right\} \right).$$

Appendix B: Air Traffic Management Conflict Region Generation

This sections details the methods used to analytically define the pair-wise state space conflict region for a given ATM control mode.

B.1 Lateral Separation

In control mode μ, each aircraft $\alpha \in \{1, 2, \ldots, A\}$ is assigned a set of n_α way-points in the three-dimensional airspace that must be visited in order. Define the set of way-points given as

$$WP_{[\mu,\alpha]} = \{(x_{[1,\alpha]}, y_{[1,\alpha]}, z_{[1,\alpha]}), (x_{[2,\alpha]}, y_{[2,\alpha]}, z_{[2,\alpha]}), \ldots, (x_{[n_\alpha,\alpha]}, y_{[n_\alpha,\alpha]}, z_{[n_\alpha,\alpha]})\}, \tag{B.1}$$

so the route of aircraft α is partitioned into a set of $(n_\alpha - 1)$ route segments (or *arcs*) defined by the airspace way-points. Thus, the total path-length for the route of aircraft α in control mode μ, denoted $l_{[\mu,\alpha]}$, is given by

$$l_{[\mu,\alpha]} = \sum_{i=0}^{n_\alpha - 1} \left\| \mathbf{a}_{[i,\alpha]} \right\|, \tag{B.2a}$$

where

$$\mathbf{a}_{[i,\alpha]} \triangleq \begin{cases} [0, 0, 0] & \text{if } i = 0, \\ [x_{[i+1,\alpha]}, y_{[i+1,\alpha]}, z_{[i+1,\alpha]}] - [x_{[i,\alpha]}, y_{[i,\alpha]}, z_{[i,\alpha]}] & \text{if } i \geq 1, \end{cases} \tag{B.2b}$$

is a vector representation of the heading of the route segment that connects way-point i to way-point $(i + 1)$. Thus, if aircraft α is traveling along route segment i, there exists some $\tau \in [0, 1]$ such that

$$[x_\alpha(t), y_\alpha(t), z_\alpha(t)] = [x_{[i,\alpha]}, y_{[i,\alpha]}, z_{[i,\alpha]}] + \mathbf{a}_{[i,\alpha]}\tau, \tag{B.3}$$

where $[x_\alpha(t), y_\alpha(t), z_\alpha(t)]$ is the three-dimensional airspace position of aircraft α as it travels along route segment i at time t.

Therefore, given aircraft α_1 and α_2 in control mode μ, such that $\alpha_1 \in \{1, 2, \ldots, A\}$, $\alpha_2 \in \{1, 2, \ldots, A\}$ and $\alpha_1 \neq \alpha_2$, the Minimum Lateral Distance (MLD) between aircraft α_1, as it travels along route segment i, and aircraft α_2, as it travels along route segment j, is given by the MLD between the any position of aircraft α_1 defined as

$$[x_{[i,\alpha_1]}, y_{[i,\alpha_1]}, z_{[i,\alpha_1]}] + \mathbf{a}_{[i,\alpha_1]}\tau_1, \tag{B.4}$$

for $\tau_1 \in [0,1]$, and any position of aircraft α_2 defined as

$$\left[x_{[j,\alpha_2]}, y_{[j,\alpha_2}, z_{[j,\alpha_2]}\right] + \mathbf{a}_{[j,\alpha_2]}\tau_2, \tag{B.5}$$

for $\tau_2 \in [0,1]$. Thus, the positions of aircraft α_1 and aircraft α_2 that achieve the MLD between aircraft α_1, as it travels along route segment i, and aircraft α_2, as it travels along route segment j, are given by

$$\left[x^*_{[i,\alpha_1]}, y^*_{[i,\alpha_1]}, z^*_{[i,\alpha_1]}\right] = \left[x_{[i,\alpha_1]}, y_{[i,\alpha_1]}, z_{[i,\alpha_1]}\right] + \mathbf{a}_{[i,\alpha_1]}\tau^*_1, \tag{B.6a}$$

$$\left[x^*_{[j,\alpha_2]}, y^*_{[j,\alpha_2]}, z^*_{[j,\alpha_2]}\right] = \left[x_{[j,\alpha_2]}, y_{[j,\alpha_2]}, z_{[j,\alpha_2]}\right] + \mathbf{a}_{[i,\alpha_2]}\tau^*_2, \tag{B.6b}$$

where $\left[x^*_{[i,\alpha_1]}, y^*_{[i,\alpha_1]}, z^*_{[i,\alpha_1]}\right]$ and $\left[x^*_{[j,\alpha_2]}, y^*_{[j,\alpha_2]}, z^*_{[j,\alpha_2]}\right]$ are the position of aircraft α_1 and aircraft α_2, respectively, that achieve the MLD between aircraft α_1, as it travels along route segment i, and aircraft α_2, as it travels along route segment j, and $\left(\tau^*_1, \tau^*_2\right)$ is the solution to the optimization problem

minimize

$$D_{L[i,j]}(\tau_1,\tau_2)^2 \triangleq \left\| \left(\left(xyz_{[i,\alpha_1]} + \mathbf{a}_{[i,\alpha_1]}\tau_1\right) - \left(xyz_{[j,\alpha_2]} + \mathbf{a}_{[j,\alpha_2]}\tau_2\right)\right) M_L \right\|^2 \tag{B.7a}$$

subject to

$$xyz_{[i,\alpha_1]} \triangleq \left[x_{[i,\alpha_1]}, y_{[i,\alpha_1]}, z_{[i,\alpha_1]}\right], \tag{B.7b}$$

$$xyz_{[j,\alpha_2]} \triangleq \left[x_{[j,\alpha_2]}, y_{[j,\alpha_2]}, z_{[j,\alpha_2]}\right], \tag{B.7c}$$

$$M_L = \begin{bmatrix} 1 & 0 & 0 \\ 0 & 1 & 0 \\ 0 & 0 & 0 \end{bmatrix}, \tag{B.7d}$$

$$0 \le \tau_1 \le 1, \tag{B.7e}$$

$$0 \le \tau_2 \le 1. \tag{B.7f}$$

where $D_{L[i,j]}(\tau_1,\tau_2)$ is the lateral distance between aircraft α_1, as it travels along route segment i, and aircraft α_2, as it travels along route segment j.

If the $\tau^*_1 \notin \{0,1\}$, then the MLD is achieved with an interior point of route segment i, and if $\tau^*_2 \notin \{0,1\}$, then the MLD is achieved with an interior point of route segment j. Therefore, if

$\tau_1^* \notin \{0,1\}$, then define the new way-point i^* at the position along route i that achieves the MLD, $\left[x^*_{[i,\alpha_1]}, y^*_{[i,\alpha_1]}, z^*_{[i,\alpha_1]}\right]$, re-define route segment i as the arc that connects way-point i to way-point i^* and define the new route segment i^* as the arc that connects way-point i^* to way-point $(i+1)$. If $\tau_2^* \notin \{0,1\}$, then define the new way-point j^* at the position along route j that achieves the MLD, $\left[x^*_{[j,\alpha_2]}, y^*_{[j,\alpha_2]}, z^*_{[j,\alpha_2]}\right]$, re-define route segment j as the arc that connects way-point j to way-point j^* and define the new route segment j^* as the arc that connects way-point j^* to way-point $(j+1)$. Thus, any pair of paths of aircraft α_1 and aircraft α_2 can be defined so that the MLD between any route segment i of aircraft α_1 and route segment j of aircraft α_2 will occur only at route segment end-points.

B.1.1 Minimum Lateral Distance of Zero.

Suppose the MLD between route segment i of aircraft α_1 and route segment j of aircraft α_2 occurs at way-point i for aircraft α_1 and way-point j for aircraft α_2, and that this MLD is zero. Then,

$$\left\| \left(xyz_{[i,\alpha_1]} - xyz_{[j,\alpha_2]}\right) M_L \right\| = 0$$

$$\implies \quad \left(xyz_{[i,\alpha_1]} - xyz_{[j,\alpha_2]}\right) M_L = [0,0,0].$$

Therefore, the lateral separation between aircraft α_1 as it moves along segment i and aircraft α_2 as it moves along segment j is given by

$$\begin{aligned}
&\left\| \left((xyz_{[i,\alpha_1]} + \mathbf{a}_{[i,\alpha_1]}\tau_1) - \left(xyz_{[j,\alpha_2]} + \mathbf{a}_{[j,\alpha_2]}\tau_2\right)\right) M_L \right\| \\
=&\left\| \left(xyz_{[i,\alpha_1]} - xyz_{[j,\alpha_2]}\right) M_L + \left(\mathbf{a}_{[i,\alpha_1]}\tau_1 - \mathbf{a}_{[j,\alpha_2]}\tau_2\right) M_L \right\| \\
=&\left\| [0,0,0] + \left(\mathbf{a}_{[i,\alpha_1]}\tau_1 - \mathbf{a}_{[j,\alpha_2]}\tau_2\right) M_L \right\| \\
=&\left\| \left(\mathbf{a}_{[i,\alpha_1]}\tau_1 - \mathbf{a}_{[j,\alpha_2]}\tau_2\right) M_L \right\|.
\end{aligned}$$

Therefore, the boundary of the pair-wise conflict region between aircraft α_1 as it moves along segment i and aircraft α_2 as it moves along segment j is given by

$$\left\| \left(\mathbf{a}_{[i,\alpha_1]}\tau_1 - \mathbf{a}_{[j,\alpha_2]}\tau_2\right) M_L \right\|^2 = (r(t))^2\,, \tag{B.8}$$

or, equivalently,

$$(\hat{c}_1)^2 + (\hat{c}_2)^2 - 2\hat{c}_1\hat{c}_2 \frac{\langle \mathbf{a}_{[i,\alpha_1]} M_L, \mathbf{a}_{[j,\alpha_2]} M_L \rangle}{\|\mathbf{a}_{[i,\alpha_1]} M_L\| \|\mathbf{a}_{[j,\alpha_2]} M_L\|} = (r(t))^2\,, \tag{B.9}$$

where $r(t)$ is the minimum allowable lateral separation between aircraft α_1 and α_2,

$$\hat{c}_1 \triangleq \tau_1 \left\| \mathbf{a}_{[i,\alpha_1]} M_L \right\| \implies \hat{c}_1 \in \left[0, \left\| \mathbf{a}_{[i,\alpha_1]} M_L \right\| \right], \tag{B.10a}$$

and

$$\hat{c}_2 \triangleq \tau_2 \left\| \mathbf{a}_{[j,\alpha_2]} M_L \right\| \implies \hat{c}_2 \in \left[0, \left\| \mathbf{a}_{[j,\alpha_2]} M_L \right\| \right]. \tag{B.10b}$$

Therefore, the boundary of the lateral conflict region in the original state space is given by

$$\mathcal{B}_{LC}^{\alpha_1,\alpha_2} \triangleq \left\{ \left(\begin{array}{c} l_{[\mu,\alpha_1]}(i) \\ + \frac{\hat{c}_1 \|\mathbf{a}_{[i,\alpha_1]}\|}{\|\mathbf{a}_{[i,\alpha_1]} M_L\|} \end{array} , \begin{array}{c} l_{[\mu,\alpha_2]}(j) \\ + \frac{\hat{c}_2 \|\mathbf{a}_{[j,\alpha_2]}\|}{\|\mathbf{a}_{[j,\alpha_2]} M_L\|} \end{array} \right) \middle| \begin{array}{rl} 0 \le \hat{c}_1 \le \left\| \mathbf{a}_{[i,\alpha_1]} M_L \right\|, & \text{(B.11a)} \\ 0 \le \hat{c}_2 \le \left\| \mathbf{a}_{[j,\alpha_2]} M_L \right\|, & \text{(B.11b)} \\ (\hat{c}_1)^2 + (\hat{c}_2)^2 \, 2\hat{c}_1 \hat{c}_2 \frac{\langle \mathbf{a}_{[i,\alpha_1]} M_L, \mathbf{a}_{[j,\alpha_2]} M_L \rangle}{\|\mathbf{a}_{[i,\alpha_1]} M_L\| \|\mathbf{a}_{[j,\alpha_2]} M_L\|} = (r(t))^2 & \text{(B.11c)} \end{array} \right\}$$

where

$$l_{[\mu,\alpha_1]}(i) \triangleq \sum_{k=0}^{i} \left\| \mathbf{a}_{[k,\alpha_1]} \right\|, \tag{B.12}$$

and

$$l_{[\mu,\alpha_2]}(j) \triangleq \sum_{k=0}^{j} \left\| \mathbf{a}_{[k,\alpha_2]} \right\|. \tag{B.13}$$

Similarly, if the MLD between route segment i of aircraft α_1 and route segment j of aircraft α_2 is zero and occurs at way-point $i+1$ for aircraft α_1 and way-point j for aircraft α_2, the boundary of the lateral conflict region in the original state space is given by

$$\mathcal{B}_{LC}^{\alpha_1,\alpha_2} \triangleq \left\{ \left(\begin{array}{c} l_{[\mu,\alpha_1]}(i) \\ + \|\mathbf{a}_{[i,\alpha_1]}\| \\ - \frac{\hat{c}_1 \|\mathbf{a}_{[i,\alpha_1]}\|}{\|\mathbf{a}_{[i,\alpha_1]} M_L\|} \end{array} , \begin{array}{c} l_{[\mu,\alpha_2]}(j) \\ + \frac{\hat{c}_2 \|\mathbf{a}_{[j,\alpha_2]}\|}{\|\mathbf{a}_{[j,\alpha_2]} M_L\|} \end{array} \right) \middle| \begin{array}{rl} 0 \le \hat{c}_1 \le \left\| \mathbf{a}_{[i,\alpha_1]} M_L \right\|, & \text{(B.14a)} \\ 0 \le \hat{c}_2 \le \left\| \mathbf{a}_{[j,\alpha_2]} M_L \right\|, & \text{(B.14b)} \\ (\hat{c}_1)^2 + (\hat{c}_2)^2 \, 2\hat{c}_1 \hat{c}_2 \frac{\langle \mathbf{a}_{[i,\alpha_1]} M_L, \mathbf{a}_{[j,\alpha_2]} M_L \rangle}{\|\mathbf{a}_{[i,\alpha_1]} M_L\| \|\mathbf{a}_{[j,\alpha_2]} M_L\|} = (r(t))^2 & \text{(B.14c)} \end{array} \right\}$$

If the MLD between route segment i of aircraft α_1 and route segment j of aircraft α_2 is zero and occurs at way-point i for aircraft α_1 and way-point $j+1$ for aircraft α_2, the boundary of the lateral conflict region in the original state space is given by

$$\mathcal{B}_{LC}^{\alpha_1,\alpha_2} \triangleq \left\{ \left(\begin{array}{c} \\ l_{[\mu,\alpha_1]}(i) \\ + \frac{\hat{c}_1 \|\mathbf{a}_{[i,\alpha_1]}\|}{\|\mathbf{a}_{[i,\alpha_1]} M_L\|} \end{array} , \begin{array}{c} l_{[\mu,\alpha_2]}(j) \\ + \|\mathbf{a}_{[j,\alpha_2]}\| \\ - \frac{\hat{c}_2 \|\mathbf{a}_{[j,\alpha_2]}\|}{\|\mathbf{a}_{[j,\alpha_2]} M_L\|} \end{array} \right) \middle| \begin{array}{rl} 0 \le \hat{c}_1 \le \left\| \mathbf{a}_{[i,\alpha_1]} M_L \right\|, & \text{(B.15a)} \\ 0 \le \hat{c}_2 \le \left\| \mathbf{a}_{[j,\alpha_2]} M_L \right\|, & \text{(B.15b)} \\ (\hat{c}_1)^2 + (\hat{c}_2)^2 \, 2\hat{c}_1 \hat{c}_2 \frac{\langle \mathbf{a}_{[i,\alpha_1]} M_L, \mathbf{a}_{[j,\alpha_2]} M_L \rangle}{\|\mathbf{a}_{[i,\alpha_1]} M_L\| \|\mathbf{a}_{[j,\alpha_2]} M_L\|} = (r(t))^2 & \text{(B.15c)} \end{array} \right\}$$

If the MLD between route segment i of aircraft α_1 and route segment j of aircraft α_2 is zero and occurs at way-point $i+1$ for aircraft α_1 and way-point $j+1$ for aircraft α_2, the boundary of the lateral conflict region in the original state space is given by

$$\mathcal{B}_{LC}^{\alpha_1,\alpha_2} \triangleq \left\{ \left(\begin{array}{cc} l_{[\mu,\alpha_1]}(i) & l_{[\mu,\alpha_2]}(j) \\ +\|\mathbf{a}_{[i,\alpha_1]}\| & +\|\mathbf{a}_{[j,\alpha_2]}\| \\ -\frac{\hat{c}_1\|\mathbf{a}_{[i,\alpha_1]}\|}{\|\mathbf{a}_{[i,\alpha_1]}M_L\|} & -\frac{\hat{c}_2\|\mathbf{a}_{[j,\alpha_2]}\|}{\|\mathbf{a}_{[j,\alpha_2]}M_L\|} \end{array} \right) \middle| \begin{array}{rl} 0 \le \hat{c}_1 \le \left\|\mathbf{a}_{[i,\alpha_1]}M_L\right\|, & \text{(B.16a)} \\ 0 \le \hat{c}_2 \le \left\|\mathbf{a}_{[j,\alpha_2]}M_L\right\|, & \text{(B.16b)} \\ (\hat{c}_1)^2 + (\hat{c}_2)^2\, 2\hat{c}_1\hat{c}_2 \frac{\langle \mathbf{a}_{[i,\alpha_1]}M_L, \mathbf{a}_{[j,\alpha_2]}M_L\rangle}{\|\mathbf{a}_{[i,\alpha_1]}M_L\|\|\mathbf{a}_{[j,\alpha_2]}M_L\|} = (r(t))^2 & \text{(B.16c)} \end{array} \right\}$$

Note that equation (B.9) is the equation of an ellipse rotated ±45 degrees, centered at the origin and intersecting the coordinates

$$(\hat{c}_1, \hat{c}_2) = (\pm r(t), 0) \tag{B.17}$$

and

$$(\hat{c}_1, \hat{c}_2) = (0, \pm r(t))\,. \tag{B.18}$$

If $\frac{\langle \mathbf{a}_{[i,\alpha_1]}M_L, \mathbf{a}_{[j,\alpha_2]}M_L\rangle}{\|\mathbf{a}_{[i,\alpha_1]}M_L\|\|\mathbf{a}_{[j,\alpha_2]}M_L\|} > 0$ then the ellipse is oriented such that the semi-major axis extends into Quadrants I and III of the c_1c_2-plane, and the values of the semi-major and semi-minor axes of the ellipse are given by

$$R_{\text{major}} \triangleq \frac{r(t)}{\sqrt{1 - \frac{\langle \mathbf{a}_{[i,\alpha_1]}M_L, \mathbf{a}_{[j,\alpha_2]}M_L\rangle}{\left\|\mathbf{a}_{[i,\alpha_1]}M_L\right\|\left\|\mathbf{a}_{[j,\alpha_2]}M_L\right\|}}} \tag{B.19}$$

$$R_{\text{minor}} \triangleq \frac{r(t)}{\sqrt{1 + \frac{\langle \mathbf{a}_{[i,\alpha_1]}M_L, \mathbf{a}_{[j,\alpha_2]}M_L\rangle}{\left\|\mathbf{a}_{[i,\alpha_1]}M_L\right\|\left\|\mathbf{a}_{[j,\alpha_2]}M_L\right\|}}}, \tag{B.20}$$

where R_{major} is the value of the semi-major axis and R_{minor} is the value of the semi-minor axis.

If $\frac{\langle \mathbf{a}_{[i,\alpha_1]}M_L, \mathbf{a}_{[j,\alpha_2]}M_L\rangle}{\|\mathbf{a}_{[i,\alpha_1]}M_L\|\|\mathbf{a}_{[j,\alpha_2]}M_L\|} < 0$ then the the ellipse is oriented such that the semi-major axis extends into Quadrants II and IV of the c_1c_2-plane, and the values of the semi-major and semi-minor axes of the ellipse are given by

$$R_{\text{major}} \triangleq \frac{r(t)}{\sqrt{1 + \frac{\langle \mathbf{a}_{[i,\alpha_1]}M_L, \mathbf{a}_{[j,\alpha_2]}M_L\rangle}{\|\mathbf{a}_{[i,\alpha_1]}M_L\|\|\mathbf{a}_{[j,\alpha_2]}M_L\|}}} \tag{B.21}$$

$$R_{\text{minor}} \triangleq \frac{r(t)}{\sqrt{1 - \frac{\langle \mathbf{a}_{[i,\alpha_1]}M_L, \mathbf{a}_{[j,\alpha_2]}M_L\rangle}{\|\mathbf{a}_{[i,\alpha_1]}M_L\|\|\mathbf{a}_{[j,\alpha_2]}M_L\|}}}. \tag{B.22}$$

B.1.2 Non-Zero Minimum Lateral Distance.

This section describes how to define the conflict region boundary if the MLD between two route segments is greater than zero.

B.1.2.1 Non-Parallel Lateral Headings.

Suppose the MLD between route segment i of aircraft α_1 and route segment j of aircraft α_2 occurs at way-point i for aircraft α_1 and way-point j for aircraft α_2, and that this MLD is greater than zero.

If $\left|\frac{\langle \mathbf{a}_{[i,\alpha_1]}M_L, \mathbf{a}_{[j,\alpha_2]}M_L\rangle}{\|\mathbf{a}_{[i,\alpha_1]}M_L\|\|\mathbf{a}_{[j,\alpha_2]}M_L\|}\right| \neq 1$, then segment i of aircraft α_1 is not parallel to segment j of aircraft α_2. Therefore, there exists some $\left(\tau_1^*, \tau_2^*\right) \in \mathbb{R}^2$ such that

$$\left\| \left(\left(xyz_{[i,\alpha_1]} + \mathbf{a}_{[i,\alpha_1]}\tau_1^*\right) - \left(xyz_{[j,\alpha_2]} + \mathbf{a}_{[j,\alpha_2]}\tau_2^*\right)\right) M_L \right\| = 0.$$

That is, the lateral projection of segment i of aircraft α_1 and the lateral projection of segment j of aircraft α_2 can be extended until they intersect. The parameters τ_1^* and τ_2^* that define the extension necessary for the lateral segment projections to intersect can be obtained from problem (B.7) by removing constraints (B.7e) and (B.7f) and solving.

After obtaining $\left(\tau_1^*, \tau_2^*\right)$ from the relaxation of problem (B.7), the lateral distance from way-point i to the point where the extended lateral projection of segment i *would* intersect with the extended lateral projection of segment j is given by

$$D_{0[i,\alpha_1]} \triangleq \left\| \left(xyz_{[i,\alpha_1]} - \left(xyz_{[i,\alpha_1]} + \mathbf{a}_{[i,\alpha_1]}\tau_1^*\right)\right) M_L \right\| \tag{B.23}$$

where $D_{0[i,\alpha_1]}$ denotes the lateral distance from way-point i to the point where the extended lateral projection of segment i would intersect with the extended lateral projection of segment j. The lateral distance from way-point j to the point where segment j *would* intersect with segment i is given by

$$D_{0[j,\alpha_2]} \triangleq \left\| \left(xyz_{[j,\alpha_2]} - \left(xyz_{[j,\alpha_2]} + \mathbf{a}_{[j,\alpha_2]}\tau_2^*\right)\right) M_L \right\|, \tag{B.24}$$

where $D_{0[j,\alpha_2]}$ denotes the lateral distance from way-point j to the point where the extended lateral projection of segment j would intersect with the extended lateral projection of segment i. Thus, segment i of aircraft α_1 can be thought of as a sub-segment of the hypothetical segment i_0 that extends from $xyz_{[i,\alpha_1]} + \mathbf{a}_{[i,\alpha_1]}\tau_1^*$ to way-point $xyz_{[i+1,\alpha_1]}$, and segment j of aircraft α_2 can be thought

of as a sub-segment of the hypothetical segment j_0 that extends from $xyz_{[j,\alpha_2]}+\mathbf{a}_{[j,\alpha_2]}\tau_2^*$ to way-point $xyz_{[j+1,\alpha_2]}$. Since the MLD between hypothetical segments i_0 and j_0 is zero, the boundary of their conflict region would be defined using equation (B.14).

Therefore, if the non-zero MLD between segment i and segment j is given by the distance between way-point i of aircraft α_1 and way-point j of aircraft α_2, the boundary of the lateral conflict region in the original state space would be given by

$$\mathcal{B}_{LC}^{\alpha_1,\alpha_2} \triangleq \left\{ \left(\begin{array}{cc} l_{[\mu,\alpha_1]}(i) & l_{[\mu,\alpha_2]}(j) \\ +\frac{\hat{c}_1\|\mathbf{a}_{[i,\alpha_1]}\|}{\|\mathbf{a}_{[i,\alpha_1]}M_L\|} & +\frac{\hat{c}_2\|\mathbf{a}_{[j,\alpha_2]}\|}{\|\mathbf{a}_{[j,\alpha_2]}M_L\|} \end{array} \right) \middle| \begin{array}{rl} 0 \le \hat{c}_1 \le \left\|\mathbf{a}_{[i,\alpha_1]}M_L\right\|, & \text{(B.25a)} \\ 0 \le \hat{c}_2 \le \left\|\mathbf{a}_{[j,\alpha_2]}M_L\right\|, & \text{(B.25b)} \\ (\tilde{c}_1)^2 + (\tilde{c}_2)^2\, 2\tilde{c}_1\tilde{c}_2 \frac{\langle \mathbf{a}_{[i,\alpha_1]}M_L, \mathbf{a}_{[j,\alpha_2]}M_L\rangle}{\|\mathbf{a}_{[i,\alpha_1]}M_L\|\|\mathbf{a}_{[j,\alpha_2]}M_L\|} = (r(t))^2\,, & \text{(B.25c)} \end{array} \right\}$$

where

$$\tilde{c}_1 \triangleq \hat{c}_1 + D_{0[i,\alpha_1]} \tag{B.26a}$$

and

$$\tilde{c}_2 \triangleq \hat{c}_2 + D_{0[j,\alpha_2]}. \tag{B.26b}$$

Similarly, if the non-zero MLD between segment i and segment j is given by the distance between way-point $i+1$ of aircraft α_1 and way-point j of aircraft α_2, the boundary of the lateral conflict region in the original state space would be given by

$$\mathcal{B}_{LC}^{\alpha_1,\alpha_2} \triangleq \left\{ \left(\begin{array}{cc} l_{[\mu,\alpha_1]}(i) & \\ +\|\mathbf{a}_{[i,\alpha_1]}\| & l_{[\mu,\alpha_2]}(j) \\ -\frac{\hat{c}_1\|\mathbf{a}_{[i,\alpha_1]}\|}{\|\mathbf{a}_{[i,\alpha_1]}M_L\|} & +\frac{\hat{c}_2\|\mathbf{a}_{[j,\alpha_2]}\|}{\|\mathbf{a}_{[j,\alpha_2]}M_L\|} \end{array} \right) \middle| \begin{array}{rl} 0 \le \hat{c}_1 \le \left\|\mathbf{a}_{[i,\alpha_1]}M_L\right\|, & \text{(B.27a)} \\ 0 \le \hat{c}_2 \le \left\|\mathbf{a}_{[j,\alpha_2]}M_L\right\|, & \text{(B.27b)} \\ (\tilde{c}_1)^2 + (\tilde{c}_2)^2\, 2\tilde{c}_1\tilde{c}_2 \frac{\langle \mathbf{a}_{[i,\alpha_1]}M_L, \mathbf{a}_{[j,\alpha_2]}M_L\rangle}{\|\mathbf{a}_{[i,\alpha_1]}M_L\|\|\mathbf{a}_{[j,\alpha_2]}M_L\|} = (r(t))^2\,, & \text{(B.27c)} \end{array} \right\}$$

where

$$\tilde{c}_1 \triangleq \hat{c}_1 + D_{0[i+1,\alpha_1]} \tag{B.28a}$$

and

$$\tilde{c}_2 \triangleq \hat{c}_2 + D_{0[j,\alpha_2]} \tag{B.28b}$$

and $D_{0[i+1,\alpha_1]}$ is the lateral distance from way-point $i+1$ to the point where the extended lateral projection of segment i would intersect with the extended lateral projection of segment j.

If the non-zero MLD between segment i and segment j is given by the distance between way-point i of aircraft α_1 and way-point $j+1$ of aircraft α_2, the boundary of the lateral conflict region in

the original state space would be given by

$$\mathcal{B}_{LC}^{\alpha_1,\alpha_2} \triangleq \left\{ \left(\begin{array}{cc} & l_{[\mu,\alpha_2]}(j) \\ l_{[\mu,\alpha_1]}(i) & \\ + \frac{\hat{c}_1 \|\mathbf{a}_{[i,\alpha_1]}\|}{\|\mathbf{a}_{[i,\alpha_1]} M_L\|} & , \quad + \|\mathbf{a}_{[j,\alpha_2]}\| \\ & - \frac{\hat{c}_2 \|\mathbf{a}_{[j,\alpha_2]}\|}{\|\mathbf{a}_{[j,\alpha_2]} M_L\|} \end{array} \right) \middle| \begin{array}{rl} 0 \leq \hat{c}_1 \leq \left\|\mathbf{a}_{[i,\alpha_1]} M_L\right\|, & \text{(B.29a)} \\ 0 \leq \hat{c}_2 \leq \left\|\mathbf{a}_{[j,\alpha_2]} M_L\right\|, & \text{(B.29b)} \\ (\tilde{c}_1)^2 + (\tilde{c}_2)^2 \, 2\tilde{c}_1\tilde{c}_2 \frac{\langle \mathbf{a}_{[i,\alpha_1]} M_L, \mathbf{a}_{[j,\alpha_2]} M_L \rangle}{\|\mathbf{a}_{[i,\alpha_1]} M_L\| \|\mathbf{a}_{[j,\alpha_2]} M_L\|} = (r(t))^2 \,, & \text{(B.29c)} \end{array} \right\}$$

where

$$\tilde{c}_1 \triangleq \hat{c}_1 + D_{0[i,\alpha_1]} \tag{B.30a}$$

and

$$\tilde{c}_2 \triangleq \hat{c}_2 + D_{0[j+1,\alpha_2]} \tag{B.30b}$$

and $D_{0[j+1,\alpha_1]}$ is the lateral distance from way-point $j+1$ to the point where the extended lateral projection of segment j would intersect with the extended lateral projection of segment i.

If the non-zero MLD between segment i and segment j is given by the distance between way-point $i+1$ of aircraft α_1 and way-point $j+1$ of aircraft α_2, the boundary of the lateral conflict region in the original state space would be given by

$$\mathcal{B}_{LC}^{\alpha_1,\alpha_2} \triangleq \left\{ \left(\begin{array}{cc} l_{[\mu,\alpha_1]}(i) & l_{[\mu,\alpha_2]}(j) \\ + \|\mathbf{a}_{[i,\alpha_1]}\| & , \quad + \|\mathbf{a}_{[j,\alpha_2]}\| \\ - \frac{\hat{c}_1 \|\mathbf{a}_{[i,\alpha_1]}\|}{\|\mathbf{a}_{[i,\alpha_1]} M_L\|} & - \frac{\hat{c}_2 \|\mathbf{a}_{[j,\alpha_2]}\|}{\|\mathbf{a}_{[j,\alpha_2]} M_L\|} \end{array} \right) \middle| \begin{array}{rl} 0 \leq \hat{c}_1 \leq \left\|\mathbf{a}_{[i,\alpha_1]} M_L\right\|, & \text{(B.31a)} \\ 0 \leq \hat{c}_2 \leq \left\|\mathbf{a}_{[j,\alpha_2]} M_L\right\|, & \text{(B.31b)} \\ (\tilde{c}_1)^2 + (\tilde{c}_2)^2 \, 2\tilde{c}_1\tilde{c}_2 \frac{\langle \mathbf{a}_{[i,\alpha_1]} M_L, \mathbf{a}_{[j,\alpha_2]} M_L \rangle}{\|\mathbf{a}_{[i,\alpha_1]} M_L\| \|\mathbf{a}_{[j,\alpha_2]} M_L\|} = (r(t))^2 \,, & \text{(B.31c)} \end{array} \right\}$$

where

$$\tilde{c}_1 \triangleq \hat{c}_1 + D_{0[i+1,\alpha_1]} \tag{B.32a}$$

and

$$\tilde{c}_2 \triangleq \hat{c}_2 + D_{0[j+1,\alpha_2]}. \tag{B.32b}$$

B.1.2.2 Parallel Lateral Headings.

Suppose the MLD between route segment i of aircraft α_1 and route segment j of aircraft α_2 is achieved at way-point i for aircraft α_1 and way-point j for aircraft α_2, and that this MLD is greater than zero. If $\left| \frac{\langle \mathbf{a}_{[i,\alpha_1]} M_L, \mathbf{a}_{[j,\alpha_2]} M_L \rangle}{\|\mathbf{a}_{[i,\alpha_1]} M_L\| \|\mathbf{a}_{[j,\alpha_2]} M_L\|} \right| = 1$, then segment i of aircraft α_1 is parallel to segment j of aircraft α_2. The *relative angle of lateral approach* between segment i and segment j is defined as

$$\theta_{[i,j]} = \arccos\left(\frac{\langle \mathbf{a}_{[i,\alpha_1]} M_L, \Delta_{[i,j]} M_L \rangle}{\|\mathbf{a}_{[i,\alpha_1]} M_L\| \|\Delta_{[i,j]} M_L\|} \right), \tag{B.33}$$

where $\Delta_{[i,j]}M_L$ is the lateral projection of the vector that connects way-point i of aircraft α_1 to way-point j of aircraft α_2.

Now, the boundary of the resulting conflict region will be evaluated by case.

1. **Divergent Segments.** If $\frac{\langle \mathbf{a}_{[i,\alpha_1]}M_L, \mathbf{a}_{[j,\alpha_2]}M_L \rangle}{\|\mathbf{a}_{[i,\alpha_1]}M_L\| \|\mathbf{a}_{[j,\alpha_2]}M_L\|} = -1$, then segment i of aircraft α_1 is oriented in the opposite direction of motion from segment j of aircraft α_2, given the MLD between route segment i of aircraft α_1 and route segment j of aircraft α_2 occurs at way-point i for aircraft α_1 and way-point j for aircraft α_2. Thus, they are considered *divergent*. In this case, as aircraft α_1 moves toward way-point $i+1$ and aircraft α_2 moves toward way-point j, the lateral distance between them will increase. Figure B.1 depicts an example of the given case.

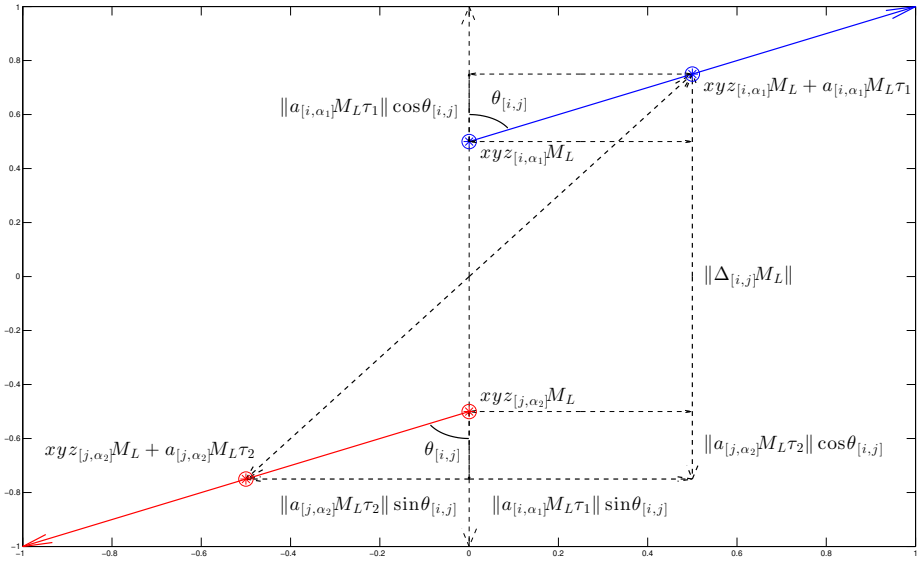

Figure B.1: Divergent Segment Geometry

From the given geometry,

$$
\begin{aligned}
&\left\| \left((xyz_{[i,\alpha_1]} + \mathbf{a}_{[i,\alpha_1]}\tau_1) - \left(xyz_{[j,\alpha_2]} + \mathbf{a}_{[j,\alpha_2]}\tau_2 \right) \right) M_L \right\|^2 \\
&= \left(\|\mathbf{a}_{[i,\alpha_1]} M_L \tau_1\| + \|\mathbf{a}_{[j,\alpha_2]} M_L \tau_2\| \right)^2 \left(\sin\theta_{[i,j]} \right)^2 \\
&\quad + \|\Delta_{[i,j]} M_L\|^2 + 2\|\Delta_{[i,j]} M_L\| \left(\|\mathbf{a}_{[i,\alpha_1]} M_L \tau_1\| + \|\mathbf{a}_{[j,\alpha_2]} M_L \tau_2\| \right) \cos\theta_{[i,j]} \\
&\quad + \left(\|\mathbf{a}_{[i,\alpha_1]} M_L \tau_1\| + \|\mathbf{a}_{[j,\alpha_2]} M_L \tau_2\| \right)^2 \left(\cos\theta_{[i,j]} \right)^2 \\
&= \left(\|\mathbf{a}_{[i,\alpha_1]} M_L \tau_1\| + \|\mathbf{a}_{[j,\alpha_2]} M_L \tau_2\| \right)^2 \\
&\quad + \|\Delta_{[i,j]} M_L\|^2 + 2\|\Delta_{[i,j]} M_L\| \left(\|\mathbf{a}_{[i,\alpha_1]} M_L \tau_1\| + \|\mathbf{a}_{[j,\alpha_2]} M_L \tau_2\| \right) \cos\theta_{[i,j]}.
\end{aligned} \tag{B.34}
$$

Therefore, the boundary of the lateral conflict region is given by

$$
\begin{aligned}
(r(t))^2 = &\left(\|\mathbf{a}_{[i,\alpha_1]} M_L \tau_1\| + \|\mathbf{a}_{[j,\alpha_2]} M_L \tau_2\| \right)^2 \\
&+ \|\Delta_{[i,j]} M_L\|^2 + 2\|\Delta_{[i,j]} M_L\| \left(\|\mathbf{a}_{[i,\alpha_1]} M_L \tau_1\| + \|\mathbf{a}_{[j,\alpha_2]} M_L \tau_2\| \right) \cos\theta_{[i,j]}.
\end{aligned} \tag{B.35}
$$

Completing the square gives

$$
\begin{aligned}
&(r(t))^2 - \|\Delta_{[i,j]} M_L\|^2 \left(\sin\theta_{[i,j]} \right)^2 \\
&= \left(\|\mathbf{a}_{[i,\alpha_1]} M_L \tau_1\| + \|\mathbf{a}_{[j,\alpha_2]} M_L \tau_2\| + \|\Delta_{[i,j]} M_L\| \cos\theta_{[i,j]} \right)^2 \\
\implies \quad &\sqrt{(r(t))^2 - \|\Delta_{[i,j]} M_L\|^2 \left(\sin\theta_{[i,j]} \right)^2} \\
&= \pm \left(\|\mathbf{a}_{[i,\alpha_1]} M_L \tau_1\| + \|\mathbf{a}_{[j,\alpha_2]} M_L \tau_2\| + \|\Delta_{[i,j]} M_L\| \cos\theta_{[i,j]} \right).
\end{aligned}
$$

Thus, the boundary of the lateral conflict region becomes

$$
\begin{aligned}
\tau_1 \|\mathbf{a}_{[i,\alpha_1]} M_L\| = &-\tau_2 \|\mathbf{a}_{[j,\alpha_2]} M_L\| \\
&-\|\Delta_{[i,j]} M_L\| \cos\theta_{[i,j]} \\
&\pm \sqrt{(r(t))^2 - \|\Delta_{[i,j]} M_L\|^2 \left(\sin\theta_{[i,j]} \right)^2}
\end{aligned} \tag{B.36}
$$

or, equivalently,

$$
\hat{c}_1 = -\hat{c}_2 - \|\Delta_{[i,j]} M_L\| \cos\theta_{[i,j]} \pm \sqrt{(r(t))^2 - \|\Delta_{[i,j]} M_L\|^2 \left(\sin\theta_{[i,j]} \right)^2} \tag{B.37}
$$

where

$$\hat{c}_1 \triangleq \tau_1 \left\| \mathbf{a}_{[i,\alpha_1]} M_L \right\| \implies \hat{c}_1 \in \left[0, \left\| \mathbf{a}_{[i,\alpha_1]} M_L \right\| \right],$$

and

$$\hat{c}_2 \triangleq \tau_2 \left\| \mathbf{a}_{[j,\alpha_2]} M_L \right\| \implies \hat{c}_2 \in \left[0, \left\| \mathbf{a}_{[j,\alpha_2]} M_L \right\| \right].$$

Therefore, the boundary of the lateral conflict region in the original state space would be given by

$$\mathcal{B}_{LC}^{\alpha_1,\alpha_2} \triangleq \left\{ \left(\begin{array}{cc} l_{[\mu,\alpha_1]}(i) & l_{[\mu,\alpha_2]}(j) \\ + \frac{\hat{c}_1 \|\mathbf{a}_{[i,\alpha_1]}\|}{\|\mathbf{a}_{[i,\alpha_1]} M_L\|} & + \frac{\hat{c}_2 \|\mathbf{a}_{[j,\alpha_2]}\|}{\|\mathbf{a}_{[j,\alpha_2]} M_L\|} \end{array} \right) \middle| \begin{array}{ll} 0 \leq \hat{c}_1 \leq \left\| \mathbf{a}_{[i,\alpha_1]} M_L \right\|, & \text{(B.39a)} \\ 0 \leq \hat{c}_2 \leq \left\| \mathbf{a}_{[j,\alpha_2]} M_L \right\|, & \text{(B.39b)} \\ \hat{c}_1 = -\hat{c}_2 - \omega_1 \pm \omega_2, & \text{(B.39c)} \end{array} \right\}$$

where

$$\omega_1 = \|\Delta_{[i,j]} M_L\| \cos\theta_{[i,j]},$$

and

$$\omega_2 = \sqrt{(r(t))^2 - \|\Delta_{[i,j]} M_L\|^2 \left(\sin\theta_{[i,j]}\right)^2}.$$

2. **Aligned Segments.** If $\frac{\langle \mathbf{a}_{[i,\alpha_1]} M_L, \mathbf{a}_{[j,\alpha_2]} M_L \rangle}{\|\mathbf{a}_{[i,\alpha_1]} M_L\| \|\mathbf{a}_{[j,\alpha_2]} M_L\|} = 1$, then segment i of aircraft α_1 is oriented in the same direction of motion as segment j of aircraft α_2, given the MLD between route segment i of aircraft α_1 and route segment j of aircraft α_2 occurs at way-point i for aircraft α_1 and way-point j for aircraft α_2. Thus, they are considered *aligned*. Figure B.2 depicts an example of the given case.

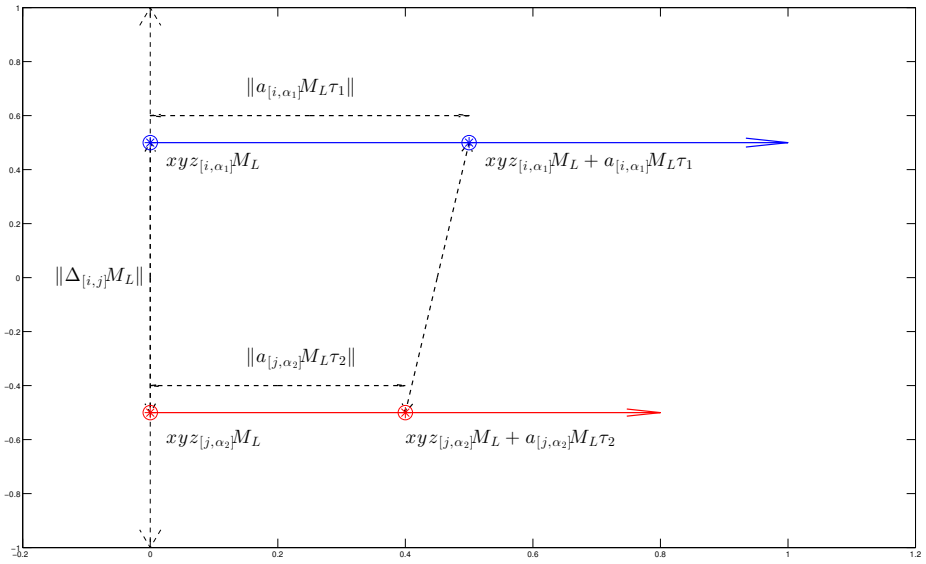

Figure B.2: Aligned Segment Geometry

From the given geometry,

$$\begin{aligned}
&\left\| \left((xyz_{[i,\alpha_1]} + \mathbf{a}_{[i,\alpha_1]}\tau_1) - \left(xyz_{[j,\alpha_2]} + \mathbf{a}_{[j,\alpha_2]}\tau_2\right)\right) M_L \right\|^2 \\
=&\|\Delta_{[i,j]}M_L\|^2 + \left(\left|\|\mathbf{a}_{[i,\alpha_1]}M_L\tau_1\| - \|\mathbf{a}_{[j,\alpha_2]}M_L\tau_2\|\right|\right)^2 \\
=&\|\Delta_{[i,j]}M_L\|^2 + \left(\|\mathbf{a}_{[i,\alpha_1]}M_L\tau_1\| - \|\mathbf{a}_{[j,\alpha_2]}M_L\tau_2\|\right)^2
\end{aligned}$$

Therefore, the boundary of the lateral conflict region is given by

$$\begin{aligned}
& (r(t))^2 = \|\Delta_{[i,j]}M_L\|^2 + \left(\|\mathbf{a}_{[i,\alpha_1]}M_L\tau_1\| - \|\mathbf{a}_{[j,\alpha_2]}M_L\tau_2\|\right)^2 \\
\implies \quad & (r(t))^2 - \|\Delta_{[i,j]}M_L\|^2 = \left(\|\mathbf{a}_{[i,\alpha_1]}M_L\tau_1\| - \|\mathbf{a}_{[j,\alpha_2]}M_L\tau_2\|\right)^2 \\
\implies \quad & \pm\sqrt{(r(t))^2 - \|\Delta_{[i,j]}M_L\|^2} = \|\mathbf{a}_{[i,\alpha_1]}M_L\tau_1\| - \|\mathbf{a}_{[j,\alpha_2]}M_L\tau_2\|.
\end{aligned}$$

Thus, the boundary of the lateral conflict region becomes

$$\tau_1\|\mathbf{a}_{[i,\alpha_1]}M_L\| = \tau_2\|\mathbf{a}_{[j,\alpha_2]}M_L\| \pm \sqrt{(r(t))^2 - \|\Delta_{[i,j]}M_L\|^2} \tag{B.41}$$

or, equivalently,

$$\hat{c}_1 = \hat{c}_2 - \pm\sqrt{(r(t))^2 - \|\Delta_{[i,j]}M_L\|^2} \tag{B.42}$$

where

$$\hat{c}_1 \triangleq \tau_1\left\|\mathbf{a}_{[i,\alpha_1]}M_L\right\| \implies \hat{c}_1 \in \left[0, \left\|\mathbf{a}_{[i,\alpha_1]}M_L\right\|\right],$$

and

$$\hat{c}_2 \triangleq \tau_2\left\|\mathbf{a}_{[j,\alpha_2]}M_L\right\| \implies \hat{c}_2 \in \left[0, \left\|\mathbf{a}_{[j,\alpha_2]}M_L\right\|\right].$$

Therefore, the boundary of the lateral conflict region in the original state space would be given by

$$\mathcal{B}_{LC}^{\alpha_1,\alpha_2} \triangleq \left\{ \left(\begin{array}{cc} l_{[\mu,\alpha_1]}(i) & l_{[\mu,\alpha_2]}(j) \\ +\frac{\hat{c}_1\|\mathbf{a}_{[i,\alpha_1]}\|}{\|\mathbf{a}_{[i,\alpha_1]}M_L\|} & +\frac{\hat{c}_2\|\mathbf{a}_{[j,\alpha_2]}\|}{\|\mathbf{a}_{[j,\alpha_2]}M_L\|} \end{array} \right) \middle| \begin{array}{rl} 0 \le \hat{c}_1 \le \left\|\mathbf{a}_{[i,\alpha_1]}M_L\right\|, & \text{(B.44a)} \\ 0 \le \hat{c}_2 \le \left\|\mathbf{a}_{[j,\alpha_2]}M_L\right\|, & \text{(B.44b)} \\ \hat{c}_1 = \hat{c}_2 - \pm\sqrt{(r(t))^2 - \|\Delta_{[i,j]}M_L\|^2}. & \text{(B.44c)} \end{array} \right\}$$

Similarly, if $\frac{\langle \mathbf{a}_{[i,\alpha_1]}M_L, \mathbf{a}_{[j,\alpha_2]}M_L\rangle}{\|\mathbf{a}_{[i,\alpha_1]}M_L\|\|\mathbf{a}_{[j,\alpha_2]}M_L\|} = 1$ and the MLD between route segment i of aircraft α_1 and route segment j of aircraft α_2 occurs at way-point $i+1$ for aircraft α_1 and way-point j for aircraft α_2, then the parallel segments are *staggered*, and the boundary of the lateral conflict region in the original state space would be given by

$$\mathcal{B}_{LC}^{\alpha_1,\alpha_2} \triangleq \left\{ \left(\begin{array}{cc} l_{[\mu,\alpha_1]}(i) & \\ +\|\mathbf{a}_{[i,\alpha_1]}\| & l_{[\mu,\alpha_2]}(j) \\ -\frac{\hat{c}_1\|\mathbf{a}_{[i,\alpha_1]}\|}{\|\mathbf{a}_{[i,\alpha_1]}M_L\|} & +\frac{\hat{c}_2\|\mathbf{a}_{[j,\alpha_2]}\|}{\|\mathbf{a}_{[j,\alpha_2]}M_L\|} \end{array} \right) \middle| \begin{array}{rl} 0 \le \hat{c}_1 \le \left\|\mathbf{a}_{[i,\alpha_1]}M_L\right\|, & \text{(B.45a)} \\ 0 \le \hat{c}_2 \le \left\|\mathbf{a}_{[j,\alpha_2]}M_L\right\|, & \text{(B.45b)} \\ \hat{c}_1 = -\hat{c}_2 - \omega_1 \pm \omega_2, & \text{(B.45c)} \end{array} \right\}$$

where

$$\omega_1 = \|\Delta_{[i,j]}M_L\|\cos\theta_{[i+1,j]},$$

and

$$\omega_2 = \sqrt{(r(t))^2 - \|\Delta_{[i+1,j]}M_L\|^2\left(\sin\theta_{[i+1,j]}\right)^2}.$$

If $\frac{\langle \mathbf{a}_{[i,\alpha_1]}M_L, \mathbf{a}_{[j,\alpha_2]}M_L\rangle}{\|\mathbf{a}_{[i,\alpha_1]}M_L\|\|\mathbf{a}_{[j,\alpha_2]}M_L\|} = 1$ and the MLD between route segment i of aircraft α_1 and route segment j of aircraft α_2 occurs at way-point i for aircraft α_1 and way-point $j+1$ for aircraft α_2, then the

parallel segments are *staggered*, and the boundary of the lateral conflict region in the original state space would be given by

$$\mathcal{B}_{LC}^{\alpha_1,\alpha_2} \triangleq \left\{ \left(\begin{array}{cc} & l_{[\mu,\alpha_2]}(j) \\ l_{[\mu,\alpha_1]}(i) & \\ + \frac{\hat{c}_1 \|\mathbf{a}_{[i,\alpha_1]}\|}{\|\mathbf{a}_{[i,\alpha_1]} M_L\|} & , \quad + \|\mathbf{a}_{[j,\alpha_2]}\| \\ & - \frac{\hat{c}_2 \|\mathbf{a}_{[j,\alpha_2]}\|}{\|\mathbf{a}_{[j,\alpha_2]} M_L\|} \end{array} \right) \middle| \begin{array}{ll} 0 \leq \hat{c}_1 \leq \left\| \mathbf{a}_{[i,\alpha_1]} M_L \right\|, & \text{(B.47a)} \\ 0 \leq \hat{c}_2 \leq \left\| \mathbf{a}_{[j,\alpha_2]} M_L \right\|, & \text{(B.47b)} \\ \hat{c}_1 = -\hat{c}_2 - \omega_1 \pm \omega_2, & \text{(B.47c)} \end{array} \right\}$$

where

$$\omega_1 = \|\Delta_{[i,j]} M_L\| \cos\theta_{[i,j+1]},$$

and

$$\omega_2 = \sqrt{(r(t))^2 - \|\Delta_{[i,j+1]} M_L\|^2 \left(\sin\theta_{[i,j+1]}\right)^2}.$$

If $\frac{\langle \mathbf{a}_{[i,\alpha_1]} M_L, \mathbf{a}_{[j,\alpha_2]} M_L \rangle}{\|\mathbf{a}_{[i,\alpha_1]} M_L\| \|\mathbf{a}_{[j,\alpha_2]} M_L\|} = -1$ and the MLD between route segment i of aircraft α_1 and route segment j of aircraft α_2 occurs at way-point $i+1$ for aircraft α_1 and way-point $j+1$ for aircraft α_2, then the parallel segments are *convergent*, and the boundary of the lateral conflict region in the original state space would be given by

$$\mathcal{B}_{LC}^{\alpha_1,\alpha_2} \triangleq \left\{ \left(\begin{array}{cc} l_{[\mu,\alpha_1]}(i) & l_{[\mu,\alpha_2]}(j) \\ + \|\mathbf{a}_{[i,\alpha_1]}\| & , \quad + \|\mathbf{a}_{[j,\alpha_2]}\| \\ - \frac{\hat{c}_1 \|\mathbf{a}_{[i,\alpha_1]}\|}{\|\mathbf{a}_{[i,\alpha_1]} M_L\|} & - \frac{\hat{c}_2 \|\mathbf{a}_{[j,\alpha_2]}\|}{\|\mathbf{a}_{[j,\alpha_2]} M_L\|} \end{array} \right) \middle| \begin{array}{ll} 0 \leq \hat{c}_1 \leq \left\| \mathbf{a}_{[i,\alpha_1]} M_L \right\|, & \text{(B.49a)} \\ 0 \leq \hat{c}_2 \leq \left\| \mathbf{a}_{[j,\alpha_2]} M_L \right\|, & \text{(B.49b)} \\ \hat{c}_1 = -\hat{c}_2 - \omega_1 \pm \omega_2, & \text{(B.49c)} \end{array} \right\}$$

where

$$\omega_1 = \|\Delta_{[i,j]} M_L\| \cos\theta_{[i+1,j+1]},$$

and

$$\omega_2 = \sqrt{(r(t))^2 - \|\Delta_{[i+1,j+1]} M_L\|^2 \left(\sin\theta_{[i+1,j+1]}\right)^2}.$$

B.2 Vertical Separation

In control mode μ, each aircraft $\alpha \in \{1, 2, \ldots, A\}$ is assigned a set of n_α way-points in the three-dimensional airspace that must be visited in order. Define the set of way-points given as

$$WP_{[\mu,\alpha]} = \{(x_{[1,\alpha]}, y_{[1,\alpha]}, z_{[1,\alpha]}), (x_{[2,\alpha]}, y_{[2,\alpha]}, z_{[2,\alpha]}), \ldots, (x_{[n_\alpha,\alpha]}, y_{[n_\alpha,\alpha]}, z_{[n_\alpha,\alpha]})\}, \quad \text{(B.51)}$$

so the route of aircraft α is partitioned into a set of $(n_\alpha - 1)$ route segments (or *arcs*) defined by the airspace way-points. Thus, the total path-length for the route of aircraft α in control mode μ, denoted $l_{[\mu,\alpha]}$, is given by

$$l_{[\mu,\alpha]} = \sum_{i=0}^{n_\alpha - 1} \left\| \mathbf{a}_{[i,\alpha]} \right\|, \tag{B.52a}$$

where

$$\mathbf{a}_{[i,\alpha]} \triangleq \begin{cases} [0,0,0] & \text{if } i = 0, \\ [x_{[i+1,\alpha]}, y_{[i+1,\alpha]}, z_{[i+1,\alpha]}] - [x_{[i,\alpha]}, y_{[i,\alpha]}, z_{[i,\alpha]}] & \text{if } i \geq 1, \end{cases} \tag{B.52b}$$

is a vector representation of the heading of the route segment that connects way-point i to way-point $(i+1)$. Thus, if aircraft α is traveling along route segment i, there exists some $\tau \in [0,1]$ such that

$$[x_\alpha(t), y_\alpha(t), z_\alpha(t)] = [x_{[i,\alpha]}, y_{[i,\alpha]}, z_{[i,\alpha]}] + \mathbf{a}_{[i,\alpha]}\tau, \tag{B.53}$$

where $[x_\alpha(t), y_\alpha(t), z_\alpha(t)]$ is the three-dimensional airspace position of aircraft α as it travels along route segment i at time t.

Therefore, given aircraft α_1 and α_2 in control mode μ, such that $\alpha_1 \in \{1, 2, \ldots, A\}$, $\alpha_2 \in \{1, 2, \ldots, A\}$ and $\alpha_1 \neq \alpha_2$, the vertical distance between aircraft α_1, as it travels along route segment i, and aircraft α_2, as it travels along route segment j, is given by the vertical distance between the any position of aircraft α_1 defined as

$$[x_{[i,\alpha_1]}, y_{[i,\alpha_1]}, z_{[i,\alpha_1]}] + \mathbf{a}_{[i,\alpha_1]}\tau_1, \tag{B.54}$$

for $\tau_1 \in [0,1]$, and any position of aircraft α_2 defined as

$$\left[x_{[j,\alpha_2]}, y_{[j,\alpha_2}, z_{[j,\alpha_2]}\right] + \mathbf{a}_{[j,\alpha_2]}\tau_2, \tag{B.55}$$

for $\tau_2 \in [0,1]$. Thus, the square of the vertical distance between aircraft α_1 and aircraft α_2 is given by

$$D_{V[i,j]}(\tau_1, \tau_2)^2 = \left\| \left([x_{[i,\alpha_1]}, y_{[i,\alpha_1}, z_{[i,\alpha_1]}] + \mathbf{a}_{[i,\alpha_1]}\tau_1 - \left[x_{[j,\alpha_2]}, y_{[j,\alpha_2}, z_{[j,\alpha_2]}\right] - \mathbf{a}_{[j,\alpha_2]}\tau_2 \right) M_V \right\|^2, \tag{B.56}$$

where $D_{V[i,j]}(\tau_1, \tau_2)$ is the vertical distance between aircraft α_1, as it travels along route segment i, and aircraft α_2, as it travels along route segment j, and

$$M_V \triangleq \begin{bmatrix} 0 & 0 & 0 \\ 0 & 0 & 0 \\ 0 & 0 & 1 \end{bmatrix} \tag{B.57}$$

Therefore, the boundary of the vertical conflict region is given by

$$\begin{aligned} & h^2 = \left\| \left([x_{[i,\alpha_1]}, y_{[i,\alpha_1}, z_{[i,\alpha_1]}] + \mathbf{a}_{[i,\alpha_1]}\tau_1 - \left[x_{[j,\alpha_2]}, y_{[j,\alpha_2}, z_{[j,\alpha_2]}\right] - \mathbf{a}_{[j,\alpha_2]}\tau_2 \right) M_V \right\|^2 \\ \implies \quad & h^2 = \left(\left(z_{[i,\alpha_1]} + \left(z_{[i+1,\alpha_1]} - z_{[i,\alpha_1]} \right) \tau_1 \right) - \left(z_{[j,\alpha_2]} + \left(z_{[j+1,\alpha_2]} - z_{[j,\alpha_2]} \right) \tau_2 \right) \right)^2 \\ \implies \quad & h = \pm \left(\left(z_{[i,\alpha_1]} + \left(z_{[i+1,\alpha_1]} - z_{[i,\alpha_1]} \right) \tau_1 \right) - \left(z_{[j,\alpha_2]} + \left(z_{[j+1,\alpha_2]} - z_{[j,\alpha_2]} \right) \tau_2 \right) \right) \end{aligned}$$

Thus, the boundary of the vertical conflict region becomes

$$\left(z_{[i+1,\alpha_1]} - z_{[i,\alpha_1]} \right) \tau_1 = \left(z_{[j+1,\alpha_2]} - z_{[j,\alpha_2]} \right) \tau_2 + z_{[j,\alpha_2]} - z_{[i,\alpha_1]} \pm h \tag{B.58}$$

or equivalently,

$$c_1 \frac{\left(z_{[i+1,\alpha_1]} - z_{[i,\alpha_1]} \right)}{\|\mathbf{a}_{[i,\alpha_1]}\|} = c_2 \frac{\left(z_{[j+1,\alpha_2]} - z_{[j,\alpha_2]} \right)}{\|\mathbf{a}_{[j,\alpha_2]}\|} + z_{[j,\alpha_2]} - z_{[i,\alpha_1]} \pm h, \tag{B.59}$$

where

$$c_1 \triangleq \tau_1 \left\| \mathbf{a}_{[i,\alpha_1]} \right\| \implies c_1 \in \left[0, \left\| \mathbf{a}_{[i,\alpha_1]} \right\| \right],$$

and

$$c_2 \triangleq \tau_2 \left\| \mathbf{a}_{[j,\alpha_2]} \right\| \implies c_2 \in \left[0, \left\| \mathbf{a}_{[j,\alpha_2]} \right\| \right].$$

Therefore, the boundary of the vertical conflict region in the original state space is given by

$$\mathcal{B}_{VC}^{\alpha_1,\alpha_2} \triangleq \left\{ (c_1, c_2) \;\middle|\; \begin{aligned} 0 \le c_1 \le \left\| \mathbf{a}_{[i,\alpha_1]} \right\|, & \qquad \text{(B.61a)} \\ 0 \le c_2 \le \left\| \mathbf{a}_{[j,\alpha_2]} \right\|, & \qquad \text{(B.61b)} \\ c_1 \delta z_1 = c_2 \delta z_2 + z_{[j,\alpha_2]} - z_{[i,\alpha_1]} \pm h, & \qquad \text{(B.61c)} \end{aligned} \right\}$$

where

$$\delta z_1 = \frac{\left(z_{[i+1,\alpha_1]} - z_{[i,\alpha_1]} \right)}{\|\mathbf{a}_{[i,\alpha_1]}\|},$$

and

$$\delta z_2 = \frac{\left(z_{[j+1,\alpha_2]} - z_{[j,\alpha_2]} \right)}{\|\mathbf{a}_{[j,\alpha_2]}\|}.$$

B.3 Three-Dimensional Conflict Region

Given the lateral conflict boundary as defined in B.1 and the vertical conflict boundary as defined in B.2, the three-dimensional conflict region is given by the intersection of the region within the lateral conflict boundary and the region within the vertical conflict boundary.

Appendix C: Settings for GPOPS-II Optimization Software

This research used the GPOPS-II Version 2.0 MATLAB software package developed by Michael A. Patterson and Anil V. Rao to evaluate the multi-objective Air Traffic Management optimization problem.

For each test case and treatment evaluated using the GPOPS-II software, the following user-defined settings were set to the values indicated:

- **setup.nlp.solver** ='snopt'

  Each test case and treatment was evaluated using the SNOPT package provided with the GPOPS software.

- **setup.nlp.snoptoptions.tolerance** = $5e-06$

  Each test case and treatment was evaluated using the SNOPT *Major Feasibility* tolerance of $1e-05$, *Minor Feasibility* tolerance of $1e-06$, *Major Optimality* tolerance of $5e-06$ and *Minor Optimality* tolerance of $1e-06$.

- **setup.nlp.snoptoptions.maxiterations** = 2000

  Each test case and treatment was evaluated using no more than 2000 *Major Iterations*.

- **setup.derivatives.supplier** = 'sparseCD'

  Each test case and treatment was evaluated using the *Central Difference* derivative estimate.

- **setup.derivatives.stepsize1** = $1e-08$

  Each test case and treatment was evaluated using a derivative estimate step-size of $1e-08$.

- **setup.derivatives.dependencies** = 'sparseNaN'

  Each test case and treatment was evaluated using the 'sparseNaN' derivatives dependencies option.

- **setup.mesh.tolerance** = $1e-03$

Each test case and treatment was evaluated using a mesh error tolerance of $1e-03$.

- **setup.mesh.maxiterations** = 1

  Each test case and treatment was evaluated using no more than 1 mesh adaptation.

- **setup.mesh.colpointsmin** = 6

  Each test case and treatment was evaluated with at least 6 collocation nodes per mesh interval.

- **setup.mesh.phase(1).colpoints** = $6 * ones(1, 15)$

  Each test case and treatment was evaluated with 15 mesh intervals.

- **setup.mesh.phase(1).fraction** = $(1/15) * ones(1, 15)$

  Each test case and treatment was evaluated with evenly allocated nodes per mesh.

- **setup.method** = 'RPM-Integration'

  Each test case and treatment was evaluated using the *integral* form of the collocation problem.

Each test case and treatment was evaluated with all other options at their default settings.

Bibliography

[1] Akella, Srinivas and S. Hutchinson. "Coordinating the motions of multiple robots with specified trajectories". *IEEE International Conference on Robotics and Automation*, volume 1, 624–631. IEEE, Washington, D.C., 2002.

[2] Arfken, George. *Mathematical Methods for Physicists*. Academic Press, Oxford, UK, 3rd edition, 1985.

[3] Arneson, Heather and M. Bloem. "Method for Scheduling Air Traffic with Uncertain En Route Capacity Constraints". *AIAA Guidance, Navigation, and Control Conference*. Chicago, IL, 2009.

[4] Asano, Tetsuo, D. Kirkpatrick, and C. Yap. "Pseudo approximation algorithms with applications to optimal motion planning". *Discrete & Computational Geometry*, 31(1):139–171, 2004.

[5] Bach, Ralph, Y.C. Chu, and H. Erzberger. *A Path-Stretch Algorithm for Conflict Resolution*. Technical report, NASA/CR–2009-214574, NASA-Ames Research Center, 2009.

[6] Barnes, Laura, M.A. Fields, and K. Valavanis. "Unmanned ground vehicle swarm formation control using potential fields". *Mediterranean Conference on Control & Automation*, 1–8. IEEE, Athens, Greece, 2007.

[7] Bazaraa, M.S., J.J. Jarvis, and H.D. Sherali. *Linear Programming and Network Flows*. John Wiley & Sons, Inc., New York, NY, 1990.

[8] Bazaraa, M.S., H.D. Sherali, and C.M. Shetty. *Nonlinear programming: theory and algorithms*. Wiley-interscience, Hoboken, NJ, 3rd edition, 2006.

[9] Benavides, Facundo, G. Tejera, M. Pedemonte, and S. Casella. "Real path planning based on genetic algorithm and Voronoi diagrams". *Robotics Symposium, 2011 IEEE IX Latin American and IEEE Colombian Conference on Automatic Control and Industry Applications (LARC)*, 1–6. IEEE, Bogota, Colombia, 2011.

[10] Bertsekas, Dimitri P. "Nondifferentiable optimization via approximation". *Mathematical Programming Studies*, 3:1–25, 1975.

[11] Bertsekas, Dimitri P. *Nonlinear Programming*. Athena Scientific, Nashua, NH, 2 edition, 1999.

[12] Bhattacharya, Priyadarshi and M.L. Gavrilova. "Voronoi diagram in optimal path planning". *4th International Symposium on Voronoi Diagrams in Science and Engineering*, 38–47. IEEE, Glamorgan, Wales, 2007.

[13] Bhattacharya, Priyadarshi and M.L. Gavrilova. "Roadmap-based path planning-Using the Voronoi diagram for a clearance-based shortest path". *Robotics & Automation Magazine, IEEE*, 15(2):58–66, 2008.

[14] Bien, Zeungnam and J. Lee. "A minimum-time trajectory planning method for two robots". *IEEE Transactions on Robotics and Automation*, 8(3):414–418, 1992.

[15] Bloem, Michael and H. Huang. "Evaluating delay cost functions with airline actions in Airspace Flow Programs". *Proc. of USA/Europe Air Traffic Management Research & Development Seminar*. Berlin, Germany, 2011.

[16] Bowe, A. and T. Lauderdale. "Selecting conflict resolution maneuvers based on minimum fuel burn". *29th Digital Avionics Systems Conference (DASC)*, 1–A. IEEE/AIAA, Salt Lake City, UT, 2010.

[17] Canny, John and J. Reif. "New lower bound techniques for robot motion planning problems". *28th Annual Symposium on Foundations of Computer Science*, 49–60. IEEE, Los Angeles, CA, 1987.

[18] Cone, Andrew C. "Effect of conflict resolution maneuver execution delay on losses of separation". *29th Digital Avionics Systems Conference (DASC)*, 3–B. IEEE/AIAA, Salt Lake City, UT, 2010.

[19] Cook, Andrew, G. Tanner, and S. Anderson. *Evaluating the true cost to airlines of one minute of airborne or ground delay*. Technical report, Eurocontrol, Brussels, Belgium, May 2004.

[20] Davis, Thomas, H. Erzberger, S. Green, and W. Nedell. "Design and evaluation of an air traffic control final approach spacing tool". *Journal of Guidance, Control, and Dynamics*, 14(4):848–854, 1991.

[21] Dijkstra, Edsger W. "A note on two problems in connexion with graphs". *Numerische mathematik*, 1(1):269–271, 1959.

[22] Dmitruk, A.V. and A.M. Kaganovich. "Maximum principle for optimal control problems with intermediate constraints". *Computational Mathematics and Modeling*, 22(2):180–215, 2011.

[23] Ehrgott, M. *Multicriteria Optimization*. Springer, Berlin, 2010.

[24] Erzberger, Heinz. "Automation of on-board flightpath management". *24th Israel Annual Conference on Aviation and Astronautics*. Tel–Aviv, Israel, 1982.

[25] Erzberger, Heinz, R.A. Paielli, D.R. Isaacson, and M.M. Eshow. "Conflict detection and resolution in the presence of prediction error". *1st USA/Europe Air Traffic Management R&D Seminar*, 17–20. Saclay, France, 1997.

[26] Federal Aviation Administration. *NextGen Implementation Plan*. Technical report, 2012.

[27] Federal Aviation Administration. *Order JO 7110.65 U*. March 2013.

[28] Francis, Michael R. *DIDO optimization of a lunar landing trajectory with respect to autonomous landing hazard avoidance technology*. Master's thesis, Naval Postgraduate School, 2009.

[29] Frazzoli, Emilio. "Decision on Manuscript". personal communication, June 2014.

[30] Garg, Divya, M. Patterson, W. Hager, A. Rao, D. Benson, and G. Huntington. "A unified framework for the numerical solution of optimal control problems using pseudospectral methods". *Automatica*, 46:1843–1851, 2010.

[31] Gelfand, I. and S.V. Fomin. *Calculus of Variations*. Dover Publications, Mineola, New York, 2000.

[32] Ghrist, Robert and D.E. Koditschek. "Safe cooperative robot dynamics on graphs". *SIAM journal on control and optimization*, 40(5):1556–1575, 2002.

[33] Ghrist, Robert, J.M. O'Kane, and S.M. LaValle. "Computing Pareto optimal coordinations on roadmaps". *The International Journal of Robotics Research*, 24(11):997–1010, 2005.

[34] Hart, P.E., N.J. Nilsson, and B. Raphael. "A Formal Basis for the Heuristic Determination of Minimum Cost Paths". *IEEE Transactions on Systems Science and Cybernetics*, 4(2):100–107, 1968. ISSN 0536-1567.

[35] Hershberger, John and S. Suri. "An optimal algorithm for Euclidean shortest paths in the plane". *SIAM Journal on Computing*, 28(6):2215–2256, 1999.

[36] Hrbacek, Karel and T. Jech. *Introduction to Set Theory*. Marcel Dekker, Inc., New York, NY, 1999.

[37] Hu, Jianghai, M. Prandini, and S. Sastry. "Probabilistic safety analysis in three dimensional aircraft flight". *Proceedings of the 42nd IEEE Conference on Decision and Control*, volume 5, 5335–5340. IEEE, Maui, HI, 2003.

[38] Hu, Jianghai, M. Prandini, and S. Sastry. "Aircraft conflict prediction in the presence of a spatially correlated wind field". *IEEE Transactions on Intelligent Transportation Systems*, 6(3):326–340, 2005.

[39] Hubbard, J. and B. Hubbard. *Vector Calculus, Linear Algebra, and Differnetial Forms*. Prentice-Hall, Inc., Upper Saddle River, NJ, 1999.

[40] Isaacson, Douglas and J.E. Robinson III. "A knowledge-based conflict resolution algorithm for terminal area air traffic control advisory generation". *AIAA Guidance, Navigation, and Control Conference*. AIAA, Montreal, Canada, 2001.

[41] Isaacson, Douglas, A.V. Sadovsky, and D. Davis. "Scheduling for Precision Air Traffic Operations: Problem Definition and Review of Prior Research". *To be submitted as a NASA Technical Memorandum*.

[42] Jung, Jae Bum and R. Ghrist. "Pareto optimal multi-robot coordination with acceleration constraints". *IEEE International Conference on Robotics and Automation*, 1942–1947. IEEE, Pasadena, CA, 2008.

[43] Kamgarpour, Maryam, V. Dadok, and C. Tomlin. "Trajectory generation for aircraft subject to dynamic weather uncertainty". *49th IEEE Conference on Decision and Control (CDC)*, 2063–2068. IEEE, Atlanta, GA, 2010.

[44] Kara, A, J. Ferguson, K. Hoffman, and L. Sherry. "Estimating Domestic US Airline Cost of Delay based on European Model". *4th International Conference on Research in Air Transportation-ICRAT*, 01–04. Budapest, Hungary, 2010.

[45] Kim, Jin-Oh and P.K. Khosla. "Real-time obstacle avoidance using harmonic potential functions". *IEEE Transactions on Robotics and Automation*, 8(3):338–349, 1992.

[46] Kirk, Donald E. *Optimal control theory: an introduction*. Dover Publications, Inc., Mineola, NY, 2012.

[47] Knorr, David and L. Walter. "Trajectory Uncertainty and the Impact on Sector Complexity and Workload". SESAR, Toulouse, France, 2011.

[48] Kosecka, Jana, C. Tomlin, G. Pappas, and S. Sastry. "Generation of conflict resolution manoeuvres for air traffic management". *Proceedings of the 1997 IEEE/RSJ International Conference on Intelligent Robots and Systems*, volume 3, 1598–1603. IEEE, Grenoble, France, 1997.

[49] Lauderdale, Todd. "The effects of speed uncertainty on a separation assurance algorithm". *Proceedings of the 10th AIAA Aviation Technology, Integration, and Operations (ATIO) Conference*. AIAA, Fort Worth, TX, 2010.

[50] Lauderdale, Todd. "Probabilistic conflict detection for robust detection and resolution". *AIAA aviation technology, integration, and operations conference*. Indianapolis, IN, 2012.

[51] Lauderdale, Todd, A.C. Cone, and A.R. Bowe. "Relative Significance of Trajectory Prediction Errors on an Automated Separation Assurance Algorithm". *Ninth USA/Europe Air Traffic Management Research and Development Seminar*. 2011.

[52] LaValle, Steven and S.A. Hutchinson. "Optimal motion planning for multiple robots having independent goals". *Proceedings of the 1996 IEEE International Conference on Robotics and Automation*, volume 3, 2847–2852. IEEE, Minneapolis, MN, 1996.

[53] Lee, Alan G., S.S. Weygandt, B. Schwartz, and J.R. Murphy. "Performance of trajectory models with wind uncertainty". *AIAA Modeling and Simulation Technologies Conference*. AIAA, Chicago, Illinois, 2009.

[54] Lee, Leng-Feng. *Decentralized motion planning within an artificial potential framework (APF) for cooperative payload transport by multi-robot collectives*. Master's thesis, State University of New York, 2004.

[55] Lewis, L. Ryan and I.M. Ross. *A pseudospectral method for real-time motion planning and obstacle avoidance*. Technical report, DTIC Document, 2007.

[56] Lewis, L. Ryan, I.M. Ross, and Q. Gong. "Pseudospectral motion planning techniques for autonomous obstacle avoidance". *46th IEEE Conference on Decision and Control*, 5997–6002. IEEE, New Orleans, LA, 2007.

[57] Liu, Lifeng and S. Zhang. "Voronoi diagram and GIS-based 3D path planning". *17th International Conference on Geoinformatics*, 1–5. IEEE, Fairfax, VA, 2009.

[58] Luenberger, David. *Optimization by Vector Space Methods*. John Wiley & Sons, Inc., New York, NY, 1994.

[59] McNally, David and C. Gong. *Concept and laboratory analysis of trajectory-based automation for separation assurance*. NASA Ames Research Center, 2006.

[60] McNally, David and D. Thipphavong. "Automated separation assurance in the presence of uncertainty". *International Council for the Aeronautical Sciences (ICAS) Congress*, 14–19. Anchorage, AK, 2008.

[61] Meckiff, Colin, R. Chone, and J.P. Nicolaon. "The tactical load smoother for multi–sector planning". *Proceedings of the 2nd USA/Europe Air Traffic Management Research and Devlepment Seminar*. Orlanda, FL, 1998.

[62] Mitchell, Joseph and M. Sharir. "New results on shortest paths in three dimensions". *Proceedings of the 20th annual symposium on Computational geometry*, 124–133. ACM, Brooklyn, NY, 2004.

[63] Neuman, Frank and H. Erzberger. *Analysis of delay reducing and fuel saving sequencing and spacing algorithms for arrival traffic*. Technical report, NASA-TM–103880, NASA-Ames Research Center, 1991.

[64] Okabe, Atsuyuki, B. Boots, K. Sugihara, and S.N. Chiu. *Spatial tessellations: concepts and applications of Voronoi diagrams*, volume 501. John Wiley & Sons, Inc., New York, NY, 2009.

[65] Patterson, Michael A. and A.V. Rao. "GPOPS- II Version 1.0: A General-Purpose MATLAB Toolbox for Solving Optimal Control Problems Using the Radau Pseudospectral Method". 2013.

[66] Peng, Jufeng and S. Akella. "Coordinating multiple double integrator robots on a roadmap: Convexity and global optimality". *Proceedings of the 2005 IEEE International Conference on Robotics and Automation*, 2751–2758. IEEE, Barcelona, Spain, 2005.

[67] Peterson, Michael, D.J. Bertsimas, and A.R. Odoni. "Models and algorithms for transient queueing congestion at airports". *Management Science*, 41(8):1279–1295, 1995.

[68] Pinedo, Michael. *Scheduling: theory, algorithms, and systems*. Prentice-Hall, Inc., Englewood Cliffs, NJ, 1995.

[69] Raghunathan, Arvind U., V. Gopal, and D. Subramanian. "Dynamic optimization strategies for three-dimensional conflict resolution of multiple aircraft". *Journal of guidance, control, and dynamics*, 27(4):586–594, 2004.

[70] Ren, Jing, K. A McIsaac, and X. Huang. "Motion planning for mobile robotics using the generalized sigmoid function". *Proceedings of the 2004 IEEE International Conference on Robotics and Automation*, volume 3, 2393–2398. IEEE, New Orleans, LA, 2004.

[71] Robinson III, John E., T.J. Davis, and D.R. Isaacson. "Fuzzy reasoning-based sequencing of arrival aircraft in the terminal area". *AIAA Guidance, Navigation and Control Conference*, 1–11. New Orleans, LA, 1997.

[72] Sadovsky, Alexander V. "Application of the Shortest-Path Problem to Routing Terminal Airspace Air Traffic". *Journal of Aerospace Information Systems*, 11(3):118–130, 2014.

[73] Sadovsky, Alexander V., D. Davis, and D.R. Isaacson. *Optimal routing and control of multiple agents moving in a transportation network and subject to an arrival schedule and separation constraints*. Technical report, NASA-Ames Research Center, 2012.

[74] Sadovsky, Alexander V., D. Davis, and D.R. Isaacson. "Separation-compliant, optimal routing and control of scheduled arrivals in a terminal airspace". *Transportation Research Part C: Emerging Technologies*, 37:157–176, 2013.

[75] Sadovsky, Alexander V., D. Davis, and D.R. Isaacson. "Efficient computation of separation-compliant speed advisories for air traffic arriving in terminal airspace". *Journal of Dynamic Systems, Measurement, and Control*, 136(4):041027, 2014.

[76] Sadovsky, Alexander V., Damek Davis, and Douglas R Isaacson. *Efficient Computation of Separation-Compliant Speed Advisories for Air Traffic Arriving in Terminal Airspace*. Technical report, NASA/TM-2012-216033, Moffett Field, California, 2012.

[77] Shin, Kang and N. McKay. "Minimum-time control of robotic manipulators with geometric path constraints". *IEEE Transactions on Automatic Control*, 30(6):531–541, 1985.

[78] Shin, Kang and Qin Zheng. "Minimum-time collision-free trajectory planning for dual-robot systems". *Robotics and Automation, IEEE Transactions on*, 8(5):641–644, 1992.

[79] Smith, Nathan and C. Arendt. "Implementing Conditional Inequality Constraints for Optimal Collision Avoidance", 2014. Manuscript submitted for publication.

[80] Soler, Manuel, A. Olivares, E. Staffetti, and P. Bonami. "En-route optimal flight planning constrained to pass through waypoints using MINLP". *Proceedings of 9th USA/Europe Air Traffic Management Research and Development Seminar*. Berlin, Germany, 2011.

[81] Sriver, Todd A. *The application of sequential convex programming to large-scale structural optimization problems*. Master's thesis, Air Force Institute of Technology, 1998.

[82] Suh, S.H. and K.G. Shin. "A variational dynamic programming approach to robot-path planning with a distance-safety criterion". *IEEE Journal of Robotics and Automation*, 4(3):334–349, 1988.

[83] Tomlin, Claire, G.J. Pappas, and S. Sastry. "Noncooperative conflict resolution [air traffic management]". *Proceedings of the 36th IEEE Conference on Decision and Control*, volume 2, 1816–1821. IEEE, San Diego, CA, 1997.

[84] Wächter, A. *An interior point algorithm for Large-scale nonlinear optimization with applications in process engineering*. Master's thesis, Carnegie Mellon University, 2002.

[85] Walter, Rudin. *Principles of Mathematical Analysis*. McGraw-Hill, New York, NY, 1964.

[86] Weisstein, Eric W. *CRC concise encyclopedia of mathematics*. CRC Press, LLC, Boca Raton, FL, 2010.

[87] Zheng, Xiaoyu and P. Palffy-Muhoray. "Distance of closest approach of two arbitrary hard ellipses in two dimensions". *Physical Review E*, 75(6), 2007.

REPORT DOCUMENTATION PAGE

Form Approved
OMB No. 0704–0188

1. REPORT DATE *(DD–MM–YYYY)*	2. REPORT TYPE	3. DATES COVERED *(From — To)*
18 Sept 2014	Dissertation	Sept 2011–Sept 2014

4. TITLE AND SUBTITLE

Optimal Control of Fully Routed Air Traffic in the Presence of Uncertainty and Kinodynamic Constraints

5a. CONTRACT NUMBER

5b. GRANT NUMBER

5c. PROGRAM ELEMENT NUMBER

6. AUTHOR(S)

Arendt, Christopher D., Major, USAF

5d. PROJECT NUMBER

5e. TASK NUMBER

5f. WORK UNIT NUMBER

7. PERFORMING ORGANIZATION NAME(S) AND ADDRESS(ES)

Air Force Institute of Technology
Graduate School of Engineering and Management (AFIT/EN)
2950 Hobson Way
WPAFB, OH 45433-7765

8. PERFORMING ORGANIZATION REPORT NUMBER

AFIT-ENS-DS-14-S-15

9. SPONSORING / MONITORING AGENCY NAME(S) AND ADDRESS(ES)

Intentionally Left Blank

10. SPONSOR/MONITOR'S ACRONYM(S)

11. SPONSOR/MONITOR'S REPORT NUMBER(S)

12. DISTRIBUTION / AVAILABILITY STATEMENT

Distribution Statement A. Approved for Public Release; Distribution Unlimited.

13. SUPPLEMENTARY NOTES

14. ABSTRACT

A method is presented to extend current graph-based Air Traffic Management optimization frameworks. In general, Air Traffic Management is the process of guiding a finite set of aircraft, each along its pre-determined path within some local airspace, subject to various physical, policy, procedural and operational restrictions. This research addresses several limitations of current graph-based Air Traffic Management optimization methods by incorporating techniques to account for stochastic effects, physical inertia and variable arrival sequencing. In addition, this research provides insight into the performance of multiple methods for approximating non-differentiable air traffic constraints, and incorporates these methods into a generalized weighted-sum representation of the multi-objective Air Traffic Management optimization problem that minimizes the total time of flight, deviation from scheduled arrival time and fuel consumption of all aircraft. The methods developed and tested throughout this dissertation demonstrate the ability of graph-based optimization techniques to model realistic air traffic restrictions and generate viable control strategies.

15. SUBJECT TERMS

Air Traffic Management Optimal Control

16. SECURITY CLASSIFICATION OF:			17. LIMITATION OF ABSTRACT	18. NUMBER OF PAGES	19a. NAME OF RESPONSIBLE PERSON
a. REPORT	b. ABSTRACT	c. THIS PAGE			Dr. James W. Chrissis (ENS)
U	U	U	UU	287	19b. TELEPHONE NUMBER *(include area code)* (937) 255-3636 x4606 james.chrissis@afit.edu